PhD degree in System Medicine (Curriculum in Molecular Oncology)

European School of Molecular Medicine (SEMM),

University of Milan and University of Naples "Federico II"

Settore Disciplinare: BIO/10

Regulation and physiological role of non-clathrin endocytosis of the epidermal growth factor receptor

Gorana Jendrišek

IEO, Milan

Matricola n. R 12424

Supervisor: Prof. **Pier Paolo Di Fiore**

IEO, Milan and University of Milan

Added supervisor: Prof. **Sara Sigismund**

IEO, Milan and University of Milan

PhD Coordinator: Prof. **Saverio Minucci**

Academic year 2021-2022

Za mamu
Za Čupku
Za Acu

Za mog Mićonija

TABLE OF CONTENTS

LIST OF ABBREVIATIONS **9**

FIGURES AND TABLES INDEX **13**

ABSTRACT **15**

1. INTRODUCTION **17**

1.1. Endocytosis **17**

1.1.1. Clathrin-dependent endocytosis 21

1.1.2. Clathrin-independent endocytosis 24

1.1.2.1. Caveolar endocytosis. 25

1.1.2.2. Flotillin. 27

1.1.2.3. CLIC/GEEC. 27

1.1.2.4. FEME. 29

1.1.2.5. EGFR-non-clathrin endocytosis. 30

1.1.3. Role of membrane microdomains - lipid rafts in endocytic pathways 30

1.1.4. Role of endocytosis in control of receptor signaling 32

1.2. Epidermal growth factor receptor **35**

1.2.1. EGFR ligands 37

1.2.2. EGFR endocytosis 40

1.2.2.1. Clathrin-dependent endocytosis of the EGFR 41

1.2.2.2. Non-clathrin endocytosis of the EGFR 42

1.2.3. EGFR signaling – different pathways 49

1.2.3.1. ERK-MAPK pathway 51

1.2.3.2. PI3K-AKT pathway 51

1.2.3.3. STAT pathway 52

1.2.3.4. PLCγ-Ca^{2+} pathway 52

1.1.1. EGFR in physiology and cancer 55

2. HYPOTHESIS AND AIMS OF THE PROJECT **57**

3. MATERIALS & METHODS **59**

3.1. Reagents **59**

3.2. Cell Culture **61**

3.3. RNA interference (RNAi) 61

3.4. Lentiviral infections 62

3.5. Biochemical assays 62

3.5.1. Western blot 62

3.5.1.1. Anti-Ub western blot 63

3.5.2. Immunoprecipitation 63

3.5.3. GST pull-down assays 64

3.5.4. Density gradient fractionation assay 64

3.6. Radioactive assays 65

3.6.1. Internalization assay with ^{125}I-EGF and ^{125}I-Tf 65

3.7. Measurements of intracellular Ca^{2+} concentration 66

3.7.1. Aequorin 66

3.7.2. GCaMP 67

3.8. Immunofluorescence assays 67

3.8.1. EGF and Tf internalization assays 68

3.8.2. In vivo CD147 internalization assay 68

3.9. Super-resolution microscopy 69

3.10. Immunoelectron Microscopy 70

3.10.1. Preparation of PM sheets and gold labeling 71

3.11. Matrigel MCF10A morphogenetic assay 72

3.12. Intestinal and mammary primary organoids from mice 72

3.13. Statistical analysis 74

4. RESULTS 75

4.1. Signaling emanating from the EGFR that influences EGFR-NCE 75

4.1.1. Specific role of PLCγ2 enzyme in NCE 75

4.1.1.1. PLCγ enzymes are phosphorylated only upon stimulation with high dose EGF 75

4.1.1.2. PLCγ2 but not PLCγ1 is critical for EGF-induced Ca^{2+} release 77

4.1.1.3. PLCγ2 but not PLCγ1 is critical for internalization of the EGFR by NCE 79

4.1.1.4. PLCγ2 is required for the fission of NCE tubular invaginations 83

4.1.2. What is the basis of PLCγ2 specificity? 85

4.1.2.1. Generation of stable HeLa cell lines expressing HA-tagged PLCγ1 or PLCγ2 85

4.1.2.2. PLCγ1 vs. PLCγ2 specific modifications - phosphorylation 88

4.1.2.3. PLCγ1 vs. PLCγ2 specific modifications – ubiquitination and binding to Ub 89

4.1.2.4. PLCγ1 vs. PLCγ2 co-clustering with different endocytosis players at the PM 92
4.1.2.5. PLCγ1 vs. PLCγ2 specific recruitment in different compartments-microdomains 97
4.1.3. Second-messenger signaling: IP3, DAG and Ca^{2+} production 100
4.1.3.1. Role of DAG kinase in NCE 100
4.1.3.2. The role of calcineurin in EGFR-NCE 103
4.2.1. EGFR signaling upon stimulation with different ligands 105
4.2.1.1. TGF-α is a weak inducer of CD147 internalization 108
4.2.1.2. TGF-α induces a weaker Ca^{2+} response that is delayed and time-restricted compared with the EGF and AREG responses 110
4.2.2. How do EGF and TGF-α induce differential NCE activation? 112
4.2.2.1. EGFR ubiquitination upon stimulation with EGF or TGF-α 112
4.2.2.2. PLCγ2 differential activation upon stimulation with EGF and TGF-α 113
4.2.2.3. EGF and TGF-α different EGFR clustering 116
4.2.3. NCE activation upon stimulation with different RTKs 118
4.3. The physiological role of EGFR-NCE 120
4.3.1. Role of NCE in cell metabolism 120
4.3.2. EGFR endocytosis in MCF10A cells and spheroids 124
4.3.3. Role of NCE in mouse intestinal and mammary organoids 127
5. DISCUSSION 129
5.1. Signaling deriving from the EGFR that regulates EGFR-NCE and Ca^{2+}release 129
5.1.1. PLCγ isozymes and their post-translational modifications 132
5.1.2. Distinct subcellular distribution of PLCγ1 and PLCγ2 134
5.1.2.1. PLCγ1 vs. PLCγ2 specific co-clustering with different endocytosis players at the PM 134
5.1.2.2. PLCγ1 vs. PLCγ2 recruitment to different PM compartments/ microdomains 135
5.1.3. PLCγ1 vs. PLCγ2 specific interactors 137
5.1.4. PLCγ2 in signaling and cell responses 138
5.1.5. The role of Ca^{2+} and other secondary messengers 140
5.2. NCE activation by other EGFR ligands and RTKs 141
5.2.1. Future plans 144
5.3. The physiological role of EGFR-NCE 144
5.3.1. NCE role in cell metabolism 145
5.3.2. NCE role in epithelial cell physiology 146
5.3.3. Future plans 147
5.4. Conclusion 148
6. APPENDIX 149

7. REFERENCES 154

ACKNOWLEDGMENTS.....174

LIST OF ABBREVIATIONS

AP2	adaptor protein 2
AREG	amphiregulin
ARF1	adenosine diphosphate-ribosylation factor 1
ARF6	adenosine diphosphate-ribosylation factor 6
ARH	autosomal recessive hypercholesterolemia
Arp 2/3	actin-related protein-2/3
AUC	area under the curve
BAR	bin/amphiphysin/rvs
BCR	B cell receptors
BTC	betacellulin
BTK	Bruton's tyrosine kinase
Cbl	Casitas B-lineage Lymphoma
CCP	clathrin-coated pit
CCV	clathrin-coated vesicle
Cdc42	cell division control protein 42
CIE	clathrin-independent endocytosis
CK	cytokeratin
CLIC	clathrin-independent carrier
CME	clathrin-mediated endocytosis
CTxB	cholera toxin B subunit
DAB2	disabled homolog 2
DAG	diacylglycerol
DGK	diacylglycerol kinase
dSTORM	Direct stochastic optical reconstruction microscopy
ECM	extracellular matrix
EGFR	epidermal growth factor receptor
EHD2	Eps15 homology domain-containing 2
EM	electron microscopy

EPG	epigen
EPR	epiregulin
Eps15	epidermal growth factor receptor pathway substrate 15
ER	endoplasmic reticulum
ERK1/2	extracellular signal-regulated kinase 1/2
EV	empty vector
FAK	focal adhesion kinase
FEME	fast endophilin-mediated endocytosis
Gab1	Grb2-associated-binding protein 1
Gal-3	galectin-3
GEEC	GPI-AP-enriched endocytic compartment
GEF	guanine nucleotide exchange factor
GLUT1	glucose transporter 1
GPCR	G protein-coupled receptor
GPI-AP	glycosylphosphatidylinositol-anchored protein
Grb2	growth factor receptor-bound protein 2
GST	glutathione S-transferase
GTP	guanosine triphosphate
HA	hemagglutinin
HB-EGF	heparin-binding EGF-like growth factor
HGF	hepatocyte growth factor
HGFR	hepatocyte growth factor receptor
IF	immunofluorescence
IL2R	interleukin-2 receptor
IP	immunoprecipitation
IP3	inositol trisphosphate
IP3R	inositol trisphosphate receptor
JM	juxtamembrane
KD	knockdown
LDLR	low-density lipoprotein receptor
LGR5	leucine-rich repeat-containing G-protein coupled receptor 5

MAPK	mitogen-activated protein kinase
MCT	monocarboxylate transporter
MEGM	mammary epithelial cell growth medium
MEM	minimum essential medium
MHC	major histocompatibility complex
MMP	matrix metalloprotease
MVB	multivesicular body
NCE	non-clathrin endocytosis
NFAT	nuclear factor of activated T-cells
NSCLC	non-small-cell lung carcinoma
NWASP	neural Wiskott-Aldrich syndrome protein
PA	phosphatidic acid
PH	pleckstrin homology
PI3K	Phosphoinositide 3-kinase
PIP2	phosphatidylinositol 4,5-bisphosphate
PIP3	Phosphatidylinositol 3,4,5-trisphosphate
PIP5K	phosphatidylinositol 4-phosphate-5-kinase
PKC	protein kinase C
PLCγ	phospholipase Cγ
PLD	phospholipase D
PM	plasma membrane
pY	phosphotyrosine
Rac1	Rac family small GTPase 1
Raf	rapidly accelerated fibrosarcoma
Ras	retrovirus associated sequence
RhoA	ras homolog family member A
RNAi	RNA interference
ROCK	rho-associated protein kinase
RPE	retinal pigment epithelium
RT	room temperature
RTK	receptor tyrosine kinase

RTN3	reticulon-3
SARA	smad anchor for receptor activation
SH2	src Homology 2
SH3	src Homology 3
SHC	src homology 2 domain-containing
SILAC	stable isotope labeling by/with amino acids in cell culture
siRNA	small interfering ribonucleic acid
SORLA	sortilin-related receptor with A-type repeats
SOS1	son of sevenless homolog 1
sPH	split PH
STAT	signal transducer and activator of transcription
STEM	scanning transmission electron microscopy
SUP	supernatant
TBS-T	tris buffered saline-Tween
TCR	T-cell receptor
Tf	transferrin
TfR	trransferrin receptor
TGF-α	transforming growth factor-α
TGFβR	transforming growth factor-β receptor
Thr	threshold
TI	tubular invagination
TIM	triosephosphate isomerase
TK	tyrosine kinase
TLR4	Toll-like receptor 4
TM	transmembrane
Ub	ubiquitin
WB	western blot
γSA	γ-specific array

FIGURES AND TABLES INDEX

Figure 1. Depiction of the main endocytic pathways. 18
Figure 2. The formation of CCV. 22
Figure 3. Distinct clathrin-mediated endocytic pathways 23
Figure 4. Formation and dynamics of caveolae. 26
Figure 5. Different CIEs mechanisms 29
Figure 6. Role of endocytosis in controlling signaling pathways. 33
Figure 7. EGFR domains and dimerization. 36
Figure 8. Schematic of the binding of different EGFR ligands to ErbB receptors. 38
Figure 9. EGFR endocytosis: integration of the CME and NCE pathways. 41
Figure 10. RTN3 is critical regulator of EGFR-NCE. 43
Figure 11. CD147 is specific cargo of NCE pathway. 45
Figure 12. Mechanism of non-clathrin endocytosis of EGFR. 46
Figure 13. RTN3 is required for the formation of TIs and ER-PM contact sites. 47
Figure 14. Ca^{2+}response and dynamin are necessary for the fission of TIs. 48
Figure 15. EGFR signaling pathways. 50
Figure 16. PLCγ structure and activation. 53
Figure 17. PLCγ1 and PLCγ2 are activated only upon stimulation with high dose of EGF. 76
Figure 18. PLCγ2 KD inhibits EGF-induced calcium signaling at the PM. 78
Figure 19. PLCγ2 KD selectively inhibits EGF internalization after stimulation of cells with high, but not low, EGF concentrations. 80
Figure 20. PLCγ2 KD and inhibition of IP3R inhibit EGF-induced CD147 internalization. 82
Figure 21. PLCγ2 is required for NCE-TI fission. 84
Figure 22. Characterization of HeLa cell lines expressing HA-tagged PLCγ enzymes. 86
Figure 23. PLCγ recruitment to PM upon EGF stimulation. 87
Figure 24. PLCγ phosphorylation upon inhibition of CME or NCE 89
Figure 25. PLCγ1-HA and PLCγ2-HA are not able to bind to Ub and they are not ubiquitinated upon stimulation with EGF 91
Figure 26. PLCγ1/2-HA and EGFR co-clustering upon EGF stimulation 94
Figure 27. PLCγ2 but not PLCγ1 specifically co-clusters with RTN3 in the vicinity of the PM in the presence of high EGF. 96
Figure 28. PLCγ2 redistributes to osmiophilic patches in HeLa cells stimulated with EGF. 98
Figure 29. PLCγ2 is enriched in raft fractions upon EGF stimulation. 100
Figure 30. DGK inhibitor decreases CD147 internalization. 102
Figure 31. Calcineurin inhibitors decrease CD147 and EGF internalization 104

Figure 32. Comparison of the activation of EGFR and downstream signaling effectors by EGF and TGF-α. 106
Figure 33. Comparison of the activation of EGFR and downstream signaling effectors by EGF and AREG. 107
Figure 34. CD147 internalization upon stimulation with different EGFR ligands. 109
Figure 35. Induction of Ca^{2+} oscillatory waves at the PM inner leaflet by different EGFR ligands. 111
Figure 36. Phosphorylation and ubiquitination of EGFR upon stimulation with high affinity ligands EGF and TGF-α. 112
Figure 37. PLCγ2 is less phosphorylated upon TGF-α stimulation as compared to EGF. 114
Figure 38. Activation of EGFR and downstream signaling effectors by EGF vs. TGF-α at different time points. 115
Figure 39. EGFR clustering upon 1 min stimulation with high dose EGF and TGF-α. 117
Figure 40. CD147 internalization upon stimulation of HeLa cells with HGF 119
Figure 41. Colocalization of MCT1with CD147 and EGF. 121
Figure 42. Colocalization of GLUT1 with CD147 and EGF. 123
Figure 43. Presence of EGFR/CD147-NCE in MCF10A cells. 125
Figure 44. Relevance of EGFR/CD147-NCE in MCF10A spheroids. 126
Figure 45. Effects of EGFR-NCE inhibitors on the growth of mammary and intestinal primary organoids. 128
Figure 46. PLCγ2 activation upon high dose EGF stimulation. 130
Figure 47. PLCγ domains and interactors 137

Appendix Figure S1. Expression of PLCγ1 and PLCγ2 in different cell lines 149
Appendix Figure S2. No differences in the co-clustering of PLCγ1 vs. PLCγ2 with CTxB upon EGF stimulation. 150
Appendix Figure S3. Rac1 KD decreased internalization of EGF and CD147 151
Appendix Figure S4. IF staining of intestinal and mammary organoids. 153

Table 1. Molecular features of the different endocytic pathways 18
Table 2. Summary of molecular characteristics of EGFR ligands 37
Table 3. Cell lines characterized for EGFR-NCE activation 49
Table 4. List of RNAi oligo sequences 59
Table 5. List of antibodies 60

ABSTRACT

The epidermal growth factor receptor (EGFR) plays a pivotal role in physiological cellular processes, but its aberrant activation is linked to cancer progression. Endocytosis is a critical regulator of EGFR activity. We have previously identified a novel endocytic route of the EGFR, non-clathrin endocytosis (NCE), which is activated only after stimulation with high doses of the ligand epidermal growth factor (EGF). Unlike canonical clathrin-mediated endocytosis (CME) that directs receptor mainly to recycling, NCE leads mostly to receptor degradation, restricting EGFR signaling and protecting cells from overstimulation.

The molecular characterization of the NCE pathway, led to the identification of a key functional regulator of NCE: the endoplasmic reticulum (ER)-shaping protein, reticulon-3 (RTN3). This regulator is necessary for the formation of contact sites between the plasma membrane (PM) and the ER during NCE internalization. Localized Ca^{2+} release at these contact sites induces the fission of NCE vesicles, completing the internalization process. In addition, CD147, a member of the immunoglobulin superfamily, was identified as a cargo co-internalizing with the EGFR in NCE vesicles. CD147 has been validated as a specific marker of NCE, and together with RTN3, represents an invaluable experimental tool for investigating this pathway.

In the present work, we have dissected the signaling pathway promoting Ca^{2+} release from the ER upon EGFR-NCE activation, uncovering a specific role of the phospholipase C γ2 (PLCγ2) enzyme. PLCγ2-dependent Ca^{2+} release at NCE sites occurs through the activation of the inositol trisphosphate receptor (IP3R) on the ER membrane and is required for the fission of EGFR/CD147-positive NCE vesicles from the PM.

At the functional level, we extended the relevance of NCE to alternative EGFR ligands, beyond the EGF. Saturating doses of the two EGFR ligands, amphiregulin (AREG) and transforming growth factor-α (TGF-α), differentially triggered EGFR/CD147 internalization via NCE: while AREG efficiently activated NCE and Ca^{2+} release at the PM, TGF-α was less effective at triggering this pathway. This finding led us to hypothesize that the differential ability of alternative EGFR ligands to activate NCE could be responsible for the differences in the EGFR fate and biological output exerted by these ligands. Interestingly, stimulation of cells with another growth factor, hepatocyte growth factor (HGF), induced CD147-NCE similarly to stimulation with EGF, implying a broader role of NCE in the regulation of surface proteins.

As a model system to test the physiological relevance of NCE, we are using organoids prepared from the non-transformed breast epithelial cell line MCF10A and from primary mouse intestinal crypt and mammary gland epithelial cells. These cells are dependent on EGFR signaling for their growth and differentiation in Matrigel. Our data showed that treatment with compounds that inhibit EGFR-NCE increase growth of mice intestinal and mammary organoids.

In conclusion, we have molecularly dissected the signaling pathway leading to EGFR-NCE and expanded its relevance to alternative EGFR ligands and other growth factors. Given its crucial role in downregulating signaling and mediating growth restriction, NCE could behave as a possible tumor suppressor pathway and its regulators could represent novel targets in cancer therapy.

1. INTRODUCTION

1.1. Endocytosis

Endocytosis is a dynamic cellular process by which cells internalize extracellular material together with surface proteins and the cell membrane. This process is mediated by the inward budding of the plasma membrane (PM) that creates invaginations that need to be pinched from PM to generate vesicles that can travel through the endosomal vesicular compartments to reach their final destination. Endocytosis plays an important role in the regulation of proliferation, cell survival, neurotransmission, embryogenesis, and cell fate determination [1, 2].

Due to the variety of cargos that are internalized by endocytosis, there are many different endocytic pathways, each with their own molecular machinery (e.g., coating, adaptor, cytoskeleton, and energy proteins), which destine their cargo to different intracellular compartments. These pathways can be either constitutive or regulated by specific signals, and are also selectively activated in specific cellular contexts.

Endocytosis is divided into different mechanisms (**Figure 1** and **Table 1**) [3-5]. Firstly, phagocytosis and macropinocytosis are processes that are mainly dependent on the remodeling of the actin cytoskeleton, and which internalize large particles >500 nm (phagocytosis) or fluids (macropinocytosis) [6, 7]. The size of the vesicles formed by these two mechanisms is much larger than the other endocytic pathways, known collectively as micropinocytosis. Micropinocytosis can be divided into several pathways based on the protein machinery that is required for the particular pathway. A major distinguishing component of these pathways is clathrin allowing the division into clathrin-dependent and -independent pathways. Within the clathrin-independent classification several pathways have been identified, such as caveolin-dependent endocytosis, flotillin-mediated endocytosis, CLIC/GEEC [clathrin-independent carrier (CLIC)/glycosylphosphatidylinositol-anchored protein (GPI-AP)-enriched endocytic compartment (GEEC)], fast endophilin-mediated endocytosis (FEME) and epidermal growth factor receptor non-clathrin endocytosis (EGFR-NCE*)* (see detailed descriptions below) [3, 8].

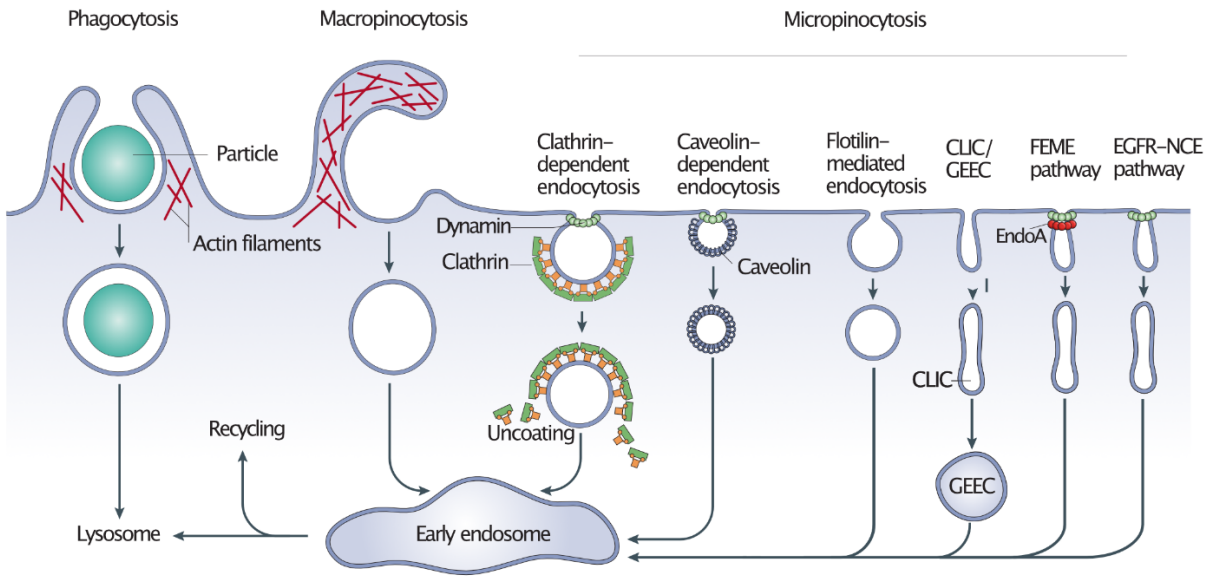

Figure 1. Depiction of the main endocytic pathways.

Phagocytosis and macropinocytosis are pathways for internalization of large particles or fluids, respectively. Micropinocytosis includes smaller invaginations (<200nm), generally divided into clathrin-dependent and -independent endocytosis. Clathrin-independent endocytosis can be further divided based on dependency on other proteins. The best-known pathways are illustrated including, caveolin-dependent endocytosis, flotillin-mediated endocytosis, CLIC/GEEC (clathrin-independent carrier/GPI-AP-enriched endocytic compartment) endocytosis, FEME (fast endophilin–mediated endocytosis) and EGFR-NCE (epidermal growth factor receptor non-clathrin endocytosis). EndoA, endofilin A. Adapted from Mayor, Nat Rev Mol Cell Biol, 2007 [8]

Table 1. Molecular features of the different endocytic pathways

	Coat	Fission machinery	Regulatory/ associated proteins	Cytoskeleton	Cargo
Phagocytosis	-	Dynamin	ARF6, Cdc42, Rac1, RhoA (depending on type), amphiphysin, adhesion proteins	Actin, microtubule, myosin	Pathogens, apoptotic remnants
Macropinocytosis	-	CtBP1, actin polymerisation	PAK1, PI3K, Ras, Src, HDAC6, ARF6,	Actin, microtubule, myosin	Fluid phase markers, RTKs

			Cdc42, Rac1, Rab5, Arp2/3		
CME	Clathrin	Dynamin, actin, Arp2/3, NWASP, cortactin, HIP/HIP1R, amphyphysin, endophilin, myosin VI, synaptojanin, auxilin, HSC70	Clathrin, AP2, SNX9, synaptojanin, amphiphysin, Rab5, ARF6, FCHO1/2, Eps15/L1, epsin 1, DAB2, ARH, AP180/CALM, NUMB, stonin, β-arrestins, intersectins, endophilin	Actin, microtubule	RTKs, GPCRs, TfR, LDLR, integrins
Caveolae	Caveolins and cavins	Dynamin	PTRF, Src, SDPR, SRBC, EHD2, pacsin, syndapins, FBP17	Actin, microtubules	CTxB, SV40, GPI-linked proteins, integrins
Flotillin	Flotillin 1 and 2	-	Fyn kinase	unclear	CTxB, CD59, TfR, E-cadherin, cationic molecules and polyplexes, proteoglycans and proteoglycan-bound ligands
CLIC/GEEC	-	Actin (Arp2/3), endophilin A2/3, dynein	Cdc42, ARF1, ARF6, GRAF1/2, Arp2/3, GBF1, PICK1, IRSp53, PI3K, endophilin A2/3	Actin	Fluid phase markers, CTxB, GPI-linked proteins, MHC class I proteins, CD59, CD98, CD44, carboxypeptidase E, myoferlin, dysferlin, shiga-toxin, CD166/ ALCAM, β_1 integrins

FEME	-	Dynamin, actin, dynein, endophilin A2, Bin1	RhoA, Rac1, PAK1/2, endophilin A2, NWASP, Arp2/3, PI3K, Dynein	-	RTKs, GPCRs, CD36, VGLUT1, AMPAR, plexin A1, ROBO1
IL2R	-	Dynamin, endophilin, actin (Arp2/3, N-WASP, cortactin)	RhoA, Rac1, PAK1, PAK2, NWASP, endophilin, PI3K	Actin	IL2R, IgE receptor, γc-cytokine receptor
EGFR-NCE	-	Dynamin	RTN3, Eps15/L1, epsin 1	-	EGFR, CD147

The table summarizes internalization pathways described in the literature. The presence or not of a coat, the fission machinery, known regulatory/associated proteins and the type of internalized cargo are showed for each internalization pathway. ARF6, Adenosine diphosphate-ribosylation factor 6; Cdc42, cell division control protein 42; Rac1, Rac family small GTPase 1; RhoA, Retrovirus associated sequence (Ras) homolog family member A; CtBP1, C-terminal binding protein 1; PAK1/2, P21-activated kinase 1/2; PI3K, Phosphoinositide 3-kinase; HDAC6, Histone deacetylase 6; Rab5, Ras- related protein in brain 5; Arp2/3, Actin-related proteins-2/3; RTK, Receptor tyrosine kinase; NWASP, Neural Wiskott-Aldrich syndrome protein; HIP1R, Huntingtin interacting protein (HIP) 1 related; HSC70, Heat shock protein 70; AP2, Adaptor protein 2; SNX9, Sorting nexin 9; FCHO1/2, Fer/Cip4 homology domain only protein 1 and 2; Eps15, Epidermal growth factor receptor pathway substrate 15; Eps15L1, Epidermal growth factor receptor pathway substrate 15 like 1; DAB2, disabled homolog 2; ARH, autosomal recessive hypercholesterolemia; CALM, Calmodulin; GPCRs, G protein-coupled receptors; TfR, Transferrin receptor; LDLR, Low-density lipoprotein receptor; PTRF, polymerase I and transcript release factor; SDPR, serum deprivation response; SRBC, SDR-related gene product that binds to c-kinase; EHD2, Eps15 homology domain-containing 2; FBP17, formin binding protein 17; CTxB, cholera toxin B; SV40, simian virus 40; GPI, glycosylphosphatidylinositol;ARF1, Adenosine diphosphate-ribosylation factor 1; GRAF-1/2, GTPase regulator associated with focal adhesion kinase-1/2; GBF1, guanine nucleotide exchange factor 1; PICK1, protein interacting with C Kinase 1; IRSp53, insulin receptor

tyrosine kinase substrate p58/53; MHC, major histocompatibility complex; ALCAM, activated leukocyte cell adhesion molecule; Bin1, bridging integrator-1; VGLUT1, vesicular glutamate transporter 1; AMPAR, a-amino-3-hydroxy-5-methyl-4-isoxazolepropionic acid receptor; ROBO1, roundabout guidance receptor 1; IL2R, interleukin-2 receptor; IgE, Immunoglobulin E; RTN3, Reticulon 3; EGFR, epidermal growth factor receptor;

1.1.1. Clathrin-dependent endocytosis

Clathrin-dependent endocytosis or clathrin-mediated endocytosis (CME), as it is also referred to, is the best characterised mechanism of protein internalisation [9]. It is active in all cellular contexts although with some differences in terms of morphology and kinetics [10, 11]. The process begins with the recognition of sorting signals in the cytoplasmic tail of the cargo by adaptor proteins [i.e., adaptor protein 2 (AP2)] (**Figure 2**, step 1). The binding of the AP2 to the cargo triggers the recruitment of clathrin and other accessory proteins, during growth phase. Clathrin is a heterohexamer protein composed of three heavy and three light chains that form a three-legged structure – a triskelion. This induces polymerisation of clathrin into a lattice that leads to membrane bending and the formation of a clathrin-coated pit (CCP) (**Figure 2**, step 2) [12]. Accessory proteins [e.g., epidermal growth factor receptor pathway substrate 15 (Eps15), epsins, disabled homolog 2 (DAB2), the autosomal recessive hypercholesterolemia (ARH)] are temporarily recruited to the CCP, helping the assembly and growth of the clathrin lattice. Dynamin, a dimeric GTPase, assembles into a helix [13] around the neck of the invaginating pit, inducing constriction and eventually fission of the membrane at the neck in a manner dependent on guanosine triphosphate (GTP) hydrolysis (**Figure 2**, step 3). This leads to the formation of a free clathrin-coated vesicle (CCV) [14], and several accessory proteins participate in this process such as amphiphysin, synaptojanin and endophilin [15, 16]. After formation of the CCV, the disassembly of the clathrin coat takes place, leaving an uncoated vesicle free to fuse with an early endosome (**Figure 2**, step 4) [17]. From early endosome cargoes are either recycled back to the PM or destined for degradation and sorted to cisternal parts of early endosomes [18]. Proteins destinated for late endosomes and lysosomes, are sorted into intralumenal vesicles that detach from endosomes, leading to appearance of multivesicular endosomes or multivesicular bodies (MVBs) [19]. Finally fusion of MVBs with lysosomes results in degradation of cargo [19].

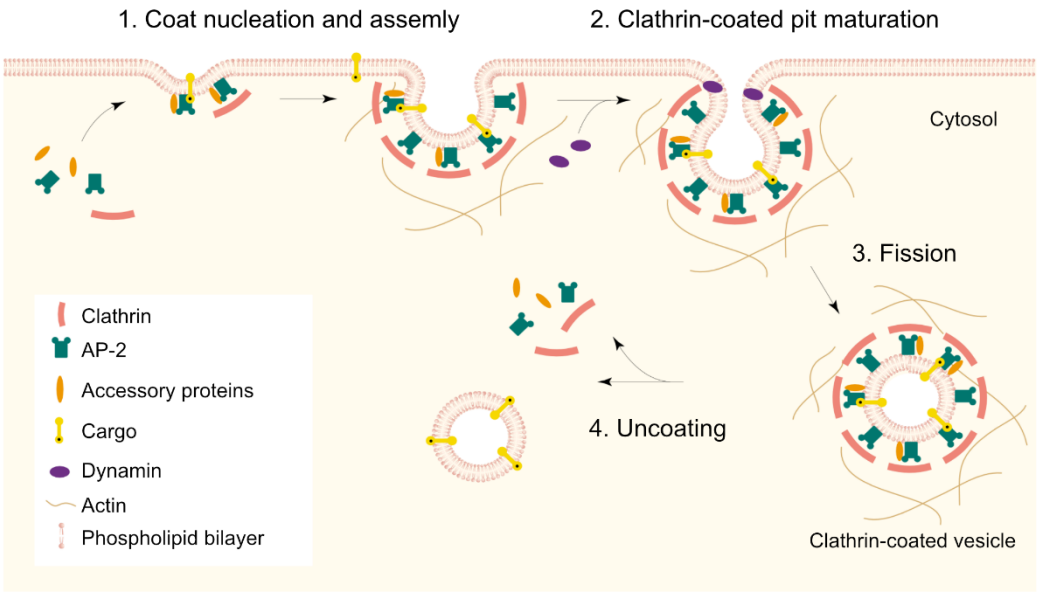

Figure 2. The formation of CCV.

Different steps involved in CME include: 1. nucleation of AP2 and adaptor proteins at the PM, and recruitment of clathrin during the growth phase; 2. maturation of CCP, stabilized by actin filaments, and finally 3. fission from the PM by the action of dynamin and formation of CCV*, followed by 4. disassembly of the clathrin coat. Adapted from Takei, Trends Cell Biol, 2001 [20]*

The best characterized cargoes endocytosed by CME (**Table 1**) are low-density lipoprotein receptor (LDLR) [21], receptor tyrosine kinases (RTKs) such as epidermal growth factor (EGF) receptor (EGFR)) [22], G protein-coupled receptors (GPCRs) and transferrin (Tf) receptor (TfR) [23], that is often used as marker of CME.

Recently, evidences are suggesting existence of distinct CME pathways that include different regulators and differentially control fate and signaling of receptors (**Figure 3**) [2]. Endocytosis of TfR depends on AP2 adaptor, and leads to recycling of Tf-TfR (**Figure 3A**) [23]. On the other side, internalization of LDLR, in addition to AP2, requires specific adaptors ARH and DAB2, and this process leads to degradation of the ligand, but recycling of empty receptor (**Figure 3B**) [24].

GPCRs-CME requires specific regulator β-arrestin and ubiquitination of receptors (**Figure 3C**). Upon binding to their ligand, GPCRs activate associated G protein and induce canonical G-protein signaling. Activated receptor is phosphorylated by G protein-coupled receptor kinase (GRK) and this leads to binding of β-arrestins, further resulting in endocytosis

of receptor and its desensitization [25]. However, depending on the type of GPCRs, β-arrestin can also trigger kinase specific non-canonical signaling pathways [26].

Even though AP2 was considered as a basic component of CCPs, some CME pathways were shown to be AP2-independent (**Figure 3D**). For instance, the EGFR can be internalized via different CMEs, depending on cell context: AP2-dependent pathway, leading to receptor recycling and consequent sustained signaling and AP2-independent pathway, leading to lysosomal degradation of receptor.

Final step of internalization, displayed as a fission of CCPs, can be done by different dynamin isoforms. While dynamin 2 is widely expressed and crucial for endocytosis in all the cells, dynamin 1 is mainly active in neurons, while it can be expressed in other cell types where it is negatively regulated by glycogen synthase kinase 3β (GSK3β)-dependent phosphorylation (**Figure 3E**). However, in cancer, this kinase can be inhibited, leading to dynamin 1 dephosphorylation and activation, finally resulting in aberrant endocytosis and signaling of cargoes (e.g., EGFR).

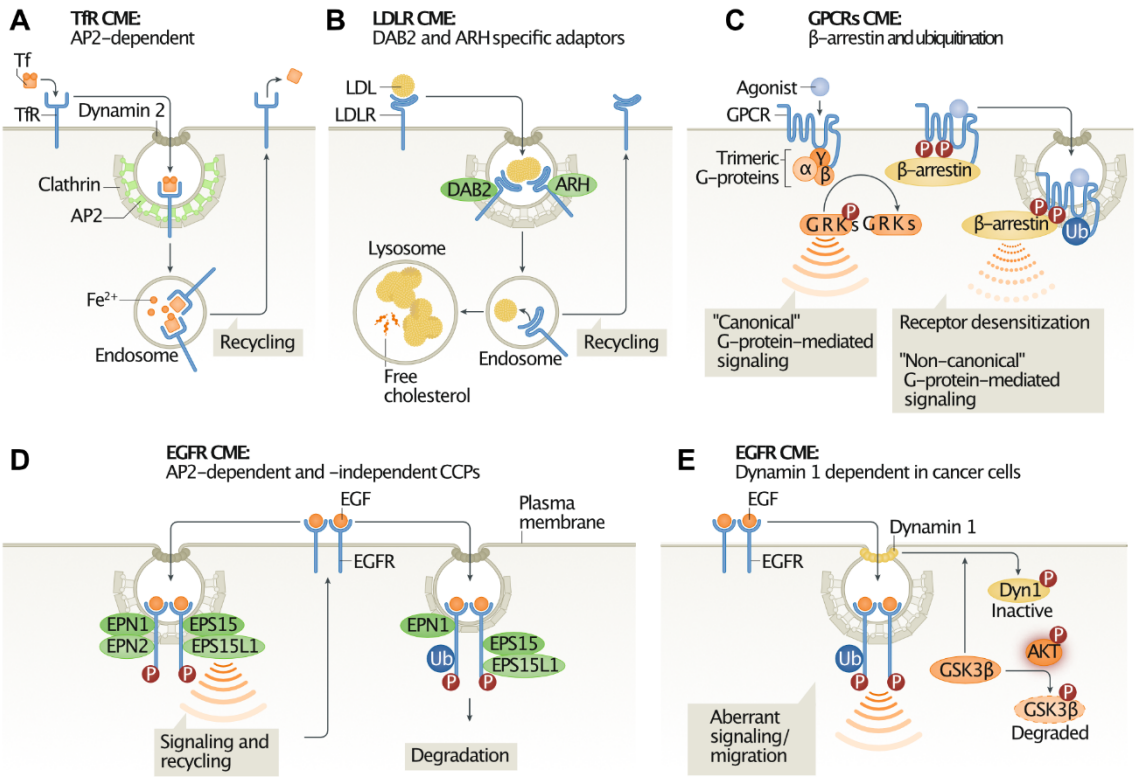

Figure 3. Distinct clathrin-mediated endocytic pathways

A. *Endocytosis of TfR is AP2 dependent and leads to recycling of receptor and ligand.* ***B.*** *LDLR internalization depends on specific adaptors DAB2 and ARH, resulting in degradation of ligand, but recycling of free receptor.* ***C.*** *Recruitment of GPCR to endocytic pathway by* β*-aresstin, induce receptor desensitization or "non-canonical" G-protein mediated signaling.* ***D.*** *EGFR can be internalized via AP2-dependent or AP2-independent pathways, that result in recycling and degradation, respectively.* ***E.*** *Degradation of* glycogen synthase kinase 3β (*GSK3β) by activation of AKT in cancer cells, leads to activation of dynamin 1 and aberrant endocytosis and signaling of EGFR. Adapted from Sigismund, Nat Rev Mol Cell Biol, 2021 [2]*

1.1.2. Clathrin-independent endocytosis

In contrast to the canonical CME pathway, clathrin-independent endocytosis (CIE) pathways are not fully defined, with information lacking on the sorting signals, adaptor proteins and the range of cargoes and their functions [4, 8]. The CIE mechanisms are highly heterogeneous and cell context-dependent, but can be broadly divided into dynamin-dependent and -independent endocytosis. They can be further categorized based on the presence or absence of a coat marking the internalized part of the PM or the involvement of small GTPases that regulate actin organization. Dynamin-dependent pathways include caveolar endocytosis, FEME and EGFR-NCE, while dynamin-independent endocytosis includes CLIC/GEEC and flotillin-mediated endocytosis [4]. These dynamin-independent endocytosis pathways are regulated by the GTPases: cell division control protein 42 (Cdc42) and adenosine diphosphate-ribosylation factor 6 (ARF6), or mediated with flotillin [8].

Nevertheless, the classification of CIE mechanisms is still under debate, and the current framework, while allowing a better organization and discussion of emerging data in this rapidly growing field, is still evolving. One of the main factors distinguishing the different mechanisms is the location of the cargo molecules in specific microdomains of the PM, i.e., lipid rafts. Initially, it was assumed that molecules located in these lipid rafts were endocytosed exclusively by CIE, however some cargoes in lipid rafts have since been shown to be endocytosed by CME [27, 28]. This finding again demonstrates the high complexity and fluid crosstalk between the different endocytic pathways.

1.1.2.1. Caveolar endocytosis. Caveolae are flask-shaped PM invaginations generally associated with CIE. They are present on all cell types but are particularly abundant in adipocytes, skeletal muscle and endothelial cells [29]. Caveolins and cavins are membrane-associated proteins that play a fundamental role in structure of caveolae [30]. Caveolin is a dimeric palmitoylated, integral membrane protein that binds cholesterol, with both the N- and the C-terminal domains localized in the cytosol, forming a hairpin-like structure inserted into the inner layer of the PM. There are three types of caveolin: caveolin-1 and caveolin-2 have broad tissue-specificity and are typically co-expressed, whereas caveolin-3 is predominantly expressed in striated muscle. Caveolin-1 and -3 are necessary and sufficient for caveolae formation, while caveolin-2 is dispensable. Caveolins are responsible for the formation of elongated and shallow invaginations and togheter wih cavins are forming coat around the bulb of caveolae (**Figure 4A**) [31]. Accessory proteins involved in caveolae formation include Eps15 homology domain-containing 2 (EHD2), pacsin/syndapins, and the Bin/Amphiphysin/Rvs (BAR) protein, formin binding protein 17 (FBP17) (**Table 1**). The actin cytoskeleton plays an important role in caveolar internalization, as its disruption results in clustering of caveolae and inhibition of their internalization [32, 33]. Fission of caveolae from PM is driven by dynamin [34]. After budding, caveolae can follow different routes. They can fuse with the early endosomes, maturate into late endosome, that fuses with or mature into lysosomes, leading to final degradation of their content. On the other side, caveolae can traffic to ER and lipid droplets, or they can return to the PM. Pathogens, such as cholera toxin B subunit (CTxB) [35] and simian virus 40 [36], were generally considered as cargoes of this pathway. However, their internalization is not exclusively driven by caveolae and potentially they can enter the cell by other endocytic mechanisms depending on the cell type, cell adherence, and the intensity of aggregation of surface molecules [37].

Caveolae are highly dynamic membrane domains, able to move laterally in the PM. They are rich in sphingolipids, cholesterol, signaling proteins and GPI-APs, similar to lipid rafts [38]. However, they can be distinguished from lipid rafts by the presence of caveolin-1/3. Also, it is been shown that EGFR is present in lipid rafts but not in caveolae [39, 40].

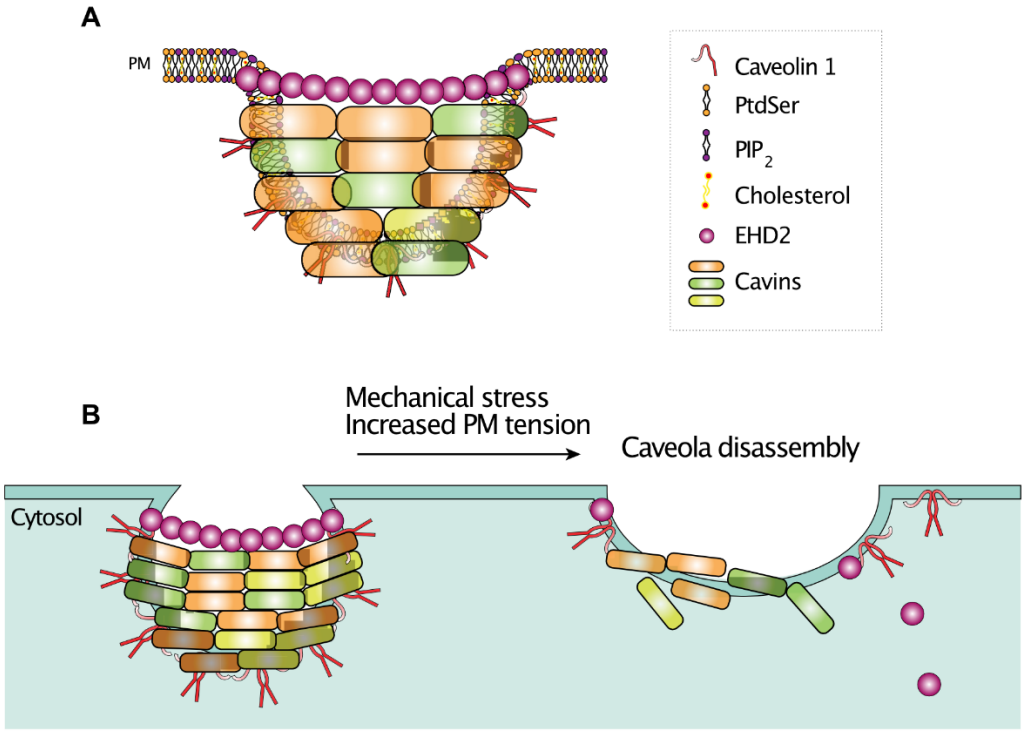

Figure 4. Formation and dynamics of caveolae.

A. *Formation of caveolae starts by caveolin insertion in cholesterol rich-PM domains, and recruitment of cavin coat proteins and accessory proteins such as EHD2. PtdSer, Phosphatidylserine. PIP2, phosphatidylinositol 4,5-bisphosphate.* ***B.*** *Mechanical stress that induces increased PM tension results in flattening of caveolae and release of cavins and EHD2, while caveolin is redistributed into the bulk PM. Adapted from Parton, Curr Opin Cell Biol, 2020 [29]*

Caveolae have a mechanoprotective role in buffering PM tension, consistent with their abundance on muscle, endothelial and adipocytes cells, which are subjected to mechanical stress at PM [41, 42]. Upon exposure of the PM to mechanical stress, e.g., during osmotic swelling and migration, caveolae numbers are reduced since they are flattened (**Figure 4B**) allowing a cell to stretch and change a shape. In contrast, low PM tension increases clustering of caveolae and possibly their internalization. Moreover, caveolae formed due to low PM tension at the rear of migrating cells are crucial for cell motility, since they are recruiting the RhoA [retrovirus associated sequence (Ras) homolog family member A] exchange factor and actomyosin machinery, required for retraction and forward migration [43].

In recent years there has been some controversy over the role and existence of caveolar endocytosis [31]. Due to lack of cargoes that are internalized specifically via this pathway [42], important question of caveolae has been raised: is it about internalizing cargoes or protecting the PM with no specificity of the proteins that are being internalized? The emerging viewpoint is that the principal role of caveolae budding is in regulating density of surface caveolae, rather than internalization and trafficking of specific cargoes.

1.1.2.2. Flotillin. Flotillin 1 and flotillin 2 are proteins with a caveolin 1-like topology, which form invaginations that are similar to caveolae but slightly larger [44]. Flotillins are found mainly in PM lipid rafts, providing a signaling platform, while they can also localize in intracellular organelles such as Golgi, endosomes, lysosomes and exosomes. The molecular mechanism of endocytosis by flotillins is not completely clear, but it was shown to be dependent on the Src family kinase Fyn (**Table 1**)[45]. Although it was first shown that flotillin-mediated endocytosis does not require dynamin [46], recently it has been described that growth factor stimulation induces flotillin-mediated endocytosis in dynamin-dependent manner [47].

Flotillin-mediated endocytosis contributes to the internalization of cargoes such as the GPI-anchored protein CD59, CTxB, cationic molecules and polyplexes, proteoglycans and proteoglycan-bound ligands (**Table 1**) [44]. Recently, flotillins are showed to play role in generation and release of exosomes, but detailed mechanism is unknown. On the other side, some studies showed role of flotillins, in association with Ras-related protein Rab-11A (Rab11a)/Sorting Nexin 4 (SNX4), in recycling of TfR and E-cadherin in epithelial cells [48].

1.1.2.3. CLIC/GEEC. CLIC/GEEC endocytosis is mediated by large uncoated tubulovesicular invaginations called CLICs, which arise directly from the PM and later mature into tubular early endocytic compartments called GEECs [4]. This pathway involves clustering of glycosylated cargoes, via extracellular galectins, that can be considered as a sort of extracellular coat [49, 50]. Clusters are formed upon galectin-3 (Gal-3) recruitment to glycosylated cargo on the PM, where it oligomerizes with glycosphingolipid-bound Gal-3. These clusters induce mechanical stress on the membrane, leading to membrane bending and the formation of CLICs [4].

The main regulators of this pathway are the small GTPases – adenosine diphosphate-ribosylation factor 1 (ARF1) and Cdc42, which are necessary for the activation of the neural Wiskott-Aldrich syndrome protein (NWASP) and of actin-related protein-2/3 (Arp 2/3) (**Table**

1). Other proteins involved in the CLIC/GEEC machinery are BAR proteins [GTPase regulator associated with focal adhesion kinase-1 (GRAF1), Insulin receptor tyrosine kinase substrate 53 kDa (IRSp53), Protein Interacting with C Kinase – 1 (PICK1)] that can interact with Arp2/3. Finally, fission is executed by endophilin A2 [51] together with the pulling forces of the actin cytoskeleton and motor proteins. The resulting CLIC fuses with endosomal GEEC, generally leading to recycling of cargoes.

CLIC/GEEC is a high-capacity endocytic sorting system, particularly active in fibroblasts and kidney epithelial cells [2], and able to turn over the fibroblast PM in 12 min [52]. This mechanism mediates the endocytosis of GPI-AP, glycoproteins, such as CD44 and CD98, and toxins (Table 1) [4]. The CLIC mechanism can also regulate PM tension, but in contrast to caveolae, CLICs are formed at the leading edge of migrating cells [52, 53].

Some CLIC/GEEC pathways are regulated by ARF6 GTPase [54]. ARF6 GTPase was shown to act by activating Rac family small GTPase 1 (Rac1), phosphatidylinositol 4-phosphate-5-kinase (PIP5K) and phospholipase D (PLD), which play an important role in remodulating the actin cytoskeleton [55]. The products of PLD activation are phosphatidic acid (PA) and diacylglycerol (DAG), which induce membrane curvature, strongly affecting all endocytosis processes, especially recycling [56]. Once an ARF6-positive vesicle is formed, it can reattach to the cell membrane very quickly after internalization, thus enabling the recycling of endocytosed molecules. It is generally considered that the ARF6 GTPase has a more significant role in the recycling process than in the endocytic process itself [57]. Furthermore, it is known that ARF6 can influence the process of CME [58], but its role may depend on the cellular context. The ARF6 GTPase plays a role in the endocytosis of major histocompatibility complex (MHC) class I molecules, CD44, CD98 and CD147 (**Table 1**) [59]. However, depending on cellular context the listed molecules can be endocytosed by other endocytosis mechanism.

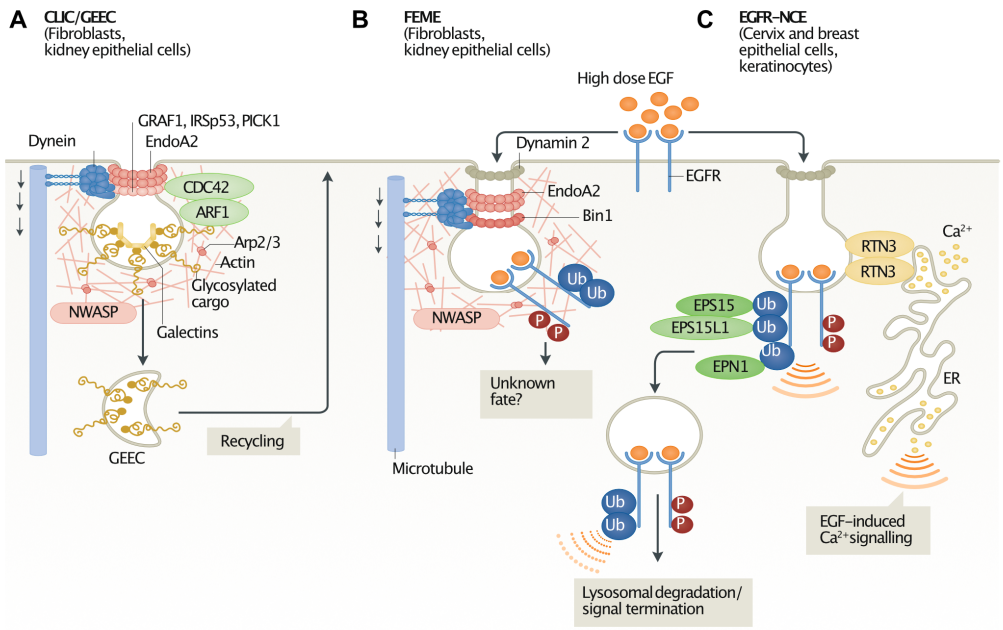

Figure 5. Different CIEs mechanisms.

A. *CLIC/GEEC depends on clustering of glycosylated cargoes, via extracellular galectins, that induce bending of membrane and small GTPases (ARF1, Cdc42), which activated NWASP and of Arp 2/3. BAR proteins (GRAF1, IRSp53, PICK1) that can interact with Arp2/3, at initial step of vesicle formation. Fission is done by endophilin A2 (EndoA2), with the pulling forces of the actin cytoskeleton and motor proteins (dynein). Internalized CLIC fuses with GEEC, leading to recycling of cargoes.* ***B.*** *FEME requires endophilin A2 for formation of vesicles, as well as actin polymerization, NWASP and BAR proteins (Bin1). Fission is done by dynamin 2, together with help of endophilin A2 and dynein. EGFR is internalized via this pathway upon stimulation with high doses of ligand.* ***C.*** *Upon stimulation with high doses of ligand, EGFR can also be internalized via EGFR-NCE requires contact sites between PM and ER, that depends on RTN3, ubiquitination of EGFR and ubiquitin (Ub) binding proteins (Eps15, Eps15L1 and EPN1, epsin1). Local* Ca^{2+} *release at these sites together with dynamin is necessary for the fission of these vesicles. EGFR-NCE targets receptor to lysosomal degradation and consequently signal termination. Adapted from Sigismund, Nat Rev Mol Cell Biol, 2021 [2]*

1.1.2.4. FEME. FEME is an extremely rapid endocytic mechanism similar to CLIC/GEEC that is mediated by tubulovesicular compartments (<1 μm), is dependent on endophilin A and is active in fibroblasts and kidney epithelial cells, like CLIC/GEEC [2]. Endophilin A recognizes cargoes through its Src homology 3 (SH3) domain, induces PM curvature with the aid of its

BAR domain (**Figure 5B**), and executes fission by the insertion of multiple amphipathic helices contained within its structure. The small GTPases that regulates this process (RhoA and Rac1) together with the adaptor NWASP, that promotes actin polymerization, are also necessary for FEME (**Table 1**) [60, 61]. Fission is mediated by dynamin, together with a help of dynein.

The formation of FEME endocytic carriers is induced upon ligand binding to specific receptors, such as GPCRs (α2a- and β1-adrenergic receptors), interleukin-2 receptor (IL2R), and RTKs (and including the EGFR) [51, 60]. At first IL2R endocytosis (Table 1) was described as separated pathway, however later was discovered that IL2R endocytosis is dependent on endophilin A2 and presents all the characteristics of FEME [60].

1.1.2.5. EGFR-non-clathrin endocytosis. Another CIE pathway is non-clathrin endocytosis of the EGFR (EGFR-NCE), which is induced upon stimulation of cells with high doses of EGF and leads to degradation of the receptor [62]. This mechanism is active in different cervical and breast epithelial cells and in keratinocytes [63]. EGFR-NCE relies on the formation interorganelle contact sites between the PM and the endoplasmic reticulum (ER) in a reticulon-3 (RTN3) dependent mechanism (**Figure 5C**) [63]. Ca^{2+} release from the inositol trisphosphate receptor (IP3R) on the ER and dynamin are required for the membrane fission step and completion of EGFR-NCE. The PM protein CD147 was identified as cargo, co-internalizing with EGFR through NCE [63]. This pathway will be described in detail in the **Section 1.2.2.2**.

At the molecular level, NCE differs from other CIE pathways described in the literature which display dependency on galectins, caveolins and endophilins [63]. In common with other pathways, however, it seems to require players such as dynamin, Eps15, Eps15L1, epsin1 (**Table 1**) [63].

1.1.3. Role of membrane microdomains - lipid rafts in endocytic pathways

The cell membrane has been described as a fluid mosaic membrane composed of a lipid bilayer randomly studded with floating proteins. According to the lipid composition, the membrane can be divided into organized microdomains (known as lipid rafts) or disorganized regions. Lipid rafts are heterogenous dynamic areas of membrane (typically 50-200 nm in diameter) with special physical characteristics that can vary depending on protein-protein and protein-lipid interactions. For example, rafts are constantly changing protein composition and sometimes size

when smaller rafts merge to form larger rafts. The lipid part of the rafts consists of cholesterol, ceramide, glycosphingolipids, sphingomyelin, and phospholipids with saturated acyl residues, which contrasts with the disorganized parts of the membrane that are made up mostly of phospholipids consisting of phosphoglycerolipids with polyunsaturated fatty acids [64-66]. The protein part consists of proteins that are either permanently located in them (e.g., flotillins, synaptophysin) or only occasionally located in them [e.g., CD44, MHC-II, T-cell receptor (TCR)] [67]. Some properties of proteins can increase their association with lipid rafts. For example, GPI-APs have a glycolipid anchor that allows their localization in rafts. Post-translation modifications of proteins (e.g., palmitoylation and myristoylation) and protein clustering can also increase the affinity of proteins to lipid rafts [68]. The latter can also stabilize rafts. In addition to the PM, lipid rafts are present also in early endosomes, recycling endosomes, and the trans-Golgi network [69].

There are different techniques for studying lipid rafts and the proteins in them. The use of non-ionic detergents is the simplest and most commonly applied method. The method relies on the strong lipid-lipid interactions in lipid rafts that make the molecules in them more resistant to dissolution in non-ionic detergents and thus float in low density fractions. Triton-X-100 is the most frequently used detergent [64, 70]. Another common method involving the removal of cholesterol (using cyclodextrins, statins and polyene antibiotics [e.g., filipin]) is based on the fact that cholesterol is very important for maintaining the integrity of lipid rafts [64]. Other possibilities for studying lipid rafts is by labeling lipid components of the membrane (e.g., gangliosides) or using different lipophilic dyes that can be followed (e.g., polycyclic aromatic hydrocarbons (PAH) dyes) [71].

It has been shown that many endocytic pathways are dependent on cholesterol. Almost all CIE pathways (e.g., caveolae, EGFR-NCE, Cdc42-dependent endocytosis) are inhibited by cholesterol depletion, but to different extents [72-74]. Also, interfering with other lipids e.g., inhibition of sphingolipid synthesis, can affect CIE, while inhibition of sphingomyelin synthesis impairs activation of both Rho GTPases Cdc42 and Rac1 [75]. However, upon depletion of clathrin and cholesterol, Shiga toxin internalization is increased, suggesting that rafts can also have a role in the prevention of internalization of some molecules and pathways.

Lipid rafts have a huge impact on cellular signaling and membrane trafficking, as they can compartmentalize signaling pathways by acting as a platform for recruitment of different players [76]. Since alteration in lipid rafts results in aberrant immune signaling (e.g.,

Immunoglobulin E (IgE), B-cell receptor (BCR)- or TCR- signaling [77, 78]) and association with cancer [76], lipid rafts and modulation of their organization may serve as a promising target in anti-cancer therapies.

1.1.4. Role of endocytosis in control of receptor signaling

Receptors present on the PM are a critical means of communication between the cell and the extracellular microenvironment. Upon activation by binding of ligands, receptors transduce signals and trigger intracellular responses. These responses can be regulated in different ways by endocytosis, for example, by controlling the number of receptors present on the PM. Typically, the activation of receptors induces endocytosis of receptor-ligand complexes, leading to a reduction of receptor surface levels, thereby downregulating receptor signaling. However, endocytosis does not only inhibit signaling, but can also determine the duration and spatial distribution of the signaling response [79-81].

The role of endocytosis in the regulation of signaling is summarized in **Figure 6** [82]. Signal downmodulation is achieved by removal of activated receptors, such as RTKs or GPCRs, from the PM and trafficking receptors to MVBs and eventually the lysosome where they are degraded (**Figure 6A)** [83]. In contrast, endocytosis can lead to signal maintenance by recycling receptors back to the PM. This can be triggered by the dissociation of ligand-receptor complexes in the gradually acidified endocytic vesicle, considering differential pH sensitivities of distinct ligand-receptor complexes. Receptors, such as TfR or LDLR, release their ligands at the stage of early endosomes, where pH is ~6.5, and they are rapidly recycled back to PM from where they can be activated again.

Endocytosis can also generate an additional layer of signaling in the cell; for example, AKT is activated at the PM by the EGFR, but to sustain its activation, cycles of EGFR endocytosis and recycling back to the PM are required [84, 85]. On the other side, when receptors are internalized, they can still interact with signaling effectors (e.g., extracellular signal-regulated kinase 1/2 (ERK1/2), signal transducer and activator of transcription 3 (STAT3) [86]) in the endosomes [87]. The endosomes therefore serve as signaling platforms (**Figure 6B**). For instance, the mitogen-activated protein kinase (MAPK) pathway with its final executor ERK is initially activated at the PM, but it remains active on endosomes (**Figure 6B**). Since different signaling effectors are present on the PM and the endosomal membranes,

endocytosis is able to generate new signals by bringing receptors to the endosomes (**Figure 6C**). Thus, endocytosis can target receptors to lysosomal degradation to switch off signaling, and also traffic receptors to recycling to sustain signaling or to different signaling compartments (endosomes) allowing the generation of new signals or the integration of signaling pathways to establish specific responses [88]. The differential distribution of signaling effectors on the PM and in the endosomal compartment contributes to the spatial and temporal regulation of signals [89].

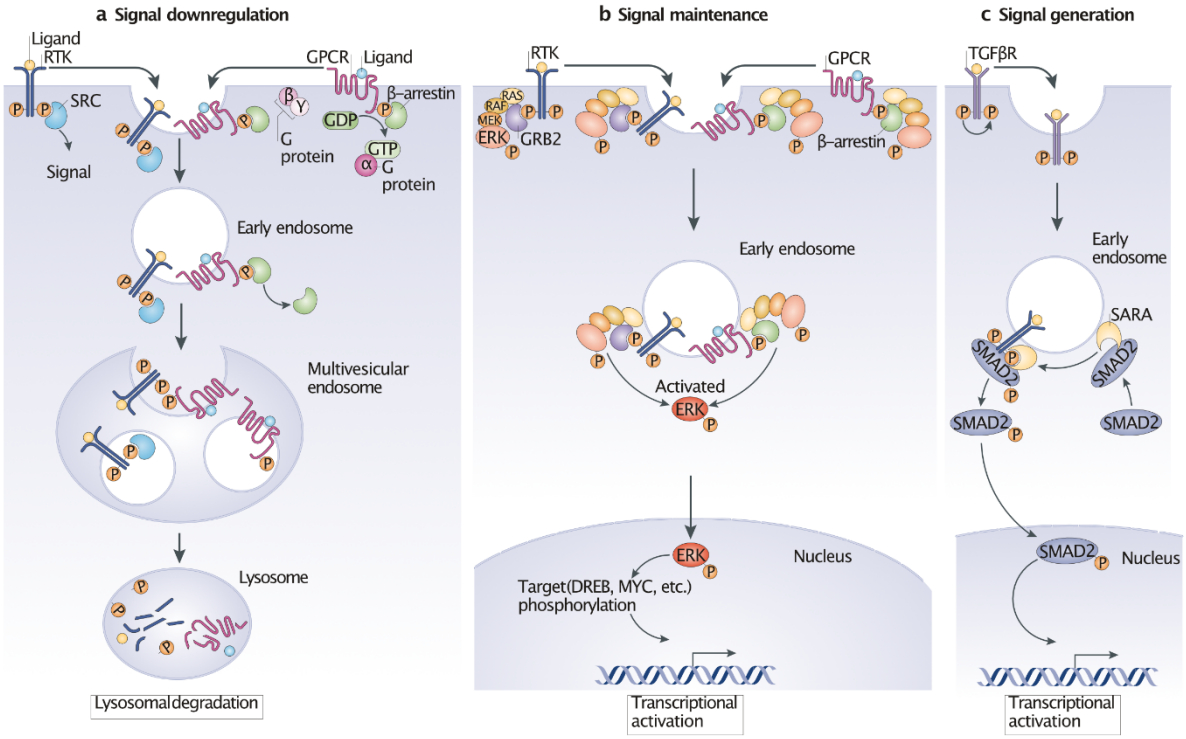

Figure 6. Role of endocytosis in controlling signaling pathways.

A. *By targeting receptors (e.g., RTK, GPCR) to lysosomal degradation, endocytosis is downmodulating the signaling.* ***B.*** *MAPK pathway (with final executor ERK) is activated at PM, but it is maintained active at early endosomes, from where ERK detaches and activates transcription in the nucleus.* ***C.*** *Transforming growth factor-β receptor (TGFβR) is activated on the PM, but only on endosomes is SMAD2 recruited to the TGFβR by the Smad anchor for receptor activation (SARA). SMAD2 is then activated and it translocates to the nucleus to induce transcriptional activation. Adapted from Dobrowolski, Nat Rev Mol Cell Biol, 2011 [82]*

Another way endocytosis can have an impact on signaling is illustrated by the trafficking of adhesion molecules, such as integrins. Integrins are receptors on the PM that communicate

with the extracellular matrix (ECM) and intracellular protein complexes, allowing the transition of signals in both directions, thus establishing a communication route between the ECM and the cell [90]. Interestingly, unlike other receptors that can be internalized and targeted to degradation, the majority of internalized integrins are recycled back to the PM. This intracellular trafficking between the PM and endosomes provides both spatial and temporal dimensions to integrin signaling which is critical for establishing specific biological responses. For example, integrin endocytosis requires integrin-mediated focal adhesion kinase (FAK) activation, and FAK signaling from endosomes has been linked to anchorage-independent growth and anoikis resistance, thus supporting metastasis [91]. Moreover, constant cycles of integrin adhesion assembly and disassembly at the PM are crucial for cell motility, and endocytic trafficking of integrins between the PM and intracellular pools is critical for fine tuning the spatial distribution and strength of focal adhesions/focal complexes and thus the generation of directional movement in response to extracellular signals [92].

Endocytosis is also a key regulator of RTK signaling. RTKs are receptors that in response to their ligands (e.g., growth factors, hormones, cytokines) become enzymatically active and, via a series of phosphorylation events, trigger different signaling cascades, thus regulating various cell signaling processes. Since their aberrant activation is linked to human disease, in particular, cancer, it is of great importance to understand how the strength, duration and spatial distribution of their signaling is regulated. Endocytosis has a critical role in this regulation of RTK, and through this action on RTK signaling, endocytosis contributes to the control of different aspects of cell function and long-term outcomes, such as organism development [93]. The integration of different endocytic pathways can also affect RTK signaling, as has been shown for the EGFR that can be internalized by both CME and NCE [74]. Upon internalization with CME, receptor is mainly recycled back to the PM while, internalization via NCE mainly leads to its degradation. While CME is active at all doses of ligand, NCE is active only at higher doses, suggesting that the integration of these two pathways can affect signaling in different ways in response to dose of ligands [74].

While the EGFR has been studied in-depth as a model of RTK endocytosis, the trafficking of other RTKs has also been shown to play an important role in their signaling [88]. ErbB2 and ErbB3 are members of same receptor family as EGFR – the ErbB family. They form ErbB2-ErbB3 heterodimers, known as the most potent signaling platforms among ErbB dimers. It has been shown that the sorting protein, sortilin-related receptor with A-type repeats (SORLA)

regulates the recycling of ErbB2 and ErbB3 and their signaling, contributing to resistance to ErbB2-targeted therapy in breast cancer [94, 95]. SORLA interacts directly with ErbB2 and ErbB3 and this interaction is necessary for SORLA-dependent proliferation of ErbB2 (also known as HER2)-positive breast cancer cell lines [94, 95].

Another example of the role of trafficking in the regulation of receptor signaling is provided by the hepatocyte growth factor receptor (HGFR)/Met. HGFR is activated after binding of HGF, its only known ligand, and it can be ubiquitinated by the E3 ligase Cbl [Casitas B-lineage Lymphoma] leading to its lysosomal degradation, similarly to EGFR [96]. Moreover, endocytosis controls the sorting of HGFR to specific endosomes and its activation of signaling effectors, such as Gab1[growth factor receptor-bound protein 2 (Grb2)-associated-binding protein 1], ERK 1/2, STAT3 and Rac1, which are implicated in cell survival, invasion and metastasis [97].

Since endocytosis is a key regulator of RTK signaling, which is frequently upregulated in cancer, aberrant endocytosis could contribute to the oncogenic function of RTKs through inefficient downmodulation of the receptor and/or aberrant activation of their downstream effectors. On the other side, acting as an attenuator of signaling, by targeting receptors to degradation, endocytosis can have possible tumor suppressor effects [79, 98].

Many of endocytic proteins that regulate receptor signaling are altered in cancer [99]. Upregulation of clathrin light chain isoform (CLCb) in non-small-cell lung carcinoma (NSCLC) cells increased cell migration and accelerated EGFR endocytosis and recycling [100]. Mutant Cbl, characterized by the loss of the E3 ligase activity, induce aberrant endocytosis of RTKs and consequent sustained signaling [101]. In the same way, mutant forms of RTKs that escape Cbl-mediated ubiquitination, showed the similar phenotype [102]. Endocytosis can also contribute to metastasis by affecting cell motility [99]. Understanding the molecular interactors and regulatory mechanisms of endocytosis could led to the discovery of novel targets in cancer therapy.

1.2. Epidermal growth factor receptor

The EGFR is known to play a pivotal role in physiological cellular processes, but its aberrant activation is linked to the development and progression of many types of cancer, including brain,

lung, colon, and breast cancer [103, 104]. It belongs to the ErbB family of RTKs that is composed of 4 members: EGFR (ErbB1), ErbB2, ErbB3, and ErbB4.

EGFR contains a cysteine-rich extracellular ligand-binding domain, a lipophilic transmembrane (TM) domain and an intracellular domain that includes the juxtamembrane (JM) regulatory region, the kinase domain, and the intracellular C-terminal regulatory tail (**Figure 7A**) [105]. The C-terminal regulatory segment contains the tyrosine residues that are trans-autophosphorylated upon ligand binding and responsible for signaling. The intracellular region also contains lysine acceptor residues, located primarily in the kinase domain, which are critical for receptor ubiquitination [106]. Upon ligand binding, EGFR homodimerizes or heterodimerizes with other ErbB receptors (**Figure 7B**). This induces a series of structural rearrangements, finally leading to transphosphorylation of tyrosine residues in the C-terminal regulatory tail [107]. Phosphotyrosine (pY) residues are docking sites for adaptor proteins that can initiate different signaling cascades (see **Section 1.2.3.**).

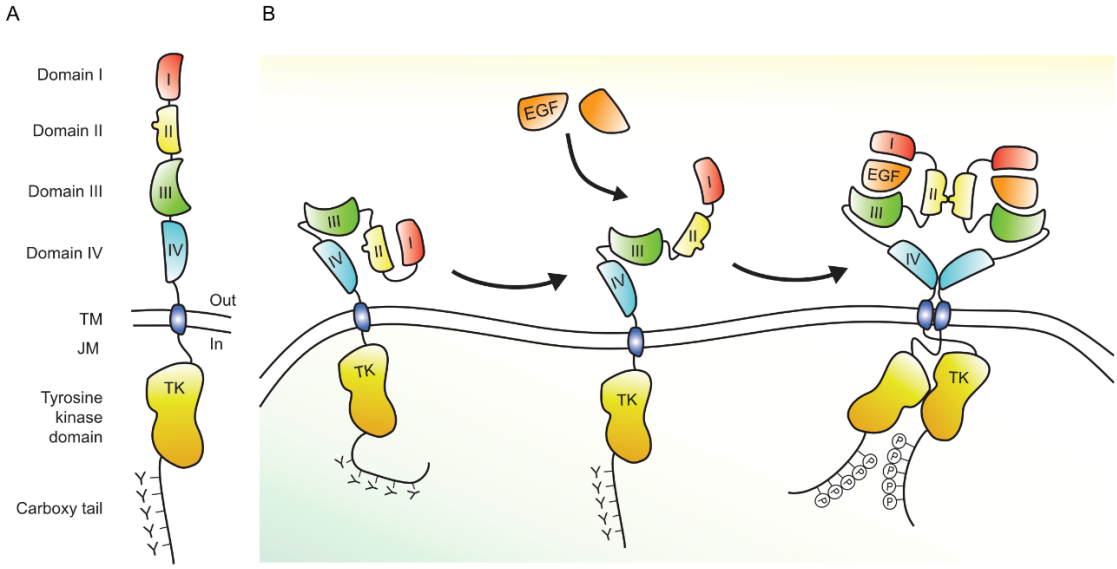

Figure 7. EGFR domains and dimerization.

A. *EGFR consist of extracellular domain (domains I, II, III and IV), transmembrane domain (TM) and intracellular domains [juxtramembrane domain (JM), tyrosine kinase domain (TK) and Carboxy tail].* ***B.*** *Upon binding to its ligand (e.g., EGF), EGFR can homo/heterodimerize, leading to transphosphorylation of carboxy tail and activation of EGFR dimers. Adapted from Sigismund, Mol Oncol, 2018 [108]*

1.2.1. EGFR ligands

Seven known EGFR ligands are responsible for the different biological outcomes of EGFR signaling: EGF, transforming growth factor-α (TGF-α), amphiregulin (AREG), epiregulin (EPR), heparin-binding EGF-like growth factor (HB-EGF), betacellulin (BTC), and epigen (EPG). These ligands can be divided into high-affinity EGFR ligands (EGF, BTC, HB-EGF, TGFα,) with a K_D of 1-100 nM and low-affinity EGFR ligands (AREG, EPR, EPG) with K_D >100 nM (**Table 2**). While EGF, TGF-α, AREG, and EPG are specific for the EGFR, the other ligands can also bind to ErbB4 (**Figure 8**). In addition, upon ligand binding, EGFR can heterodimerize with the other family members, including the orphan receptor ErbB2, leading to the activation of specific signaling effectors. The overexpression of EGFR and of the other ErbB family members, and the increased secretion of EGFR ligands are associated with tumorigenesis [109].

Table 2. Summary of molecular characteristics of EGFR ligands

Ligand	Binding affinity (K_D)	Predicted mass (kDa)	Group
EGF	High affinity ~ 0.1 nM Low affinity ~ 10 nM	6.4	High affinity
TGF-α	9.2 nM	5.5	
BTC	1.4 nM	9.8	
HB-EGF	7.1 nM	9.7	
AREG	350 nM	11.3	Low affinity
EPR	350 nM	5.6	
EPG	> 500 nM	7.9	

The table summarizes features of EGFR ligands, invoving their binding affinity (in nM) and predicted molecular mass (in kDa).

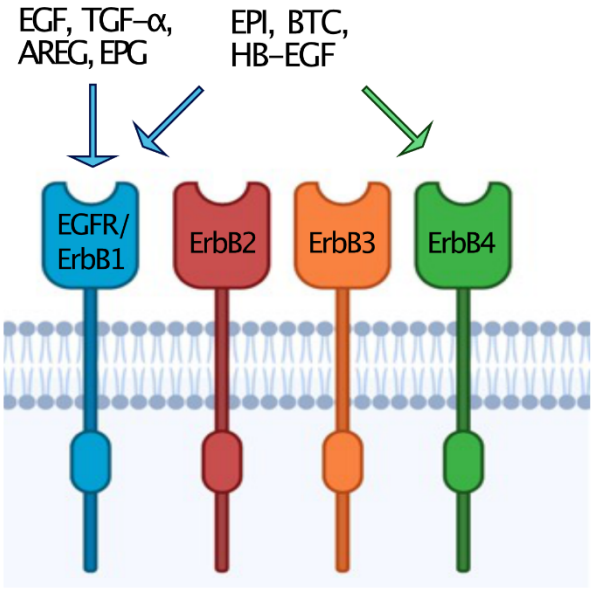

Figure 8. Schematic of the binding of different EGFR ligands to ErbB receptors.
From seven known EGFR ligands, EGF, TGF-α, AREG, and EPG are specific for the EGFR (blue), while EPR, BTC and HB-EGF can also bind to ErbB4 (green). ErbB2 (red) has no known ligand, while ErbB3 and ErbB4 can bind to neuregulins. Created with biorender.com

Each EGFR ligand appears to activate the receptor in the same way: through ligand binding, receptor dimerization, receptor trans-autophosphorylation, and the recruitment of signaling proteins or adaptors. In addition, all EGFR ligands induce EGFR internalization and trafficking to early endosomes [104]. Despite these similarities, the different EGFR ligands stimulate different downstream signals and biological outcomes starting from the activation of same receptor [24,97]. This occurs even when the ligands are present at saturating doses and therefore cannot be explained by their quantitative differences in binding affinities. Thus, these distinctions in signaling are independent of ligand affinity or potency and appear to reflect differences in the intrinsic ligand activity or efficacy.

Several theories have been proposed to explain how different ligands can produce different signaling patterns and biological outcomes. For example, the ligands could bind preferentially to specific EGFR/ErbB receptor dimers [110], receptor dimers could have different stabilities [111], differential conformations of dimerized receptors could result in the distinct recruitment of signaling players to the C-terminus [109], and differences in the trafficking (recycling *vs.* degradation) of receptor-ligand complexes after internalization [112]. Since differential endocytic sorting of RTKs is considered a fundamental process regulating

signaling duration and long-term responses, it could be that the differential responses induced by EGFR ligands are due the differential activation of endocytic pathways.

Two major ligands of EGFR, EGF and TGF-α, share similar three-dimensional structures, but induce different downstream biological responses. TGF-α is the most potent EGFR mitogenic ligand and this correlates with the fact that this ligand induces scarce EGFR ubiquitination and targets receptors to recycling [113, 114]. This effect cannot be interpretated by the quantitative differences in biological activities, because TGF-α and EGF bind to the receptor with a similar K_D and induce receptor autophosphorylation at similar concentrations. A possible explanation could be the different pH sensitivities of the ligand binding to EGFR. While at neutral pH both EGF and TGF-α have similar affinities for the receptor, at lower pH, the EGF/EGFR complex remains stable, while TGF-α is dissociated from the EGFR, leading to receptor deubiquitination and recycling before entering the lysosomal compartment. However, AREG is acid-resistant and remains bound to the receptor at lower pH, but still induces EGFR recycling [112]. This finding can be explained by the fact that AREG induces lower levels of ubiquitination and recruitment of Cbl to the EGFR than EGF (due to lack of phosphorylation of Y1045).

EGF is a growth factor whose concentration is regulated locally and not systemically like hormones; thus, EGF concentration varies depending on the organ. For example, EGF is found at high concentrations (50–500 ng/mL) in bile, urine, milk, and prostate fluid, at medium concentrations (5–50 ng/mL) in tears, follicular fluid, sperm, and seminal plasma, and at low concentrations (1–2 ng/mL) in plasma, serum, and saliva [93,94]. However, EGF knockout mice do not exert defeats, probably due to the presence of other EGFR ligands. While EGF is extensively studied, in the last years increased knowledge of other ligands has become available. Although the exact concentration that different ligands can reach in organs is unknown, in some types of cancer they can reach very high levels (e.g., TGF-α and HB-EGF in breast cancer [115]). In NSCLC patients, the levels of TGF-α and AREG in the serum correlate with tumor aggressiveness, while the EGF levels does not correlate and they are lowered in NSCLC patients than in healthy individuals [116].

AREG is mainly expressed in placenta and breast, where it plays an important role in the morphogenesis and differentiation of the mammary gland [117]. AREG is distributed widely in normal tissues (mainly breast and placenta) – inducing ductal morphogenesis in breast [118] – and can be found in many forms of cancer. Controversial data about AREG-induced cell

growth are present in literature: while it promotes growth of normal epithelial cells, fibroblasts and keratinocytes, AREG inhibits growth of certain aggressive carcinoma cell lines [119].

TGF-α is widely expressed in many normal tissues, while its concentration is elevated in tumors. It has been implicated in cell migration, growth and differentiation. TGF-α expression correlates with more aggressive breast tumors than EGF [115]. Similarly, also increased expression of AREG and decreased expression of EGF were observed in early hyperplastic precursors of breast cancer [120]. Both TGF-α and AREG stimulate equivalent levels of DNA synthesis in MDCK, canine kidney, cells [121]. In the same cells, AREG stimulates a morphologic change and redistribution of E-cadherin, while TGF-α does not. In MCF10A human mammary epithelial cells, AREG stimulates greater motility and invasiveness than EGF [122].

Together these data indicate that each ligand–EGFR pair influences signaling events and duration in specific ways and dependent of cell context, induce different biological outcomes.

1.2.2. EGFR endocytosis

EGFR can be internalized constitutively, without ligand stimulation. This pathway exhibits a slow rate of internalization and regulates EGFR steady-state levels at the PM. In the presence of ligand, EGFR can be internalized via CME or NCE, and the choice of the route depends on ligand concentration, cell context, the nature of homo-/hetero-dimers of the receptor, and the presence of specific endocytic signals in the intracytoplasmic tail [74, 123, 124] (**Figure 9**).

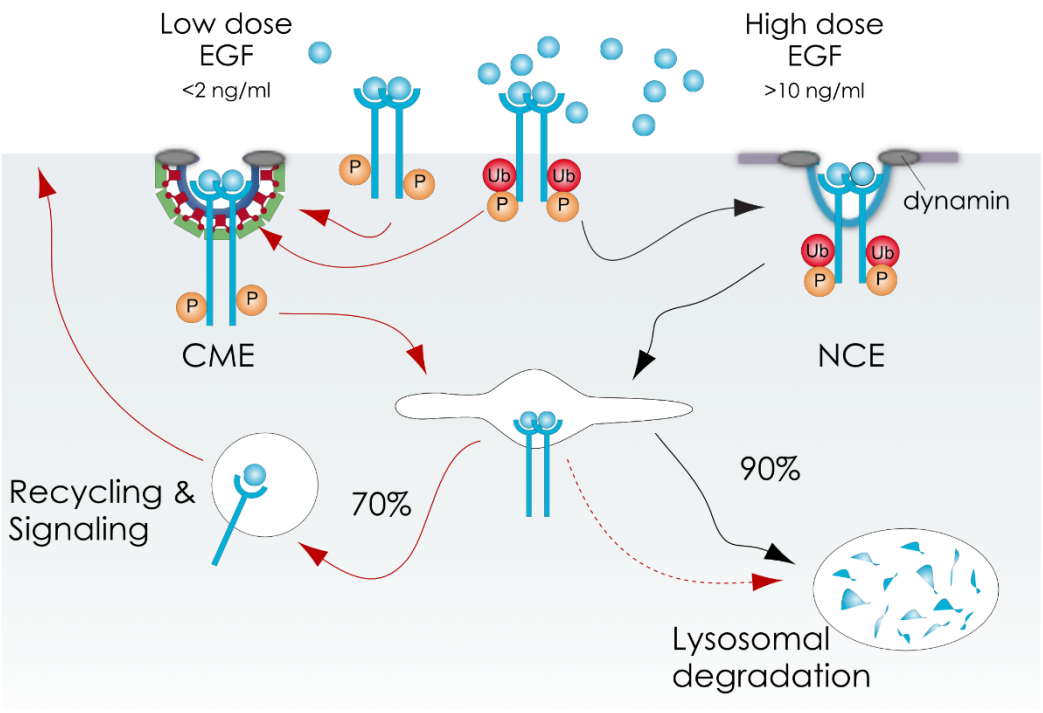

Figure 9. EGFR endocytosis: integration of the CME and NCE pathways.

Upon stimulation with low doses of EGF (~1 ng/ml), EGFR is internalized via clathrin-mediated endocytosis (CME). In the presence of high, yet physiologically relevant, EGF concentrations (>10 ng/ml) the EGFR can be internalized through both, CME and non-clathrin endocytosis (NCE). While CME mainly targets EGFR to recycling, NCE mostly leads to its degradation. Adapted from Barbieri, Curr Opin Cell Biol, 2016 [125]

1.2.2.1. Clathrin-dependent endocytosis of the EGFR

Clathrin-dependent endocytosis is active at all doses of ligand stimulation and destines the majority of EGFRs to recycling (~70%), although a fraction of receptors (~30%) is also targeted to degradation by this pathway. In the canonical CME pathway, upon stimulation of EGFR, AP2 recognizes sorting signals on the activated receptor and recruits clathrin and other accessory proteins of the CME machinery (e.g., Eps15, Eps15L1, epsin 1), inducing the formation and maturation of CCPs. The fission of the pits is exerted by dynamin, leading to formation of free CCVs in the cytosol that fuse with endosomes.

In addition to the canonical AP2-dependent CME pathway, EGFR can also be internalized via AP2-independent CME (**Figure 3D**). This mechanism relies on Eps15, Eps15/L1 and epsin 1 (note that these proteins are also necessary for AP2-dependent CME).

Interestingly, the two CME routes target EGFR to distinct intracellular fates. While AP2-dependent CME of the EGFR leads to its recycling and is required for sustained AKT signaling and cell migration, AP2-independent CME destines the receptor to degradation [126]. While the precise role of eps15/L1/epsin1 in AP2-independent CME needs to be resolved, it is possible that ubiquitin (Ub) and ubiquitin-binding domains can play a role in mediating the protein-protein interactions occurring in AP2-independent CME. Indeed, it has been shown that monoubiquitination of endocytic adaptors is necessary for AP2-independent EGFR-CME. For example, ubiquitination of Eps15, Eps15/L1 and epsin1 by NEDD4 [Neural Precursor Cell Expressed, Developmentally Down-Regulated 4] E3 ligase was shown to be critical for AP2-independent EGFR-CME [127].

1.2.2.2. Non-clathrin endocytosis of the EGFR

NCE is a novel endocytic route of the EGFR, which is activated only after stimulation with high, but physiologically relevant, doses of EGF (>10 ng/ml). Unlike canonical AP2-dependent CME, NCE leads mostly to receptor degradation [74, 123]. Thus, NCE appears to be a negative regulator of EGFR signaling, protecting cells from overstimulation when ligand concentrations are high [128]. Loss of this route has therefore been speculated to lead to the aberrant regulation of EGFR signaling in cancer. The integration of the NCE and CME pathways seems to be coupled with the different concentrations of EGF found in biological fluids: CME would protect the EGFR from a degradative fate in conditions of low ligand availability and sustain signaling, while NCE would protect cells from overstimulation in conditions of high ligand concentration and maximal receptor activation.

NCE is dependent on EGFR ubiquitination and requires the ubiquitin-binding proteins Eps15, Eps15L1 and epsin 1, and cholesterol-enriched PM microdomains [62, 123]. Indeed, in HeLa cells the KD of these adaptor proteins or the disruption of cholesterol -enriched rafts using filipin inhibited EGFR degradation specifically at high EGF doses [123]. In addition through KD experiments and analysis of EGFR mutated at specific pY sites, it was established that the E3 ligase Cbl is recruited to the active receptor both directly via the EGFR autophosphorylation site pY1045 [129] and indirectly through Grb2, the latter binding to pY1068 and Y1086 [130]. Cbl then ubiquitinates the EGFR stimulating recruitment of adaptor proteins with ubiquitin-binding domains (Eps15, Eps15L1 and epsin 1) and internalization by NCE. Notably, Cbl-

mediated ubiquitination of the EGFR occurs over a narrow range of EGF doses between 1-10 ng/ml, resulting in a ubiquitination threshold that correlates with EGFR internalization by NCE [62].

In order to identify NCE regulators and cargoes co-trafficking with EGFR via NCE, an unbiased proteomics approach was undertaken in our laboratory to isolate EGFR-containing NCE vesicles [63]. This strategy involved the immunopurification of EGFR-NCE vesicles coupled to stable isotope labeling by/with amino acids in cell culture (SILAC)-based mass spectrometry. Proteins specifically enriched in the NCE vesicle preparation were identified. Among these proteins, selective NCE regulators were identified through small interfering ribonucleic acid (siRNA) screening and the analysis of the impact of siRNAs on EGFR endocytosis; candidates with a role in EGFR-NCE, but not in EGFR-CME were selected for high-resolution studies.

Several functional NCE regulators were identified and, among them, the ER-shaping factor RTN3 had the strongest effect on EGFR internalization at high doses of ligand when knocked down (KD) (**Figure 10A, bottom**), with minimal impact at low EGF concentration (**Figure 10A, top**). Consistent with the role of NCE in EGFR degradation, RTN3 KD inhibited EGFR degradation and increased EGFR-dependent signaling (**Figure 10B**).

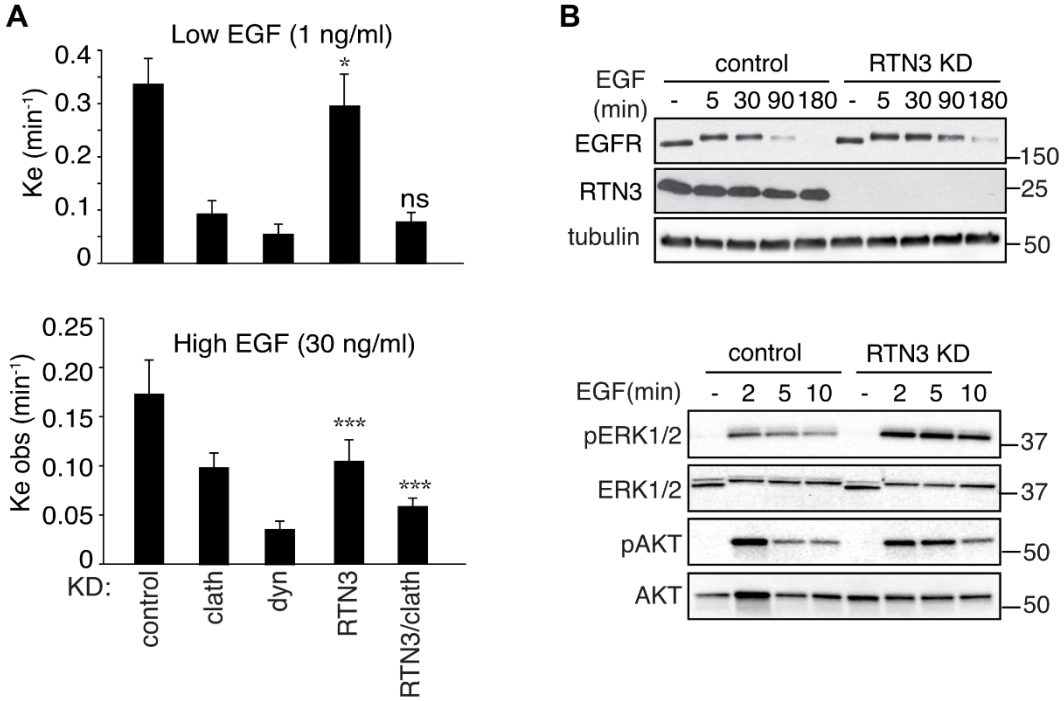

Figure 10. RTN3 is critical regulator of EGFR-NCE.

A. *EGFR endocytic rate constants (Ke) at low (1 ng/ml) and high (30 ng/ml) EGF doses in HeLa cells silenced for the indicated proteins (clath, clathrin; dyn, dynamin; RTN3, reticulon-3). RTN3 KD reduced EGF internalization at a high EGF dose, when NCE is active. The double RTN3 and clathrin KD (RTN3/clath) reduced EGF internalization almost to the levels of dynamin KD, which inhibits both EGFR-CME and -NCE. P-value, Student's t-test two tailed; *, P<0.05; ***, P<0.005. ns, not significant.* ***B.*** *Immunoblots showing the effect of RTN3 KD on total EGFR levels (upper blot) and EGFR downstream signaling effectors (lower blot). RTN3 KD delayed EGFR degradation and increased EGF-induced signaling, as shown for phosphoERK1/2 (pERK1/2) and phosphoAKT (pAKT). Total ERK1/2 and AKT levels are shown as controls. Tubulin, loading control. Adapted from Caldieri, Science, 2017 [63]*

In addition to functional regulators, NCE-specific cargoes were also identified in the SILAC-based proteomics analysis, among them, CD147 (**Figure 11**). CD147 is an integral membrane glycoprotein, that induces the activation of extracellular matrix metalloproteases (MMP) and binds to different partners (e.g., other CD147 molecules, integrins, monocarboxylate transporters (MCTs), cyclophilins, annexin II and caveolin1) [131]. Through these interactions, CD147 is involved in variety of processes (such as cell adhesion, tissue repair and remodeling, interaction with the ECM and embryo implantation) [131]. CD147 is highly expressed on the surface of some cancer cells and is associated with tumor progression/invasion and poor prognosis [132]. CD147 was previously shown to enter HeLa cells through a slow constitutive a clathrin- and dynamin-independent endocytic pathway together with CD44, CD98 and MHCI [59]. CD147, CD44 and CD98 appear to directly enter recycling tubules thus avoiding trafficking to lysosomes and degradation [133].

In the presence of high EGF doses, CD147 was shown to enter the cell and to colocalize with EGFR in a clathrin-independent, but RTN3- and dynamin-dependent manner. Thus, in this setting, CD147 can be used as a specific NCE marker [63]. Interestingly, as a partner of MCTs (that can transport lactate and pyruvate) and the glucose transporter 1 (GLUT1), CD147 has been shown to regulate aerobic glycolysis and promote cancer cell growth when its cell surface expression is altered [134, 135]. Thus, EGFR signaling, through the regulation of these transporters by CD147-NCE, might influence cell metabolic functions not typically connected with the EGFR pathway.

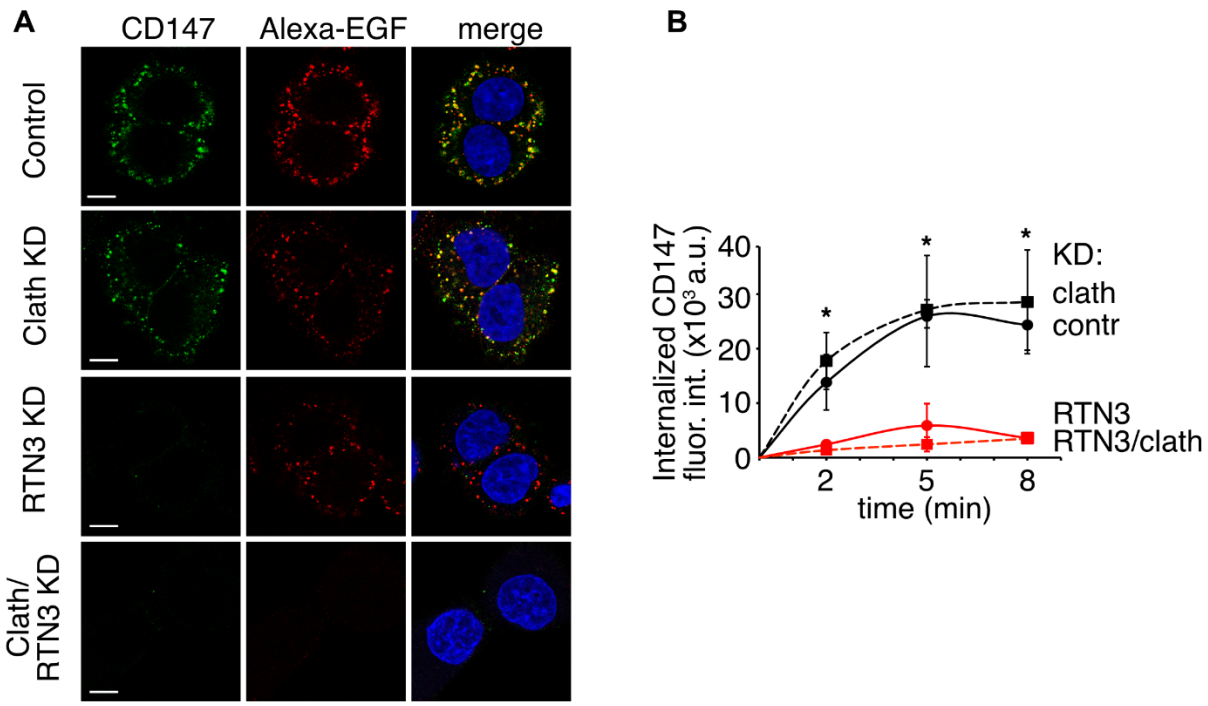

Figure 11. CD147 is specific cargo of NCE pathway.

A*. Immunofluorescence analysis of CD147 internalization in HeLa cells subjected to the indicated KD. CD147 is a specific marker of NCE that internalize in HeLa cells only upon stimulation with high doses of EGF and colocalizes with EGF. Its internalization was abolished by RTN3 KD. CD147 internalization was followed for 8 min at 37℃ in the presence of Alexa-555-EGF using a specific antibody applied to cells in vivo. Cells were subjected to acid wash prior to fixation to remove PM signal and visualize only internalized CD147/EGF. Bars, 10 μm.* ***B****. Time course of CD147 internalization after EGF addition measured through a plugin designed ad hoc. Mean integrated fluorescence density +/- SD is reported (a.u., arbitrary units). *, P<0,05 (RTN3 KD vs. control). Clath, clatrhin; contr, control; RTN3, reticulon-3. Black dotted line with squares, clatrhin KD; black solid line with circles, control; red solid line with circles, RTN3 KD; red dotted line with squares, RTN3/Clathrin KD. Adapted from Caldieri, Science, 2017 [63]*

Recently, different steps of the NCE pathway were mechanistically characterized (**Figure 12)** [63]. Firstly, the morphology of EGFR endocytic structures was revealed by employing electron microscopy (EM) in HeLa cells upon stimulation with high dose of EGF, where EGFR has been labeled with gold. It was found that NCE is mediated by tubular

invaginations (TIs), structures that were persistent in clathrin KD (**Figure 13A, B**). Interestingly, RTN3 KD decreased the number of TIs, suggesting that RTN3 is involved in the early step of TI formation.

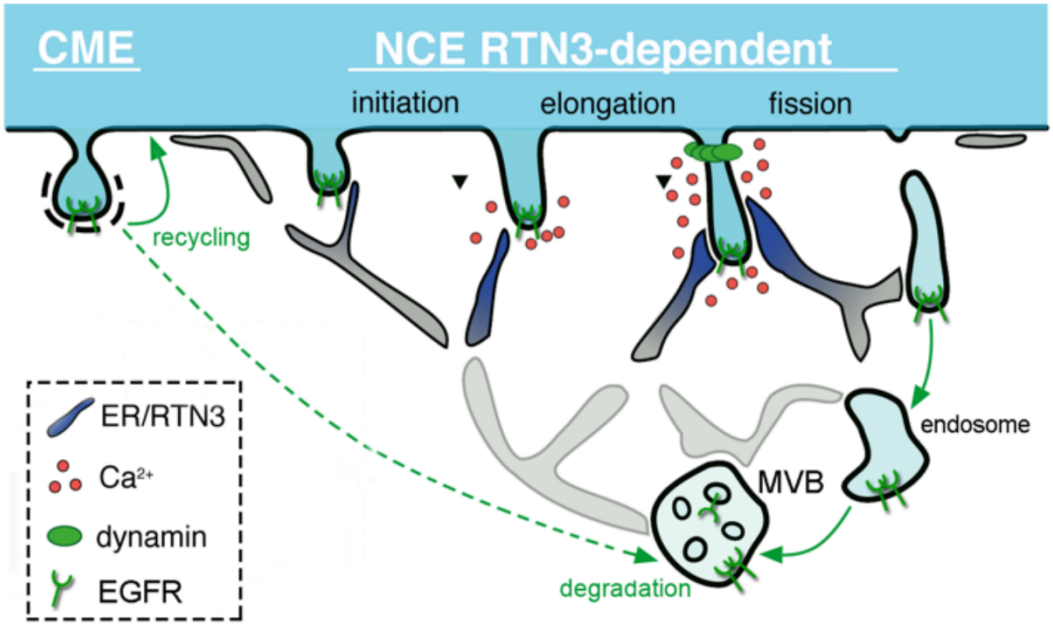

Figure 12. Mechanism of non-clathrin endocytosis of EGFR.

Schematic showing the different steps of NCE. For initiation of the formation of TIs, NCE requires ER-PM contact sites, that depends on RTN3. At these sites there is local Ca^{2+} release, necessary for the final step – fission of TIs, together with dynamin, and completion of TI internalization. Adapted from Caldieri, Science, 2017 [63]

RTN3 is necessary for the formation of ER-PM contact sites (**Figure 13C, D**). To visualize contacts between the ER and EGFR-containing endocytic structures, high-resolution EM is performed on HeLa cells, in which cortical ER was labeled by transient transfection with the HRP-KDEL construct [136] and EGFR was gold-labeled. Contacts sites were observed between the ER and TIs, but not with CCPs, indicating that TIs are a distinctive feature of EGFR-NCE. Moreover, RTN3 KD strongly affected formation contact sites.

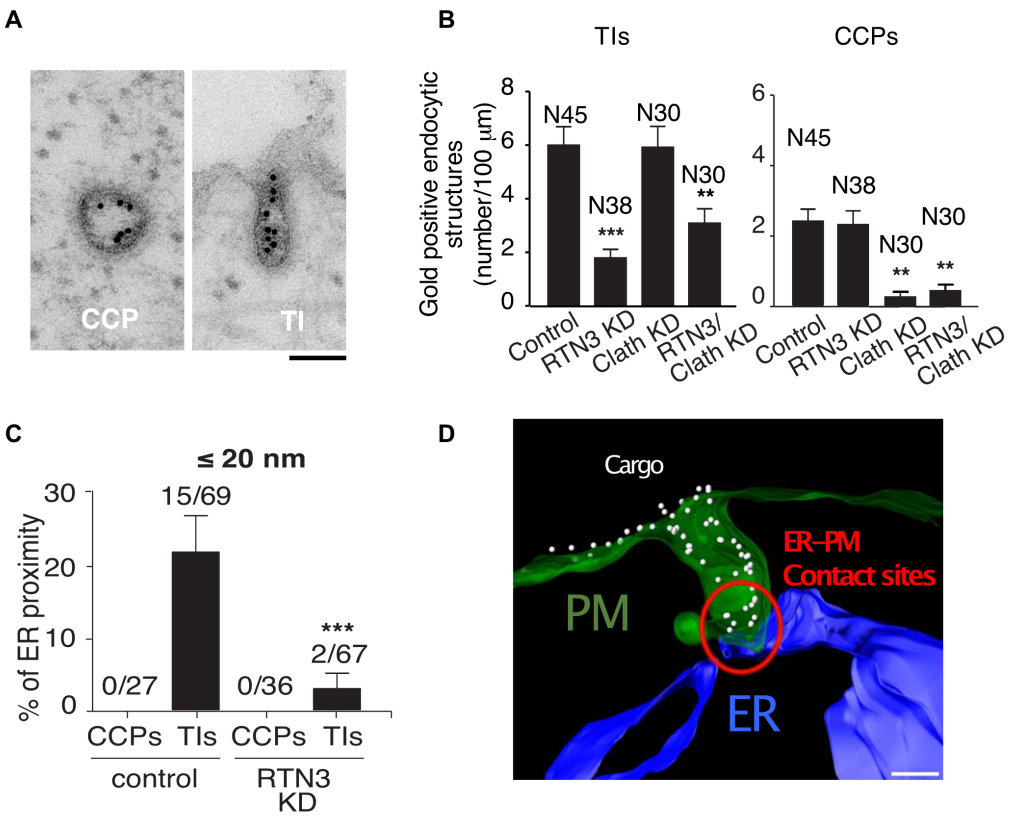

Figure 13. RTN3 is required for the formation of TIs and ER-PM contact sites.

A. *Representative EM image of EGFR congaing structures – CCPs and TIs, upon stimulation with high EGF. Bar 100 nm.* ***B.*** *Quantification of gold-labeled EGFR-positive endocytic structures (TIs and CCPs) upon stimulation with high dose of EGF in HeLa cells silenced for the indicated proteins. RTN3 KD decreased numbers of TIs, alone or in combination with clathrin KD, while it did not affect CCPs. N, number of analyzed cell profiles. Data are expressed as the number of gold-positive structures, normalized to PM profiles of 100-µm length, ± SD.* ***C.*** *Contacts between the ER and EGFR-containing endocytic structures are analysis by EM upon stimulation with high EGF, labeling ER with HRP-KDEL and EGFR with gold. The proximity analysis of labeled ER structures with gold-labeled EGFR in TIs vs. clathrin-coated pits (CCPs) at distance ≤ 20 nm. Contact sites were observed between ER and TIs, but not CCPs, in RTN3 dependent manner. Quantification showed as a percentage of structures in contact with ER on total number of structures expressed as percentage ± SD. The number of counted structures in contact with the ER is indicated.* ***D****. 3D reconstruction of a contact sites formation between PM – TI (in green), internalizing the cargo CD147 (white dots), and cortical ER (in blue) that depends on RTN3 function. The 3D image represents the*

*segmentation of the tomogram. Bar, 200 nm. P values, *P < 0.05, **P < 0.01, ***P < 0.001. Adapted from Caldieri, Science, 2017 [63]*

At these ER-PM contact sites, there is localized Ca^{2+} release, observed by PM tagged-Ca^{2+} sensor, that was again dependent on RTN3 (**Figure 14A**). Ca^{2+} response is mediated by the IP3R located on the ER, and its inhibition by xestospongin C, as inhibition of the GTPase dynamin, was shown to reduce length but not the number of TIs (**Figure 14 B-D**). This argues that the role of dynamin and Ca^{2+} is in promotion of the fission of NCE TIs and completion of the internalization process [63].

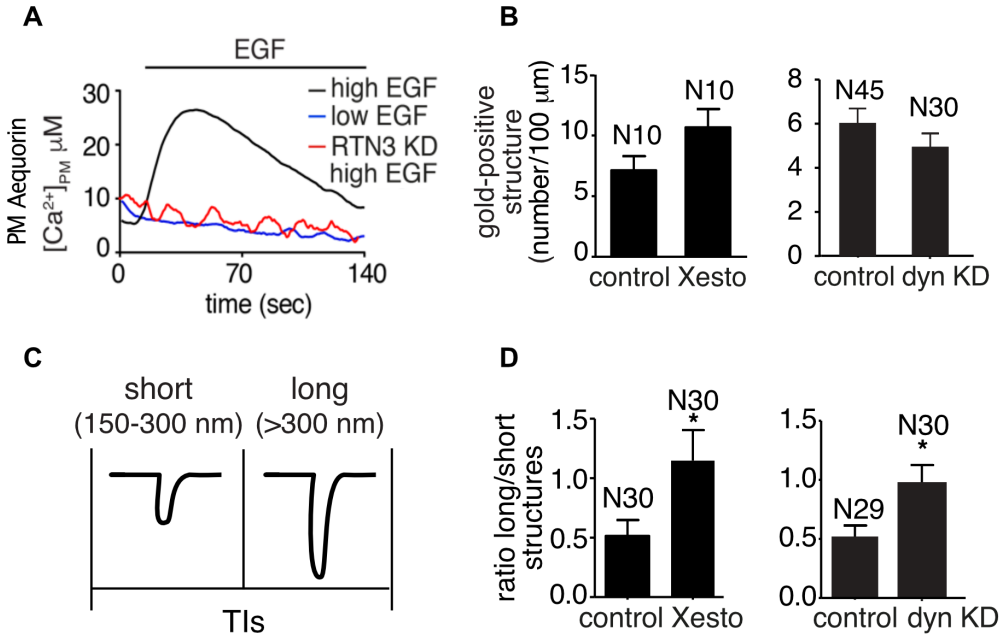

Figure 14. Ca^{2+}response and dynamin are necessary for the fission of TIs.

A. *The Ca^{2+} sensor aequorin was fused to a PM-targeting sequence. PM-aequorin detected a peak of Ca^{2+} release induced by high, but not low, EGF doses, that was reduced in RTN3 KD cells.* ***B.*** *Quantification of gold-labeled EGFR-TIs upon stimulation with high dose of EGF in HeLa cells inhibited with xestospongin C (Xesto) or silenced for dynamin. N, number of analyzed cell profiles. Data are expressed as the number of gold-positive structures, normalized to PM profiles of 100-µm length, ± SD.* ***C.-D.*** *Morphometric analysis of the length of EGFR gold-positive TIs. Both xestospongin C and dynamin KD increase the length of TIs. Data expressed as the ratio between the number of long vs. short structures normalized to PM profiles*

*of 100-µm length ± SD. N, cell profiles analyzed. *P < 0.05. Adapted from Caldieri, Science, 2017 [63]*

EGFR-NCE has been shown to be cell context dependent, with only specific cell types, such as cervical and breast epithelial cells, skin and keratinocytes, showing activation of this pathway upon stimulation with high doses of EGF (**Table 3**) [62, 63]. One of parameters that seems to be relevant for NCE activation in different cells is the number of EGFRs on cell surface. For instance, while NCE has a critical role in EGFR endocytosis and signaling in the HeLa Milan clone used in our laboratory, another HeLa clone (called HeLa Oslo) that has fewer surface EGFRs, is inactive for the NCE pathway [62, 63]. Other parameters might also be relevant for NCE activation in different cell contexts and this issue is under further investigation. In addition, it is not known whether the NCE pathway is also relevant to other growth factors or RTKs.

Table 3. Cell lines characterized for EGFR-NCE activation

Cell Line	Cell type	Surface EGFRs/cell	NCE
HeLa - Milan	Cervix adenocarcinoma	2.5-3.0 x 10^5	YES
HeLa - Oslo	Cervix adenocarcinoma	0.8 x 10^5	NO
NR6-EGFR	Fibroblast normal	2.5 x 10^5	YES
HaCaT	Keratinocyte normal	4.0 x 5^5	YES
A431	Skin carcinoma	1.2 x 10^6	YES
BT20	Breast carcinoma	1 x 10^6	YES
MCF10A	Breast normal	2.9 x 10^5	YES/NO
BT549	Breast ductal carcinoma	0.8 x 10^5	NO
HCT116	Colorectal carcinoma	0.5 x 10^5	NO

The presence of EGFR-NCE was evaluated by the ^{125}I-EGF (high vs. low dose) and/or CD147 internalization assays, in control, RTN3 KD, clathrin KD and/or dynamin KD cells. ^{125}I-EGF saturation binding assay was used to measure EGFR surface number/cell.

1.2.3. EGFR signaling – different pathways

Upon activation by its ligands, EGFR undergoes a transition from an inactive monomer to an active EGFR dimer, which stimulates its intrinsic intracellular protein tyrosine kinase activity

and results in the trans-autophosphorylation of several tyrosine residues in the C-terminal domain of EGFR (**Figure 15A**). There are nine tyrosine residues in the intracellular domain of the EGFR that can be phosphorylated. These pY sites act as docking sites for the recruitment of different proteins harboring domains capable of binding to pY, such as those with Src homology 2 (SH2) or pY binding (PTB) domains. The recruitment of these signaling effectors then triggers a variety of signaling cascades, including the ERK/MAPK, phosphoinositide 3-kinase/protein kinase B (PI3K/AKT), STAT, phospholipase Cγ (PLCγ) - Ca^{2+} pathways (**Figure 15B**) [137]. As these pathways are interconnected, the activation of the EGFR stimulates an entire signaling network associated with a wide number of biological outcomes, such as cell proliferation, differentiation, migration, and survival. In the following sections, the different downstream signaling cascades are described, focusing in particular on the PLCγ pathway since it leads to Ca^{2+} release from ER and as such, could have role in EGFR-NCE.

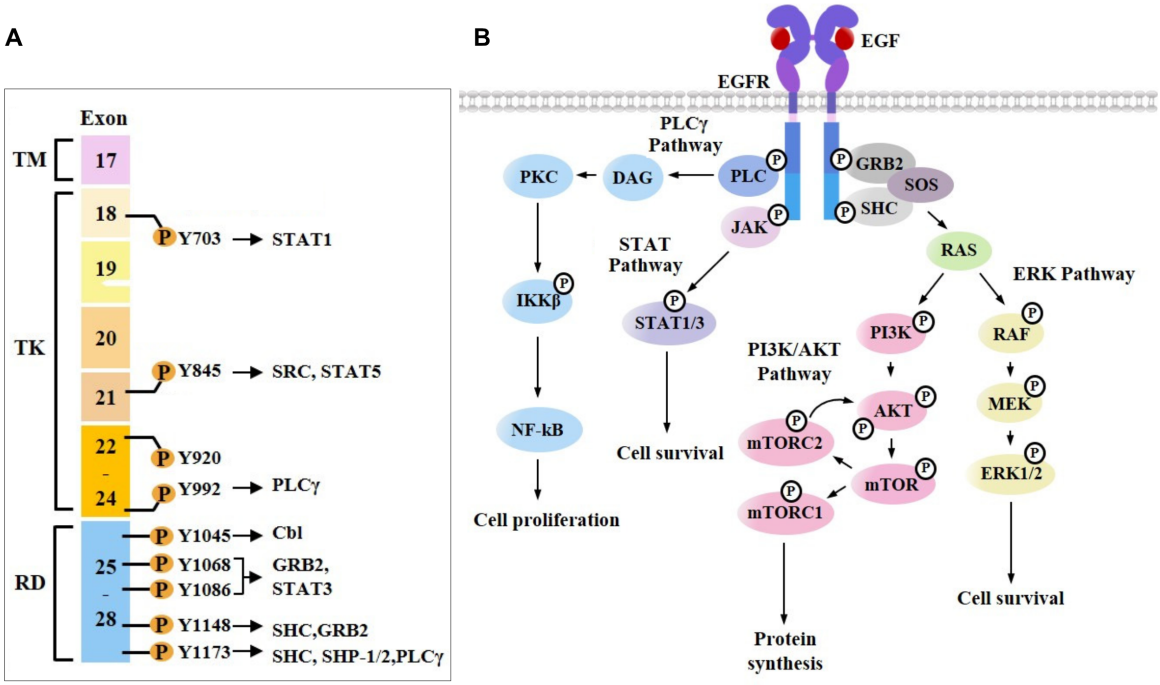

Figure 15. EGFR signaling pathways.

A. *Schematic representation of the EGFR transmembrane (TM) and intracellular domain composed of the tyrosine kinase domain (TK) and the regulatory domain (RD). The exons encoding each domain are shown as well as the sites of the nine pY residues and proteins recruited to these docking sites.* ***B.*** *Summary of the different signaling cascades and associated biological outcomes that can be triggered from activated EGFR homodimers. Adapted from Kwon, Cancers, 2019 [138]*

1.2.3.1. ERK-MAPK pathway

The ERK-MAPK pathway starts with the recruitment of Grb2 and Src homology 2 domain-containing (SHC) protein to the EGFR autophosphorylation sites (Grb2 recruitment to: pY1068, pY1086 or pY1148; and SHC recruitment to pY1148 or pY1173). Grb2 also binds to phosphorylated SHC and recruits SOS1 [Son of sevenless homolog 1], a guanine nucleotide exchange factor (GEF) for Ras small guanosine triphosphatase (GTPase). SOS1 activates Ras by inducing it to exchange guanosine diphosphate (GDP) to GTP. Ras then activates the MAPK signaling pathway by activation of rapidly accelerated fibrosarcoma (Raf) kinase that in turn activates mitogen-activated protein kinase/extracellular signal-regulated kinase (MEK1/2), also known as MAPK kinase (MAPKK), which then phosphorylates ERK1/2. The ERK Ser/Thr kinase then phosphorylates downstream substrates located in the cytosol or the nucleus, which eventually leads to various biological responses, such as chromatin remodeling, ribosome synthesis, and protein translation implicated in cell survival and proliferation [139].

1.2.3.2. PI3K-AKT pathway

The PI3K-AKT signaling pathway plays a role in controlling cell metabolism, proliferation and survival. PI3K is activated downstream of the EGFR (Figure 7B) [139]. PI3K is composed of the p85 regulatory subunit and the p110 catalytic subunit. Binding indirectly to the activated EGFR through the adaptor Gab1, allows the p110 subunit to phosphorylate the membrane lipid, phosphatidylinositol 4,5-bisphosphate (PIP2), producing phosphatidylinositol (3,4,5)-trisphosphate (PIP3) [140]. PI3K can also be activated by Ras downstream of the activated EGFR (**Figure 15B**) [139]. Ras binds to the PI3K p110 subunit promoting its membrane recruitment. Activation of PI3K leads to recruitment and activation of the Ser/Thr kinase AKT. In addition, EGF-induced ubiquitination of AKT also recruits AKT to the PM. PM-recruited AKT is phosphorylated at Thr308 and Ser473. While phosphorylation of Thr308 is necessary and sufficient for AKT activation, maximal activation is got by phosphorylation at Ser473. Activated AKT can result in proliferation, metabolism, migration, protein synthesis and cell survival. AKT can also activate mammalian target of rapamycin (mTOR) signaling, leading to increased protein synthesis.

1.2.3.3. STAT pathway

Phosphorylated EGFR can activate STATs by phosphorylating their tyrosine residues via Janus kinase family (JAK) dependent [141] or JAK-independent mechanisms [142]. Activated STATs form dimers that translocate to the nucleus where they activate transcription of target genes. Active STAT1, STAT3 and STAT5 are known to have role in cancer through stimulation of cell proliferation, survival and oncogenesis [143].

1.2.3.4. PLCγ-Ca^{2+} pathway

PLCγ is membrane-associated enzyme that belongs to the PLC family consisting of 13 isozymes in six families (β, γ, δ, ε, ζ, η) that differ in structure [144]. PLCγ exists as two isozymes, PLCγ1 and PLCγ2, which are recruited and phosphorylated by the EGFR following EGF stimulation. This leads to their activation and results in the hydrolysis of PIP2 into DAG and inositol trisphosphate (IP3) [145]. IP3 is needed for Ca^{2+} release from the ER via the IP3R [146], the main Ca^{2+} channel on the ER membrane. DAG and the released Ca^{2+} activate protein kinase C (PKC) which has many substrates, including EGFR and Raf kinase [147].

Common to all PLC isozymes, PLCγ consists of an N-terminal pleckstrin homology (PH) domain, four EF hands, a catalytic region, and a C-terminal C2 domain [148] (**Figure 16A**). The PH domain regulates the activation and translocation of PLCγ to the PM by anchoring it to PIP2 and PIP3, allowing them to interact with other signaling players. In addition, it is involved in the binding of PLCγ to the dimeric protein complex Gβγ (a component of heterotrimeric G proteins). The four EF hands are helix-loop-helix motifs with calcium-binding ability. The catalytic region consists of the triosephosphate isomerase (TIM) barrel, an X and Y catalytic domain and an X-Y linker. The TIM barrel is highly conserved among the PLCs, with 60–70% sequence identity. The X and Y domain form the Ca^{2+}-binding site and a catalytic active site. This region serves for the hydrolysis of PIP2 into DAG and IP3. The C-terminal C2 domain is tightly packed against the TIM barrel and maintains the structural integrity of the catalytic core. In addition, it also enhances membrane recruitment of the enzymes upon Ca^{2+} release.

Specific to the PLCγ isozymes is γ-specific array (γSA) part, consisting of a split PH (sPH) domain, tandem SH2 domains, and an SH3 domain. These different domains present different levels of homology between PLCγ1 and PLCγ2 (**Figure 16A**). The sPH domain shows

affinity for PIP2 and binding proteins that control PLCγ activity and intracellular localization. The C-terminal half of the PH domain can interact with the TRPC3 Ca^{2+}channel.

In the absence of signal, PLCγs are autoinhibited (**Figure 16B**). PLCγs are recruited to receptors through the binding of the nSH2 domain to pY residues on RTKs; these interactions induce phosphorylation and activation of PLCγ1/2. Binding of pY783 of PLCγ1 or pY759 of PLCγ2 to the cSH2 domain is necessary for their activation and these sites are primary sites of phosphorylation coupled to enzyme activation [149, 150]. Other Tyr residues that are phosphorylated following activation of the EGFR are Y771, Y775, Y783, and Y1254 for PLCγ1; and Y753, Y759, Y1197, and Y1217 for PLCγ2. Interaction between primary pY sites of PLCγ and cSH2 induces a conformational change, reorienting the X-Y linker to allow the substrate to access the active site. Although phosphorylation of pY775 for PLCγ1 or pY753 for PLCγ2 is necessary to increase lipase activity, alone it could not induce the activation of PLCγ1/2.

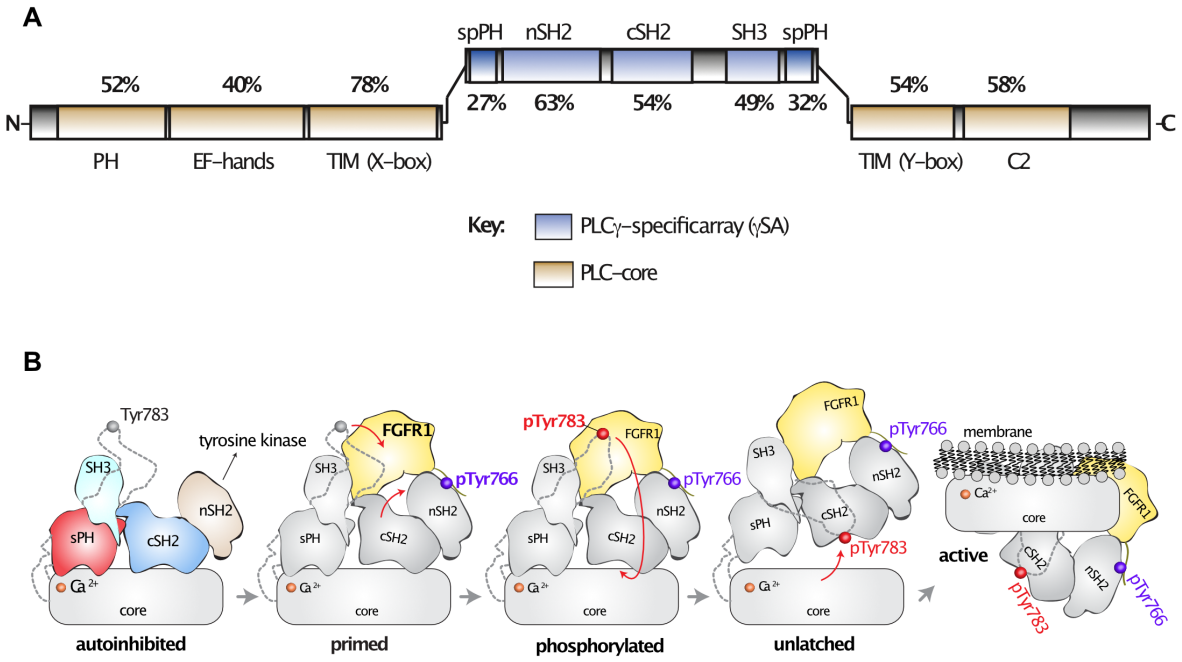

Figure 16. PLCγ structure and activation.

A. *PLCγ structure with percentage of similarity between PLCγ1 and PLCγ2. PLCγ consists of the PLC core (an N-terminal PH domain, EF-hands, TIM-barrel-like fold, a C2 domain) and the γSA (sPH domain, two SH2 domains (nSH2 and cSH2), and one SH3 domain). Adapted from Koss, Trends Biochem Sci, 2014 [151]* ***B.*** *Activation of PLCγ by RTKs (here shown for PLCγ1 and fibroblast growth factor receptor 1[FGFR1]). At steady state, PLCγ1 is autoinhibited, while upon activation of receptor, in this case FGFR1, the nSH2 domain of PLC1γ regulates its*

recruitment to receptor. The nSH2 domain binds to pY of receptor (pY766), and this binding leads to destabilization of the interaction between the cSH2 and C2 domains of PLCγ1, priming the lipase for phosphorylation-dependent activation. PLCγ1 is then phosphorylated on Tyr783, which leads to the full dissociation of the cSH2 domain from the C2 domain and the catalytic core, *and finally leading to activation of PLCγ1 and membrane binding and hydrolysis of PIP2. Adapted from Hajicek, Elife, 2019 [148]*

The SH3 domain of PLCγ binds to proline-rich sequences on the target protein, such as scaffolding proteins [Cbl, Strumpellin and WASH-interacting protein homolog (SWIP), lymphocyte cytosolic protein 2 (Lcp2)], cytoskeleton components (dynamin, cortical actin complexes, microtubule-associated proteins), and signaling proteins (AKT, TrpC3 [Transient Receptor Potential Cation Channel Subfamily C Member 3] channels, SHIP1 [Src homology 2 (SH2) domain containing inositol polyphosphate 5-phosphatase 1]). In the case of Grb2, it negatively regulates PLCγ1 by competing with PLCγ1 for binding to fibroblast growth factor receptor 2 (FGFR2) via the SH3 domain, and by direct interaction with PLCγ1 [152, 153]. The SH3 domain of PLCγ1 also can act as a GEF for PI3K Enhancer (PIKE) and dynamin-1 [154]. PLCγ2 activity is stimulated by the small GTPases Rac1 and Rac2. Rac2 binds the sPH domain of PLCγ2 and this induces a conformational change in PLCγ2 and movement of the X-Y linker from an autoinhibitory position [155]. The activation by Rac is independent of phosphorylation and is also associated with translocation of PLCγ2 to the PM. PLCγ1 is not activated by Rac1 and Rac2; however, the requirement of PLCγ1 in Rac1-mediated nuclear factor of activated T-cells (NFAT)5 activation was suggested [156].

PLCγs are also stimulated by high concentrations (40–100 μM) of PIP3 [157]. This activation of PLCγ by PIP3 is mediated by both the N-terminal PH domain and the cSH2 domains of PLCγ.

PLCγ1 is widely expressed with a prominent role in T cell and natural killer cell function, whereas PLCγ2 expression is mainly restricted to immune cells, such as mast cells, natural killer cells, B cells, and platelets [151, 158]. However, PLCγ2 is also found to play role in brain. It is known that activating mutations of PLCγ1 are the most frequent mutations in adult T cell leukemia/lymphoma [159, 160], while activating mutations in PLCγ2 have high frequency in patients with B cell leukemias treated with ibrutinib, an inhibitor of Bruton's tyrosine kinase (BTK), a kinase that is active downstream of the BCR. Therefore, ibrutinib prevents

downstream activation of PLCγ2 and finally, blocks downstream BCR signaling. Nevertheless, ibrutinib resistance due to acquired mutations in BTK and PLCγ2 has been documented [160]. Mutated forms of PLCγ2 isozymes were also found in other cancers mainly linked to immune responses [161, 162]. Moreover, an activating mutation in PLCγ2 was found to have protective role in Alzheimer's disease [163] highlighting the fact that the same mutations can have different effects depending on cellular context. Although the activation of PLCγ enzymes is associated with cancer progression, their regulation and interactors are not fully characterized [164].

1.1.1. EGFR in physiology and cancer

EGFR activated by its different ligands plays a crucial role in physiology and tissue homeostasis. Its ability to induce cellular proliferation, migration and differentiation, means that EGFR plays crucial role in development and organogenesis. EGFR is implicated in the morphogenesis of many organs and EGFR knockout mice display an embryonic lethal phenotype with profound defects in many organs, including gastrointestinal tract [165]. Also, EGFR ligands are involved in morphogenetic processes. For example, EGF together with WNT is involved in maintaining the stem cell compartment of intestinal crypts, as EGFR is enriched in stem and progenitor cells [166]. Intestinal crypts consist of stem cells (in the bottom of the crypt, leucine-rich repeat-containing G-protein coupled receptor 5 (LGR5)-cells), Paneth cells, transit amplifying cells and +4 cells (cells on position +4 from the base of the crypt). EGF is mainly secreted by Paneth cells and together with other factors [WNT, Notch, and bone morphogenetic protein (BMP)], it regulates the survival, self-renewal and differentiation of intestinal stem cells. In addition to EGF and EGFR, other ErbB receptors (e.g., ErbB2, ErbB3) and ligands (e.g., AREG, EPR) are important components of the intestinal crypts [167, 168].

Overexpression (with or without gene amplification) or activating mutations of EGFR have been associated with cancers, including lung, glioblastoma and epithelial tumors of the head and neck [169]. Moreover, mutations of other members of the ErbB family, ErbB2, are implicated in 15-30% breast carcinomas [170]. For these reasons, many cancer therapies are focused on downmodulating the levels of ErbB receptors and their signaling, by using TK inhibitors (e.g., gefitinib, erlotinib) or monoclonal antibodies (e.g., cetuximab, panitumumab) [108, 171-174]. Even though they have been approved for treatment of cancer (TK inhibitors for lung and pancreatic cancers [171, 172] and monoclonal antibodies for colorectal cancer and

head and neck cancer [173, 174]), they show to have limited response and evoke resistance in patients [108] so improvements of cancer therapies are of key importance.

Mechanism of action of monoclonal antibodies is to prevent ligand binding and therefore block receptor activation and downstream signaling. However, antibodies induce EGFR dimerization and further endocytosis of antibody-bound EGFR in low-rate internalization and usually are recycled back to PM [175]. Interestingly, combination of EGFR antibodies against different epitopes showed increased internalization of EGFR and its degradation [176], implicating that regulation of EGFR trafficking can act as a possible point for improvement of targeted therapies [175]. Thus, a better understanding of EGFR trafficking will allow future advances in drug discovery and cancer treatments.

2. HYPOTHESIS AND AIMS OF THE PROJECT

Since NCE promotes EGFR degradation and leads to extinction of EGFR signaling in the presence of high doses of EGF, we hypothesize that it could have a critical role in cell physiology, protecting cells from excessive activation of the EGFR pathway and its associated biological responses, e.g., proliferation, differentiation, and survival. It follows therefore that loss of NCE function could contribute to the oncogenic function of EGFR through the inefficient downmodulation of the receptor, arguing for a possible tumor suppressor role of NCE. Detailed molecular characterization of the EGFR-NCE pathway could therefore highlight novel targets for cancer therapy.

Several critical regulators of EGFR-NCE have already been characterized, e.g., Cbl-mediated ubiquitination of EGFR is necessary for the recruitment of endocytic adaptors (Eps15/L1, epsin1) and the initiation of NCE [62, 123, 129], RTN3 is critical for the formation of PM-ER contact sites and the release of Ca^{2+} from the ER via the IP3R which is needed for dynamin-mediated fission of NCE TIs and completion of the internalization step [63]. However, the involvement of the various signaling cascades triggered by the activated EGFR in the regulation of the NCE machinery is still unclear, as are the exact physiological and pathological roles of the NCE pathway.

The present study was undertaken to decipher the signaling pathways emanating from the EGFR that can influence NCE, and to expand our understanding of the potential physiological and pathological relevance of NCE by investigating whether other EGFR ligands and growth factors are internalized by this pathway. To investigate these issues, we have addressed the following specific aims:

1) Characterization of the signaling events originating from the activated EGFR that are critical for EGFR-NCE. Initially, we investigated whether activation of the EGFR downstream signaling pathways correlates with EGFR-NCE activation. This led to the identification of PLCγ as a potential regulator of NCE. A series of experiments were then carried out to define the precise role of PLCγ in EGFR-NCE focusing on its known role as a regulator of Ca^{2+} release from the ER;
2) Characterization of the specific involvement of the PLCγ2 isozyme (but not PLC γ1) and its associated second messengers in EGFR-NCE;

3) Identification of other EGFR ligands and RTKs that can be internalized by NCE, in order to expand the relevance of NCE to the regulation of other signaling molecules;
4) Characterization of the possible physiological role of NCE focusing on its potential involvement in cell metabolism due to the known function of CD147 in the regulation of glucose transporters;
5) Characterization of the presence of EGFR/CD147-NCE in non-tumorigenic breast epithelial cells and its involvement in the growth of primary mammary and intestinal organoids to gain insights into the relevance of NCE in cell physiology.

3. MATERIALS & METHODS

3.1. Reagents

Ligands used for receptor stimulation: EGF, TGF-α, AREG (Peprotech) and HGF (R&D) were used at the indicated concentrations. Alexa-labeled EGF was used at a concentration (400 ng/ml or 1 μg/ml of the conjugated species) corresponding to an actual EGF concentration of ~40 ng/ml and ~100 ng/ml, as indicated. Alexa-EGF and Alexa-Tf were from Molecular Probes. List of oligos and antibodies used are showed in Tables 4 and 5. Inhibitors were used at the following concentrations: DAG kinase inhibitor (R59949) – 10 μM, cyclosporine A (CsA) – 10 μM, FK506 – 5 μM, xestospongin C – 2 μM, gefitinib – 10 μM, PPMP – 5 μM.

Table 4. List of RNAi oligo sequences

ID	Sequence
PLCγ1 Smart pool Dharmacon	5'-GCAGCAAGAUCUACUACUC-3' 5'-GAUGGGAUGCCAGUUAUUU-3' 5'-GAGACAACCGCCUCUAGUU-3' 5'-GAAUGGAAUUUCGCCUGAA-3'
PLCγ2 Dharmacon	5'-GGGAUGCCCUGGUUAAAGA-3'
IP3R Ribox Smart pool	5'-AUUAAGGUAAACUGAGUCCCCC-3' 5'-UUAUUCUUGUCAGUCCACGCCCCC-3' 5'-UAUAGAUGUUAUGGCCCACCCCC-3'
RTN3 Stealth	5'-CCCUGAAACUCAUUAUUCGUCUCUU-3'
Clathrin heavy chain Riboxx	5'-UAAAUUUCCGGGCAAAGAGCCCCC-3'
DAG kinase (DGK) α Stealth	5'-CGAGGAUGGCGAGAUGGCUAAAUAU-3'
Dynamin 1 Riboxx	5'-UUUCACAAUGGUCUCAAAGCCCCC-3'
Dynamin 2 Riboxx	5'-UGAACUGCAGGAUCAUGUCCCCC-3'
Rac1 Stealth	5'-CCGGUGAAUCUGGGCUUAUGGGAUA-3'

Table 5. List of antibodies

Antibody	Producer	Clone or Epitope	Catalog number	Dilution
AKT	Cell Signaling		#9272	1:1000
CD147	BD	HIM 6	555961	1:300
CD147	Biolegend	OX114	123701	1:50
Clathrin	BD	clone 23	610499	1:1000
DGKα	Abcam	Amino acids 331-370	ab64845	1:500
EGFR	Genentec	Clone 13A9	13A9	1:2000
EGFR	In-house	806 serum		IF 1:200 WB 1:10000
ERK1/2	Sigma	ERK-1, 351-368	M7927	1:5000
GAPDH	Santa cruz	6C5	sc-32233	1:3000
HA	Biolegend	16B12	901503	WB, IF 1:5000
HGFR	R&D	Glu25-Thr932	AF276	1:200
IP3R	BD	Clone 2	610312	1:500
Cytokeratin (CK) 5	Abcam	Amino acids 541-590	ab53121	1:200
CK 8	In-house	TROMA-1		1:200
LGR5	Abcam	Amino acids 689-719	ab75732	1:200
pAKT	Cell Signaling	Thr308	# 9275	1:500
pERK1/2	Cell Signaling	Thr202/Tyr204	#9106	1:1000
PLCG1	BD	Clone 10	558575	1:500
PLCG2	R&D	346404	MAB3716	1:500
pPLCG1	Cell Signaling	Tyr1783	#2821	1:1000
pPLCG2	R&D	Tyr759, Clone #744757	MAB7377	1:500
pSHC	Cell Signaling	Tyr239/240	#2434	1:500
pTyr	Millipore	4G10	05-321MG	1:1000
pY 1045 EGFR	Cell Signaling	Tyr 1045	#2237	1:1000
pY 1068 EGFR WB	Cell Signaling	Tyr 1068, D7A5	#3777 (XP)	WB 1:1000

				IF 1:200
pY 1173 EGFR	Cell Signaling	Tyr 1173, 53A5	#4407	1:1000
pY 992 EGFR	Cell Signaling	Tyr 992	#2235	1:1000
RTN3	In-house	Amino acids 1-47		1:250
SHC	BD	Clone 20	#610878	1:500
Tubulin	In-house	serum		1:500
Ub	Santa Cruz	P4D1	sc-8017	1:1000
Vinculin	Sigma	clone hVIN-1	V9131	1:5000

WB: western blot; IF: immunofluorescence.

3.2. Cell Culture

Human epithelial cervical cancer HeLa cells were cultured in Minimum Essential Medium (MEM, Sigma) supplemented with 10% FBS, 2 mM glutamine, sodium pyruvate 1 mM (Euroclone), 0.1 mM non-essential amino acids (Euroclone). The inducible clathrin KD HeLa clone was grown in the same medium as HeLa cells but supplemented with 10% TET-System Approved FBS (PAA) instead of standard FBS. Non-tumorigenic epithelial breast MCF10A cell line was cultured in a 1:1 mixture of DMEM and HAM'S-F12 (Gibco, Life Technologies), supplemented with 5% horse serum (Invitrogen), 2 mM Glutamine, 50 ng/ml cholera toxin, 10 µg/ml insulin, 500 ng/ml hydrocortisone (Sigma) and fresh 20 ng/ml human EGF (Invitrogen). In the case of ligand stimulation, different concentrations of human recombinant ligands were added to serum-starved medium for the indicated time points. All cells were cultured at 37°C and 5% CO_2.

3.3. RNA interference (RNAi)

RNAi was performed with Lipofectamine RNAimax from Invitrogen, according to the manufacturer's protocol: for RTN3 KD (Stealth), Clathrin heavy chain KD (Riboxx) and Rac1 KD (Stealth), cells were transfected with 2 cycles of 8 nM of oligos; for PLCγ1 KD and PLCγ2 KD, cells were transfected with 2 cycles of 16 nM of oligos; for Dynamin KD (Riboxx), cells were transfected with 1 cycle of 8 nM of oligo.

Briefly, 1.5 x 10^6 cells in a 10 cm culture plate were transfected in reverse: liposome complexes carrying siRNAs were formed for 15 min at room temperature (RT) and then added to trypsinized cells in suspension. The next day, cells were transfected in forward, adding the liposome/siRNA complexes to cells in adhesion. On the fourth day, cells were plated at the required concentration for the assays the next day. KDs were verified after 5 days, and as a negative control, cells were transfected with lipofectamine alone. See **Table 4** for the nucleotide sequence of siRNAs employed.

3.4. Lentiviral infections

HeLa and the inducible-clathrin KD cells were infected with lentiviral pLVX vectors: empty vector (EV) or vectors encoding for PLCγ1-hemagglutinin (HA) and PLCγ2-HA. 293T packaging cells were cultured in a humid atmosphere containing 5% CO_2 in DMEM supplemented with 10% FBS, 2 mM glutamine, 100 U/ml penicillin and 100 µg/ml streptomycin. Medium was changed 2 h before transfection and cells at 70% confluence were transfected overnight with the calcium-phosphate procedure with a mixture of 5 µg GAG-POL, 5 µg ENV, 5 µg REV, and 10 µg of lentiviral vector. The medium of 293T cells was replaced after 12-16 h post-transfection and the viral supernatant was collected at 36 h post-transfection and filtered with a 0.45 µm syringe-filter and added to 40-50% confluent target cells for overnight infection at 37°C. The following day, the appropriate medium for the target cells was added and cells were passaged.

3.5. Biochemical assays

3.5.1. Western blot

Cells were lysed by adding RIPA buffer (50 mM Tris–HCl, 150 mM NaCl, 1 mM EDTA, 1% Triton X-100, 1% sodium deoxycholate, 0.1% SDS), plus protease inhibitor cocktail (CALBIOCHEM) and phosphatase inhibitors (20 mM sodium pyrophosphate pH 7.5, 50 mM NaF, 2 mM PMSF, 10 mM Na3VO4 pH 7.5), directly to cell plates. Lysate was clarified by centrifugation at 13,200 rpm for 20 min at 4°C. Protein concentration was measured by the

Bradford Assay (Biorad) and 30µg of protein was prepared in Laemmli 1x buffer (2% SDS, 62.5 mM Tris HCl, pH 6.8, 10% Glycerol, 0.1% Bromophenol blue, 5% β-Mercaptoethanol). For detection of pPLCγ2 and total PLCγ2, due to low expression of PLCγ2 in HeLa cells and inefficient antibodies, 45µg of proteins were prepared. Protein samples were run on pre-cast gels with a gradient 4-20% (Biorad) and transferred to a nitrocellulose membrane (Biorad) using Trans-Blot (Biorad) according to manufacturer's instructions. Membranes were blocked with 5% milk diluted in tris buffered saline 0.1% Tween (TBS-T) and then incubated overnight with primary antibody according to the datasheet. Following 3 washes with TBS-T, membranes were incubated with the appropriate secondary antibody conjugated to horseradish peroxidase. After 3 more washes, the signal was detected at Chemidoc (Biorad) using ECL from Amersham or Biorad. See **Table 5** for the list of antibodies employed.

3.5.1.1. Anti-Ub western blot

After resolving protein lysates on pre-casts gels as above, proteins were transferred to a PVDF (polyvinylidene fluoride) membrane (Biorad), previously activated by incubation in 100% MeOH for 5 min at RT. Ponceau staining was avoided since it might interfere with antibody recognition. After transfer, membranes were subjected to denaturing solution (6 M guanidium chloride, 20 mM Tris, pH 7.4, 1 mM PMSF, 5 mM β-mercaptoethanol) for 30 min at 4°C, in order to denature Ub and facilitate the recognition of latent Ub epitopes by the anti-Ub antibody resulting in intensification of the anti-Ub signal. After extensive washing in TBS-T buffer, membranes were blocked overnight at 4°C in 5% BSA (dissolved in TBS-T). After blocking, membranes were incubated with the the P4D1 antibody (Santa Cruz, 1:1000) against Ub, diluted in TBS-T 5% BSA, for 1h at RT, followed by 3 washes of 10 min each in TBS-T. Membranes were then incubated with the appropriate secondary antibody conjugated with horseradish peroxidase. After 3 more washes, the signal was detected at Chemidoc (Biorad) using ECL from Amersham or Biorad.

3.5.2. Immunoprecipitation

Cells were serum starved overnight and then stimulated for the indicated times with 100 ng/ml of EGF or TGF-α. Lysates prepared in JS buffer (50 mM HEPES pH 7.5, 50 mM NaCl, 1%

glycerol, 1% Triton X-100, 1.5 mM MgCl, 25 mM EGTA) were incubated in the presence of specific antibodies (about 1-2 μg/mg of lysates) for 2h at 4°C with rocking. Assays were performed using 1 mg of lysate, respectively. Protein G Sepharose beads (Zymed) were then added, and samples were left for an additional hour at 4°C, rocking. immunoprecipitants were then washed 4 times in JS buffer.

To detect ubiquitination of PLCγ-HA, anti-HA antibody (Biolegend) was used for immunoprecipitation and anti-Ub antibody for Ub recognition. Cells expressing Eps15-HA were used as a positive control for ubiquitinated protein. To detect different post-translational modifications upon stimulation with EGF or TGF-α, EGFR was immunoprecipitated using an anti-EGFR antibody produced in-house (see Table 5).

3.5.3. GST pull-down assays

For the glutathione S-transferase (GST) pull-down assays, cells were serum starved overnight, stimulated with EGF 100 ng/ml for 5 min and then 1 mg of lysate (PLCγ-HA or Eps15-HA as positive control) in JS buffer was incubated with 20 μg of GST-3Ub or GST alone (as a negative control) for 2 h at 4°C. Beads were then washed 4 times with JS buffer, before elution of bound proteins by the addition of Laemmli buffer 2x.

3.5.4. Density gradient fractionation assay

Cells were serum starved for 4 h, followed by stimulation with EGF 100 ng/ml for 1 min. Cells were lysed in Triton-X-100 lysis buffer (1% Triton-X-100, 150 nM NaCl, 25 mM TrisHCl, 5 mM EDTA, with protease inhibitor cocktail). 1 mg of lysates in 1 ml volume was added to 2 ml of cold Optiprep 60%, to give a 3 ml sample with 40% final concentration. This fraction was put at the bottom of the tube. On the top of it, 6 ml of Optiprep 30% was added, following by 2.5 ml of Optiprep 5%. Tubes are centrifugated for 16 h in a SW41 rotor at 120,000g (25,000 rpm) at 4°C. After the overnight centrifugation of gradients, fractions of 1 ml were collected starting from the top of each gradient. Proteins were precipitated in these fractions with 5X trichloroacetic acid/Na-deoxycholate (TCA/DOC) solution to give a final concentration of 10% TCA, 0.4 mg/mL DOC. After mixing, samples were kept on ice for 1.5 h, followed by

centrifugation for 10 min at 13,000 rpm 4°C. Pellet was washed twice with cold acetone, and after drying resuspended in 50 µl of 2X Laemmli buffer.

3.6. Radioactive assays

3.6.1. Internalization assay with ^{125}I-EGF and ^{125}I-Tf

Cells were serum starved for at least 2 h and then incubated at 37°C in the presence of radiolabeled ligands, ^{125}I-EGF or ^{125}I-Tf, in binding buffer (MEM, BSA 0.1%, Hepes pH 7.4 20 mM) for 2, 4 and 6 min. For low dose stimulations, 1 ng/ml ^{125}I-EGF was used. For high dose stimulations, 1 ng/ml ^{125}I-EGF + 29 ng/ml unlabeled EGF were used. ^{125}I-Tf was used at a concentration of 1 ng/ml. After the incubation time, cells were put on ice, washed three times in PBS, and then incubated for 5 min at 4°C in 300 µl of acid wash solution pH 2.5 (acetic acid 0.2 M, NaCl 0.5 M). Then, the solution was removed from the cells and the radioactivity present in this solution was measured. This measurement represents the amount of ^{125}I-EGF/Tf bound to the receptor on the cell surface. Cells were then lysed with 300 µl of a solution containing 1 M NaOH and radioactivity was measured. This sample represents the amount of internalized ^{125}I-EGF/Tf. The unspecific binding was measured at each time point in the presence of an excess of non-radioactive EGF/Tf (300x and 500x, respectively). After being corrected for non-specific binding, the rate of internalization was expressed as the ratio between internalized and surface-bound radioactivity. Endocytic rate constants [Ke and Ke obs, [177] were calculated from the slope of the trend-line. Results are expressed as the internalization rate constant (Ke or Ke obs) or as a % of Ke in control cells, as indicated, and are the mean of duplicate or triplicate points. Statistical analysis was performed using JMP 10.0 statistical software (SAS Institute, Inc).

3.6.2. Downmodulation assay

Cells were serum starved for at least 2 h in binding buffer and incubated for various times (60', 30', 10', 5', 0') with 100 ng/ml of EGF/TGF-α at 37 °C, washed with cold PBS, and surface-bound EGF was removed by treatment with mild acid/salt wash buffer (pH 4.5) for 5 min. This mild acid/salt treatment removed more than 90% of the total ^{125}I-EGF bound to the cells at 4°C

without affecting cell permeability, EGF receptor binding, internalization, or degradation. The number of binding sites at the different time points was then determined by incubating the cells at 4°C for 4 h with 100 ng/ml of ^{125}I-EGF: 10 ng/ml of ^{125}I-EGF + 90 ng/ml of unlabeled EGF. Cells were washed 3 times with cold PBS and lysed in 1 N NaOH. The lysate was collected and the radioactivity present in it was measured. This sample represents the amount of EGFR at the PM at the different time points. Non-specific binding was measured for each time point in the presence of 30 μg/ml (300x 100 ng/ml) of unlabeled EGF, and generally was not more than 3-4% of the total counts and was subtracted from the total radioactivity. After correction for non-specific binding, the rate of downmodulation was expressed as a percentage of EGFR remaining at the cell surface with respect to the initial amount (100%, calculated at time=0).

3.7. Measurements of intracellular Ca^{2+} concentration

3.7.1. Aequorin

Aequorin measurements were performed as previously described [63]. Briefly, cells were grown on 13-mm-round glass coverslips at 50% confluence and were transfected with PM-targeted aequorin. PM-aequorin was obtained by fusing aequorin with SNAP25, a neuronal protein that is recruited to the PM after the post-translational addition of a lipid anchor [178]. Aequorin constructs and protocols were previously described [179]. All aequorin measurements were performed in Krebs-Ringer modified buffer (KRB) (135 mM NaCl, 5 mM KCl, 0.4 mM KH_2PO_4, 1 mM $MgSO_4$, 20 mM HEPES and 5.5 mM glucose, pH 7.4), supplemented with 1 mM Ca^{2+}. When EGTA treatment was performed, aequorin measurements were recorded in KRB buffer plus 100 μM EGTA. Stimulation with EGF was performed as specified in the figure legends. The experiments were terminated by lysing the cells with 0.01% Triton in a hypotonic Ca^{2+}-rich solution (10 mM $CaCl_2$ in H_2O), thus discharging the remaining aequorin pool. The light signal was collected and calibrated into [Ca^{2+}] values, as previously described [179]. Extents of Ca^{2+} waves were expressed as area under the curve (AUC) and maximal value of peak in box plot graphs. Statistical analysis was performed using GraphPad Prism.

3.7.2. GCaMP

GCaMP measurements were performed using a more sensitive Ca^{2+}-probe, GCaMP6f. GCaMPs were developed for imaging rapid Ca^{2+} peaks, like the one observed at ER-PM NCE contact sites. To localize the probe to the PM, where NCE contact sites are formed, we added the same tag (SNAP25) as used for Aequorin [178]. Cells were grown on 24-mm coverslips and transfected with the construct 48 h prior to the acquisition of images. For image acquisition, cells were washed and supplemented with 1 mM Ca^{2+}/KRB. To determine the PM Ca^{2+} response, cells were placed in an open Leyden chamber on a 37°C thermostat-controlled stage and exposed to 494/402 nm wavelength light using the Olympus xcellence multiple-wavelength high-resolution fluorescence microscopy system equipped with an ORCA ER CCD camera (Hamamatsu Photonics) and an Uplan FLN 40X oil objective (Olympus). After registration of baseline ratio, cells were stimulated with EGF, TGF-α and AREG at the indicated concentrations. Fluorescence data collected were expressed as emission ratios. The extent of Ca^{2+} peaks was expressed as AUC in box plot graphs. Statistical analysis was performed using GraphPad Prism. One-way ANOVA was used to calculate statistical significance between different samples.

3.8. Immunofluorescence assays

For immunofluorescence (IF) experiments, cells were plated on glass coverslips the day before the experiment. For PLCγ-HA recruitment to PM upon EGF stimulation, cells were serum starved for 2 h prior to stimulation for 1 min with 100 ng/ml of EGF-Alexa-488. Then, cells were transferred on ice, washed with ice-cold PBS and fixed in 4% paraformaldehyde for 10 min, washed with PBS and permeabilized in 0.1% Triton X-100, 1% BSA/PBS for 8 min at RT. To prevent non-specific binding of the antibodies, cells were then incubated with blocking solution (1% BSA/PBS) for 30 min at RT. Next, cells were incubated for 1 h with primary antibody in blocking solution (anti-HA 1:5 000), washed 3 times with 1X PBS and incubated for 30 min with fluorescently-labeled secondary antibodies. After 3 washes with PBS, nuclei were DAPI-stained for 5 min and washed again 3 times with 1X PBS. Coverslips were mounted with glycerol mounting media. Images were obtained using a Leica TCS SP8 confocal

microscope equipped with a 63X oil objective (Leica HCX PL APO CS, 1.4NA) and processed using ImageJ (see **Table 5** for list of antibodies employed).

3.8.1. EGF and Tf internalization assays

HeLa cells, plated on glass coverslips, were incubated at 37°C for the indicated times with indicated doses of Alexa-EGF or Alexa-Tf. When indicated, cells were treated with acid wash (100 mM Glycine-HCl, pH 2.2) 3 times for 45'' at 4°C, in order to visualize only internalized ligand. Samples were then washed and fixed. After permeabilization, nuclei were stained with DAPI. Images were obtained using Leica TCS SP8 confocal microscope equipped with a 63x oil immersion objective using a 1024x1024 scan format and a 2.5x optical zoom (74 nm pixel size). EGF or Tf signal was highlighted applying an intensity-based threshold (Default method), and then fluorescence intensity per field was calculated using the "Measure" command, limiting measurement to threshold. This value was then divided for the number of nuclei in the field, counted using the DAPI signal, in order to calculate the EGF or Tf fluorescence intensity per cell. Data are the mean ±SD, calculated on ~5-10 different fields.

3.8.2. *In vivo* CD147 internalization assay

For antibody internalization assays, cells were incubated with anti-CD147 antibody for 30 min at 4°C. Cells were then stimulated with high doses of different ligands (Alexa-EGF, EGF, TGF-α, AREG or HGF) at 37°C for the indicated times. As a control, we also incubated CD147 in the absence of ligands and we observed no detectable CD147 internalization. After internalization, cells were acid wash-treated as previously. Cells were then fixed and processed for IF. After permeabilization, proteins of interest (EGFR, GLUT1, MCT1, HGFR) were labeled with adequate primary antibodies in 1% BSA/PBS, followed by incubation with specific secondary antibodies. Alexa-488 secondary antibody was used to label the internalized CD147 antibody.

Images were acquired with a Leica TCS SP8 confocal microscope equipped with a 63x oil immersion objective using a 1024x1024 scan format and a 2.5x optical zoom (74 μm pixel size). Quantification of CD147 internalization was done using Fiji plugin or intensity-based threshold method. Fiji plugin was used to quantify only CD147 fluorescence density from

EGFR-positive vesicles, as described before [63]. Briefly, plugin was developed to calculate CD147 integrated fluorescence intensity per cell (expressed as arbitrary units). We used the Alexa-EGF signal to identify EGFR-positive vesicles. In order to enhance the signal *vs.* background and identify the vesicles, the image was filtered with a Laplacian of Gaussian filter [using the FeatureJ-Laplacian plugin with a smoothing scale parameter of 2], then a histogram-based threshold was applied. The threshold ($Thr_{vesicle}$) is calculated with this formula: $Thr_{vesicles} = I_{max} - 0.05 * (I_{max}-I_{mode})$, where I_{max} is maximum intensity and I_{mode} is the mode intensity of the histogram. Only those pixels that deviate from the maximum intensity by less than 5% of the difference between the maximum intensity and the mode intensity were considered to belong to a vesicle. We then measured the CD147 integrated fluorescence intensity within the recognized vesicles for each field. This value was then divided for the number of nuclei in the field, in order to calculate the CD147 integrated fluorescence intensity per cell. The nuclei were identified using the DAPI signal and their boundaries were outlined by applying a histogram normalization and then an intensity-based threshold (Li method). When it was not possible to identify EGFR-positive vesicles (e.g., upon stimulation with different ligands) CD147 signal was highlighted applying an intensity-based threshold (Default method), and then fluorescence intensity per field was calculated using the "Measure" command, limiting measurement to threshold. This value was then divided for the number of nuclei in the field, counted using the DAPI signal, in order to calculate the CD147 fluorescence intensity per cell. Data are the mean ±SD, calculated on ~5-10 different fields. Data are the mean ±SD, calculated on ~5-10 different fields.

3.9. Super-resolution microscopy

HeLa cells overexpressing PLCγ-HA were plated on 35 mm dish, No. 1.5 Coverslip, 14 mm Glass Diameter (MatTek). On the following day, cells were serum starved for 2 h and stimulated with 100 ng/ml of the indicated ligand for 1 min. Immediately after stimulation, cells were transferred on ice, washed with ice-cold PBS and fixed in 4% paraformaldehyde for 10 min, washed with PBS and permeabilized in 0.1% Triton X-100 in 1% BSA/PBS for 8 min at RT. To prevent non-specific binding of the antibodies, cells were then incubated with blocking solution (1% BSA/PBS) for 30 min at RT. After permeabilization, staining was performed with appropriate antibodies against proteins-of-interest (EGFR, HA, RTN3, CLATH) or with Alexa-

tagged CTxB (Thermofisher) in 1% BSA/PBS, followed by incubation with specific secondary antibodies. Samples were post-fixed in 4% paraformaldehyde and analyzed by direct stochastic optical reconstruction microscopy (dSTORM). Briefly, super-resolution localization imaging is based on blinking on and off of the fluorescent molecules induced by reducing agents included in the imaging medium [180]. If few molecules are fluorescent at each time point, meaning that the diffraction limited spots corresponding to individual fluorophores are well separated, the position of each molecule can be quantified with higher accuracy than the resolution limit [181]. By acquiring multiple images of the same field (tens to hundreds of thousands) and storing the position of the localized molecules at each frame, it is possible to obtain an image of the sample with a resolution higher than the diffraction limit.

Imaging was performed on a super-resolution Nikon N-STORM microscope configured for oblique incidence excitation (N-STORM module 2, Nikon instruments) in STORM buffer [Buffer A: 10 mM Tris (pH 8.0) + 50 mM NaCl], an oxygen-scavenging system "GLOX" [56 mg/mL glucose oxidase (Sigma-Aldrich), 3.4 mg/mL catalase (Sigma-Aldrich) and 1M Mercaptoethylamine (MEA) (Sigma-Aldrich)]. Alexa-Fluor 647 dye was excited by using 647 nm laser (120 m Watts nominal power), while Cy3 was excited with a 561 nm laser (70 m Watts) (LU-NV laser unit, Nikon instruments, Tokyo, Japan). 15,000 frames were collected for each channel with 20 ms exposure time. Only localization events occurring at the periphery of the cell were considered (within 40 nm from the PM). Image cross-correlation spectroscopy (ICCS), for nanoscale colocalization analysis was performed as described [182]. Briefly, image cross correlation functions were obtained by averaging over the pixels contained in a selected region of interest. The amplitude parameters from the resulting curves were employed to calculate two coefficients of localizations whose arithmetic mean provides the colocalizing fraction fICCS – cross correlation coefficient. For visualization purposes, the super-resolution images were reconstructed by rendering each of the detected molecules as a Gaussian distribution, with width equal to the localization precision of each event.

3.10. Immunoelectron Microscopy

EGFR-containing endocytic structures (CCPs and TIs) were identified by EM. Serum-starved cells, knocked down for indicated proteins, were incubated with anti-EGFR 13A9, followed by incubation with rabbit anti-mouse, and, finally, with Protein-A Gold 10 nm (30 min incubation

on ice/each step). Cells were then incubated at 37°C for 2 min with 30 ng/ml EGF. A control sample left at 37°C for 5 min without EGF was included in the experiment to control that no internalization was induced by the antibody in the absence of ligand. Cells were then washed in PBS and fixed for 1h at RT in 1.2% glutaraldehyde in 66 mM sodium cacodylate buffer pH 7.2 containing 0.5 mg/ml of ruthenium red. After quick washes with 150 mM sodium cacodylate buffer, the samples were post-fixed in 1.3% osmium tetroxide in a 66 mM sodium cacodylate buffer (pH 7.2) containing 0.5 mg/ml ruthenium red for 2h at RT. Cells were then rinsed with 150 mM Na-cacodylate, washed with distilled water and enbloc stained with 0.5% uranyl acetate in dH20 overnight at 4°C in the dark. Finally, samples were rinsed in dH2O, dehydrated with increasing concentrations of ethanol, embedded in Epon and cured in an oven at 60°C for 48 h.

3.10.1. Preparation of PM sheets and gold labeling

Preparation of PM sheets was described previously [183]. The coverslips were rapidly chilled by immersion in ice-cold Hepes buffer (25 mM Hepes, pH 7, 25 mM KCl, and 2.5 mM MgAcetate) and inverted onto nickel EM grids that had been coated with formvar and carbon and, on the day of the experiment, glow-discharged and floated on poly-L-lysine (0.8 mg/ml for 30 min, followed by 10 s dH2O rinse and air drying). Pressure was applied to the coverslip for 20 s by bearing down with a cork. The coverslips were lifted, leaving sections of the upper cell surface adherent to the poly-L-lysine–coated grid. Membranes were rinsed in 4°C Hepes buffer and fixed in 2% paraformaldehyde for 10 min. All membranes were labeled from the inside by inverting the grids onto droplets containing primary antibodies or biotin-phalloidin (5 units/ml) followed by gold-conjugated secondary reagents. Incubations were for 30 min. Intermediate washes in PBS were performed by inverting the grids onto droplets. Primary antibody was diluted in PBS, 0.1% BSA at the following concentrations: HA 1:1000. gold-conjugated secondary reagents were diluted 1:20 from commercial stocks in PBS-BSA. The samples were post-fixed in 2% glutaraldehyde in PBS and incubated overnight in PBS. Next, samples were stained for 10 min with 1% OsO4 prepared in 0.1 M cacodylate buffer and washed 5 min with cacodylate buffer and twice for 5 min in dH2O. Samples were then processed for 10 min in 1% aqueous tannic acid, followed by two 5-min rinses with dH2O, 10 min with 1% aqueous uranyl acetate and two 1-min rinses with dH2O. Grids were air-dried and examined using a Hitachi

600 transmission EM. Samples were analyzed employing the Ripley's K function [184] tool that tests spatial randomness of molecules and explains molecular distribution.

3.11. Matrigel MCF10A morphogenetic assay

MCF10A cells were suspended in their culture medium containing 5 ng/ml EGF (instead of 20 ng/ml as in standard medium) and 2% of growth factor reduced Matrigel (Corning). Cells (4000 cells/well) were plated in 8-well chambers (chamber slide system, Lab-Tek II) on a thin layer of Matrigel (~40 µl, previously allowed to solidify on the bottom of the plate). Cells were incubated at 37°C, 5% CO_2 for 10 days. Medium was changed every 3 days. After 10 days, acini were starved for 3 h, stimulated with 500 ng/ml EGF and fixed with 4% paraformaldehyde for 20 min at RT and permeabilized with 0.5% Triton X-100 in PBS for 10 min. Slides were rinsed three times with PBS/Glycine (100 mM), 10 min/wash at RT. Blocking was in 10% donkey serum in PBS (with 0.1% BSA, 0.2% Triton X-100, 0.05% Tween-20). Primary antibodies (anti-CD147, anti-EGFR, anti-pEGFR) were diluted in blocking solution and incubated overnight at 4°C. Secondary antibodies [donkey anti-mouse or anti-rabbit, Alexa-488- or Alexa-647-conjugated (Thermo Fisher); donkey anti-mouse or anti-rabbit Cy3 (Jackson ImmunoResearch)] were diluted 1:200 in blocking solution and incubated for 40 min at RT. Nuclei were counterstained with DAPI. Images were acquired on glass-wells with a Leica TCS SP8 AOBS confocal microscope with Las-X software (v3.5, Leica Biosystems) and processed using ImageJ software (v1.52, NIH).

3.12. Intestinal and mammary primary organoids from mice

The intestines were harvested from 8-15 week-old mice and prepared as described [185]. Briefly, the proximal part of the intestine was collected, opened longitudinally and washed with ice-cold PBS. The luminal side of the intestine was scraped using a glass slide to remove luminal content and villious structures. After a second wash with ice-cold PBS, the intestine was cut into 2–4-mm pieces with scissors. The pieces were transferred to a tube and further washed with cold PBS (5–10 times) with gentle vortexing. Intestinal fragments were incubated in PBS containing 20 mM EDTA, for 20 min on ice. The supernatant was discarded, and cold PBS was

added to the fragments. Crypts were released by manually inverting the tube for 5-10 times. The supernatant was collected and passed through a 70-μm strainer. The remaining tissue fragments were again resuspended in cold 1% FBS PBS and triturated 5–10 times, and the supernatant was passed through a 70-μm strainer. The previous step was repeated once again. The isolated crypts were then pelleted by centrifugation at 100×*g* for 5 min and seeded on top of Matrigel that was previously polymerized to form a droplet. 500 μl of growth medium was added to each well to maintain the culture at 37°C in a humidified incubator with 5% CO_2.

To obtain mammary organoids with a double acini layer, inguinal and thoracic mammary glands from mice of 8-15 weeks of age were used. Bilayered organoids were prepared essentially as described [186], with modifications. Briefly, mammary glands were minced with scissors and partially digested on a rotating wheel (1×*g*) for 1 h at 37°C (5% CO_2) in the following digestion medium: 1:1 mixture of DMEM and Ham's F12 medium (DMEM/F12, Gibco, Life Technologies), 1% penicillin–streptomycin antibiotics, trypsin 2.5% and collagenase type-1a 1 mg/ml (Sigma-Aldrich, Merck Millipore). Then, mammary glands were centrifuged for 5 min at 350 ×*g* and a three-layer suspension was obtained. The liquid interface was discarded, while the fat layer (on the top) was transferred into a new tube, diluted with PBS and centrifuged for 10 min at 350×*g*. The pellet was resuspended in DMEM/F12 and added to the pellet of the first centrifugation. Samples were centrifuged again, and the pellet was treated with ACK lysis buffer (Gibco, Life Technologies) for 1 min to lyse blood cells, followed by dilution with PBS and centrifugation for 5 min at 350×*g*. The pellet was resuspended in mammary epithelial cell growth medium (MEGM) supplemented with the Bullet kit (Lonza) and incubated for 30 min in a cell culture dish to allow the attachment of fibroblasts. Then, supernatant containing non-attached cells was passed through a 40-μm diameter filter, and the filtered organoids were resuspended in MEGM seeded on the top of the Matrigel.

Mammary and intestinal organoids were treated with gefitinib, PPMP and xestospongin C and their growth and morphology were followed using a phase-contrast microscope (Evos) at days 6 and 8. For IF staining of organoids, slides were fixed directly in the 8-well chamber slides with 4% paraformaldehyde for 20 min at RT. Permeabilization was performed with 0.2% Triton X-100 in PBS for 30 min at 4°C and 30 min at RT. Slides were rinsed three times with PBS (10 min/wash at RT). Blocking was in 1% bovine serum albumin in PBS (with 0.1% BSA, 0.2% Triton X-100, 0.05% Tween-20). Primary antibodies (anti-CK-5, anti-CK-8, anti-CD147, anti-EGFR), were diluted in blocking solution and incubated overnight at 4 °C. Secondary antibodies

[donkey anti-mouse or anti-rabbit, Alexa-488- or Alexa-647-conjugated (Thermo Fisher); donkey anti-mouse or anti-rabbit Cy3 (Jackson ImmunoResearch)] were diluted 1:200 in blocking solution and incubated for 2.5h at RT. Nuclei were counterstained with DAPI for 30 min. Images were acquired on glass-wells with a Leica TCS SP8 AOBS confocal microscope with Las-X software (v3.5, Leica Biosystems) and processed using ImageJ software (v1.52, NIH).

3.13. Statistical analysis

Two-sided student's T-test was employed to obtain statistical significance of experimental differences; p-value <0.05 *, p-value <0.01 **, p-value <0.005 ***, p-value <0.001 ****.

4. RESULTS

4.1. Signaling emanating from the EGFR that influences EGFR-NCE

Upon activation of the EGFR by EGF stimulation, several signaling cascades are known to be activated (see **Section 1.2.3**, **Figure 15B**). The major signaling effectors of the EGFR include PI3K-AKT, ERK-MAPK, SHC-Ras, and PLCγ-PKC among others. The aim of our first set of experiments was to determine whether the activation of signaling effectors downstream of the EGF-EGFR ligand-receptor complexes, correlates with the activation of NCE, and therefore could be involved in the regulation of this endocytic pathway.

Interestingly, our results (described in detail below) point to an involvement of the PLCγ pathway in NCE. This pathway is the best-characterized signaling pathway that promotes Ca^{2+} release from the ER [145], which we have shown to be essential for completion of internalization by NCE [63]. PLCγ enzymes are recruited to the activated EGFR and are phosphorylated by it, leading to their activation and the hydrolysis of phosphatidylinositol 4,5-bisphosphate into DAG and IP3. IP3 then binds to the IP3R on the ER leading to Ca^{2+} release [110, 111]. Therefore, we have performed an in-depth characterization of the role of PLCγ in EGFR-NCE.

4.1.1. Specific role of PLCγ2 enzyme in NCE

4.1.1.1. PLCγ enzymes are phosphorylated only upon stimulation with high dose EGF

We investigated which of the EGFR downstream signaling pathways are activated selectively at high dose EGF when NCE occurs. Using HeLa cells, we found that both members of the PLCγ family, PLCγ1 and PLCγ2, are activated selectively upon stimulation with high EGF dose (100 ng/ml) for different time points, at variance with other signaling effectors (e.g., AKT, ERK1/2, SHC) (**Figure 17A**). Moreover, at 2 min of stimulation with increasing doses of EGF, we detected a sharp increase in the EGF-induced phosphorylation of PLCγ enzymes between 3

and 10 ng/ml of EGF, reaching a maximum at 30 ng/ml (**Figure 17B**). This PLCγ phosphorylation dose response was similar to that of the ubiquitination of the EGFR, which increases rapidly above 1 ng/ml EGF reaching a maximum at 10 ng/ml [62]. In contrast, the phosphorylation of SHC can be observed already at low doses of EGF (0.3 ng/ml) (**Figure 17B**).

Thus, the activation of PLCγ appears to correlate with the activation of NCE.

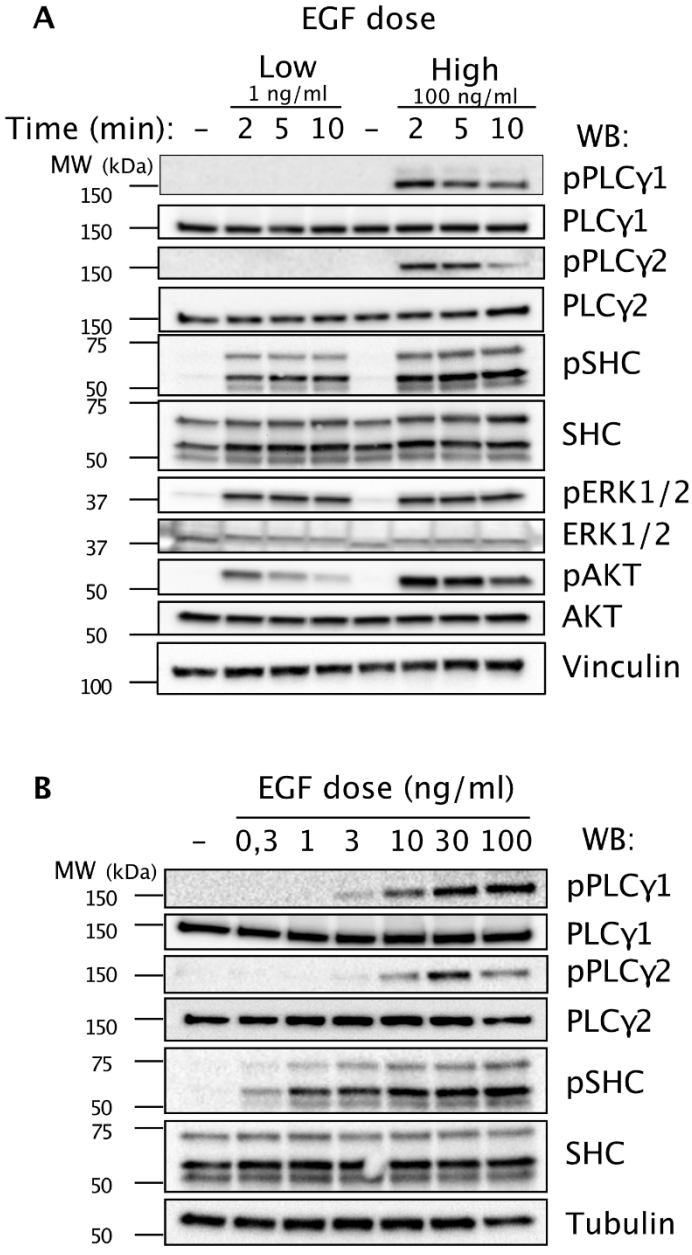

Figure 17. PLCγ1 and PLCγ2 are activated only upon stimulation with high dose of EGF.

A. *HeLa cells were stimulated with low (1 ng/ml) and high (100 ng/ml) EGF concentrations for the indicated time points. Total cellular lysates were analyzed for the indicated signaling effectors by western blot (WB). Vinculin, loading control.* ***B.*** *HeLa cells were stimulated with*

EGF for 2 min at the indicated EGF concentrations. Lysates were subjected to WB as shown. Tubulin, loading control. Data is representative of three independent experiments. MW: Molecular weight markers are shown on the left of the blots.

4.1.1.2. PLCγ2 but not PLCγ1 is critical for EGF-induced Ca^{2+} release

Based on the WB data, we hypothesized that PLCγ enzymes might have a role in NCE, in particular, in EGF-dependent Ca^{2+} signaling at NCE sites. To investigate this possibility, we used the Ca^{2+} probe, aequorin, which upon Ca^{2+} binding emits light that can be measured by a luminescence reader. We previously showed that high, but not low doses of EGF were able to induce a localized Ca^{2+} wave in proximity of the PM, detected using a PM-targeted aequorin probe [63].

Interestingly, using this probe, we observed that only PLCγ2 seems to have a specific role in the activation of EGF-dependent Ca^{2+} signaling at NCE sites, since the increase in intracellular Ca^{2+} concentration at the PM under high EGF conditions was abolished upon PLCγ2 knockdown (KD), but not PLCγ1 KD (**Figure 18A, B**). As a control, we also performed the KD of the Ca^{2+} channel on the ER, IP3R, which as expected completely inhibited EGF-dependent Ca^{2+} signaling similarly to PLCγ2 KD (**Figure 18A, B**), consistent with our previously published data [63]. The efficiency of KD of PLCγ1, PLCγ2 and IP3R was confirmed by WB (**Figure 18C**).

Thus, the activation of PLCγ2 downstream of EGFR activation appears to have a critical role in the generation of Ca^{2+} wave at the PM, which we know is essential for the completion of the NCE pathway [63].

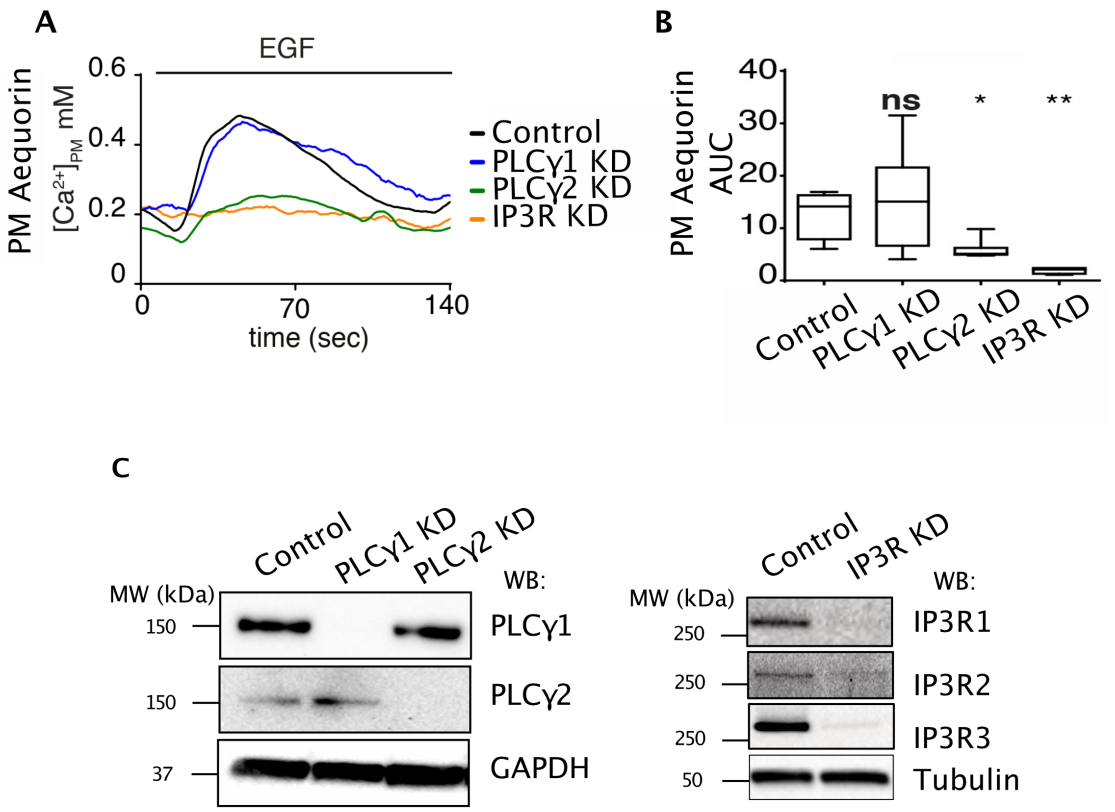

Figure 18. PLCγ2 KD inhibits EGF-induced calcium signaling at the PM.

A. *HeLa cells were transfected with PM-targeted aequorin, subjected to the indicated KD and stimulated with high dose EGF (100 ng/ml). The kinetics of Ca^{2+} release at the PM was measured by a luminescence reader.* ***B.*** *Quantification of the Ca^{2+} response shown in "A". The area under the curve (AUC) ± SD of an experiment performed in triplicate (bottom). P-value, Student's t-test two tailed; *, P<0.05; **, P<0.01. ns, not significant.* ***C.*** *Efficiency of the indicated KDs was assessed by WB. KD of three IP3R isoforms is shown. GAPDH and tubulin, loading controls. MW: Molecular weight markers are shown on the left. The experiments were performed with the help of Elisa Barbieri and Giusi Caldieri from our lab, in collaboration with Prof. Paolo Pinton's Lab (Section of Pathology, Oncology and Experimental Biology, and Laboratory for Technologies of Advanced Therapies Center, Department of Morphology, Surgery and Experimental Medicine, University of Ferrara, Ferrara, Italy).*

4.1.1.3. PLCγ2 but not PLCγ1 is critical for internalization of the EGFR by NCE

To understand the role of PLCγ enzymes in EGFR endocytosis, we followed EGFR internalization using the radiolabeled iodinated EGF ligand, ^{125}I-EGF, in HeLa cells upon KD of the PLCγ1 and PLCγ2 alone or in combination with clathrin KD. As a control of inhibition of EGFR endocytosis, we also used the KD of clathrin to inhibit CME and of dynamin to inhibit both CME and NCE.

After stimulation with low dose EGF (1 ng/ml), the KD of clathrin resulted in marked decrease (~70%) of EGF internalization compared to control (**Figure 19A**). The fact that internalization was not completely inhibited by clathrin KD can be explained by an incomplete KD of the protein, allowing some CME to occur. Alternatively, the data could be consistent with the existence of a clathrin-independent endocytic route that is mediating EGFR endocytosis at low EGF ligand concentrations, possibly the constitutive pathway of EGFR endocytosis [62].

At high dose EGF (30 ng/ml), clathrin KD reduced EGF internalization by ~45% (**Figure 19B**). These data are consistent with EGFR being internalized by both CME and NCE at high EGF doses [74].

Next, we assessed the role of PLCγ enzymes, both at high and low doses of EGF, in order to clarify whether they have a specific role in EGFR-NCE. At low dose of EGF, KD of PLCγ1 or PLCγ2 did not affect EGF internalization in comparison with control cells (**Figure 19A**). Interestingly, at high dose of EGF, PLCγ2 KD reduced the internalization of EGF by ~35% that is compatible with the inhibition of NCE (**Figure 19B**). This effect of PLCγ2 KD was specific since PLCγ1 KD at high EGF dose did affect EGF internalization (**Figure 19B**).

These findings are consistent with PLCγ2 having an essential role in EGFR-NCE.

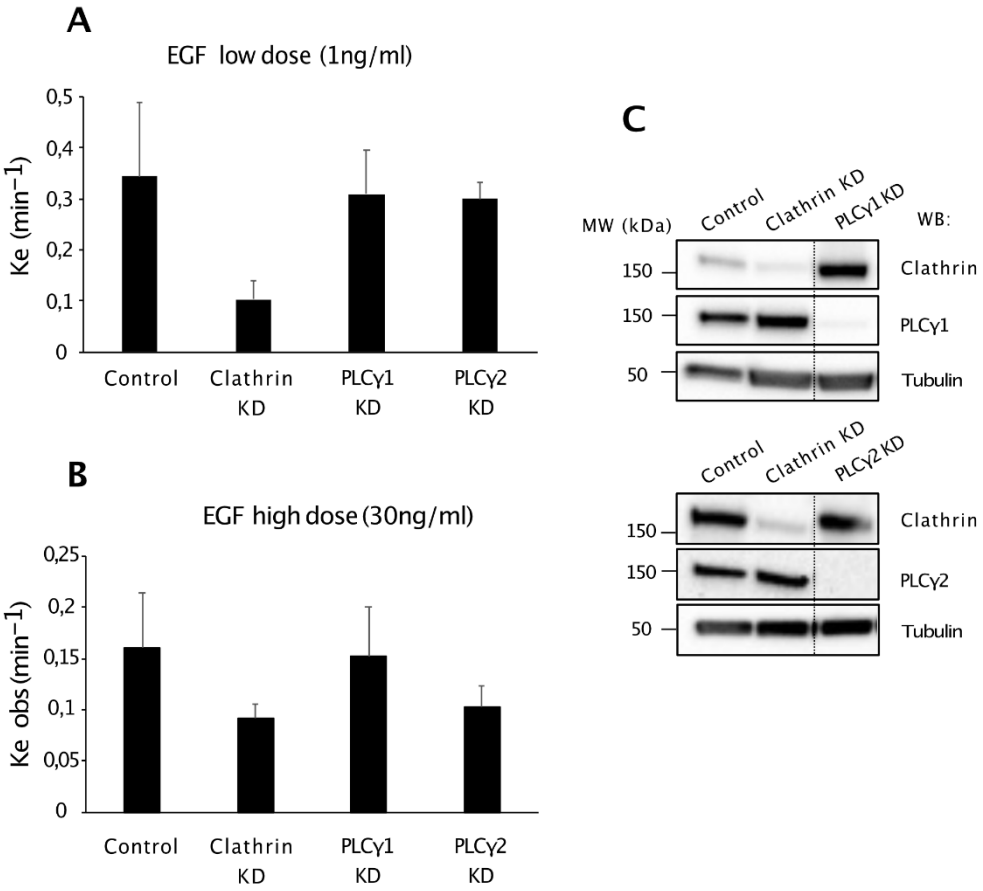

Figure 19. PLCγ2 KD selectively inhibits EGF internalization after stimulation of cells with high, but not low, EGF concentrations.

A.-B. *Kinetics of ^{125}I- EGF internalization at high (**A.**) or low (**B.**) doses were followed at early time points (0-8 min) upon KD of the indicated proteins in HeLa cells. Internalization constants (Ke) were extrapolated from the internalization curves and correspond to the slopes of the best-fitting curves.* ***C.*** *Efficiency of the indicated KDs was assessed by WB. The blot shows samples from the same membrane, but splicing out irrelevant lines (indicated by dotted line). Tubulin, loading control. MW: Molecular weight markers are shown on the left. Experiments are average of two biological replicates. Experiments were performed with the help of Giusi Caldieri from our lab*

In agreement, confocal fluorescence microscopy analysis of HeLa cells stimulated with high dose of fluorescently labeled ligand, Alexa-555-EGF, for 8 min confirmed that PLCγ2 KD alone is able to inhibit the internalization of EGF and of the NCE-specific cargo, CD147 (**Figure**

20A-C). CD147 internalization was assessed *in vivo* by IF as described previously [63]. In contrast, PLCγ1 KD did not show any impairment of EGF or CD147 internalization (**Figure 20A-C**), confirming that it does not play a functional role in NCE.

The inhibition of CD147 internalization by PLCγ2 KD was quantitatively comparable to that achieved upon KD of IP3R (**Figure 20B**), arguing that the role of PLCγ2 in NCE is exerted through the IP3 second messenger and Ca^{2+}. These results are in line with our previous data showing that Ca^{2+} is required for NCE [63].

To provide further confirmation that PLCγ2 has a specific role in NCE and not CME, we investigated the effect of its KD on the internalization of the CME-specific cargo, Tf, using the fluorescently labeled ligand, Alexa-488-Tf. The results clearly showed that PLCγ2 KD, as well as that PLCγ1 KD, did not affect Tf internalization (**Figure 20D, E**).

Thus, these results confirm the relevance and specificity of PLCγ2 function in EGFR/CD147-NCE.

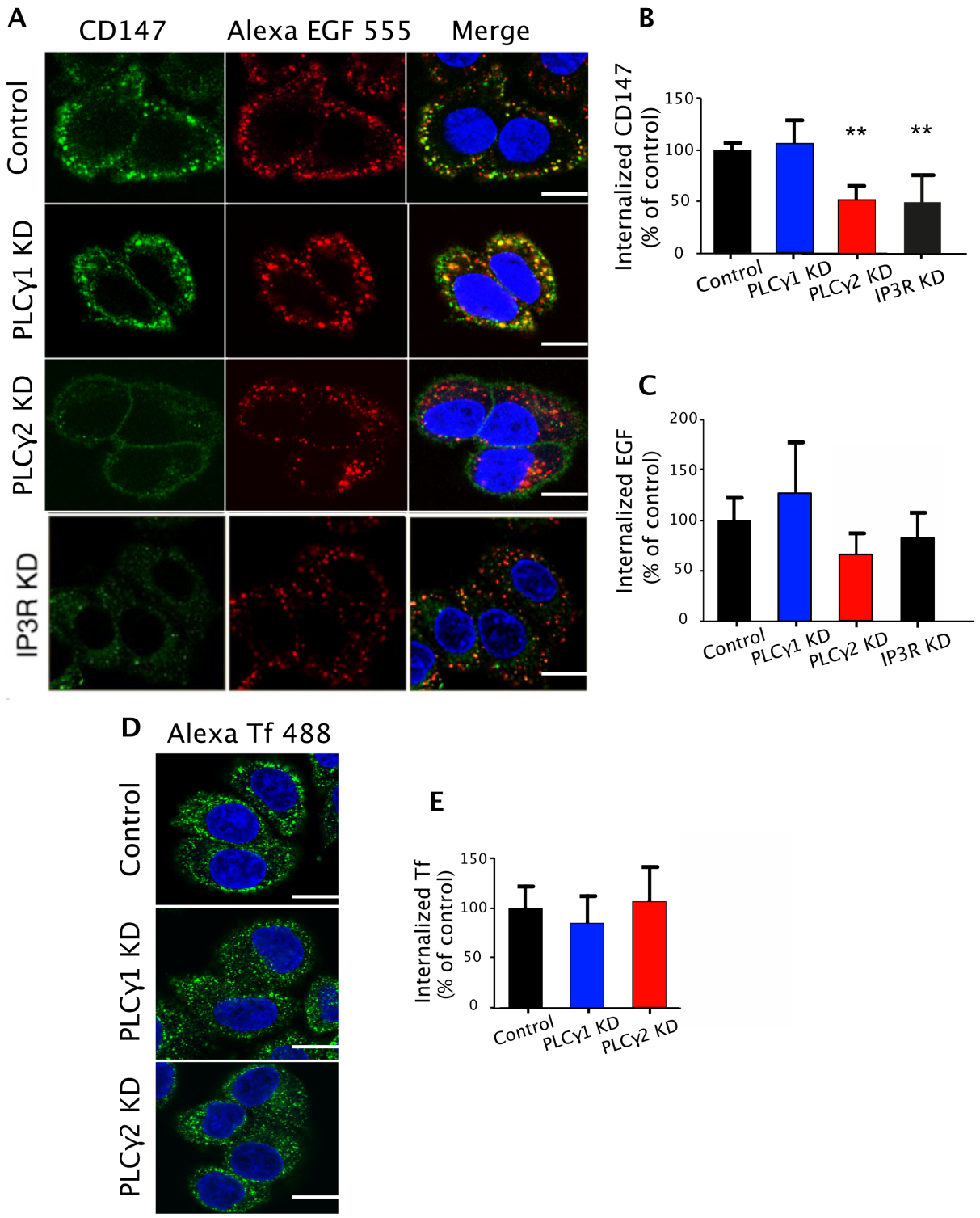

Figure 20. PLCγ2 KD and inhibition of IP3R inhibit EGF-induced CD147 internalization.

A-C. *HeLa cells were subjected to the indicated KD. Cells were then stimulated with high dose Alexa-555-EGF (~30 ng/ml, red) for 8 min and EGF and CD147 internalization were followed in vivo by confocal fluorescence microscopy. Alexa-555-EGF internalization was measured directly while CD147 internalization was measured by IF using an anti-CD147 antibody as*

previously described [63]. Cells were subjected to an acid wash treatment prior to fixation to remove the PM-bound antibody. Internalized CD147 was revealed with an Alexa-488 secondary antibody (green) on permeabilized cells. Blue, DAPI. Bar, 20 μm. ***B.*** *Internalized CD147 was quantified with an ad hoc designed ImageJ macro. Mean integrated fluorescence intensity ± SD is reported as % of control cells. P-value, Student's t-test two-tailed; **, P<0.01, in comparison with control.* ***C.*** *Internalized EGF was quantified using ImageJ program. Alexa-555-EGF signals were highlighted applying an intensity-based threshold (Default method), and then fluorescence intensity per field was calculated using the "Measure" command, limiting measurement to the threshold. This value was then divided by the number of nuclei in the field, counted using the DAPI signal, to calculate the EGF fluorescence intensity per cell. Mean integrated fluorescence intensity ± SD, reported as % of control cells.* ***D.*** *HeLa cells as in "A" were stimulated with Alexa-488-Tf (50 μg/ml, green) for 8 min and subjected to acid wash before fixation. Internalization of Tf was followed by confocal fluorescence microscopy (**D**) and quantified (**E**) as described in "C". Blue, DAPI. Bar, 20 μm. Experiments were performed in biological triplicate with the help of Giusi Caldieri and Deborah Salvi Mesa from our lab.*

4.1.1.4. PLCγ2 is required for the fission of NCE tubular invaginations

Given the requirement of PLCγ2 for EGF induced Ca^{2+} wave generation at the PM (**Figure 18A, B**) and the known involvement of Ca^{2+} signaling in the fission of NCE TIs [63], we hypothesized that PLCγ2 is specifically involved in TI fission, rather than initiation and elongation. To investigate this, we performed EM experiments employing gold-labeled EGFR to visualize EGFR internalizing structures (*i.e.,* CCPs, NCE TIs) in cells stimulated with high dose EGF for 5 min. KD of PLCγ1 and PLCγ2 did not affect the number of TIs indicating that they are not involved in TI formation (**Figure 21A**). However, PLCγ2 KD increased the ratio of long (>300 nm) *vs.* short TIs (150-300 nm), while PLCγ1 KD caused only a minor increase that was statistically non-significant (**Figure 21B, C**). The effects of PLCγ2 KD were comparable to those achieved upon inhibition of the IP3R by xestospongin C [63] arguing that PLCγ2 exerts its role in NCE through the IP3 second messenger and Ca^{2+} (**Figure 21C**). The KD of dynamin, which we previously showed is involved in the fission step of NCE [63], also caused a similar increase in long *vs.* short TIs, consistent with an involvement of PLCγ2 in TI fission (**Figure**

21C). No significant effects of PLCγ1 and PLCγ2 KD were observed on number or length of EGFR-containing CCPs (**Figure 21D**), confirming the selective functional involvement of PLCγ2 in NCE over CME. Thus, these results support a scenario where the PLCγ2/IP3 circuitry and Ca^{2+} appear to be required for NCE-TI fission, in concert with the action of dynamin.

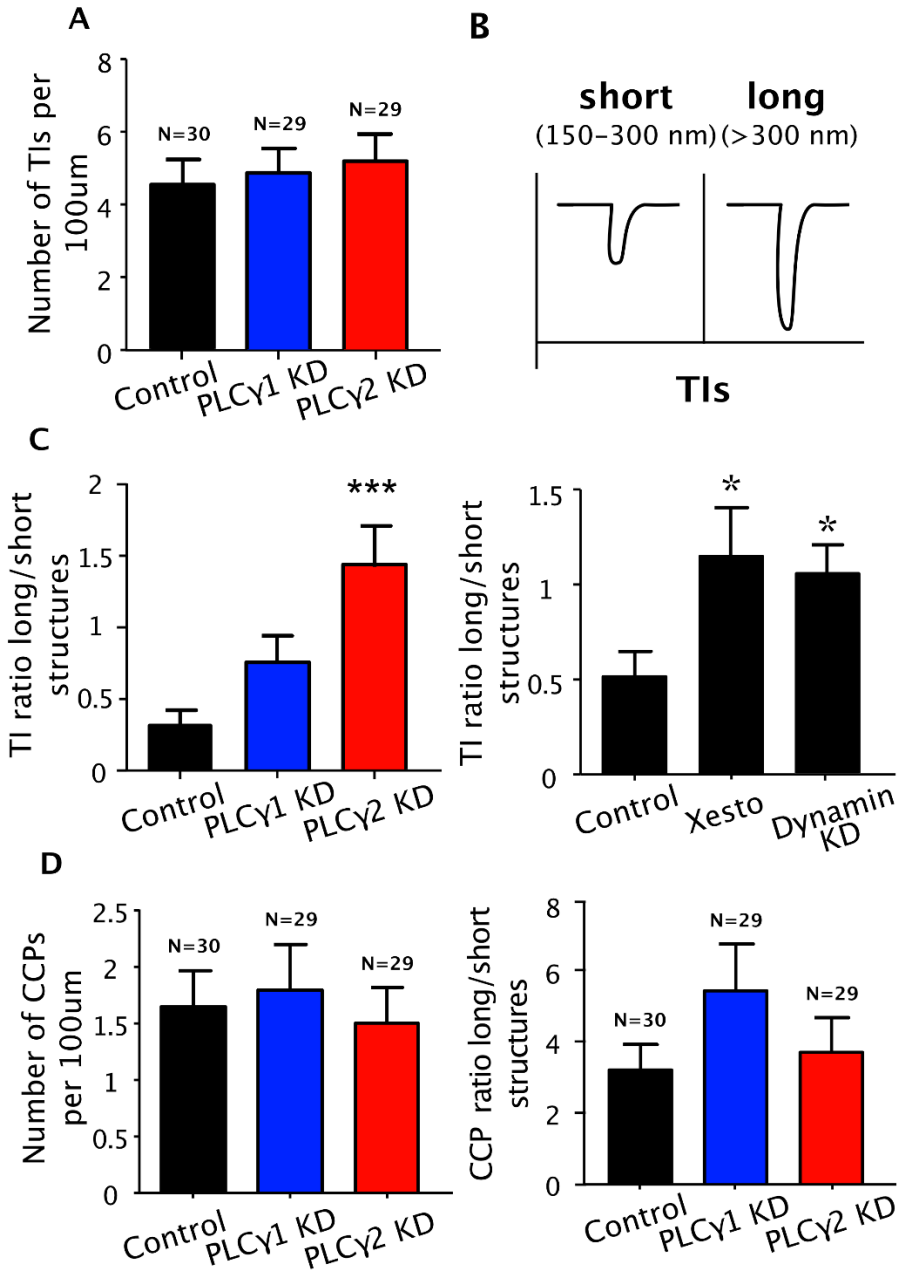

Figure 21. PLCγ2 is required for NCE-TI fission.

A. *HeLa cells were subjected to the indicated KD and stimulated with high dose EGF (30 ng/ml) for 5 min. NCE TIs were quantified using gold-labeled EGFR and EM. Data are expressed as the number of gold-positive structures, normalized to PM profiles of 100 μm length ± SEM.* ***B.***

Definition of short and long TIs used for morphometric analysis of the length of EGFR gold-positive TIs. ***C.*** *Right, the ratio of long to short TI structures was quantified in HeLa cells as in "A". Left, the effects of dynamin KD or xestospongin C (Xesto) treatment (2 μM for 16 h) were also analyzed and used as a positive control for TI fission inhibition. Data are expressed as normalized to PM profiles of 100 μm length ± SD.* ***D.*** *Quantification of the number of EGFR gold-labeled CCPs (left) and the ratio of long to short CCPs (right) in cells treated as in "A". N, cell profiles analyzed. P-value, Student's t-test two-tailed; *, P<0.05; ***, P<0.005. Experiments were performed with the help of Elisa Barbieri and Giusi Caldieri from our lab, and Andrea Raimondi from Prof. Carlo Tacchetti's Lab (Centro Imaging Sperimentale, San Raffaele Scientific Institute, Milan, Italy).*

4.1.2. What is the basis of PLCγ2 specificity?

4.1.2.1. Generation of stable HeLa cell lines expressing HA-tagged PLCγ1 or PLCγ2

The specificity of PLCγ2 in NCE was unexpected since PLCγ1 is the best-characterized member of this enzyme family and is widely expressed, while PLCγ2 displays a more restricted and regulated expression, dependent on cellular context, with a prominent role in immune cells platelets [151, 158].

To investigate the nature of PLCγ2 specificity in NCE, we first needed to generate experimental tools for studying this enzyme. Due to the lack of antibodies against the total and phosphorylated forms of PLCγ2 that are suitable for IF assays, we generated stable HeLa transfectants expressing HA-tagged PLCγ1 or PLCγ2 in the WT HeLa background or in a HeLa clone (referred to as "clone 53") stably transfected with a doxycycline-inducible clathrin KD system [63] (that will serve us for future examination of role of PLCγ2 in clathrin KD condition). We verified that these populations express similar levels of PLCγ1-/PLCγ2-HA by WB (**Figure 22A**). Then, we evaluated the EGF-induced phosphorylation of HA-tagged PLCγ1 or PLCγ2 by EGF, as well as EGFR phosphorylation upon stimulation with high dose EGF for 2 and 10 min. WB analysis of total cellular lysates revealed no change in the phosphorylation of EGFR (at pY992 and pY1068) in HeLa-PLCγ1-HA (**Figure 22B**) or HeLa-PLCγ2-HA (**Figure 22C**) cells compared with the EV control implying that EGFR activation is not affected by overexpression of the HA-tagged PLCγ forms. EGF-induced phosphorylation of PLCγ1-HA (**Figure 22B**) and

PLCγ2-HA (**Figure 22C**) was also detectable indicating that the HA-tag is not interfering with the post-translation modification.

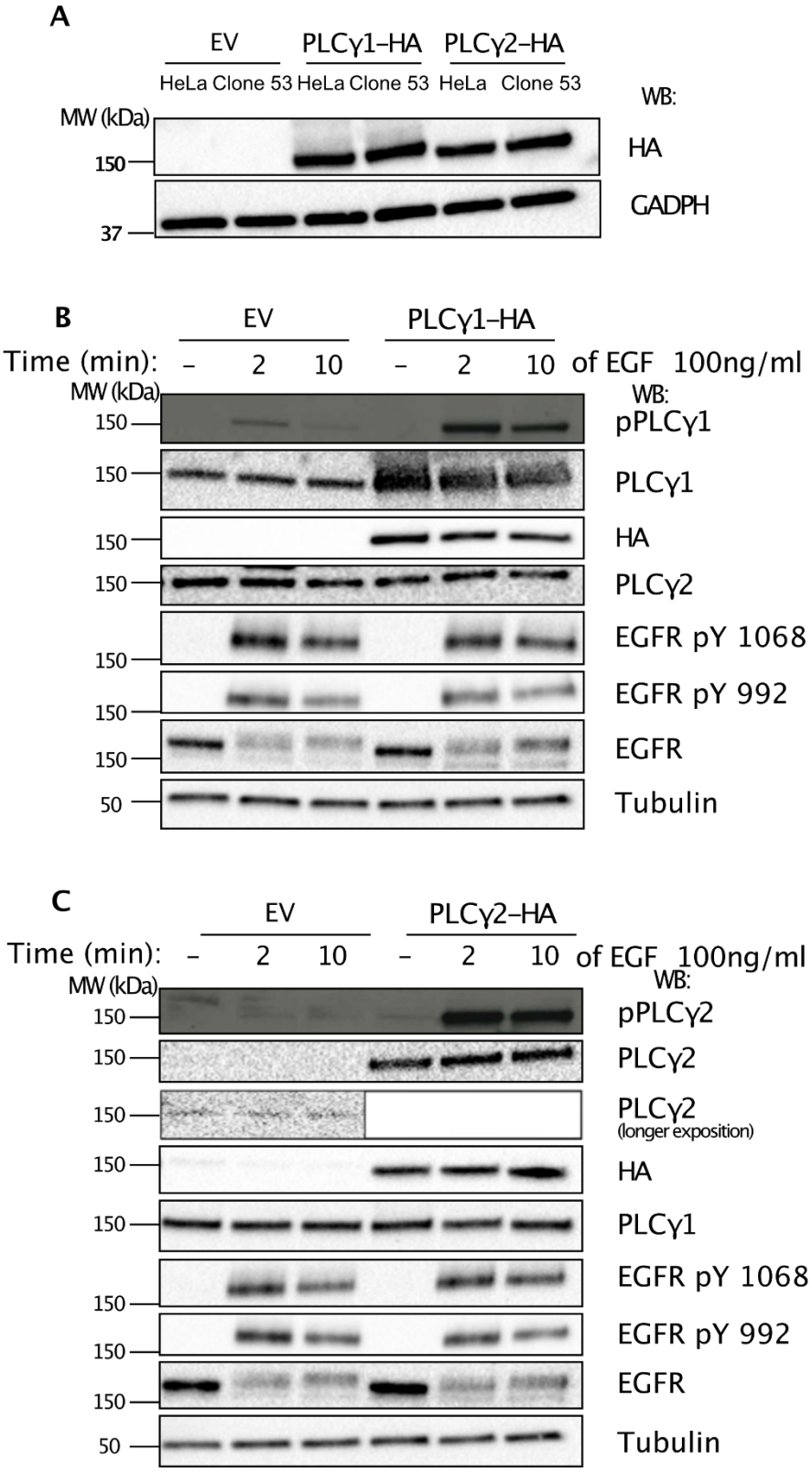

Figure 22. Characterization of HeLa cell lines expressing HA-tagged PLCγ enzymes.

A. *Western blot (WB) analysis of levels of expression of HA-tagged PLCγ enzymes in stable HeLa clones derived from a WT HeLa (HeLa) background or clone 53 transfected with a doxycycline-inducible clathrin KD system. HA was detected using anti-HA antibody. GAPDH is a loading control.* ***B-C.*** *WB analysis of the phosphorylation of EGFR (pY992, pY1068) and HA-tagged PLCγ1 (B) or PLCγ2 (C) in the indicated stable WT HeLa clones upon stimulation with high dose EGF (100 ng/ml) for the indicated times. EV, empty vector control. Tubulin is a loading control. MW: Molecular weight markers are shown on the left. Experiments are performed once.*

Having generated the stable PLCγ-HA clones, we used them to investigate whether EGF treatment affects the subcellular localization of PLCγ enzymes. After stimulation with high dose Alexa-555-EGF (100 ng/ml), cells were fixed and the localization of PLCγ enzymes was determined using the anti-HA antibody and a fluorophore (Alexa-488)-labeled secondary antibody. In unstimulated cells, both enzymes showed homogenous localization in the cytosol, while after high dose EGF stimulation, relocalization to the PM was evident, with colocalization of PLCγ enzymes and EGF (**Figure 23**).

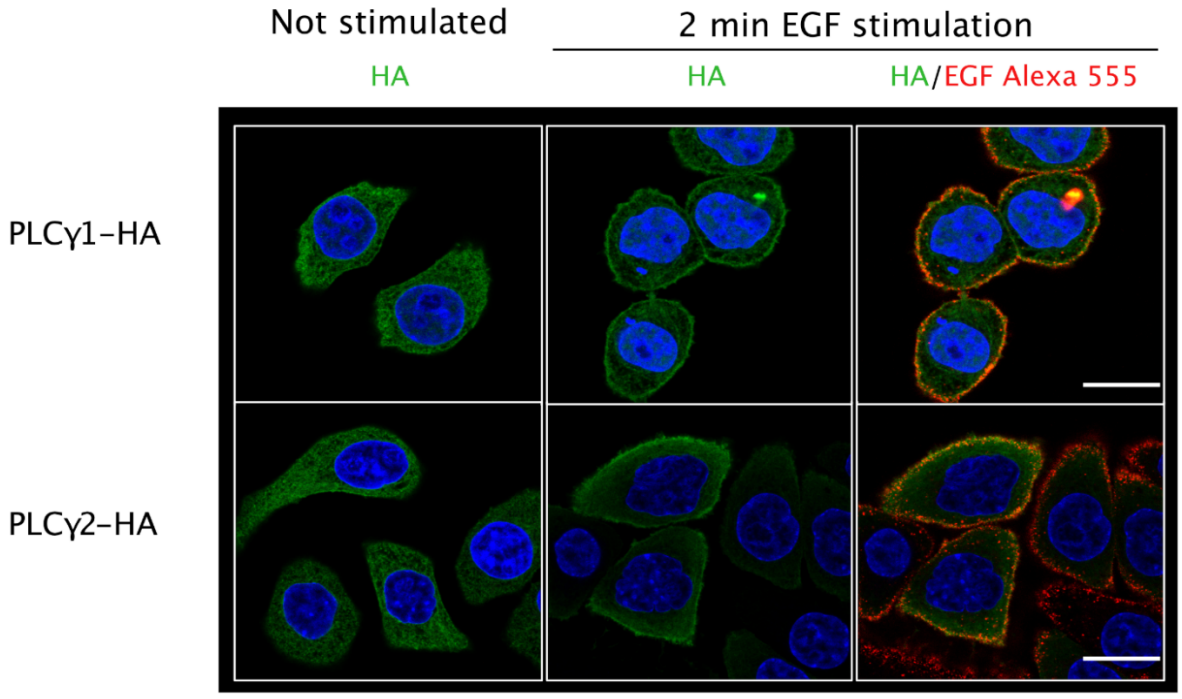

Figure 23. PLCγ recruitment to PM upon EGF stimulation.

The effect of EGF stimulation on the subcellular localization of PLCγ-HA enzymes in stable HeLa clones. Immunofluorescence was performed with the mouse anti-HA antibody and the Alexa-488 anti-mouse secondary antibody (green). Left panels: unstimulated cells. Middle panels: 2 min stimulation with high dose Alexa-555-EGF. Right panels: merge of Alexa-555-EGF (red) and Alexa-488 (green). Blue, DAPI. Bar, 20 μm.

4.1.2.2. PLCγ1 *vs.* PLCγ2 specific modifications - phosphorylation

Previously, we showed that both PLCγ enzymes are phosphorylated only upon stimulation with high doses of EGF (**Figure 17**). We decided to check whether the PLCγ phosphorylation status in HeLa cells is altered upon depletion of different NCE or CME regulators: RTN3 (NCE is inhibited), AP2 (CME is inhibited) and Cbl (NCE is inhibited). RTN3 KD and AP2 KD did not affect phosphorylation of PLCγ1, PLCγ2 or EGFR, the latter measured as phosphorylation of the EGFR Tyr residues pY1173 and pY992 (**Figure 24**). In contrast, Cbl KD reduced both PLCγ1 and PLCγ2 phosphorylation. However, since it also reduced the levels of total and phosphorylated EGFR, other RNAi oligos will be tested to verify whether this is a specific effect of Cbl KD or not. In either case, these results are not very promising for our investigation on the differential roles of PLCγ1 and 2, since Cbl KD affects equally the activation of both enzymes.

Since no difference between the phosphorylation of PLCγ1 and PLCγ2 were scored, these data suggest that the activation of these enzymes is not affected by their recruitment to specific endocytic structures and it is likely that PLCγ activation occurs upstream of the two endocytic pathways.

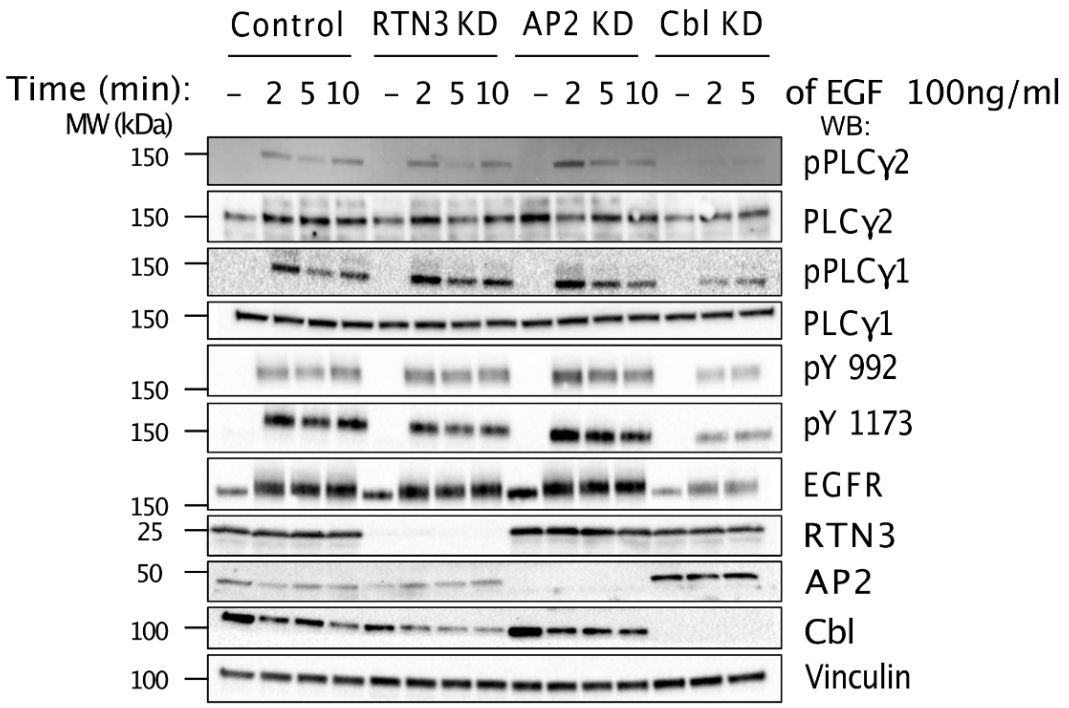

Figure 24. PLCγ phosphorylation upon inhibition of CME or NCE

HeLa cells were subjected to the indicated KD and treated with 100 ng/ml of EGF for indicated time points. Lysates were analyzed by western blot (WB) for the expression of the indicated endocytic proteins and signaling effectors. Vinculin, loading control. Experiment was perfomed once.

4.1.2.3. PLCγ1 *vs.* PLCγ2 specific modifications – ubiquitination and binding to Ub

Given that EGFR ubiquitination is the signal triggering EGFR-NCE, we investigated whether PLCγ1 and PLCγ2 have different Ub-binding abilities by performing *in vitro* pulldown assays. To this aim, total cellular lysates of HeLa cells stably expressing HA-tagged PLCγ1 or PLCγ2 were subjected to pulldown assays with a linear chain of three Ub moieties fused to GST (GST-3Ub) or with GST alone as a specificity control. As a positive control, we tested the efficacy of GST-3Ub to pulldown proteins known to bind Ub: 1) Eps15 from lysates of cells expressing Eps15-HA; and 2) endogenous Rabex-5 from lysates of cells expressing PLCγ1-HA or PLCγ2-HA. Our data show that while Eps15 and Rabex-5 were able to bind specifically to GST-3Ub as expected, PLCγ1-HA and PLCγ2-HA appeared to bind to GST alone and this binding did not

change in the GST-3Ub pulldown (**Figure 25A**). This result suggests that PLCγ1 and PLCγ2 do not bind significantly to Ub.

We then tested whether PLCγ1, PLCγ2 and Eps15 (as a positive control) undergo ubiquitination after high dose EGF stimulation of HeLa cells stably expressing the HA-tagged versions of these proteins. HA-tagged proteins were then immunoprecipitated from cell lysates and immunoprecipitates were assessed for ubiquitination by an anti-Ub WB. While Eps15 ubiquitination was found to increase upon EGF stimulation, as previously reported [127], PLCγ1 and PLCγ2 did not appear to be ubiquitinated in response to EGF stimulation (**Figure 25B**). However, some ubiquitination of these enzymes was observed in unstimulated cells, a result that needs to be verified. Since PLCγ1 and PLCγ2 ubiquitination was not affected by the addition of EGF, and considering that there were no apparent differences between PLCγ1 and PLCγ2 in terms of ubiquitination and Ub-binding abilities, we concluded that these factors were not determinants for their differential roles in NCE.

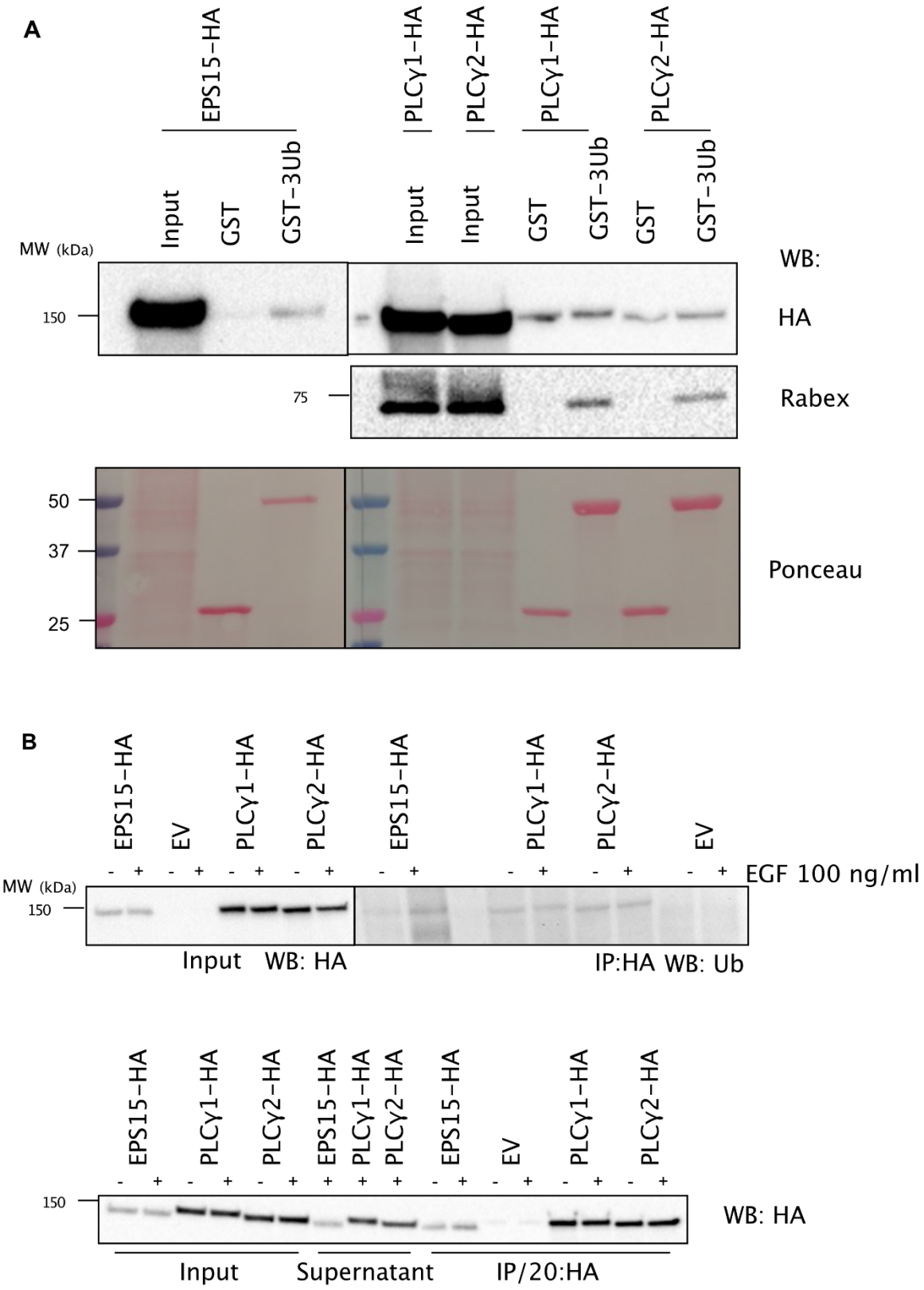

Figure 25. PLCγ1-HA and PLCγ2-HA are not able to bind to Ub and they are not ubiquitinated upon stimulation with EGF

A. *HA-tagged Eps15, PLCγ1, PLCγ2, and endogenous Rabex-5 expressed in the indicated HeLa cell lines were assessed for their Ub-binding abilities in a GST-3Ub (linear change of 3Ub molecules) pulldown assay. Total cell lysates (500 μg) were subjected to pulldown by incubation with equimolar concentrations of GST-3Ub and GST (the latter was used to assess binding specificity). The amount of HA-tagged protein (Eps15, PLCγ1, PLCγ2) pulled-down was evaluated by western blotting (WB) using an anti-HA antibody. The amount of Rabex-5 positive control was evaluated using an anti-Rabex antibody. Lower panel: Ponceau staining was used as a GST-protein loading control. Data are representative of two independent experiments.* ***B****. HeLa cells as in "A" or empty vector (EV) control cells were stimulated or not with 100 ng/ml EGF for 10 min. Total cellular lysates (1 mg) were subjected to anti-HA immunoprecipitation (IP). Ubiquitination of immunoprecipitated HA-tagged proteins was evaluated by WB using the anti-Ub antibody (upper blot, right). Anti-HA was performed on the input (15 μg) as a control of the MW of the HA-tagged proteins (upper blot, left) and on the supernatant and 1/20th of the IP samples to check for IP efficiency (lower blot). Data are representative of two independent experiments. MW: Molecular weight markers are shown on the left.*

4.1.2.4. PLCγ1 *vs.* PLCγ2 co-clustering with different endocytosis players at the PM

To understand whether the differential role of PLCγ1 *vs.* PLCγ2 in EGFR-NCE is due to their localization in specific membrane subdomains and/or PM-localized endocytic compartments, we employed STORM super-resolution technology. The STORM technique combines fluorescent dyes that photo-switch in specific buffers upon laser irradiation, allowing blinking from dark to emission states. Imaging of photo-switchable fluorophores over time allowed us to resolve the background signal coming from the presence of multiple fluorophores and to determine the precise location of individual molecules, thus enabling us to quantify the distribution and clustering of specific molecules. We exploited this technique to characterize the distribution and possible colocalization of PLCγ enzymes and the EGFR. Cells expressing PLCγ-HA forms were stimulated for 1 min with high dose EGF (100 ng/ml). After stimulation, cells were fixed, permeabilized and stained with anti-HA and anti-EGFR primary antibodies, followed by staining with appropriate secondary antibodies.

In non-stimulated cells, we scored EGFR (red) mainly on the PM, while PLCγ1/2 (green) were homogenously distributed in the cytosol (**Figure 26A**). Upon EGF stimulation, recruitment of PLCγ to EGFR was observed. Cross-correlation of PLCγ1/2 and EGFR was performed as described [182]. Briefly, cross-correlation was obtained by averaging over the pixels contained in a selected region of interest. The amplitude parameters from the resulting curves were employed to calculate two coefficients of localization whose arithmetic mean provides the colocalizing fraction and we used a mask to quantify specifically the PM-proximal signal (**Figure 26B**). We found an increase in the proximity between the two signals quantified as co-clustering for both PLCγ1 and PLCγ2 with EGFR at the PM upon stimulation with high dose EGF in comparison to non-stimulated cells. This was not surprising as we expected from the literature that PLCγ1/2 are recruited to the activated EGFR.

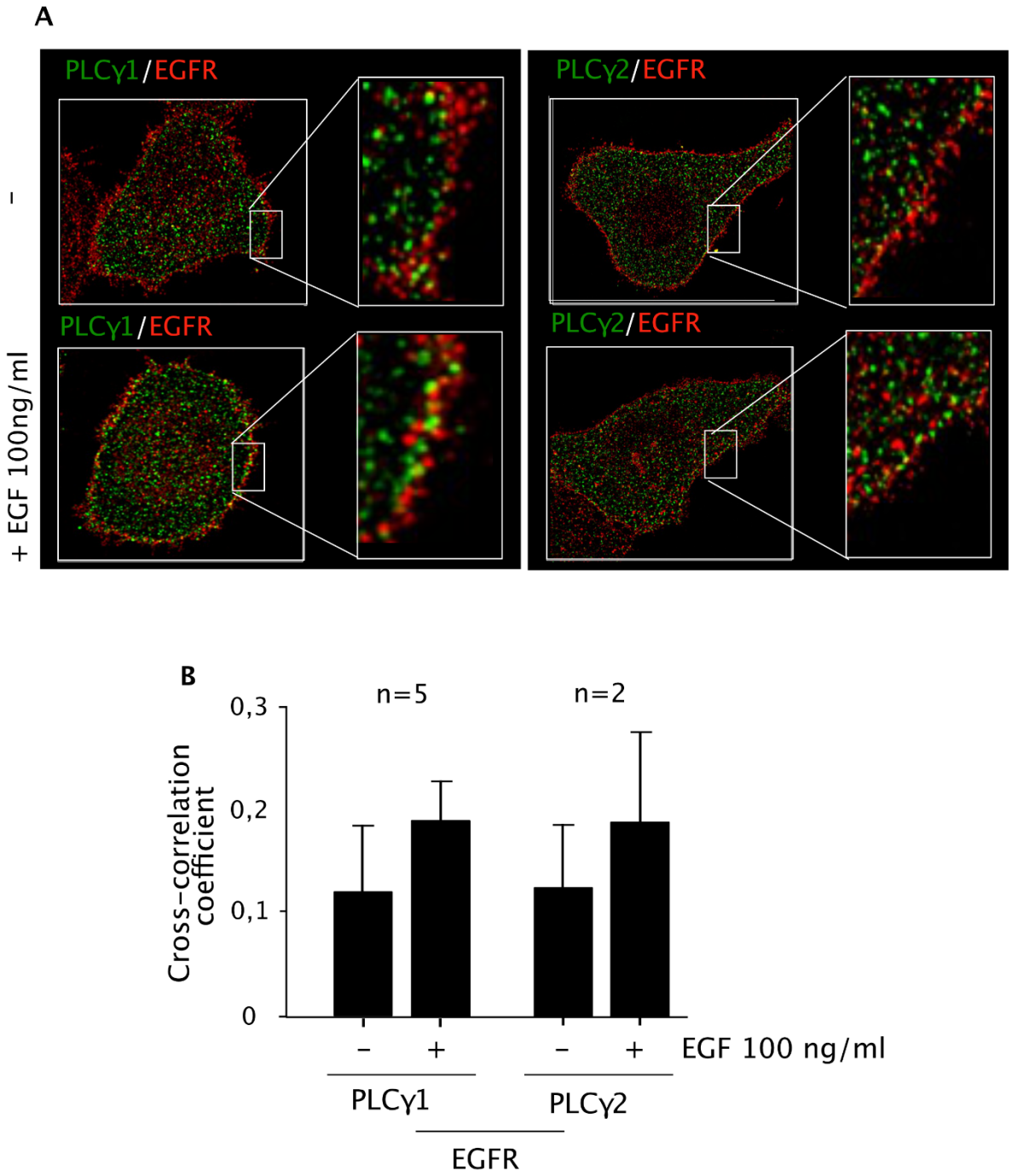

Figure 26. PLCγ1/2-HA and EGFR co-clustering upon EGF stimulation.

A. *HeLa cells expressing HA-tagged PLCγ1 or PLCγ2 were stimulated for 1 min with EGF (100 ng/ml) at 37°C, then fixed, permeabilized and stained with anti-HA and anti-EGFR that were revealed with an Alexa-CY3 (green) and Alexa-647 (red) secondary antibody, respectively. Cells were analyzed by STORM. A representative median section of the cell is shown for each condition.* ***B.*** *Cross-correlation analysis between red and green signals within 40 nm from PM*

is shown. n, cell number analyzed. Experiments were performed with the help of Stefano Freddi from our lab, and Simone Pelicci and Mario Faretta (Imaging Development Unit, IEO).

To understand if the differential role of PLCγ2 and PLCγ1 in NCE is linked to differences in their colocalization with regulators of NCE or CME (i.e., RTN3 and clathrin), we performed the STORM experiment as previously described, but this time we stained with antibodies against RTN3 and clathrin heavy chain instead of EGFR (**Figure 27A**). Only localization events occurring at the periphery of the cell were considered for quantification of co-clustering. Interestingly, we observed significantly higher co-clustering of RTN3 with PLCγ2 than with PLCγ1, while little co-clustering of PLCγ2 or PLCγ1 with clathrin was observed (**Figure 27B**). These results suggests that PLCγ2 is located in PM subdomains in close contact with RTN3-enriched ER. Since EGFR-NCE involves PM-ER contact sites containing RTN3, then the differential recruitment of PLCγ2 *vs.* PLCγ1 to these sites could explain its specific role in NCE. Although we observed the co-clustering of PLCγ2 and RTN3 in the vicinity of the PM in the presence of high EGF, we still need to demonstrate that this proximity is induced by ligand stimulation. However, given that we have shown the PLCγ2 in unstimulated cells is homogenously distributed in the cytosol, while upon EGF stimulation it is recruited to the PM (**Figure 23**), it is likely that this co-clustering of PLCγ2 and RTN3 is specifically induced by EGF.

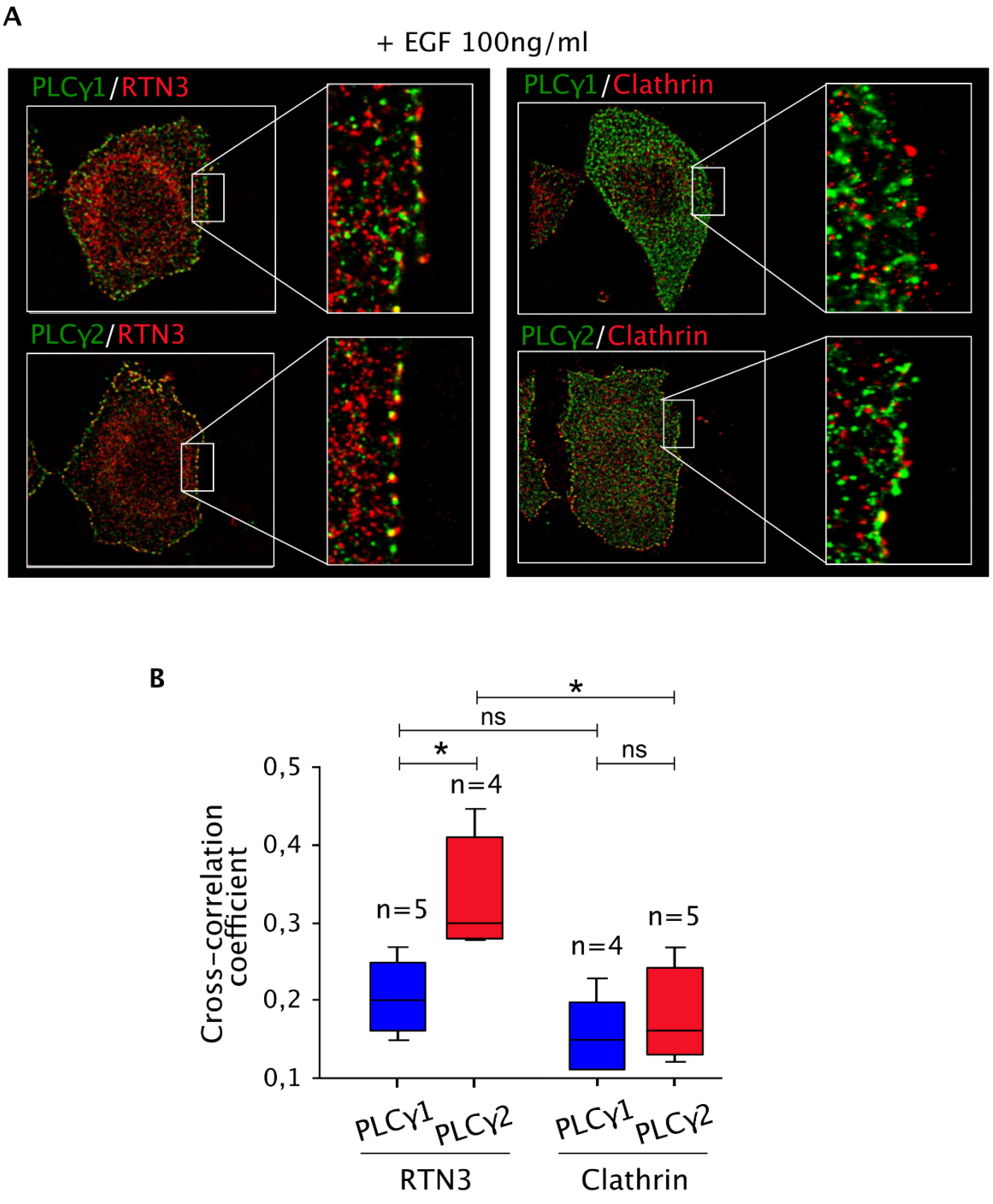

Figure 27. PLCγ2 but not PLCγ1 specifically co-clusters with RTN3 in the vicinity of the PM in the presence of high EGF.

A. *HeLa cells expressing HA-tagged forms of PLCγ1 or PLCγ2 were stimulated for 1 min with EGF (100 ng/ml) at 37°C, then fixed, permeabilized and stained with anti-HA and anti-RTN3/clathrin heavy chain that were revealed with an Alexa-CY3 (green) and Alexa-647 (red) secondary antibody, respectively. Cells were analyzed by STORM. A representative median*

section of the cell is shown for each condition. ***B.*** *Cross-correlation analysis between red and green signals within 40 nm from PM is shown. n, cell number analyzed. P-value, Student's t-test two-tailed; *, P<0.05. Experiments were performed with the help of Stefano Freddi from our lab, and Simone Pelicci and Mario Faretta (Imaging Development Unit, IEO).*

4.1.2.5. PLCγ1 *vs.* PLCγ2 specific recruitment in different compartments-microdomains

Since PLCγ1 and PLCγ2 have a high degree of sequence identity and an almost identical domain structure (**Figure 16**), but differ in their involvement in EGFR-NCE, we hypothesized that this difference in function might arise from their differential recruitment to EGFR pools located in different PM microdomains, as also suggested by our STORM analysis. In agreement with this possibility, it was shown that upon mast cell activation, PLCγ2 was relocalized predominantly to lipid rafts (together with activated IgE receptors), at variance with PLCγ1, which was mainly relocalized outside lipid rafts [187]. Since NCE is known to be dependent on lipid rafts [123], we investigated whether PLCγ2 is specifically recruited to lipid rafts in our model system.

To this aim, we employed the protocol previously described for mast cells [183]: PM sheets from HeLa cells expressing PLCγ1-HA and PLCγ2-HA were immunolabeled with anti-HA antibody and stained with osmium, which stains membrane regions enriched in unsaturated fatty acids (as in lipid rafts) and can be visualized as an electron dense staining in EM. Staining with anti-HA in EV cells was performed to quantify non-specific binding. Upon stimulation with EGF 100 ng/ml for 2 min, we were able to score clustering of PLCγ2, but not PLCγ1, in osmiophilic patches enriched in unsaturated lipids (**Figure 28A**). To analyze molecular distribution, we employed the Ripley's K function [184] tool that tests spatial randomness of molecules. With this analysis, we found that PLCγ1 was localized in small uniform dispersed clusters, while PLCγ2 formed larger clusters of 300-400 nm (**Figure 28B**). We hypothesized that these large clusters could correspond to NCE active sites.

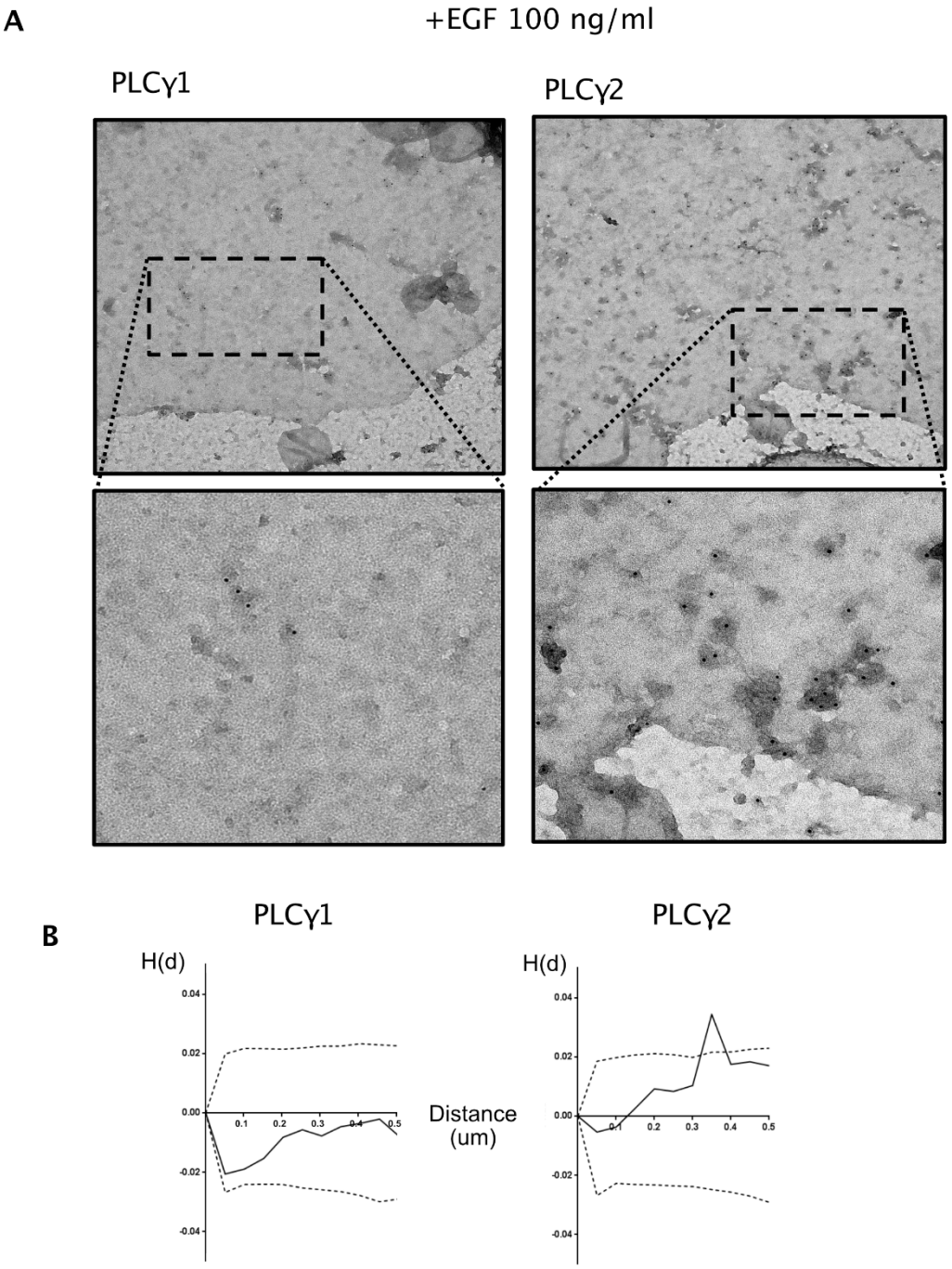

Figure 28. PLCγ2 redistributes to osmiophilic patches in HeLa cells stimulated with EGF.

A. *PM sheets from HeLa cells expressing HA-tagged forms of either PLCγ1 or PLCγ2 were prepared after stimulation with EGF (100 ng/ml for 2 min). Sheets were labeled with anti-HA monoclonal antibody followed by incubation with rabbit anti-mouse secondary antibody, and, finally, with Protein-A gold 10 nm, visualized on images with black dots. Osmium staining is showed by dark grey areas. Top, representative images are shown. Bottom, magnifications.* ***B.*** *Analysis of the spatial organization of molecules with Ripley's K function. The normalized and*

centered Ripley's K function H(d) is proportional to the number of pairs of points that are closer in distance than the probability for the field of view. Signal is clustered if H(d)>0 and higher than the objective level (showed with dotted boundaries). In contrast, signal is considered dispersed if H(d)<0 and lower than the boundaries. If H(d) is within boundaries, signal is uniform. H(d) of the PLCγ1 signal (left) is uniform, since it is not significantly different from 0, while H(d) of the PLCγ2 signal (right) is clustered since it is significantly different from 0. Experiments were performed with the help of Andrea Raimondi from Prof. Carlo Tacchetti's Lab (Centro Imaging Sperimentale, San Raffaele Scientific Institute, Milan, Italy).

As a complementary approach, we performed a density gradient fractionation assay of total cell lysates to separate detergent-soluble and insoluble (*i.e.,* lipid rafts) PM fractions from HeLa cells expressing HA-tagged PLCγ2. Briefly, cells were stimulated with high EGF concentrations for 2 min and then lysates were loaded onto the gradient, in order to isolate different fractions. As a marker of lipid rafts, we used flotillin and caveolin, while tubulin was used as a marker of soluble fractions. In a preliminary experiment, at steady state, PLCγ2-HA and endogenous PLCγ1 were present in raft fractions (5-7) and in non-raft fractions (9-12) (**Figure 29**). Upon stimulation with EGF some PLCγ2 shifted to fraction 3, which corresponds to the lipid raft fraction with the highest level of raft markers, caveolin and flotillin. A similar increase in fraction 3 was scored also for Rac1 (see Discussion). A very faint band of PLCγ1, if any, was also visible in fraction 3.

While this experiment needs to be repeated, also for PLCγ1-HA expressing cells, our preliminary result suggests the differential recruitment of PLCγ2 *vs.* PLCγ1 to lipid rafts upon EGF stimulation. If confirmed, this result would support our hypothesis that the specificity of PLCγ2 for EGFR-NCE resides in its ability to be specifically recruited to the activated EGFR present in lipid rafts.

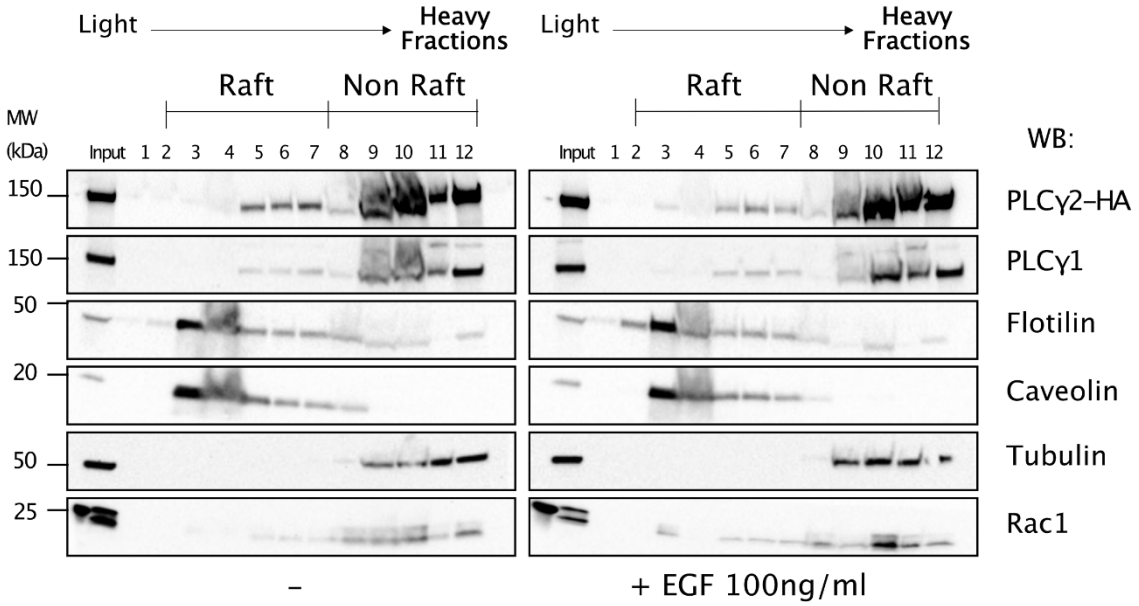

Figure 29. PLCγ2 is enriched in raft fractions upon EGF stimulation.

HeLa cells expressing HA-tagged PLCγ2 were stimulated with 100 ng/ml of EGF for 2 min. Total cell lysates were subjected to density gradient fractionation and the presence of proteins in each fraction was determined by WB analysis with the indicated antibodies. Flotillin and caveolin were used as markers of lipid rafts, while tubulin is used as a marker of non-raft fractions. PLCγ1 is endogenous protein. Experiment was performed once.

4.1.3. Second-messenger signaling: IP3, DAG and Ca^{2+} production

We have previously described the role of IP3 in EGFR-NCE and shown that inhibition of Ca^{2+} release impairs NCE by inhibiting the last step of NCE-TI fission, phenocopying the TI elongation effect observed upon dynamin 1/2 KD [63]. However, the precise role of other second messengers, e.g., DAG (that is produced with IP3 during the conversion of PIP2 by PLCγ enzymes) and the molecular target of Ca^{2+} are still unknown. Some preliminary, yet interesting experiments regarding the role of DAG and Ca^{2+} were performed and will be discussed briefly in the following two paragraphs.

4.1.3.1. Role of DAG kinase in NCE

From literature, it is known that DAG can be converted into PA by DAG kinase (DGK) and that PA induces the negative curvature of the PM that could possibly lead to recruitment of dynamin

[188]. Moreover, it was shown DGKα can can bind to Ca^{2+} and this binding regulates DGK activity [189]. Therefore, we hypothesized that DGK could be a target of Ca^{2+} and regulator of last step of an NCE.

To test this hypothesis, we knocked down DGKα in HeLa cells or treated cells with an allosteric pan DGK inhibitor (R59949). We found that DGKα KD appeared to increase internalization of the NCE specific marker, CD147 (although the result was not statistically significant), while the DGK inhibitor had the opposite effect (**Figure 30A, B, D**). Interestingly, no effect on EGF internalization was scored upon DGKα KD or upon treatment with DGK inhibitor (**Figure 30A, C**).

These results suggest that DGKα does not have a major regulatory role in EGFR-NCE, as no effects on EGF internalization were scored. In contrast, DGK appears to have a regulatory role in CD147 internalization, perhaps controlling its recruitment to the EGFR-NCE pathway or to other endocytic pathways. Indeed, the opposite effects of KD and inhibitor on CD147 internalization can be explained by the fact that the DGK inhibitor is affecting all forms of DGK, with at least one of them playing a positive regulatory function, while DGKα might exert a negative role on NCE. An alternative explanation might be related to the fact that the KD of DGKα was performed for 5 days, thus representing a chronic inhibition, at variance with the inhibitor treatment that is instead administered acutely (30 min at 37°C plus the time needed for the CD147 internalization protocol). Indeed, from our previous experience, we know that chronic inhibition of one endocytic pathway could upregulate other compensatory endocytic mechanisms. Thus, in the DGKα KD condition, an alternative endocytic route could be upregulated that can internalize CD147, but not EGF.

More experiments are required to discriminate between these possibilities. Also, we plan to check the role of DGK in CME, by performing Tf internalization assays.

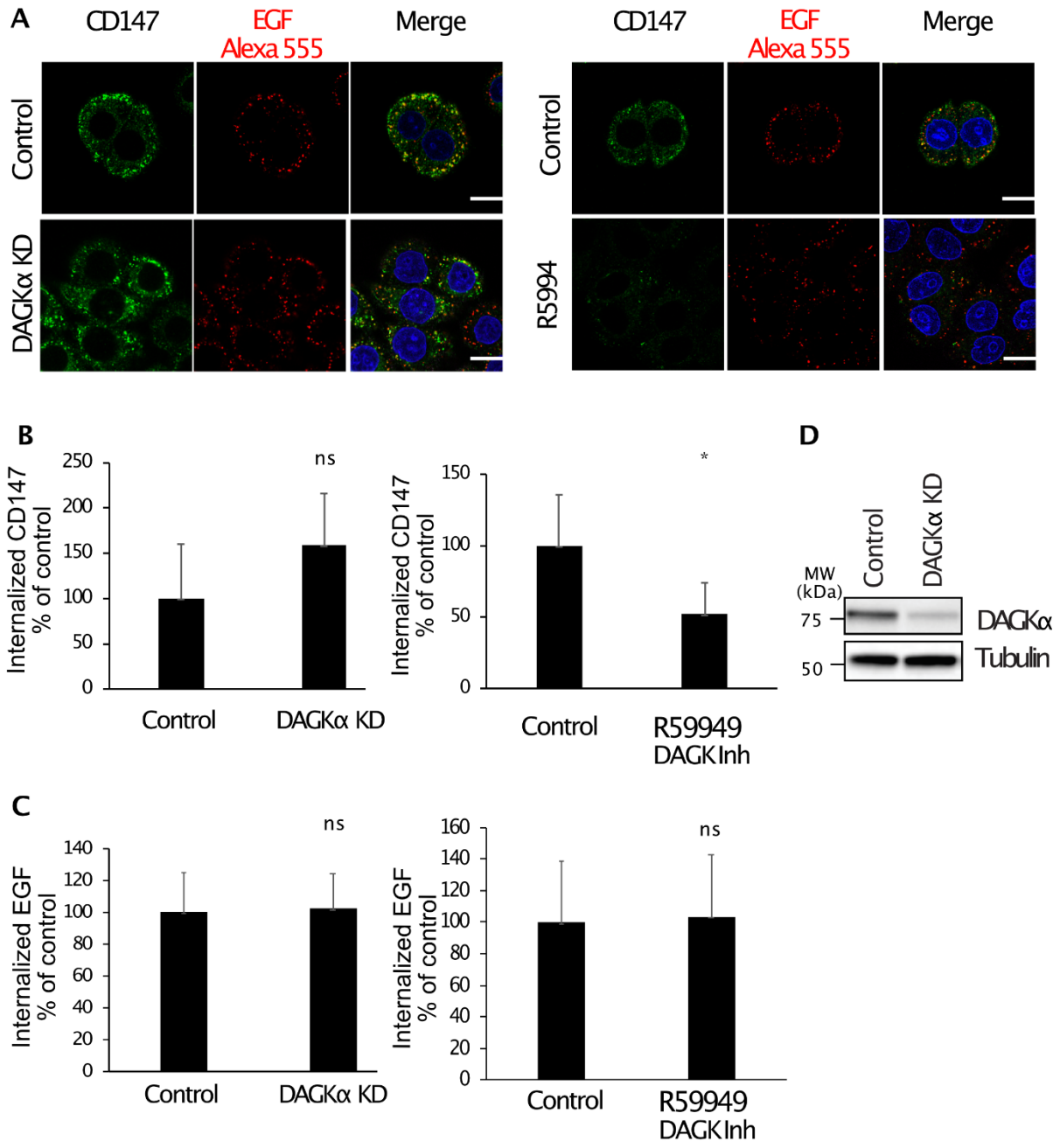

Figure 30. DGK inhibitor decreases CD147 internalization.

A. *HeLa cells were subjected to the indicated KD or treated with DGK inhibitor (10 μM; 30 min at 37°C + time of CD147 internalization protocol) and then stimulated with high dose Alexa-555-EGF (~30 ng/ml). DMSO was used as the vehicle control for DGK inhibitor. Confocal fluorescence microscopy was performed to monitor internalization of Alexa-555-EGF (red) and CD147 (detected with an anti-CD147 antibody and an Alexa-488 secondary antibody; green). Blue, DAPI. Bar, 20 μm.* ***B.*** *Internalized CD147 was quantified with an ad hoc designed ImageJ macro. Mean integrated fluorescence intensity ± SD is reported as % of control cells.*

C. *Using ImageJ program, Alexa-555-EGF signal was highlighted applying an intensity-based threshold (Default method), and then fluorescence intensity per field was calculated using the "Measure" command, limiting measurement to the threshold. This value was then divided by the number of nuclei in the field, counted using the DAPI signal, to calculate the EGF fluorescence intensity per cell. Mean integrated fluorescence intensity ± SD, reported as % of control cells.* ***D.*** *Efficiency of DGKα KD was assessed by WB. Tubulin, loading control. MW: Molecular weight markers are shown on the left. Experiment was performed in biological triplicate. P-value, Student's t-test two-tailed; ***, P<0.005. Experiments were performed with the help of Elisa Barbieri from our lab.*

4.1.3.2. The role of calcineurin in EGFR-NCE

Dynamin is dephosphorylated by the calcium–calmodulin-activated protein phosphatase calcineurin, which leads to its activation. Since Ca^{2+} and dynamin are required for the last step of NCE, we tried to understand if Ca^{2+} regulates dynamin function through calcineurin. To this aim, we stimulated HeLa cells with high dose EGF in the presence of a combination of calcineurin inhibitors, namely CsA and FK506 [190, 191]. Our preliminary experiment showed that calcineurin inhibitors decreased CD147 and EGF internalization by 20-30% (**Figure 31A-C**). In contrast, the inhibitors did not affect Tf internalization, which occurs through CME, suggesting that calcineurin is selectively involved in NCE (**Figure 31D**).

To confirm the efficacy of calcineurin inhibitors, we checked NFAT phosphorylation, since calcineurin is known to dephosphorylate this protein [190, 191]. Upon treatment of HeLa cells with the inhibitors, in the presence and absence of EGF stimulation, we observed a shift up in the NFAT band in WB, consistent with increased phosphorylation (**Figure 31E**). This result indicates that the inhibitors are functioning correctly.

These preliminary data suggest that calcineurin might be a regulator of NCE. However, more work is required to understand the role of calcineurin for EGFR-NCE. In addition, we will need to demonstrate the link between calcineurin activation and NCE-dependent Ca^{2+} release.

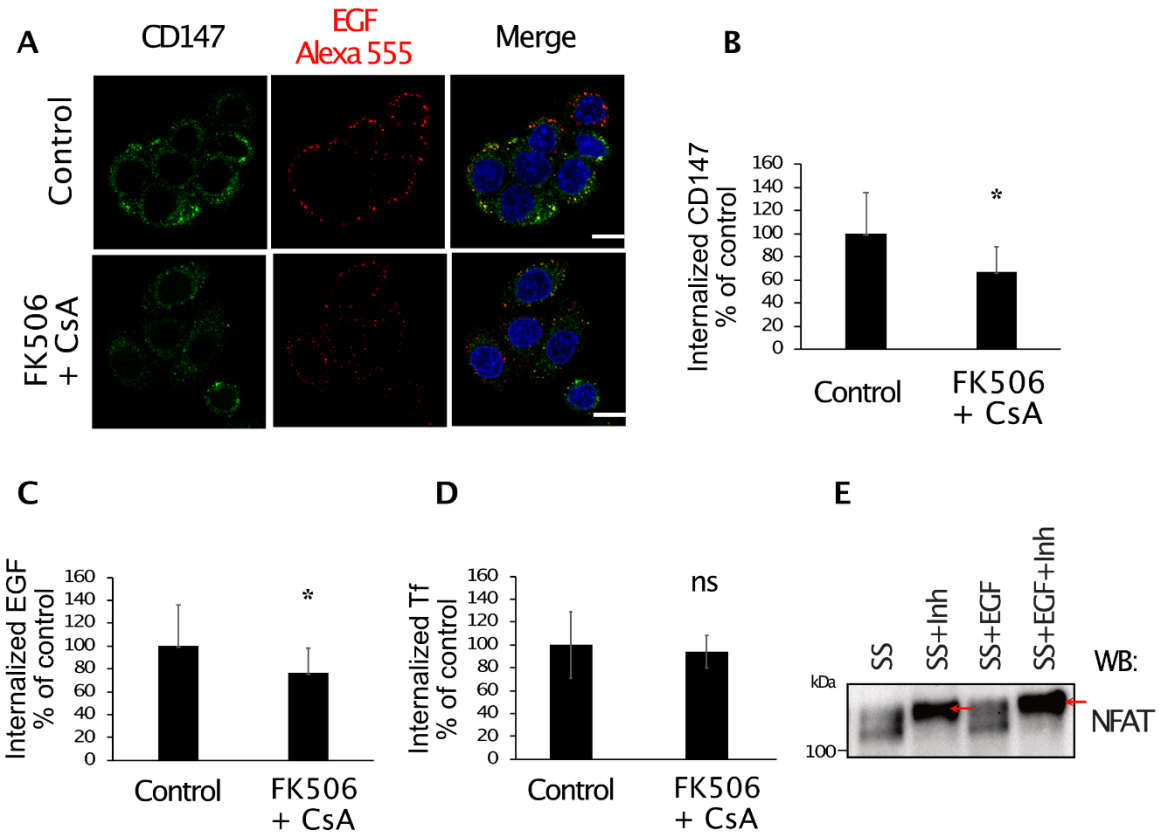

Figure 31. Calcineurin inhibitors decrease CD147 and EGF internalization

A. *HeLa cells were treated with calcineurin inhibitors (FK506, 5 μM; CsA, 10 μM) for 1 h prior to stimulation with high dose Alexa-555-EGF (~30 ng/ml). Confocal fluorescence microscopy was performed to monitor internalization of Alexa-555-EGF (red) and CD147 (detected with an anti-CD147 antibody and an Alexa-488 secondary antibody; green). Inhibitor treatments were maintained throughout the whole CD147 internalization protocol. Blue, DAPI. Bar, 20 μm.* ***B.*** *Internalized CD147 was quantified with an ad hoc designed ImageJ macro. Mean integrated fluorescence intensity ± SD is reported as % of control cells.* ***C.-D.*** *The effect of calcineurin inhibitors on internalized Alexa-555-EGF (**C.**) or Alexa-488-Tf (**D.**) was measured as following: signals were highlighted applying an intensity-based threshold (Default method), and then fluorescence intensity per field was calculated using the "Measure" command, limiting measurement to the threshold. This value was then divided by the number of nuclei in the field, counted using the DAPI signal, to calculate the EGF/Tf fluorescence intensity per cell. Mean integrated fluorescence intensity ± SD, reported as % of control cells.* ***E.*** *Efficiency of the calcineurin inhibitors FK506 and CsA shown on NFAT phosphorylation (red arrow pointing to higher MW form of NFAT corresponding to phosphorylated protein). MW: Molecular weight*

*markers are shown on the left. Experiment was performed in triplicate. Experiments were performed with the help of Elisa Barbieri from our lab. P-value, Student's t-test two-tailed; *, P<0.05.*

4.2. NCE activation by other EGFR ligands and RTKs

To investigate if NCE is specific for EGF-EGFR or if it has a broader function in the cell, we tested whether other EGFR ligands can induce NCE. Different EGFR ligands can induce different biological outcomes starting from the activation of the same receptor [192]. Since these differences cannot be explained simply by quantitative differences in ligand affinities, we are investigating if the differential activation of endocytic pathways by different ligands could contribute to determining specific biological outcomes. We decided to focus initially on TGF-α and AREG, since they are specific for the EGFR and not for the other ErbB family members. TGF-α is the most potent EGFR mitogenic ligand and has been shown to induce scarce EGFR ubiquitination and to target EGFR to recycling [112, 193], providing an alternative framework to test the relevance of ubiquitination to NCE and signal extinction. Similar properties were shown for AREG, although it is less studied in literature [112]. TGF-α and EGF are high affinity ligands with a K_D of binding to the EGFR in range of 0.1-10 nM [194] (**Table 2**). In contrast, AREG is considered a low affinity ligand having a K_D of ~350 nM [194].

4.2.1. EGFR signaling upon stimulation with different ligands

Initially, we characterized the activation of the EGFR and its downstream signaling effectors upon stimulation with TGF-α or AREG in a dose response experiment, in comparison to EGF. Saturating concentrations of ligands (100ng/ml for EGF and TGF-α or 5μg/ml for AREG) were calculated from molarities (15.62 nM EGF, 18.18nM TGF-α and 442.48nM AREG) that correspond to values that are above K_D of each ligand.

By WB analysis, we found that the high affinity ligands EGF and TGF-α induced a similar activation of EGFR and downstream effectors, although the intensity of EGFR phosphorylation (pY1068, pY992 and pY1045) appeared slightly less upon TGF-α stimulation compared with EGF (**Figure 32**). However, phosphorylation of SHC, AKT, PLCγ1/2 and ERK1/2 were very similar as was the total EGFR level (**Figure 32**).

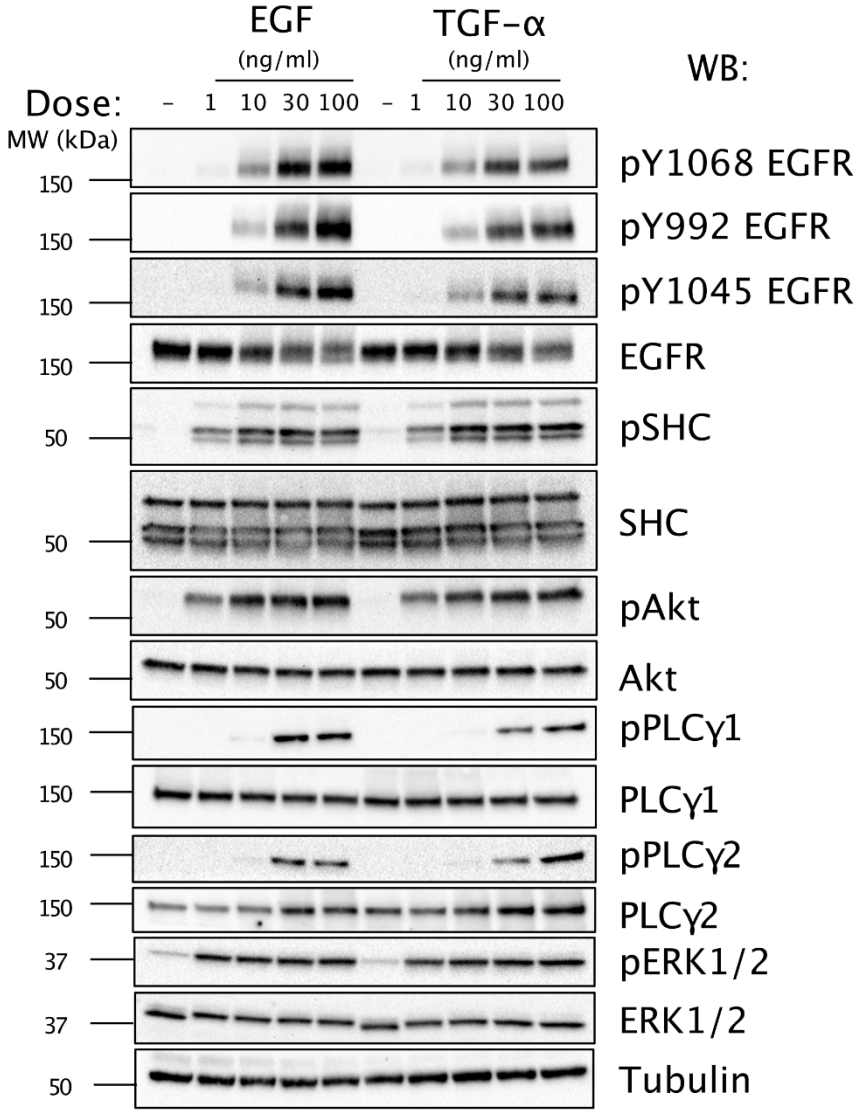

Figure 32. Comparison of the activation of EGFR and downstream signaling effectors by EGF and TGF-α.

HeLa cells were stimulated with increasing concentrations of high affinity EGFR ligands for 2 min. Total cell lysates were analyzed by WB using antibodies specific for the indicated signaling effectors and EGFR pY sites. Tubulin, loading control. MW: Molecular weight markers are shown on the left. Blot is representative of two repeats.

In contrast, compared to EGF, the low affinity ligand AREG induced a lower level of phosphorylation of the EGFR residues Y992 and Y1068, but a similar phosphorylation of EGFR-Y1173 (**Figure 33**). Notably, AREG also induced a higher phosphorylation of SHC and AKT compared to EGF, while the phosphorylation of ERK1/2, PLCγ1, and PLCγ2 was similar (**Figure 33**).

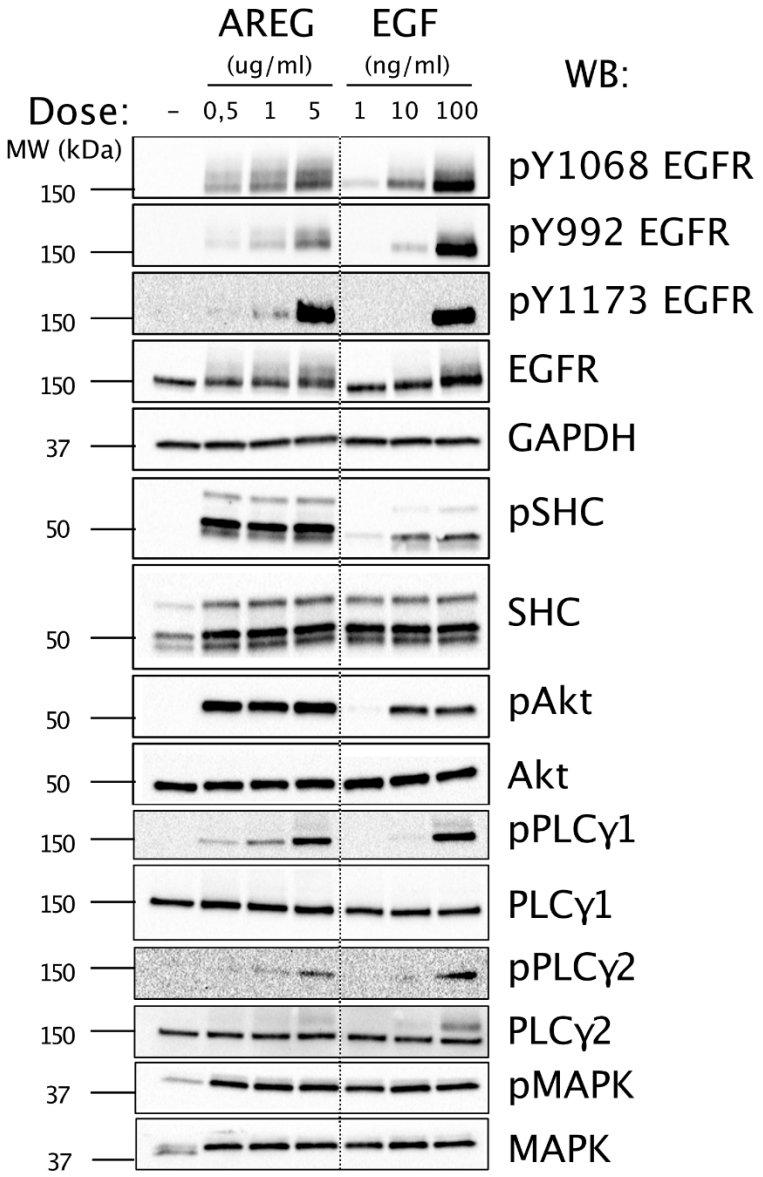

Figure 33. Comparison of the activation of EGFR and downstream signaling effectors by EGF and AREG.

HeLa cells were stimulated with increasing concentrations of EGF and AREG ligands for 2 min. Total cell lysates were analyzed by WB using antibodies specific for the indicated signaling effectors and EGFR pY sites. The blot shows samples from the same membrane, but with irrelevant lines splicing out (indicated by dotted line). MW: Molecular weight markers are shown on the left. Blot is representative of two repeats.

4.2.1.1. TGF-α is a weak inducer of CD147 internalization

We then followed CD147 endocytosis triggered by EGF (high dose), AREG or TGF-α in HeLa cells, interfered or not for RTN3 (NCE inhibited) or clathrin (CME inhibited). CD147 internalization was followed using an anti-CD147 antibody that recognizes its extracellular domain without interfering with endocytosis [63]. We also followed localization of EGFR, staining it with a specific antibody after fixation of HeLa cells.

In unstimulated cells, the EGFR signal was mainly localized at the PM while only a small amount of CD147 signal was detectable and located in intracellular vesicles (**Figure 34A**). Upon EGF and AREG stimulation for 8 min, CD147 was internalized and colocalized with EGFR via a clathrin-independent process (insensitive to clathrin KD) that was inhibited by RTN3 KD indicating NCE activation (**Figure 34A, B, D**). In contrast, TGF-α was a weak inducer of CD147 internalization (**Figure 34A, C**). Indeed, in the RTN3 KD sample, EGFR internalization looked similar to control, whereas in the clathrin KD there was more evident EGFR staining on the cell surface, suggesting that internalisation is through a CME pathway and not a NCE pathway. This is consistent with the CD147 result too, as only a minor fraction of CD147 is internalized in this setting (**Figure 34A, C**), suggesting that CD147-NCE is not efficiently activated by TGF-α, at variance with EGF and AREG. In the RTN3/clathrin KD, most of EGFR and CD147 staining is on the PM, while some residues of signal inside the cell, can be explained by non-CME/NCE routes or the constitutive pathways [62]. Since in this experiment, staining of EGFR was done after fixation, we cannot distinguish between PM, internalized and newly synthesized EGFR and this disables proper quantification of the internalized EGFR. Further experiments following *in vivo* EGFR internalization, by using an antibody against its extracellular domain can provide us with more information about clear endocytic routes activated by different ligands.

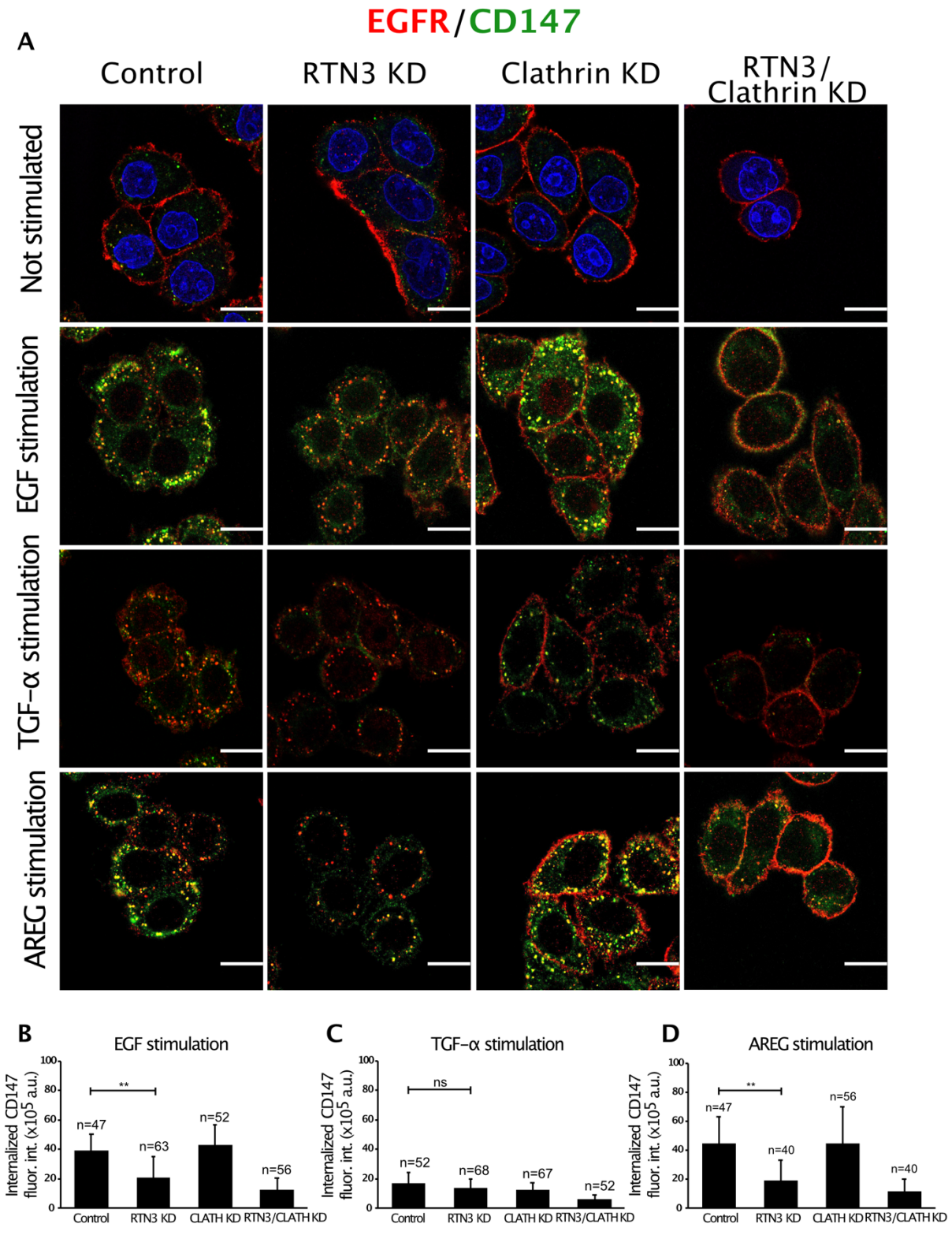

Figure 34. CD147 internalization upon stimulation with different EGFR ligands.

A. *HeLa cells were subjected to the indicated KD and treated with EGF (~30 ng/ml), TGF-α (100 ng/ml) and AREG (5.5 μg/ml) for 8 min. CD147 internalization was followed in vivo, in the absence (not stimulated) or presence of the different ligands, using an anti-CD147 antibody*

and an Alexa-488 secondary antibody (green). EGFR was stained with a specific primary and secondary antibody after fixation (red). Blue, DAPI. Bar, 20 μm. ***B-D.*** *Quantification of CD147 internalization in cells described in "A". Signal was highlighted applying an intensity-based threshold (Default method) and then fluorescence intensity per field was calculated using the "Measure" command, limiting measurement to threshold. This value was then divided by the number of nuclei in the field, counted using the DAPI signal, to calculate the CD147 fluorescence intensity per cell. Mean integrated fluorescence intensity ± SD. n, cell number analyzed. P-value, Student's t-test two-tailed; **, P<0.01, ns, not significant.*

4.2.1.2. TGF-α induces a weaker Ca^{2+} response that is delayed and time-restricted compared with the EGF and AREG responses

Since we scored differential effects of EGFR ligands on CD147 internalization, we explored their effects on EGF-dependent Ca^{2+} release in proximity of the PM. We used the Ca^{2+} probe GCAMP6f, a modified GFP that increases fluorescence upon binding to Ca^{2+} and that allows changes in Ca^{2+} concentration to be followed at the single cell level [195]. We targeted this probe to the inner leaflet of the PM to be able to measure Ca^{2+} released in proximity of NCE sites, with the same strategy we previously used to target PM-Aequorin (see **Figure 18A** and [63]). Using the PM-GCAMP6f probe, we observed that stimulation with EGF (high dose) and AREG induces Ca^{2+} oscillatory waves at the PM inner leaflet with a similar magnitude, while TGF-α induced a much weaker Ca^{2+} response (**Figure 35A, B**). Interestingly, high doses of AREG induce more of Ca^{2+} release than EGF and this feature we will investigate in the future. On the other side, singe cell track analysis revealed that TGF-α induced Ca^{2+} oscillations that were delayed with respect to EGF-induced oscillation and were also time restricted (**Figure 35C**). This limited Ca^{2+} response might explain the poor ability of TGF-α to induce NCE.

Together, these data indicate that different EGFR ligands can differentially activate Ca^{2+} signaling at the PM and, consequently, EGFR-NCE, and this might account for differences in biological outcome, something we aim to test.

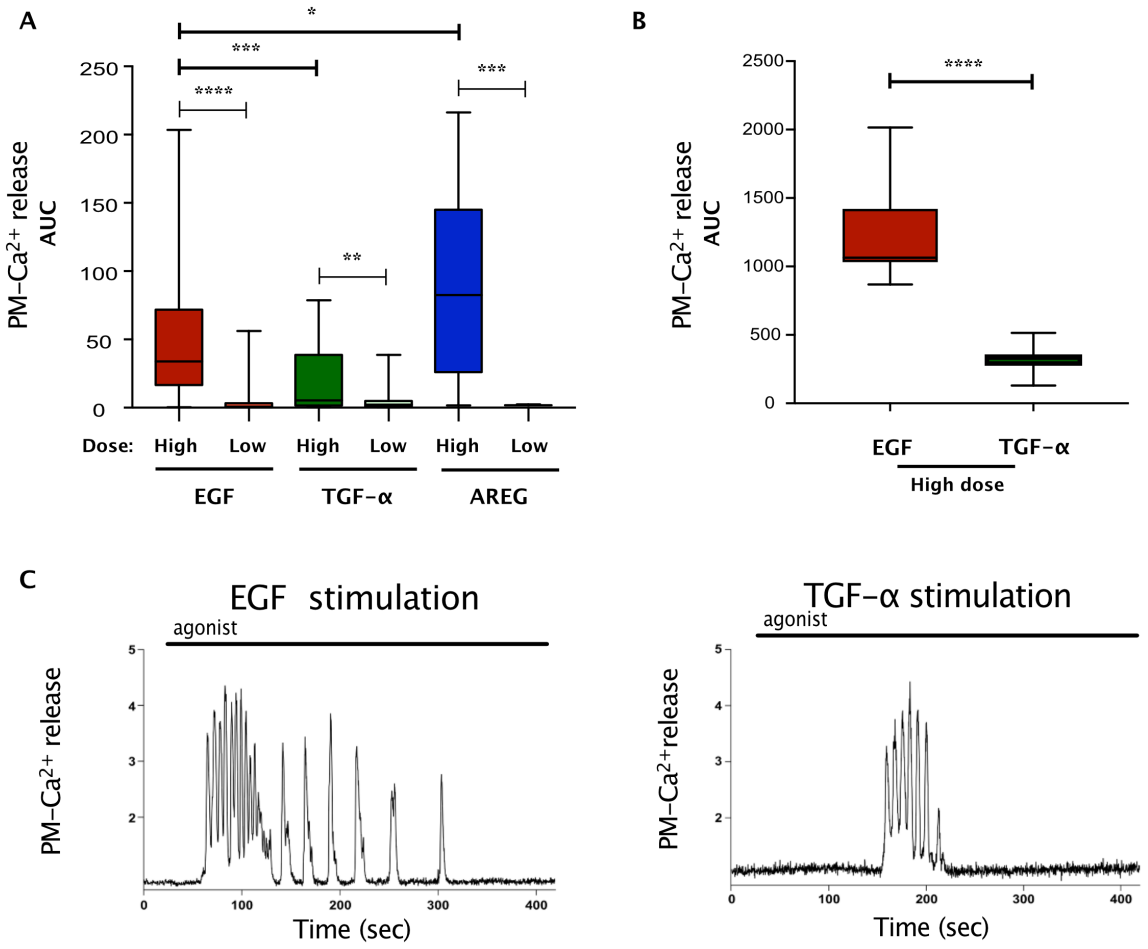

Figure 35. Induction of Ca^{2+} oscillatory waves at the PM inner leaflet by different EGFR ligands.

A. *HeLa cells were transfected with PM-targeted GCaMP6f Ca^{2+} sensor and stimulated with high and low doses of EGF (100 ng/ml and 1 ng/ml), TGF-α (100 ng/ml and 1 ng/ml) and AREG (5 μg/ml and 500 ng/ml). The area under the curve (AUC) ± SD of the Ca^{2+} response at the PM is presented in the box plot.* ***B.*** *HeLa cells were stimulated with high doses of EGF and TGF-α (100 ng/ml), and Ca^{2+} response is observed using PM-targeted GCaMP6f. The area under the curve (AUC) ± SD of the Ca^{2+} response at the PM is presented in the box plot.* ***C.*** *Single-cell traces of PM-Ca^{2+} release from experiment in "B" are. The kinetics of the Ca^{2+} response is presented as the ratio of fluorescence at 488/405 nm emission. P-value, Student's t-test two-tailed; *, P<0.05; **, P<0.01; ***, P<0,005; ****, P<0.001. The experiments in "A" were performed with the help of Deborah Salvi Mesa from our lab, in collaboration with Prof. Paolo Pinton's Lab (Section of Pathology, Oncology and Experimental Biology and Laboratory for Technologies of Advanced Therapies Center, Department of Morphology, Surgery and*

Experimental Medicine, University of Ferrara, Ferrara, Italy). The experiments in "B" and "C" were performed with the help of Giorgia Miloro from our lab.

4.2.2. How do EGF and TGF-α induce differential NCE activation?

4.2.2.1. EGFR ubiquitination upon stimulation with EGF or TGF-α

EGFR-NCE is activated when receptors are fully phosphorylated and ubiquitinated [62]. EGFR ubiquitination, in particular, is the signal that triggers NCE [62]. Thus, we investigated if EGFR is differentially phosphorylated or ubiquitinated upon stimulation with EGF or TGF-α, as this might easily explain the differential activation of NCE. HeLa cells were treated with different doses of ligands before performing immunoprecipitation of EGFR and analyzing receptor phosphorylation and ubiquitination by WB. Initial experiments showed a small decrease in total EGFR phosphorylation upon TGF-α stimulation compared to EGF stimulation (**Figure 32**), in agreement with what we observed with antibodies against specific EGFR pY sites (**Figure 36**). A subtle change in the migration pattern of ubiquitinated EGFR was also observed that needs to be eventually further investigated (**Figure 36**). However, no major differences in the total phosphorylation or ubiquitination of the EGFR were apparent after stimulation with the two ligands.

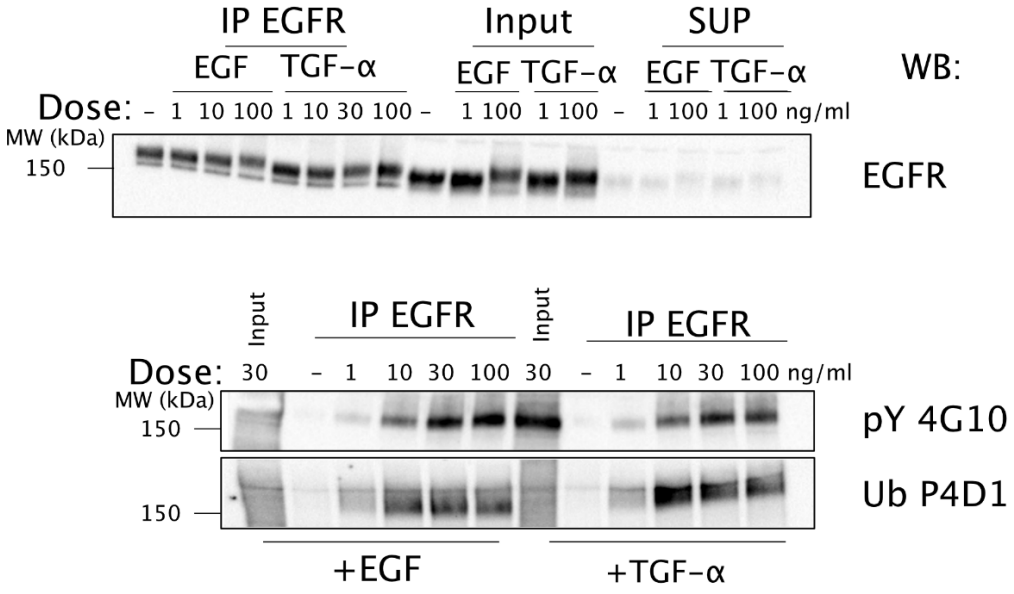

Figure 36. Phosphorylation and ubiquitination of EGFR upon stimulation with high affinity ligands EGF and TGF-α.

HeLa cells were treated increasing doses of EGF and TGF-α for 2 mins. Immunoprecipitation (IP) of EGFR with anti-EGFR antibody was then performed on total cell lysates (0.5 mg) and immunoprecipitates were analyzed by WB. Top, control WB to test IP efficiency, showing total EGFR levels in the immunoprecipitates (~40 μg), the input (30 μg) and supernatant (SUP, 30 μg). We could observe an enrichment of EGFR in the IP and depletion in the supernatant (SUP), as compared to input (>90% efficiency). Bottom, 50 μg or 450 μg of immunoprecipitate was analyzed by WB for pY-EGFR using the generic anti-phosphotyrosine antibody 4G10 or Ub-EGFR using the anti-Ub P4D1 antibody respectively. A representative input (30 μg) of samples stimulated with 30 ng/ml of ligand was loaded as a control.

4.2.2.2. PLCγ2 differential activation upon stimulation with EGF and TGF-α

To understand if differential NCE activation by EGF and TGF-α and delayed and time restricted Ca^{2+} response upon TGF-α might be due to inefficient activation of PLCγ2 upon TGF-α, we checked the phosphorylation of PLCγ2 after stimulation at different time points with ligands. We found that both PLCγ1 and PLCγ2 were less phosphorylated upon TGF-α stimulation compared to EGF (**Figure 37**), however the decrease in PLCγ2 was much stronger (~46%) as compared to PLCγ1 (~14%) at 1 min of stimulation. In addition, we also observed a decrease in EGFR phosphorylation at different pY sites, with ~30% reduction in pY1068 and pY992, as well as a reduction in pY1045 and pY1173 (**Figure 38)**. Thus, these data are compatible with TGF-α inducing less efficient EGFR phosphorylation, which is translated in a reduced recruitment and phosphorylation of PLCγ2, causing inefficient activation of the NCE. However, while some decrease in STAT3 phosphorylation was scored upon TGF-α, no effect were observed on SHC, AKT and ERK1/2 phosphorylation.

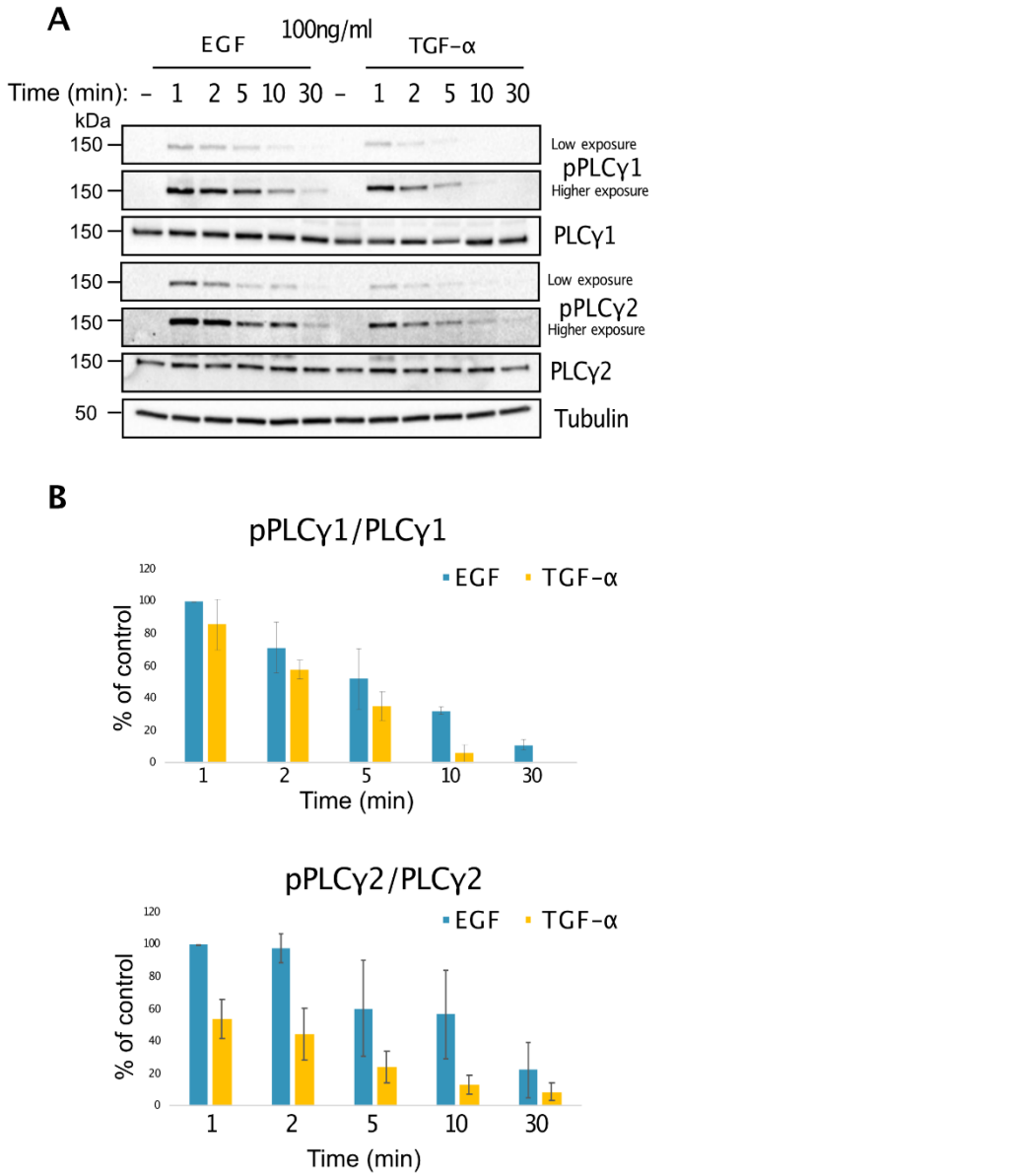

Figure 37. PLCγ2 is less phosphorylated upon TGF-α stimulation as compared to EGF.

A. *HeLa cells were stimulated with 100 ng/ml of either EGF or TGF-α for the indicated time points. Lysates were were analyzed by WB for total and phosphorylated PLCγ1 and PLCγ2. Tubulin, loading control.* ***B.*** *Quantification of WB signal shown as % of sample stimulated with EGF for 1 min. Experiment was performed twice.*

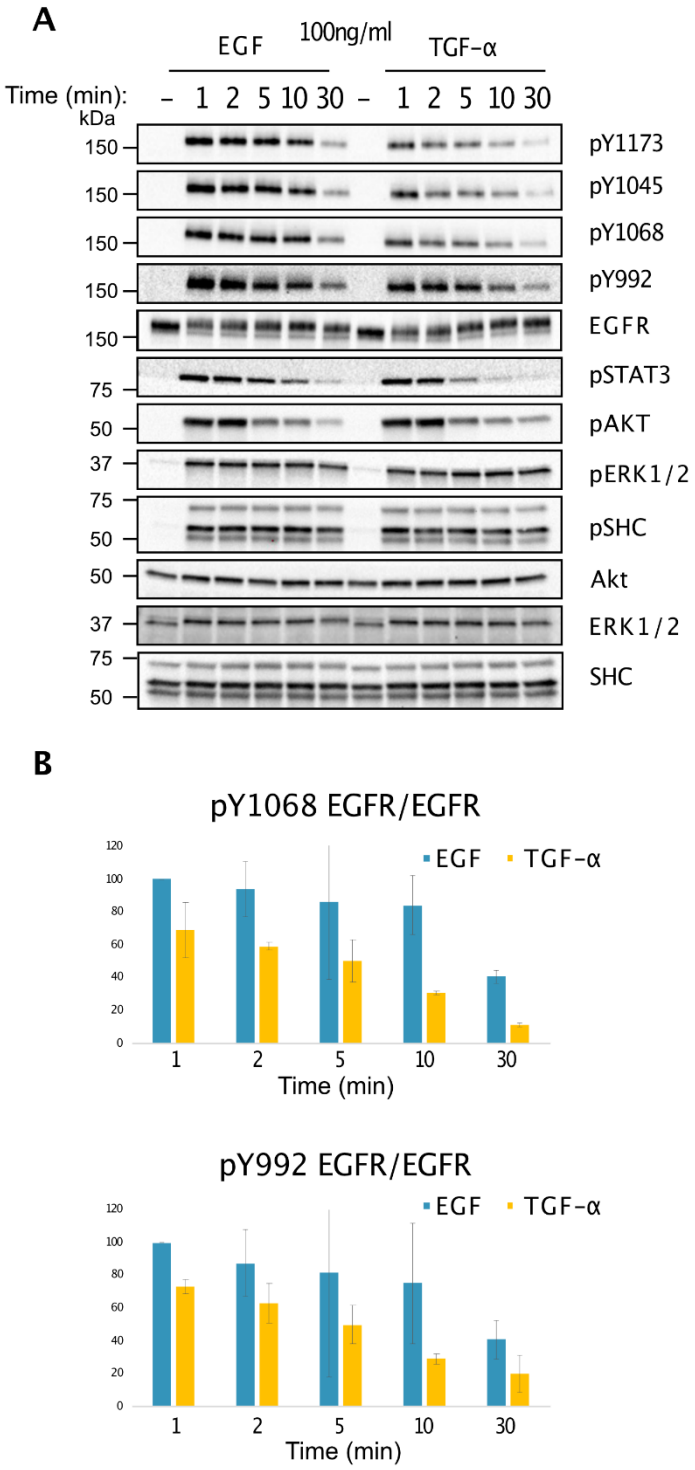

Figure 38. Activation of EGFR and downstream signaling effectors by EGF vs. TGF-α at different time points.

A. *HeLa cells were stimulated with 100 ng/ml of either EGF or TGF-α for the indicated time points. The indicated signaling effectors and EGFR pY sites were analyzed by WB.* ***B.***

Quantification of WB signal shown as % of sample stimulated with EGF for 1 min. Experiment performed twice.

The largest difference in signaling activation upon TGF-α *vs.* EGF stimulation was observed at 10 min post-stimulation, as assessed by EGFR and effector phosphorylation in WB (**Figure 38)**. However, the WB method is semi-quantitative and the differences observed were variable among experiments (**Figure 32** vs. **Figure 37**) and not very strong. For this reason, we should employ more quantitative methods to assess signaling players, such as flow cytometry or ELISA assays.

4.2.2.3. EGF and TGF-α different EGFR clustering

Since NCE is active only in cells with a high number of activated EGFRs, i.e., in cells with a high level of surface EGFR and stimulated with high dose EGF (>10 ng/ml), and it is dependent on lipid rafts that facilitate receptor oligomerization, we speculated that NCE could represent a mechanism for the internalization of EGFR clusters/oligomers. EGFR is known to form clusters that range in size from a few to >30 receptor molecules per cluster in the PM of different cell types [196]. For example, EGFR clusters are present on both normal lung epithelial cells and lung cancer cells, but cluster diameter and number of EGFR was higher in cancer cells [197]. Considering these data, we hypothesized that EGF activating and inducing internalization of more clusters compared to TGF-α.

To test this hypothesis, we examined EGFR clustering upon stimulation with high doses (100 ng/ml) of EGF or TGF-α employing STORM super-resolution technology. We quantified the size of EGFR clusters close to PM. While smaller clusters (<0.03 μm^2) were present in TGF-α stimulated sample, larger clusters (>0.08 μm^2) were found upon EGF stimulation (**Figure 39**). These data suggest that EGF is inducing EGFR clustering more efficiently than TGF-α. In future experiments, we plan to examine role of PIP2 and lipid rafts in the recruitment/stabilization of EGFR clusters using pharmacological or genetic inhibitors/enhancers of PIP2, and drugs that affect lipid rafts (e.g., PPMP, methyl-β-cyclodextrin). We can also employ different techniques for investigating clusters such as optogenetics, a tool for fast light-induced and reversible protein clustering [198].

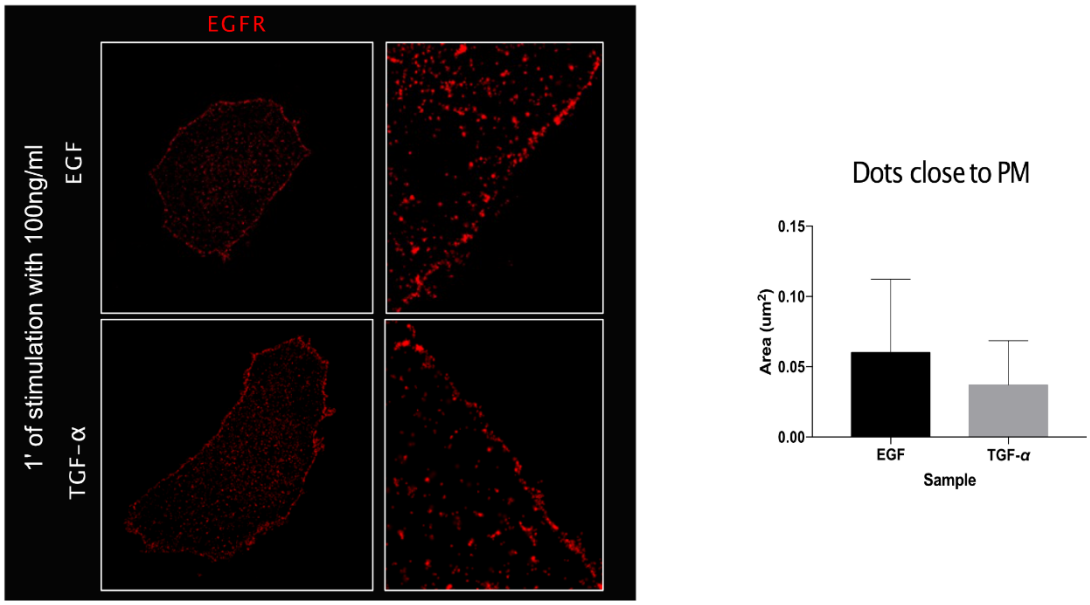

C

Surface area	EGF	TGF-α	Total
Area $< 0.03\ \mu m^2$	806	1259	2065
$0.03\ \mu m^2 \leq$ Area $< 0.05\ \mu m^2$	752	812	1563
$0.05\ \mu m^2 \leq$ Area $< 0.08\ \mu m^2$	838	507	1345
Area $\geq 0.08\ \mu m^2$	883	271	1154
Total	3278	2849	6127

Figure 39. EGFR clustering upon 1 min stimulation with high dose EGF and TGF-α.

A. *HeLa cells were stimulated for 1 min with EGF or TGF-α (100 ng/ml) at 37°C, then fixed, permeabilized and stained with anti-EGFR that was revealed with an Alexa-647 secondary (red). Cells were analyzed by STORM.* ***B.*** *Quantification of total area of red signal close (~2μm) to PM upon EGF and TGF-α simulation.* ***C.*** *Quantification of the number of clustered EGFR signals close to the PM upon EGF and TGF-α simulation, with different surface areas, as indicated.* ***Experiments*** *were performed with the help of Stefano Freddi from our lab, and Simone Pelicci and Mario Faretta (Imaging Development Unit, IEO).*

4.2.3. NCE activation upon stimulation with different RTKs

We have started to investigate whether other growth factors might induce internalization of their receptor and of CD147 similarly to EGF-EGFR. We initially studied HGFR/Met which is highly expressed and its signaling is relevant in HeLa cells. Interestingly, HGFR is activated by its only known ligand, HGF, and like EGFR it can be ubiquitinated by Cbl, is endocytosed and targeted for lysosomal degradation [199].

We therefore stimulated HeLa cells with saturating doses of HGF (100 ng/ml for 8 min) and followed CD147 internalization using an anti-CD147 antibody that recognizes its extracellular domain without interfering with endocytosis [63] and HGFR localization, staining it with specific antibody after fixation of HeLa cells. In unstimulated cells, the HGFR signal was mainly localized at the PM while only a small amount of CD147 signal was detectable in intracellular vesicles (**Figure 40A**).

Upon HGF stimulation, HGFR internalization was induced as expected (**Figure 40A**). HGF stimulation also induced internalization of CD147, with colocalization observed for HGFR and CD147 (**Figure 40A**). Notably, CD147 internalization was independent of clathrin but required RTN3 (**Figure 40A, B**). The efficiency of the KD of RTN3, clathrin or the double RTN3/clathrin KD was verified by WB (**Figure 40C**). While it seems that HGF stimulation activates CD147-NCE, we still need to understand what effect if HGFR is endocytosed by CME, NCE or combination of these pathways. In this experiment, as in one with EGFR (**Figure 34**) staining of HGFR was done after fixation, disabling us to distinguish between PM, internalized and newly synthesized HGFR and consequently to quantify only internalized HGFR. Further experiments following *in vivo* HGFR internalization, by using an antibody against its extracellular domain can provide us with more information about endocytic route of this receptor.

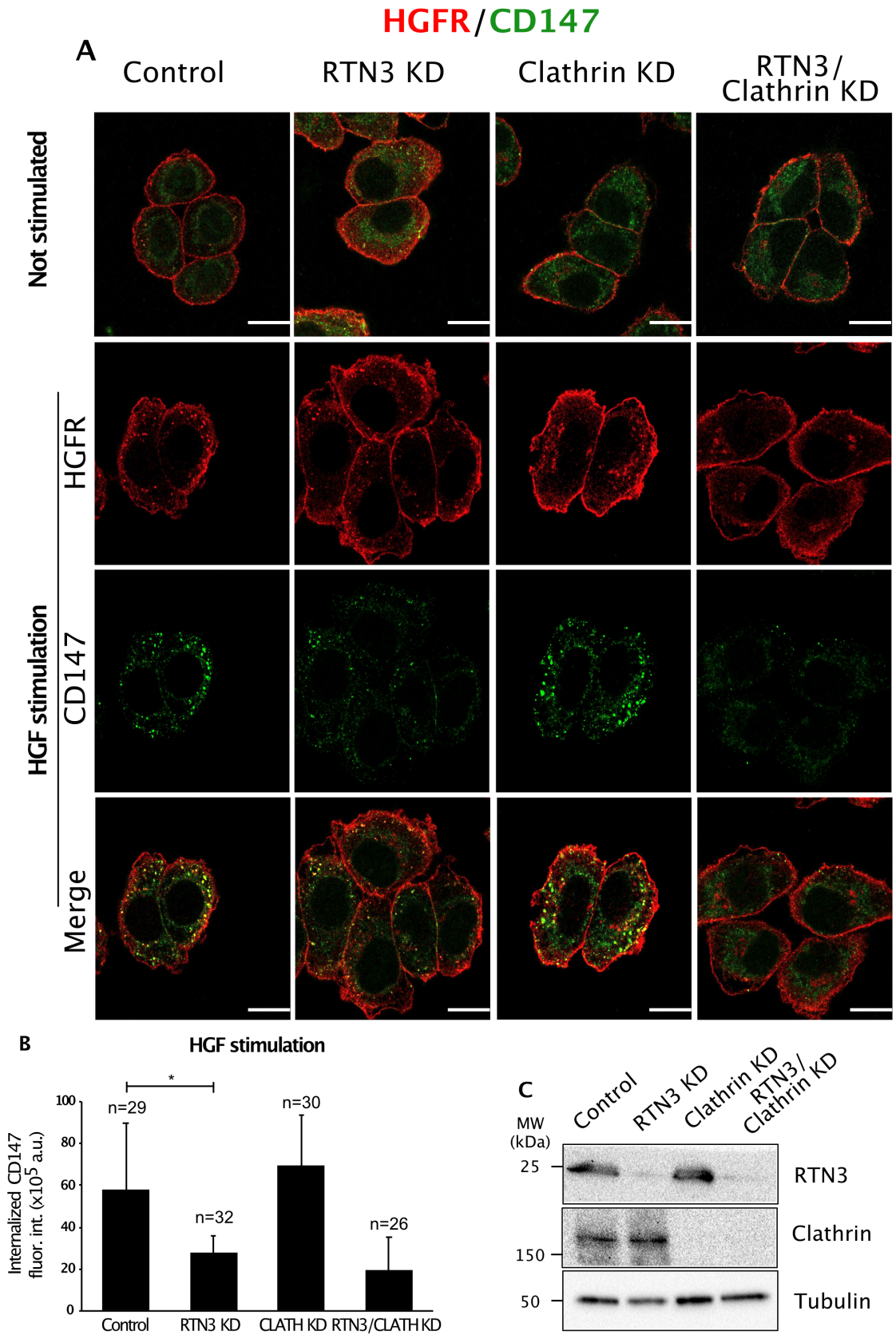

Figure 40. CD147 internalization upon stimulation of HeLa cells with HGF.

A. *HeLa cells were subjected to the indicated KD. CD147 internalization was followed for 8 min, using a specific mouse antibody applied to cells in vivo [63] in the absence (not stimulated) or in the presence of HGF (100 ng/ml). Cells were subjected to acid wash treatment prior to fixation, then stained for CD147 with the Alexa-488 secondary antibody (green). HGFR was stained with a specific antibody after fixation (red). Bar, 20 μm.* ***B.*** *Quantification of CD147 internalization in cells treated as described in A. CD147 signal was highlighted applying an intensity-based threshold (Default method), and then fluorescence intensity per field was calculated using the "Measure" command, limiting measurement to threshold. This value was then divided for the number of nuclei in the field, counted using the DAPI signal, in order to calculate the CD147 fluorescence intensity per cell. Mean integrated fluorescence intensity ± SD.* ***C.*** *Efficiency of the indicated KD was verified by WB analysis. n, cell number analyzed. P-value, Student's t-test two-tailed; *, P<0.05. Experiment performed once.*

4.3. The physiological role of EGFR-NCE

4.3.1. Role of NCE in cell metabolism

CD147 was shown to play a crucial role in cell metabolism, working as a chaperone regulating the PM localization of the glucose transporter GLUT1 and monocarboxylate transporters like MCT1, thus promoting glucose entry and lactate extrusion [200, 201]. Thus, NCE might regulate localization, trafficking and fate of these transporters possibly influencing cell metabolism. In order to investigate this issue, we performed colocalization experiments of EGF-induced internalized CD147 with MCT1 (**Figure 41**) or GLUT1 (**Figure 42**). Again, in these experiments, CD147 internalization was followed *in vivo*, while staining of MCT1 and GLUT1 was done after fixation.

Upon stimulation with high dose Alexa-555-EGF, we observed the colocalization of both CD147 and EGF with MCT1, which was maintained in clathrin KD cells, but abrogated in RTN3 KD cells (**Figure 41A**). The efficiency of the KD of RTN3 or clathrin was verified by WB (**Figure 41B).** These results suggest that MCT1 could be co-internalizing with EGF and CD147 via the NCE pathway upon EGF stimulation. Thus, it is possible that EGF-EGFR signaling, by regulating the PM levels and fate of this transporter, could influence metabolic cell functions such as lactate transport; a possibility that merits further investigation.

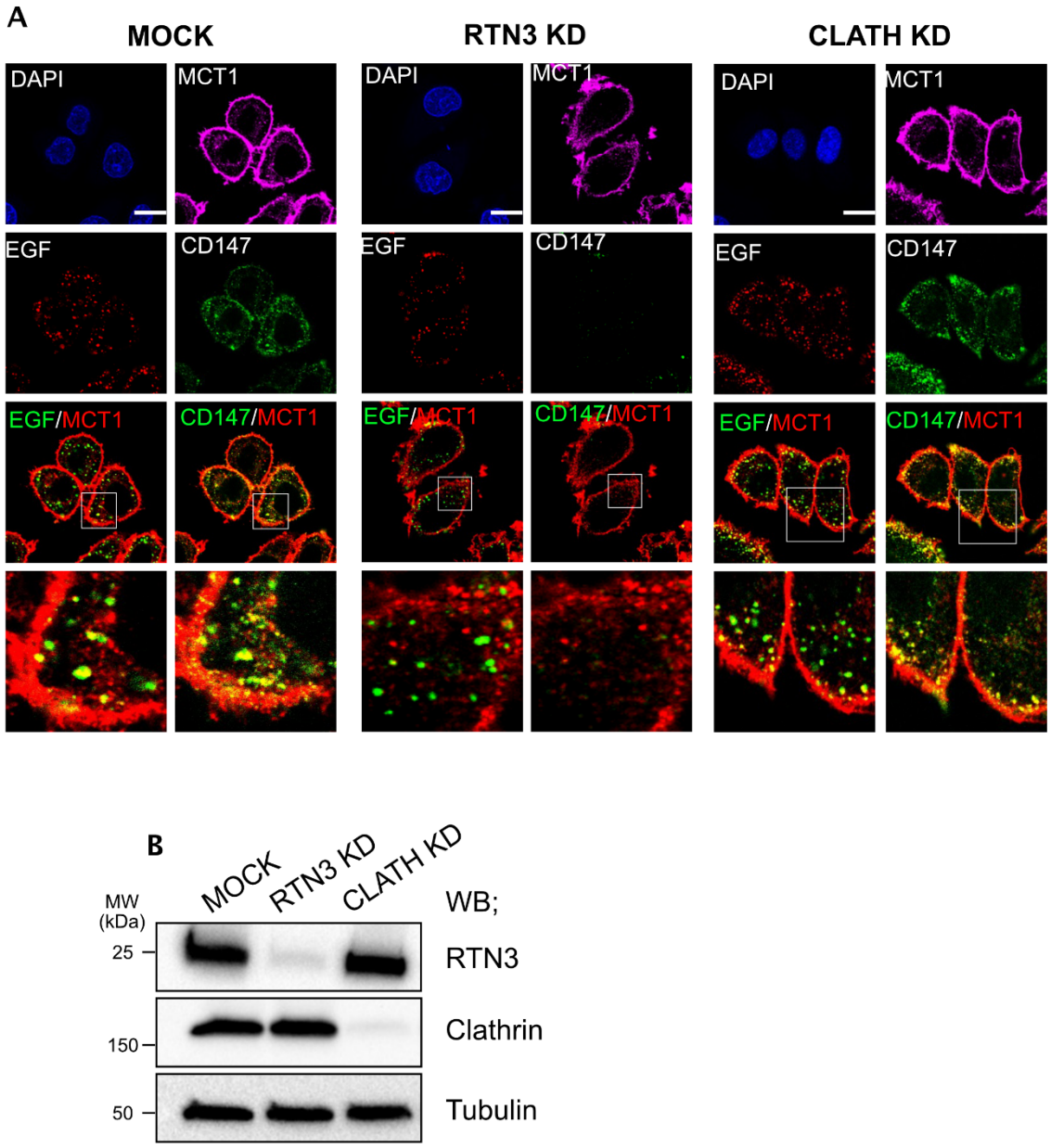

Figure 41. Colocalization of MCT1with CD147 and EGF.

A. *HeLa cells subjected to the indicated KDs were stimulated with high dose Alexa-555-EGF (red) for 8 min and CD147 internalization was followed in vivo with a mouse antibody recognizing the extracellular domain of the protein. Cells were subjected to acid wash treatment to remove CD147-bound antibody at the PM, followed by fixation and staining with an Alexa-488 secondary antibody (green). An anti-MCT1 antibody and Alexa-647 secondary antibody were used to visualize MCT1 (purple). Single channels and double merged channels are shown with EGF/MCT1 or CD147/MCT1 pseudocolored in green/red. Magnification of merged*

channels are shown at the bottom. Bar, 20 μm. ***B.*** *Efficiency of the indicated KD was verified by WB analysis. Tubulin, loading control. Experiment was performed once.*

We then performed the same assay for GLUT1 (**Figure 42**). In control unstimulated cells there was more GLUT1 on the PM (some signal was observed inside cell, showing a GLUT1 cytosolic fraction), in comparison to EGF stimulated cells, suggesting that some part of GLUT1 can be internalized upon EGF stimulation. It seems that GLUT1 was internalized primarily via CME, since more colocalization between GLUT1 and EGF was observed in control and RTN3 KD cells compared with clathrin KD cells.

Interestingly, from these preliminary experiments, it seems that both MCT1 and GLUT1 are internalized upon EGF stimulation, but via different pathways. However, more controlled experiments need to be conducted in order to understand the internalization mechanism of MCT1 and GLUT1, e.g., *in vivo* internalization with specific extracellular antibodies against these transporters upon stimulation of EGF. Since both transporters are involved in glycolysis, which is required for rapid energy production, in the future, it will be important to address how endocytosis is affecting this process.

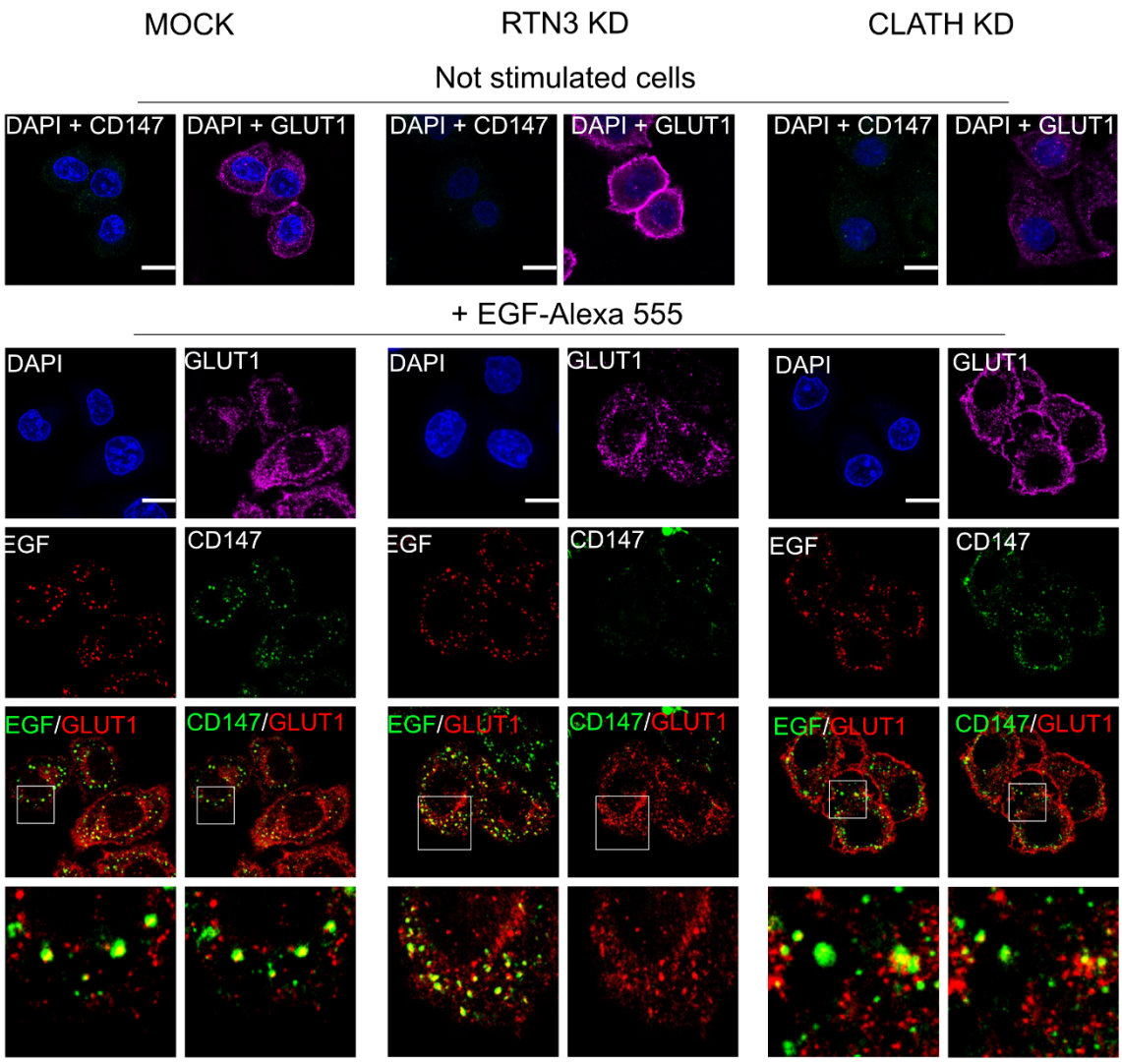

Figure 42. Colocalization of GLUT1 with CD147 and EGF.

HeLa cells subjected to the indicated KDs were stimulated with high dose Alexa-555-EGF (red) for 8 min and CD147 internalization was followed in vivo with an antibody recognizing the extracellular domain of the protein. Cells were subjected to acid wash treatment to remove CD147-bound antibody at the PM, followed by fixation and staining with an Alexa-488 secondary antibody (green). An anti-GLUT1 antibody and Alexa-647 secondary antibody were used to visualize GLUT1 (purple). Single channels and double merged channels are shown with EGF/GLUT1 or CD147/GLUT1 pseudocolored in green/red. Magnification of merged channels are shown at the bottom. Bar, 20 μm. Experiment was performed once.

4.3.2. EGFR endocytosis in MCF10A cells and spheroids

We previously found that NCE is active in different human cell lines, including cervical and breast tumor cell lines as well as normal keratinocytes, while it is not active in mouse embryonic fibroblasts and other cell types [63]. An interesting case is represented by MCF10A non-tumorigenic breast epithelial cells that showed only a minor activation of EGFR-NCE, if any [63]. However, since these cells are cultured in the continuous presence of EGF, with concentrations of 20 ng/ml in the medium, we decided to re-examine them for EGFR internalization upon starvation of EGF and serum for 3 h prior to EGF stimulation for 8 min at high dose. Using CD147 as a marker of EGFR-NCE, we identified a subset of cells where CD147 is internalized and colocalized with EGF indicating the presence of the NCE pathway (**Figure 43**). In RTN3 KD cells, we qualitatively observed a reduction of CD147 internalization; however, since MCF10A grow in adherence (not allowing the acid wash to completely detach antibodies), we still have signal of CD147 at PM. For this reason, it was not possible to quantify CD147 internalization with methods we usually use (Macro or Threshold method). In future experiments, we will try to optimize conditions for following CD147 internalization in MCF10A cells, with stronger and prolonged acid washes and also, we will prolong time of starvation of MCF10A from EGF and serum in order to allow accumulation of EGFR on PM.

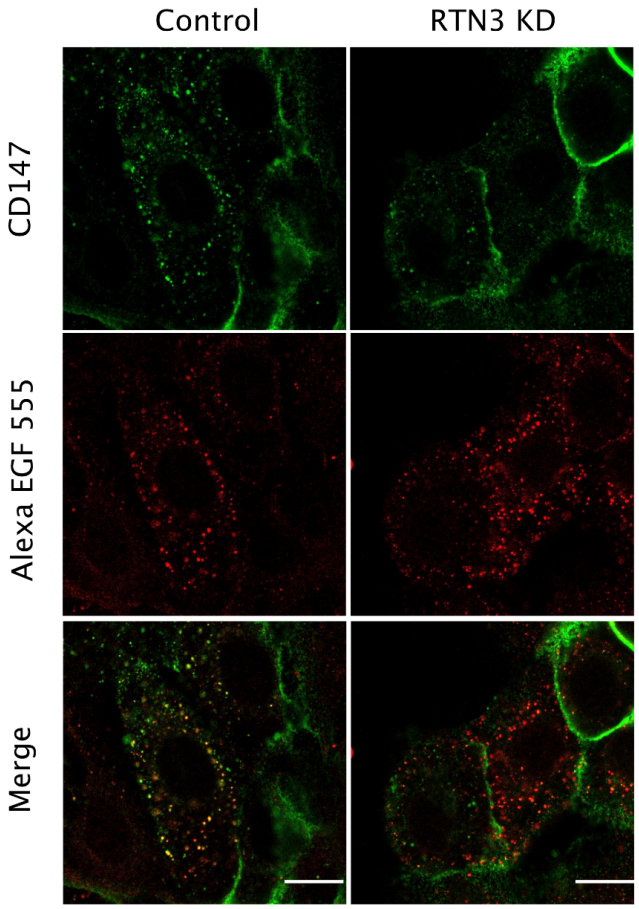

Figure 43. Presence of EGFR/CD147-NCE in MCF10A cells.

Confocal fluorescence microscopy images of MCF10A control or RTN3 KD cells, EGF and serum-starved for 3 h and treated with Alexa-555-EGF (100 ng/ml, red). CD147 internalization was followed for 8 min, using a specific anti-CD147 antibody applied to cells in vivo [63]. Cells were subjected to acid wash treatment prior to fixation, then stained for CD147 with the Alexa-488 secondary antibody (green). Bar, 20 μm.

Interestingly, MCF10A cells were clonally derived from mammary stem cells, which, by undergoing self-renewal and differentiation, generate in 3D culture organoids that possess an organized architecture that resembles acini-like structures of the mammary gland [202]. Therefore, to gain insights into the physiological relevance of NCE, we decided to use MCF10A organoids as a model system since they recapitulate many of the features of the mammary gland. We have set up protocols for the analysis of MCF10A organoids by IF and have been able to visualize EGFR phosphorylation and internalization in organoids stimulated with high dose EGF. We grew MCF10A organoids for 10 days, after which they were starved of EGF and

serum for 3 h before stimulation with 500 ng/ml EGF for 30 min. Organoids were then fixed and permeabilized, and stained with anti-CD147, anti-EGFR and anti-pEGFR primary antibodies and appropriate fluorochrome-labeled secondary antibodies. Using this approach, we were able to stain CD147 and EGFR in unstimulated cells, and EGFR and pEGFR in stimulated cells (**Figure 44**). Further experiments will be performed to characterize the presence of NCE in these organoids.

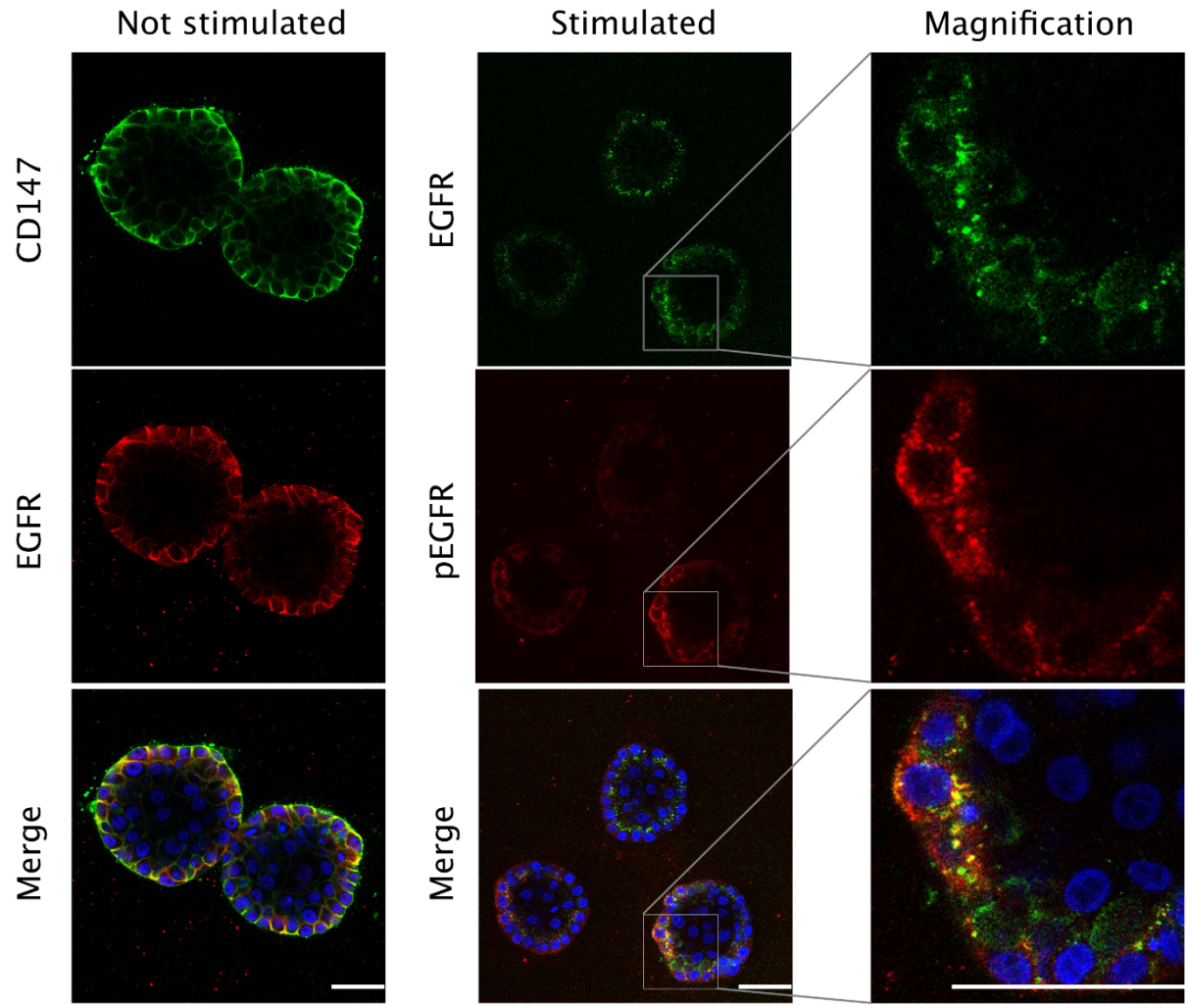

Figure 44. Relevance of EGFR/CD147-NCE in MCF10A spheroids.

Immunofluorescence staining of MCF10A organoids with the indicated antibodies (EGFR, CD147, pEGFR). Organoids were EGF and serum starved for 3 h and then stimulated or not for 30 min with EGF (500 ng/ml). Staining was done after fixation. Blue, DAPI. Bar, 50 μm.

4.3.3. Role of NCE in mouse intestinal and mammary organoids

To understand the physiological role of NCE in growth and differentiation, and in the stem cell *vs.* progenitor compartment, we have also established procedures for culturing organoids derived from primary cells from the mouse intestinal crypts or mammary glands. These organoids are highly dependent on a cocktail of factors, including high EGF concentrations, to grow and differentiate *ex vivo* in Matrigel. The intestinal organoids are obtained from crypts from mice intestine (as described [185]), while mammary organoids with double acini layer were obtained from inguinal and thoracic mammary glands [186]. We followed growth of these organoids upon treatment with different drugs (6 days for mammary and 8 days for intestinal). Interestingly, treatment with the EGFR kinase inhibitor, gefitinib, almost completely blocked organoid growth (**Figure 45**) [203]. Preliminary experiments also showed that treatment with compounds that inhibit EGFR-NCE*, i.e.,* PPMP and xestospongin C [63], have the opposite effect to gefitinib, promoting increased organoid growth (**Figure 45**). Although these two drugs act through different mechanisms (xestospongin C blocks Ca^{2+} release from the ER, while PPMP interferes with glycosphingolipid synthesis), both induced an increase in organoid number and size. One explanation of these results is that if we block NCE there is an increase of EGFR levels leading to increased proliferation and growth of these organoids. However, we should take into consideration that these drugs can affect many cellular targets, thus inhibiting not only NCE but other processes that can lead to the result we observed. To correlate effects of drugs to NCE, we should firstly examine levels of EGFR in organoids upon different treatments. However, we cannot distinguish effects on specific cells from organoids that are possibly affected by the drugs.

Although these results will be further verified through molecular genetic experiments (KD of specific NCE/CME players with shRNAs), they indicate that EGFR-NCE might have an important role in the regulation of organoid development, and moreover, a potential function in organ homeostasis.

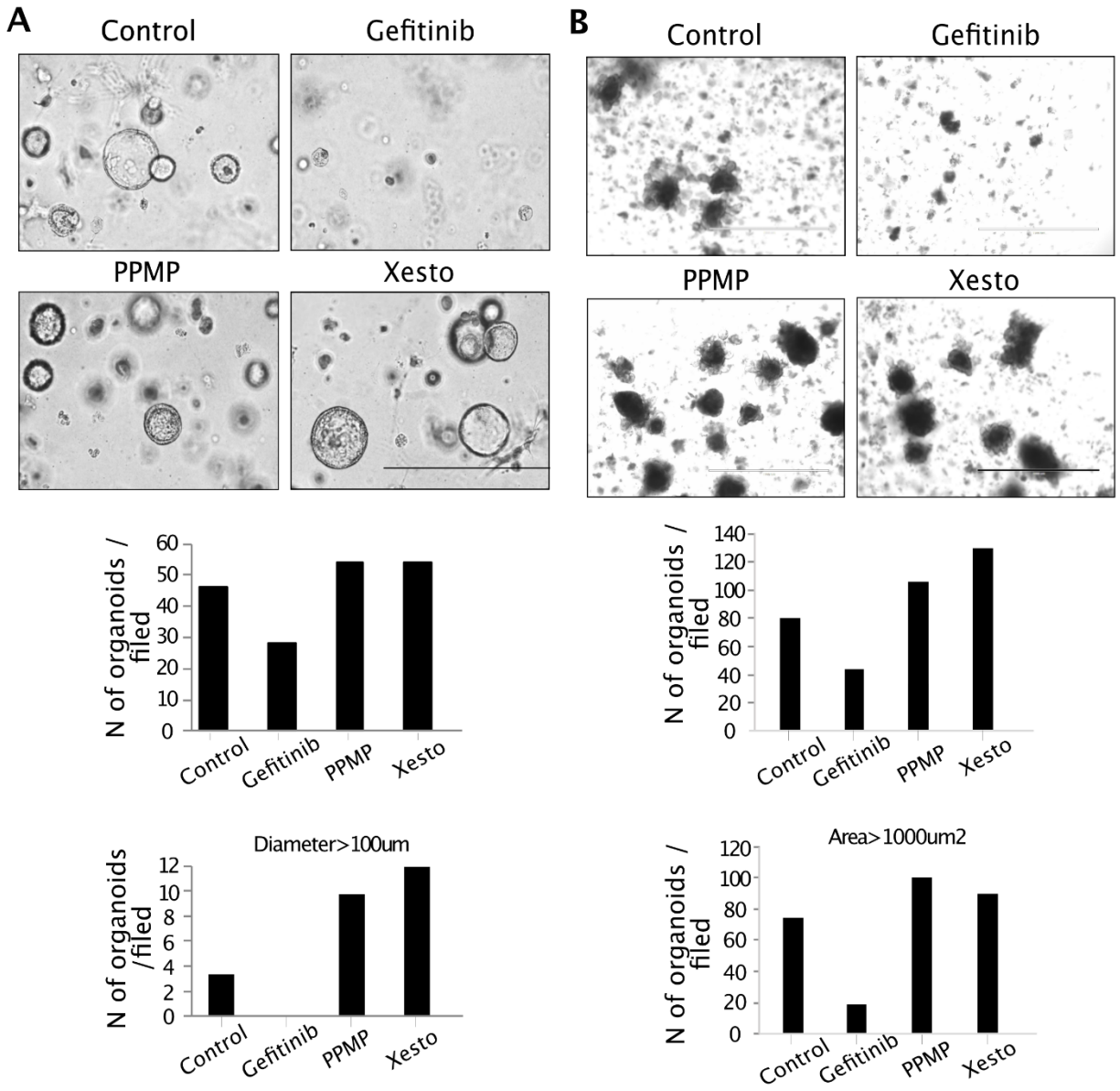

Figure 45. Effects of EGFR-NCE inhibitors on the growth of mammary and intestinal primary organoids.

A. Mammary organoids were treated for 6 days with gefitinib (10 μM), PPMP (5 μM), xestospongin C (Xesto; 2 μM) or vehicle control. Bar, 400 μm. Quantification of the number and size of organoids per field of view (1360x1024 pixels) is shown below representative images of the organoids. B. Intestinal organoids were treated for 8 days with gefitinib (10 μM), PPMP (5 μM) or xestospongin C (Xesto; 2 μM). Bar, 1000 μm. Quantification of the number and size of organoids per field of view (1024x768 pixels) as in "A". Experiment performed once.

5. DISCUSSION

We have previously described a novel non-clathrin endocytic pathway, defining its uniqueness compared to other endocytic routes described in literature. EGFR-NCE relies on several players not previously linked to endocytosis (e.g., RTN3) [63]. In the present work, we have dissected the signaling pathway promoting Ca^{2+} release, uncovering a specific role of the PLCγ2 enzyme, at variance with PLCγ1. Both PLCγ1 and PLCγ2 are recruited and phosphorylated by EGFR only at high doses of EGF, which leads to their phosphorylation. However, only PLCγ2 is able to induce a productive Ca^{2+} release through the IP3R, the main Ca^{2+} channel on the ER, in proximity of the PM (and, we hypothesize, close to NCE sites) that is ultimately required for the fission of EGFR-NCE vesicles from the PM. We uncovered that this specificity of PLCγ2 *vs.* PLCγ1 appears to be determined by the specific localization of PLCγ2 in specific regions of the PM, the so-called "lipid rafts", where NCE vesicles are generated and where contact sites between the PM and ER cortical tubules enriched in RTN3 are taking place [63].

At the functional level, we extended the relevance of NCE to EGFR ligands other than EGF. Saturating doses of the two EGFR ligands, AREG and TGF-α, differentially triggered EGFR internalization via NCE: while AREG efficiently activated NCE and Ca^{2+} release at the PM, TGF-α was much less effective, suggesting that this differential ability could be responsible for the specific biological outputs exerted by the two ligands. Interestingly, stimulation of cells with HGF, the only known ligand for the HGFR/Met, induced CD147 internalization similarly to EGF, providing evidence of the relevance of this novel NCE pathway to the regulation of other signaling receptors.

5.1. Signaling deriving from the EGFR that regulates EGFR-NCE and Ca^{2+}release

In present work, we unveiled a critical role of the PLCγ2 isozyme, but not PLCγ1, in NCE. Although both PLCγ1 and PLCγ2 are phosphorylated upon stimulation of HeLa cells with EGF, with a dose response correlating with the activation of NCE (i.e., only at high EGF doses), molecular genetic studies showed that PLCγ2 KD alone was able to inhibit EGFR- and CD147-

NCE, while PLCγ1 KD had no effect. PLCγ2 together with the IP3R were essential for the NCE-associated Ca^{2+} signaling at the PM, which was required for NCE-TI fission, in concert with the action of dynamin. Inhibition of IP3R had the same effects as PLCγ2 KD, suggesting that the role of PLCγ2 is exerted through the IP3 second messenger. Thus, the PLCγ2/IP3R/Ca^{2+} signaling axis appears to be a specific and essential component of the NCE mechanism (**Figure 46**).

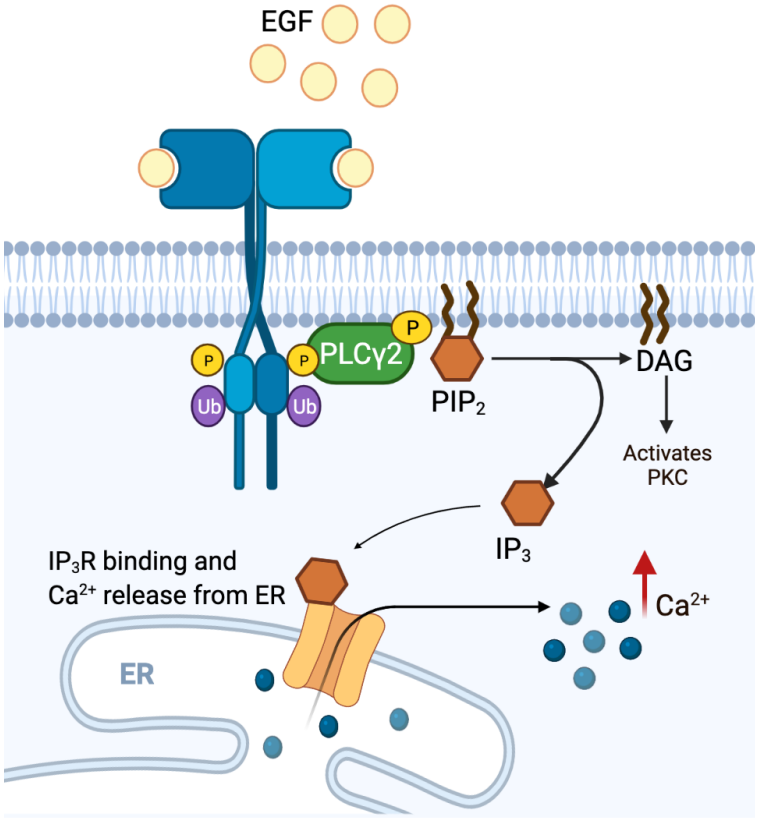

Figure 46. PLCγ2 activation upon high dose EGF stimulation.

Upon EGFR activation in the presence of high dose EGF, PLCγ2 is recruited to the receptor and activated by phosphorylation, leading to hydrolysis of the phospholipid PIP2 in the PM into DAG and IP3. IP3 then binds to the IP3R on the ER and opens it, inducing Ca^{2+} release from the ER lumen, which is necessary for the fission of NCE TIs. Created with biorender.com

A role of PLCγ2 in endocytosis was previously shown for Toll-like receptor 4 (TLR4) in macrophages, where PLCγ2/IP3R/Ca^{2+} inhibition blocked the translocation of TLR4 from the PM to the endosomes [204]. In addition, a hyperactive variant of PLCγ2 was found to increase the internalization of amyloid beta in microglia and macrophages [205]. We discovered here a

specific role of PLCγ2 in EGFR endocytosis that has not been reported previously. Ca^{2+} signaling activated downstream of PLCγ2 did not affect EGFR-CME, but was necessary for the fission of NCE TIs, showing the same phenotype as dynamin 2 KD. Interestingly, in the literature it has been reported that PLCγ1 and Ca^{2+} have a critical role in EGFR-CME in retinal pigment epithelium (RPE) cells at all doses of EGF stimulation [206]. Since, we demonstrated that the activation of NCE is dependent on cell context (**Table 3**, [62, 63]), this finding in RPE cells could be rationalized by the possibility that NCE is not present in these cells. Nevertheless, the involvement of the PLCγ1/IP3R/Ca^{2+} circuitry in endocytosis does not necessarily conflict with the involvement also of PLCγ2/IP3R/Ca^{2+} in the same cells. Since both PLCγ isozymes are activated at high doses of EGF, it is possible that PLCγ1 can play a role in trafficking events downstream of EGFR-CME and/or in Ca^{2+} signaling in other compartments than PM, while PLCγ2 is acting specifically on early steps of EGFR-NCE, possibly inducing a more localized Ca^{2+} response at PM-ER contact sites.

The specificity of PLCγ2 was unexpected as PLCγ1 is the best-characterized member of the family and widely expressed in different tissues, while PLCγ2 is expressed in a much more tissue-restricted manner, being highly expressed (and having a prominent role) in immune cells [151]. Similarly, as NCE is highly cell context dependent (**Table 3,** [62, 63]) and PLCγ2 is a critical player in this pathway, we hypothesized that the restricted expression of PLCγ2 might explain the activation of NCE only in specific cells. Indeed, in our screening, using RNA sequencing technology, of three cell lines (HeLa Milan, HaCaT [two cell lines known to have EGFR-NCE pathway] and HeLa Oslo [cell line that does not have EGFR-NCE]) we revealed that PLCγ2 expression correlates with activation of NCE (**Figure S1A**). We found less expression of PLCγ2 in HeLa Oslo, where NCE is not active, in comparison to cell lines that do have NCE, HeLa Milan, and HaCaT. Moreover, these data were confirmed by WB (**Figure S1C**). On the other side, no significant difference of PLCγ1 expression was observed between HeLa cell lines, while HaCaT cells show decreased expression of PLCγ1 in comparison to HeLa Oslo (**Figure S1B, C**). We will perform further analysis to evaluate expression of these enzymes in other NCE-relevant cell lines. However, understanding PLCγ2 vs. PLCγ1 specificity might give important insights on how NCE is regulated, also considering that the activation of this mechanism of endocytosis is dependent on the cell context and the strength of stimulation.

5.1.1. PLCγ isozymes and their post-translational modifications

To address the mechanism of PLCγ2 specificity in NCE and due to the lack of an antibody against the PLCγ2 enzyme suitable for IF assays, we have generated stable HeLa cell lines expressing HA-tagged PLCγ1 or PLCγ2, with and without inducible clathrin KD (for studying only NCE). We used control HeLa cells expressing endogenous PLCγ and HeLa cells expressing the HA-tagged PLCγ enzymes, to evaluate the basis of the differential involvement of PLCγ1 and PLCγ2 in NCE.

In this system, we initially checked for any differences in the phosphorylation of PLCγ enzymes by EGFR, as it is known that RTK-mediated phosphorylation of PLCγ enzymes is responsible for their activation [145]. Since we showed that upon stimulation with high dose EGF both PLCγ enzymes are similarly relocated from the cytosol to the PM and similarly phosphorylated, we hypothesized that there might be differences in the precise PM locations where phosphorylation occurs. In particular, we reasoned that PLCγ2 might be phosphorylated and activated specifically at sites of NCE-TIs, while PLCγ1 phosphorylation might be occurring in other regions of the PM – perhaps in CCPs where part of the activated EGFR fraction is located. Therefore, selectively abrogating NCE might affect PLCγ2 phosphorylation but not PLCγ1. To check this, we performed RTN3 KD and Cbl KD (NCE inhibited – early stage) or AP2 KD (CME inhibited) and looked at PLCγ phosphorylation status in HeLa cells. No major differences were observed in the phosphorylation status of the PLCγ enzymes in any of the KD conditions. It should be noted that the experiment with Cbl KD needs repeating as the total levels of EGFR appeared to be downmodulated in these cells. However, given that PLCγ1 and 2 showed similar phosphorylation patterns in all conditions, it would appear that their recruitment to the EGFR and their phosphorylation is occurring upstream of RTN3, AP2 and possibly Cbl function. It appears that the differential NCE involvement of the PLCγ enzymes cannot be explained from these data.

In the above scenario, we have considered PLCγ phosphorylation only as an activation mechanism, however, it is possible that the phosphorylation of specific residues has different effects on enzyme activity, with some phosphorylation reactions resulting in inhibition of enzymatic activity. For example, phosphorylation of serin 1248 of PLCγ1 by PKA or PKC upon EGF stimulation results in inhibition of the catalytic activity of PLCγ1 [207, 208]. Sequence alignments showed that this residue (Ser1248) is not conserved in PLCγ2, so hypothetically

soon after stimulation with EGF, the activation of its downstream effector PKC could cause the inhibition of PLCγ1, explaining why it is not playing a role in NCE; while PLCγ2 is kept active inducing Ca^{2+} release that is necessary for NCE. To test this possibility, we plan to check the PLCγ1-Ser1248 phosphorylation status upon EGF stimulation in our cell system and, if this site is phosphorylated, we will mutate it and then examine, in PLCγ2 KD cells, if the mutant PLCγ1 can compensate PLCγ2 role in NCE.

Since we have used phosphorylation as proxy for PLCγ enzyme activation and have not directly assessed their lipase activity, future experiments will be undertaken to understand if both isozymes are enzymatically activated after EGF stimulation. To this end, we plan to measure levels of their substrate PIP2 and reaction products, IP3 and DAG, upon stimulation with high EGF in PLCγ1/2 KD conditions, to have an indication of their activity levels.

Ubiquitination is necessary for NCE, since it depends on EGFR-Ub and several Ub-binding proteins, such as Eps15/L1 and epsin1 [62]. There are some indications in literature that PLCγ1 can be ubiquitinated. In particular, it was shown that the CISH (cytokine-inducible SH2 containing protein) E3 ligase is able to form a complex with PLCγ1, leading to its ubiquitination in T cells [209]. Moreover, upon TCR stimulation, overexpression of Cbl-b in human T lymphocyte Jurkat cells increased ubiquitination of PLCγ1. Accordingly, Cbl-$b^{-/-}$ T cells showed reduced levels of PLCγ1 ubiquitination [210]. In Cbl-$b^{-/-}$ B cells, B cell receptor stimulation induced prolonged PLCγ2 phosphorylation and Ca^{2+} fluxes, although no evidence on PLCγ2 ubiquitination status was reported [211]. These experiments were performed in immune cells upon T or B cell receptor stimulation, however, in terms of the EGFR system little is known about PLCγ ubiquitination. It was shown that PLCγ1 binds c-Cbl in an EGF-dependent way in the A431 epidermoid carcinoma cell line but ubiquitination of PLCγ1 was not observed [212]. Although there is not direct evidence that PLCγ2 is ubiquitinated, the PhosphositePlus tool suggests that both isozymes of PLCγ have ubiquitination sites (https://www.phosphosite.org/homeAction; PLCγ1; PLCγ2).

Since Ub can act as a signal to recruit adaptor proteins to the activated EGFR in NCE, we assessed whether PLCγ1 and PLCγ2 have Ub-binding abilities by performing *in vitro* pulldown assays with GST-3Ub. Moreover, given that Ub-binding adaptors play a specific role in NCE (i.e., Eps15/L1 and epsin1 [123]), we also checked if PLCγ1 and PLCγ2 undergo ubiquitination upon EGF treatment by performing immunoprecipitation of HA followed by anti-Ub WB. Our data suggest that there is no major binding of PLCγ1-HA and PLCγ2-HA to Ub

upon EGF stimulation, while we were able to confirm the increased Ub-binding of known interactors Eps15 and Rabex-5. However, since we scored some unspecific binding of HA-tagged proteins to GST, we plan to repeat pulldown assays with endogenous PLCγ. Moreover, the PLCγ enzymes do not appear to be ubiquitinated upon EGF stimulation, as evidenced in immunoprecipitation and WB experiments, in which we were able to score an increase in Eps15-Ub. Interestingly, is this experiment PLCγ1/2 appeared to be ubiquitinated at steady state, suggesting that these proteins can be ubiquitinated. However, this ubiquitination might simply be due to the high levels of expression of the HA-tagged proteins, and the removal of excess protein through ubiquitination and proteasomal degradation. To investigate this possibility, we can repeat these experiments in endogenous setting, by immunoprecipitating ubiquitinated proteins with an anti-Ub antibody and performing a WB against PLCγ1 and PLCγ2.

In conclusion, no post-translational modifications were identified that could account for the specific role of PLCγ2 in NCE.

5.1.2. Distinct subcellular distribution of PLCγ1 and PLCγ2

5.1.2.1. PLCγ1 *vs.* PLCγ2 specific co-clustering with different endocytosis players at the PM

We hypothesized that PLCγ isozymes might be enriched/recruited to different EGFR pools or PM compartments. To understand this, we first checked how EGF treatment affects the subcellular localization of PLCγ enzymes by confocal IF microscopy using the anti-HA antibody and fluorophore-labeled secondary antibodies. As known from the literature, PLCγ is recruited to the pY992 residue of the EGFR [213], leading to its phosphorylation by EGFR and catalytic activation. The activated enzymes are retained at the PM by binding to PIP3. In agreement, we showed relocalization of PLCγ-HA enzymes to the PM after high dose EGF stimulation, while at steady state both enzymes were homogenously localized in the cytosol. To understand if, in our system, PLCγ1 and PLCγ2 are recruited to the activated EGFR at the PM, we employed STORM super-resolution technology. We were able to see recruitment of both PLCγ-HA enzymes to EGFR clusters at the PM. In particular, using a mask to quantify signal only at the cell periphery (close to the PM), we observed increased co-clustering of EGFR and HA upon high EGF stimulation. However, although both enzymes are recruited to and

phosphorylated by the EGFR, we observed that only PLCγ2 is localized in PM subdomains co-clustering with RTN3, likely representing PM-ER contact sites where NCE takes place. In contrast, there was little co-clustering of RTN3 and PLCγ1 signals. Moreover, no co-clustering was observed between clathrin and PLCγ enzymes, confirming the specificity of PLCγ2-RTN3 co-clustering and suggesting that the critical role of PLCγ2 in EGFR-NCE is exerted through its specific subcellular localization. In the future, we will evaluate co-clustering of PLCγ1 and PLCγ2 with other proteins involved in NCE (*e.g.,* CD147) or CME (*e.g.,* AP2) as a negative control, upon both high *vs.* low EGF stimulation. Moreover, we will examine if RTN3/PLCγ2 co-clustering depends on i) phosphorylation of PLCγ2; ii) specific pattern of EGFR phosphorylation (e.g., pY992 or pY1173 that are docking sites of PLCγ2); iii) specific adaptors (e.g., Rac, see **Section 5.1.3.**) that can recruit PLCγ2 to RTN3.

5.1.2.2. PLCγ1 *vs.* PLCγ2 recruitment to different PM compartments/ microdomains

The different co-clustering patterns of PLCγ2 *vs.* PLCγ1 led to the hypothesis that upon EGF stimulation, PLCγ2 is recruited specifically to lipid rafts where NCE takes place. Interestingly, it was shown upon B cells activation that PLCγ2 is recruited to lipid rafts from where it starts signaling from the B cell receptor [214]. Moreover, upon mast cell activation, PLCγ2 is relocalized predominantly to osmiophilic patches, the so-called "primary signaling domains", together with IgE receptors and other signaling molecules, at variance with PLCγ1, which was mainly relocalized to PM outside these patches [187]. The osmiophilic patches are regions of the PM (e.g., unsaturated fatty acids, sphingomyelins, cholesterol [215]) that stain darkly with osmium in comparison to other parts of membrane. Here, we showed that PLCγ2, but not PLCγ1, is specifically recruited to osmiophilic patches in our model system using EM and immunogold labeling of HeLa membrane sheets stained with an anti-HA antibody that reveals the localization of PLCγ1/2-HA enzymes. This finding is in line with the STORM analysis and provides further support to the differential localization of PLCγ enzymes at the PM.

As a complementary approach, we performed a protein flotation assay to isolate detergent-soluble and insoluble ("lipid rafts") PM fractions from cells stimulated high EGF concentrations. We found that upon EGF stimulation, PLCγ2 was enriched in the floating

fraction with highest expression of flotillin and caveolin (markers of lipid rafts). For PLCγ1, we did not score differences in localization between fractions in cells stimulated or not with EGF. However, this experiment was performed in cells expressing PLCγ2-HA and future assays will be repeated in both PLCγ1-HA and PLCγ2-HA expressing cells, in order to verify the differential recruitment of PLCγ1 *vs.* PLCγ2 to lipid rafts under the same overexpression settings.

In order to investigate further whether PLCγ1 and PLCγ2 are recruited to specific PM domains, we also employed STORM super-resolution microscopy and evaluated the co-clustering of PLCγ1 and PLCγ2 with CTxB. CTxB can bind to five GM1-ganglioside receptors, located in lipid rafts of PM, and for this reason CTxB is generally considered as a marker of lipid rafts [71]. However, no differences were scored between the co-clustering of PLCγ1 and PLCγ2 with CTxB upon EGF stimulation (**Figure S2**). This can be explained by the fact that in some cases CTxB can bind also to other sugar components on PM, such as galactose [216], thus not labeling only lipid rafts. Moreover, it has been found that CTxB/GM1 can be internalized through CME [217, 218]. To overcome this issue, we will evaluate co-clustering of PLCγ1 *vs.* PLCγ2 with other more specific markers of lipid rafts (e.g., GPI-anchored proteins such as CD55, CD58, and CD59), or we will try to disrupt lipid rafts (e.g., by depleting cholesterol with methyl-β-cyclodextrin) and then check the localization/recruitment of PLCγ to EGFR upon EGF stimulation.

Recruitment and catalytic activity of PLCγ largely depends on the lipid content of membrane. It has been shown that PLCγ1 is relatively inert towards PIP2 unless it is first bound to a tyrosine kinase [219]. It could be that PLCγ2 is more stably bound to PIP2, since the engineered cSH2 domain of PLCγ2 was shown to have higher affinity (almost double) to lipids at the PM in comparison to the cSH2 domain of PLCγ1 [220]. PIP2 is also required for PLCγ signaling. Earlier studies showed that in NR6 cells, EGF-induced signaling of PLCγ1 was restricted to the PM in comparison to intracellular compartments (e.g., endosomes) even though both EGFR and PLCγ1 were still phosphorylated in these compartments. This was explained by limited access to PIP2 by PLCγ1 in endosomes [221]. However, recent studies showed that the presence of PIP2 in endosomes is dynamically controlled and its localization could be also cell dependent [222], so it would be interesting to evaluate its role and signaling in NCE.

5.1.3. PLCγ1 *vs.* PLCγ2 specific interactors

Tyrosine kinase receptors are known as main activators of PLCγ, however, they are not the only proteins that can bind and stabilize PLCγ at PM; for instance, the scaffolding protein SLP-76 [SH2-domain-containing leukocyte protein of 76 kDa] binds to the SH3 domain of PLCγ1 [223], while Rac binds to sPH of PLCγ2 [224] (**Figure 47**). We hypothesized that the specificity of PLCγ2 *vs.* PLCγ1 in EGFR-NCE could be explained by their differential interactors. Importantly, only PLCγ2, and not PLCγ1, is activated by the Rho family of small GTPases - Rac1, Rac2 and Rac3 in their GTP-bound forms - and this activation is independent of phosphorylation of tyrosine residues on PLCγ. The sPH domain of PLCγ2, is both necessary and sufficient for activation of PLCγ2 by Rac [225], and the crystal structure of PLCγ2 sPH:Rac complexes revealed a hydrophobic pocket with set of specific amino acids, not conserved in PLCγ1, that are necessary for Rac-mediated activation of PLCγ2 [226]. Indeed, mutation of one of those amino acids, F897Q, blocked interaction PLCγ2 with active Rac.

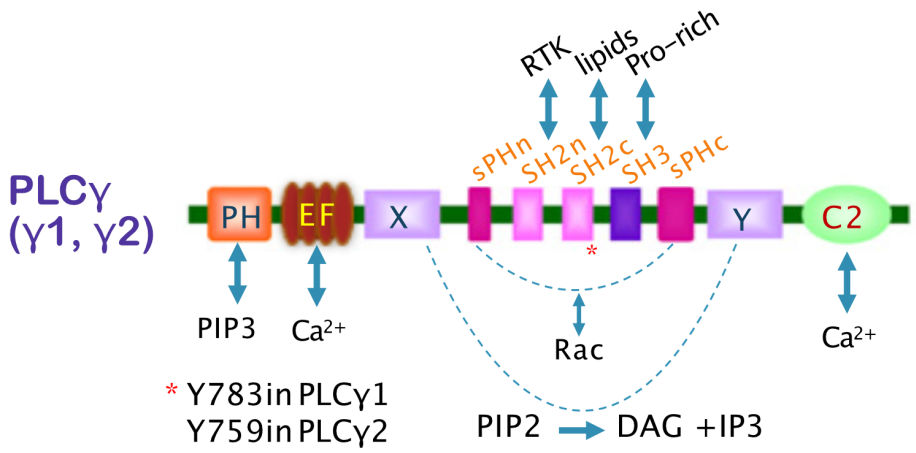

Figure 47. PLCγ domains and interactors.

PLCγ are multidomain enzymes that can bind different targets (PH – PIP3; EF – Ca^{2+}, sPH - Rac, SH2n – RTKs, SH2c-lipids, SH3 – Pro rich protein domains, C2 - Ca^{2+}). Red star shows pY (783 in PLCγ1 and 759 in PLCγ2). Adapted from Choi, Adv Enzyme Regul, 2007 [227]

Rac1 is the major form of Rac expressed in HeLa Milan cells, and we found that its KD inhibited EGF internalization at both low and high doses of EGF (**Figure S3A, C**). Rac1 KD also inhibited Tf internalization, suggesting that Rac1 plays a role in CME (**Figure S3B, E**).

Thus, it is possible that Rac1 is involved in just CME or both CME and NCE. In support of the latter, at high EGF doses, in the KD of Rac1, in combination with clathrin KD, further decrease of EGF internalization (though not statistically significant) in comparison to clathrin KD alone was scored, arguing that it can also affect NCE. Moreover, KD of Rac1 inhibited internalization of the NCE specific cargo, CD147 (**Figure S3D**). Although these data still need to be verified, they suggest that Rac1 could play a role in both EGFR-CME and -NCE.

Rac is not able to disrupt autoinhibition of PLCγ2, but rather it stabilizes the active conformation of PLCγ2 once it is recruited to PM [228]. Since also Rac was shown to localize in membrane rafts [229], we hypothesized that it could be involved in the recruitment and stabilization of PLCγ2 in these membrane subdomains upon EGFR activation. To test our hypothesis, we will employ different approaches. We will check: 1) recruitment of PLCγ2 to the PM (and/or EGFR) -/+ EGF, in the HeLa cells depleted of Rac1 or expressing Rac1 dominant-negative or dominant-active forms; 2) colocalization of PLCγ2 and Rac1 upon EGF stimulation, using the probe for active Rac1 [230]; 3) EGF and CD147 internalization in Rac1 dominant-negative or dominant-active expressing cells; 4) EGF and CD147 internalization in cells expressing PLCγ2 mutants (F897Q) unable to bind to Rac1.

While the role of Rac1 will be molecularly dissected, we will evaluate other possible interactors. For example, Grb2 was shown to interact with phosphorylated Y783 of PLCγ1, inhibiting its activation upon EGF stimulation and consequent catalytic activity [152]. In contrast, no evidence of Grb2 interaction with PLCγ2 was found in literature. Thus, one possible scenario in our model system is that upon EGF stimulation, phosphorylated PLCγ1 is inhibited by Grb2, while PLCγ2 is free to carry out its catalytic activities, explaining their differential roles. In addition, we can also look for novel PLCγ2 interactors by immunoprecipitation of PLCγ1/2-HA in conditions of +/- EGF and mass spectroscopy to identify co-immunoprecipitating proteins. This approach could lead to the discovery of novel regulators of endocytosis and might allow us to better understand the role of PLCγ2 in EGFR endocytosis.

5.1.4. PLCγ2 in signaling and cell responses

PLCγ2 is involved in endocytosis and signaling originating from BCRs. In the literature, it is reported that mutations that activate PLCγ2 contribute to its pathological role related to dysfunction of the immune system: *e.g.,* autoinflammation and autoimmunity, and drug

resistance in chronic lymphocytic leukemia [162, 231]. However, one mutation that activates PLCγ2 has been linked to the protection from the development of Alzheimer's disease [232] due to increased endocytosis of dextran and beta amyloid [205]. This is interesting, since it shows that aberrant activation of PLCγ2 can have advantageous or pathological properties, depending on the cell context. Endocytosis of dextran and beta amyloid were blocked upon inhibition of both CME (with chlorpromazine [233]) or CIE (with Methyl-β-cyclodextrin [234]) [205], so further studies should be performed to understand the role of this mutant in EGFR-NCE.

The NCE cargo, CD147, is highly expressed in immune cells: T and B lymphocytes, dendritic cells, monocytes and macrophages [131]. Given these observations, an intriguing scenario – which we would like to evaluate – is that NCE might play a critical role in the immune system. One of our future directions is the evaluation of the activation of NCE in immune cells (e.g., macrophages or microglia).

Interestingly, it was recently shown that the SARS-CoV-2 virus can use CD147 as an alternative receptor to ACE2 to enter the cells (*e.g.,* in lung and kidney epithelial cells) [235]. Potentially, immune cells might also be infected by SARS-CoV-2 and participate in the local and systemic spread of the virus [236]. Thus, NCE could be a mechanism of viral entry into cells expressing CD147, and PLCγ2 could be a novel regulator of virus infection. Future studies are required to investigate this possibility, which could pave the way for the development NCE-targeted drugs, such as PLCγ2-specific inhibitors.

Given its role in the downregulation of EGFR signaling, we propose here that NCE could have a potential tumor suppressor function and its dysregulation could contribute to aberrant EGFR signaling, as frequently observed in several human tumors. Indeed, inhibition of NCE leads to sustained ERK1/2 and AKT signaling in HeLa cells [63] and, as shown here, it induces increased growth of primary mammary and intestinal organoids. Thus, loss of NCE could contribute to tumor growth. However, this is a simplistic view, as we know that NCE is not only a negative regulator of the EGFR downstream signaling cascade, but it is also a positive regulator of Ca^{2+} signaling, which might be important for cell adhesion and migration. Indeed, signaling from the EGFR can lead to different cell responses, including cell proliferation, survival, differentiation and migration, and these responses are mediated via different signaling pathways [237]. The EGFR-activated PLCγ-dependent pathway has been associated with cell migration: EGF-dependent cell migration was blocked by inhibition of either PLCγ itself [238], EGFR kinase activity or phosphorylation of the pY992 phosphosite in the EGFR cytoplasmic

tail (the site of PLCγ recruitment) [239]. Mechanistically, it was proposed that PIP2-bound actin regulatory proteins are released upon PLCγ activation, restoring their ability to remodel cortical actin filaments, a process required for filopodia/lamellipodia extension and retraction in motile cells [240, 241]. In agreement, EGFR activation of PLCγ leads to actin reorganization and contributes to the initiation of the motile phenotype [242]. PLCγ2 activity has been previously linked with activation and mobilization of the actin cytoskeleton in myeloid cells [243, 244] and Rac (an activator of PLCγ2), also plays a role in actin polymerization [245]. In addition, many actin-regulatory proteins are Ca^{2+}-dependent and might be therefore regulated by PLCγ through IP3-mediated Ca^{2+} signaling [246]. We have initial data showing that the Arp2/3 complex, a major actin regulator, is relocalized to the PM upon EGF stimulation and that an inhibitor of Arp2/3 is able to block CD147 internalization. Moreover, preliminary experiments show a possible involvement of NCE in wound healing in HaCaT cells, a normal keratinocyte cell line where NCE is active (Salvi Mesa D., unpublished data). Further studies are needed to clarify the role of PLCγ2 in NCE, EGFR signaling and biological response, to understand whether the NCE-PLCγ2 axis is altered in cancer and if PLCγ2 mutations have positive or negative effects on NCE, promoting or inhibiting cancer-related phenotypes.

5.1.5. The role of Ca^{2+} and other secondary messengers

We have dissected the role of the IP3 second messenger (from PLCγ signaling) in Ca^{2+} release from the ER and in NCE, however, the function of DAG was not investigated. DAG can be converted to PA by DGK and PA is important for negative curvature of the membrane, which could lead to recruitment of dynamin and EGFR endocytosis [247]. In addition, from the literature it is known that some forms of DGK can be activated by binding to Ca^{2+}. We tested the possible involvement of DGK in NCE by ablating DGKα with siRNA and by inhibition of all DGK family of enzymes with an allosteric inhibitor. We found that the inhibitor of DGK inhibited CD147 internalization, while DGKα KD did not. Thus, it is possible that the DGKα isoform does not a have function in NCE, while other isoforms of DGK can play a crucial role; this will be further investigated.

Another point to be clarified is the role of Ca^{2+}. As known from literature Ca^{2+} activates dynamin 1 [248], while dynamin 2 is necessary for NCE [62]. In neurons Ca^{2+} binds to and activates calcineurin, a phosphatase that is able to regulate different proteins including ones

involved in endocytosis, such as dynamin, Eps15, epsin1 [249]. To understand effect of calcineurin on NCE, we checked EGF and CD147 internalization upon treatment with specific calcineurin inhibitors (CsA and FK506). We scored a partial decrease in the internalization of both EGF (~25%) and CD147 (~35%), suggesting that NCE is partly inhibited but not completely blocked. Since the mechanism of regulation of NCE appears complex and may require different regulators, it is possible calcineurin is one of them, but future experiments will be performed in order to discard off-target effects of the calcineurin inhibitors.

Another role of DAG and Ca^{2+} in NCE could be in the translocation of PLCγ2 to the PM: in B cells it was shown that C2 domain of PLCγ2 specifically interacts with Ca^{2+} and PM, inducing translocation of PLCγ2 and amplification Ca^{2+} signaling [250]. This mechanism depends on Ca^{2+} influx generated by DAG-dependent activation of PM Ca^{2+} channels (RACC), and IP3R. Translocation of PLCγ2 leads again to hydrolysis of PIP2 into DAG and IP3, leading to a second Ca^{2+} wave by IP3R, and amplification of Ca^{2+} signaling. Since these events are happening close to the PM, they could be involved in NCE and they might explain why we detected repetitive Ca^{2+} pulses with PM-targeted Ca^{2+} sensors (**Figure 35C**). Interestingly, mutations that lead to PLCγ2 constitutive activation, as for instance deletion of the C2 domain, can induce a continuous release of Ca^{2+} from ER [251]. Moreover, deletion of some parts in the C2 domain showed loss in response to EGF, suggesting that this domain can play a role in EGF signaling [251]. Of note, although the C2 domain is present in PLCγ1 and its structure seems to be similar to that in PLCγ2, there is no evidence in literature that it can be regulated by Ca^{2+}. Thus, it is possible that the C2 domain is critical for the stepwise activation of PLCγ2 and for the generation of Ca^{2+} waves at the PM, determining the specific role of PLCγ2 in NCE. Further investigations are required to verify this possibility.

5.2. NCE activation by other EGFR ligands and RTKs

While the identification of players involved in NCE-EGFR signaling is critical to reveal endocytic molecular interactors and regulatory mechanisms that could represent novel targets in cancer therapy, it is also important to understand other potential activators of NCE. Since different EGFR ligands can induce different biological outcomes starting from the activation of the same receptor [192], we hypothesized that they might exert this differential function through the induction of different endocytic routes. Indeed, by regulating signaling duration and spatial

distribution, endocytosis has a key role in controlling the final biological response [128]. Therefore, the study of extracellular cues that can promote EGFR-NCE, or are unable to do so, should contribute to our understanding of the oncogenic function of these activators, since the ones that do not induce NCE could lead to an inefficient downmodulation of the receptor. Along this line, we showed a substantial activation of EGFR-NCE upon AREG and EGF stimulation but a weak activation upon TGF-α treatment. While EGF and AREG efficiently induced internalization of CD147, TGF-α failed to do so. Surprisingly, we could not detect differential EGFR phosphorylation and/or ubiquitination or differential activation of early signaling effectors (e.g., PLCγ, AKT, ERK1/2, SHC) at 2 min of stimulation with EGF and TGF-α (note that some differences between AREG and EGF were observed), suggesting that these effectors are not responsible for the differential entry into NCE. Interestingly, both EGF and AREG induced a strong Ca^{2+} response at the PM, while TGF-α induced it with a delay and the response was time restricted. Indeed, with EGF, we could score Ca^{2+} oscillations already 20 sec after ligand stimulation, and it lasted more than 5 min, while for TGF-α, the window of response started from 1.5 min and lasted for 1 min. Thus, this restricted Ca^{2+} response might be caused by inefficient activation of NCE and it might be not sufficient the NCE fission step. The differential activation of NCE by EGF and TGF-α can give us more insights into the mechanisms of this pathway. In this direction, it has been shown in proteomics studies that 8 min of stimulation with EGF and TGF-α led to the highest ligand-specific diversity [252]. In order to explain this difference, we examined activation of signaling effectors at different time points, upon stimulation with high doses of EGF and TGF-α. We were able to score decrease in PLCγ2 phosphorylation upon TGF-α, that could possibly explain differences in Ca^{2+} response, but since data were variable between experiments and as WB is only semi-quantitative method, we could not draw strong conclusions. Further experiments employing more quantitative techniques will help in understanding this. Moreover, we put forward additional hypotheses, including that EGF and TGF-α could induce distinct 1) conformations of the EGFR JM domain [253, 254], or 2) EGFR clustering, thus determining their different abilities to activate NCE.

EGF and TGF-α binding to extracellular domain of EGFR results in different conformations of the intracellular JM domain of the EGFR [253, 254]. Formation of different conformations was followed with bipartite tetracysteine display; briefly, two different amino acids within the JM domain of EGFR were substituted with two cysteines [253, 254]. Upon dimerization of these mutants, if the cysteines are in close contact, the assembled tetracysteine

motif is able to bind the substrate – the bis-arsenical dye ReAsH – and emit fluorescence. With this system, it was shown that binding of EGF to the extracellular domain of the EGFR induces the formation of a discrete antiparallel coiled-coil conformation of the JM domain (EGF-type), while TGF-α induced an alternative helical interface that is an ‘‘inside-out’’ version of the EGF-induced JM structure (TGF-α-type). Interestingly, point mutations in the TM domain of the EGFR affected the JM coil-coiled structure, inducing the formation of an EGF-type JM interface upon stimulation with TGF-α (or *vice versa*) [254]. The interplay between TM (that is in direct communication with extracellular space) and the JM domain provides the basis for further research. It is possible that alternative JM conformations can target receptor to different endocytic pathways and induce different signaling. If the JM conformation of EGFR is necessary for its endocytosis, we can check if different mutations (that induce EGF- or TGF-α-types of JM structure) are differentially targeting EGFR to NCE or CME.

The EGFR JM domain was found to play an important role in EGFR clustering and in the formation of lipid-protein interactions through interaction with anionic lipid PIP2 [197]. Mutation or deletion of the JM domain resulted in a decrease in the number of EGFR clusters in COS-7 cells and inhibited the formation of clusters with more than eight EGFR proteins [255]. One of the major anionic lipids of the PM that can bind to positively charged residues in the JM domain is PIP2. This phospholipid forms clusters at the PM that colocalize with EGFR (60% of EGFR clusters colocalize with PIP2) [197]. PIP2 depletion in the PM impaired EGFR cluster formation and led to the dissociation of a genetically engineered JM domain from the PM. Moreover, in the COS-7 monkey kidney cell line, EGFR forms clusters in lipid rafts at both the basal and apical surfaces, but the diameter of the clusters is larger at the apical surface [255]. The disruption of lipid rafts with methyl-β-cyclodextrin weakens EGFR clustering in these cells [255].

Interestingly, our preliminary results suggest that EGF is inducing EGFR clustering more efficiently than TGF-α. If we verify these data, together with decreased activation of PLCγ2 upon TGF-α, an interesting scenario could be that EGF is able to induce the formation and internalization of clusters compared to TGF-α, and PLCγ2 is recruited to clusters of EGFRs, while PLCγ1 is recruited more to single dimers. Indeed, it was shown that the formation of EGFR clusters also affects its signaling [256]. Decreased EGFR phosphorylation was scored upon mutation or deletion of the JM region (for EGFR pY1173), or PIP2 depletion (pY992), while overexpression of PIP5KIα (the enzyme that leads to PIP2 formation) led to increased

phosphorylation of Y992 [257]. Interestingly, these sites are binding sites of PLCγ2, suggesting that PLCγ2 could be recruited to EGFR clusters. There is also some evidence in the literature suggesting that clustering of platelet low affinity Fcγ receptor IIA involves activation of PLCγ2 [258].

5.2.1. Future plans

Given that other EGFR ligands and another RTK (i.e., HGFR) promote CD147 internalization in a clathrin-independent, RTN3-dependent manner, similarly to EGF, while another EGFR ligand (TGF-α) does not, we will further characterize NCE activation upon stimulation with different ligands/growth factors, by investigating: i) ER-PM contact site formation; ii) TI formation; iii) receptor fate, degradation *vs.* recycling of EGFR (upon stimulation with TGF-α/AREG) and of HGFR (upon stimulation with HGF); iv) downstream EGFR/HGFR signaling, extending the analysis that we have already performed.

This work will help us to understand if NCE is specific for the EGFR or if it has a broader function in the cell. Finally, to understand whether the differential activation of NCE and of Ca^{2+} signaling at PM-ER contact sites by the different EGF ligands determines a differential biological response, we will investigate cell growth and proliferation (*e.g.,* BrdU incorporation assays, growth curves, colony assays in 2D-culture and in 3D-semisolid medium, see also point 3), cell migration and invasion (*e.g.,* wound healing, Transwell Matrigel assays) upon stimulation with the different ligands/growth factors in control cells or cells inhibited for NCE (*i.e.,* KD of RTN3, PLCγ2).

5.3. The physiological role of EGFR-NCE

Some of the NCE players, such as CD147, EGFR [104, 259], are mutated in tumors, suggesting a possible tumor suppressive role of NCE, however there is no direct evidence that NCE is implicated in cancer. Overexpression and overactivation of the EGFR and increased secretion of its ligands are associated with tumorigenesis, and its trafficking is elevated in many cancers (such as, lung or glioblastoma) [104, 259]. Extending the relevance of NCE from our model system (HeLa cells) to physiologically more relevant cell-based systems and, finally, to *ex vivo* organoid models that recapitulate the differentiation and organogenesis programs seen in tissues

in vivo, will help us understand how NCE activation might affect cell signaling responses and could provide insights into EGFR (and other oncogenic RTKs) signaling in cancer.

5.3.1. NCE role in cell metabolism

The specific NCE cargo, CD147, is a membrane glycoprotein, highly expressed on the cell surface of various types of cancer [260]. CD147 induces the activation of extracellular matrix metalloproteases (MMPs) and binds to a variety of proteins (*e.g.,* integrins, monocarboxylate transporters, P-glycoprotein, annexin II and caveolin1) [260]. It regulates aerobic glycolysis and promotes cancer cell growth and its overexpression is associated with unfavorable tumor outputs [261]. Thus, dysfunction of NCE could represent a mechanism by which cancer cells upregulate surface levels of CD147.

CD147 is known to be a chaperone of monocarboxylate transporters (MCTs) and the glucose transporter, GLUT1, promoting glucose entry and lactate extrusion [262]. Tumor cells use glycolysis for rapid energy production, and they extrude the excess lactate via the CD147-MCT complex to avoid toxicity. As the tumor size increases, expression of CD147 and MCTs is boosted to enhance lactate export. Thus, through the regulation of CD147 and these transporters, NCE might influence cell metabolic functions not typically connected with this pathway. Since upon stimulation of EGF, CD147 is internalized, we tested if together with CD147 also MCT1 and GLUT1 are internalized via NCE. Interestingly, it seems that MCT1 is internalized in NCE vesicles, where it colocalize with EGF and CD147, in clathrin-independent way, suggesting that NCE might regulate MCT1 levels on the PM and lactate extrusion, something that will be further investigated. For GLUT1, the results were less clear: while it also seems to be internalized upon EGF stimulation and to colocalize with EGF, no colocalization was observed with CD147, suggesting that GLUT1 internalization might mainly occur via the clathrin-dependent pathway. GLUT1 was shown to co-immunoprecipitate with EGFR in T lymphocytes [263], so it is possible that it interacts with the EGFR and co-internalizes with it possibly via a CME pathway.

5.3.2. NCE role in epithelial cell physiology

We showed that AREG is able to induce EGFR-NCE even more efficiently than EGF. Interestingly, AREG is known to induce a greater motility in non-tumorigenic breast epithelial MCF10A cells than EGF, by a mechanism that is yet to be defined [122]. One possible explanation could be the increased internalization of AREG-EGFR via NCE, enhanced PLCγ2 activation and Ca^{2+} signaling. Interestingly, AREG has a prominent role in mammary gland development: AREG KO mice show impairment of ductal morphogenesis [264]. Thus, we hypothesized that EGFR-NCE could be involved in regulation of normal breast tissue. In this direction, we recently found that MCF10A cells overexpressing the small GTPase Rab5 - which is overexpressed in breast cancer and correlates with poor prognosis [265] - acquire a collective motility phenotype called "unjamming transition", which is dependent, at least in part, on the upregulation of EGFR-NCE and is inhibited by RTN3 KD [265]. The unjamming transition is relevant for wound repair and branching morphogenesis during mammary gland development and plays a critical role in breast carcinoma dissemination [265]. These data point to a role of EGFR-NCE in the migration and invasion potential of breast epithelial cells and in mammary morphogenesis. To investigate this, we have started setting up and characterizing different mammary epithelial model systems, including MCF10A cells grown in 2D culture or as 3D organoids, and murine mammary organoids derived from primary breast tissue.

We have also established primary organoid cultures from mouse intestinal crypts to investigate the role of EGFR signaling and NCE in intestinal morphogenetic program. As both mammary and intestinal organoids are highly dependent on high doses of EGF and EGFR signaling (together with cocktail of other factors), in order to grow and differentiate *ex vivo* in Matrigel, we hypothesis that NCE can have a role in differentiation and organogenesis of these organoids. Moreover, treatment with the EGFR kinase inhibitor, gefitinib, almost completely blocked their growth [203]. Preliminary experiments showed that treatment with compounds that affect EGFR-NCE, *i.e.,* PPMP (that interferes with glycosphingolipid synthesis) and xestospongin C (that blocks the Ca^{2+} release from the ER) had the opposite effect to gefitinib, promoting organoid growth. Although these two drugs act through different mechanisms, both induce an increase in organoid number and size, suggestive of upregulated EGFR signaling when NCE is inactivated. These results suggest that EGFR-NCE might have an important role in the regulation of organoid development, however they need further verification through

molecular genetic experiments. For this reason, we have designed shRNA-based lentiviral vectors for human and mouse RTN3/4 and PLCγ1/2.

5.3.3. Future plans

To investigate the role of NCE in morphogenetic and growth processes, we will use: i) MCF10A-derived organoids; ii) breast and intestinal primary organoids derived from WT mice (as in **Figure 45**). We will generate organoids starting from single cells, manipulated *ex vivo* to inhibit CME *vs.* NCE by KD of clathrin, AP2, RTN3 or PLCγ1/2 using shRNA-based lentiviral vectors. In these cultures, we will follow: i) organoid dimension, morphology (*e.g.,* regular, irregular, invasive) and number (in mammary and intestinal organoids); ii) luminal *vs.* basal epithelial markers (in mammary organoids); iii) $LGR5^+$ cell number, the emergence of Paneth cells and crypt formation (in intestinal organoids); iv) EGFR/CD147 levels and localization by imaging. These experiments will be also performed upon stimulation in the presence of different EGFR ligands to see if they have different morphogenetic abilities that could be linked to NCE. To this end, we are setting up procedures for IF imaging of EGFR/CD147 endocytosis in a 3D organoid assay to investigate the level and localization of EGFR and CD147. We identified EGFR, CD147, leucine-rich repeat-containing G-protein coupled receptor 5 (LGR5), CK5 and CK8 specific antibodies suitable for IF in control organoids (**Figure S4**). LGR5, the intestinal stem cell marker, stained a specific single cell as expected (**Figure S4A)**. EGFR and CD147 stainings in intestinal crypts showed their expression pattern on surface of all cells (**Figure S4A)**. In mammary organoids, the CK5 and CK8 identified basal and luminal layered organoids as expected (**Figure S4B)**. EGFR staining was present on the surface of mammary organoid cells, while CD147 seem to present on particular types of cells (**Figure S4B)**, that could be basal cells, but further investigation and double staining of CD147 and markers of different layers (e.g., CKs) will let us understand better the type of CD147-positive cells. MCF10A cells and primary breast mouse epithelial cells derived from the normal mammary gland will also be used in *ex vivo* migration/invasion assays (*e.g.,* wound healing, Transwell Matrigel assay, chemotaxis assays, 3D-organoid growth/invasion in Matrigel) upon inhibition of CME *vs.* NCE, as above. Our research will allow us to uncover how broad the impact of NCE is on cell physiology, its role in organoid development and morphogenesis, and its relevance to breast cancer.

5.4. Conclusion

In conclusion, we have gained a deeper understanding of EGFR-NCE by revealing endocytic molecular players and regulatory mechanisms.

1) We unveil the signaling pathway by showing that:

- The PLCγ/IP3R signaling pathway is activated downstream of the EGFR and leads to Ca^{2+} release at the PM;
- PLCγ2 plays a critical role in EGFR/CD147-NCE at variance with PLCγ1;
- PLCγ2/IP3R circuitry and Ca^{2+} signaling are involved in the fission step of NCE tubular invaginations together with dynamin.

2) We expanded role of NCE demonstrating that:

- Although similar, there were some differences in EGFR activation and downstream signaling activated by the 3 EGFR ligands (EGF, AREG and TGF-α);
- AREG induces CD147-NCE similarly to EGF, while TGF-α was a weak inducer;
- AREG induces Ca^{2+} signaling at the PM similarly to EGF, while TGF-α induces a delayed and time-restricted Ca^{2+} response;
- Activation of HGFR by its ligand HGF induces CD147-NCE.

3) We set organoid system to investigate role of EGFR-NCE in the morphogenesis and development and we showed that:

- Compounds that affect EGFR-NCE, *i.e.,* PPMP and xestospongin C had the opposite effect to gefitinib (that inhibit EGFR kinase function), promoting organoid growth.

This knowledge can be applied not only to the study this endocytic mechanism in cell physiology and cancer, but also in the development of targeted therapies in the future.

6. APPENDIX

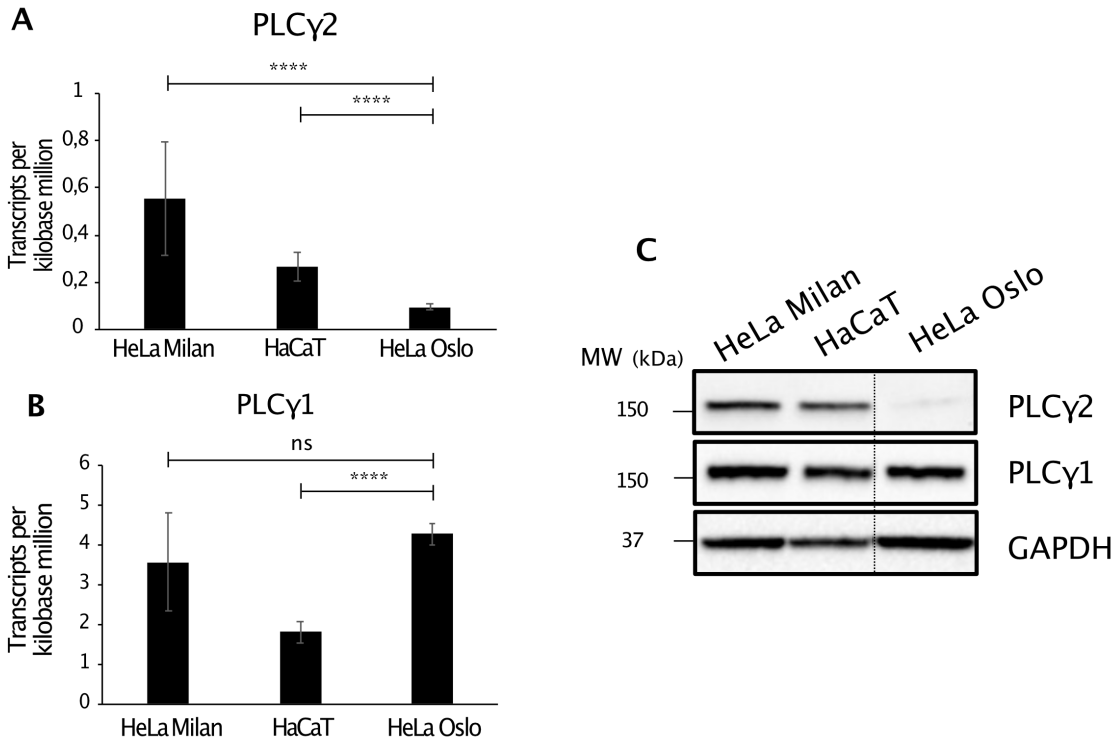

Appendix Figure S1. Expression of PLCγ1 and PLCγ2 in different cell lines

A.-B. *Expression of PLCγ2 (**A.**) or of PLCγ1 (**B.**) are showed as transcripts per kilobase million in three cell lines (HeLa Milan, HaCaT and HeLa Oslo), as indicated. All analysis were made using EdgeR software; ****, P<0,001; ns, non-significant. The experiments were performed with the help of Stefano Confalonieri from our lab, and Thelma Capra and Luca Rotta (Genomics Unit, IEO).* ***C.*** *WB analysis of expression of PLCγ1 and PLCγ2 in same three cell lines from "A", as indicated. The blot shows samples from the same membrane, but splicing out irrelevant lines (indicated by dotted line). GAPDH, loading control. MW: Molecular weight markers are shown on the left.*

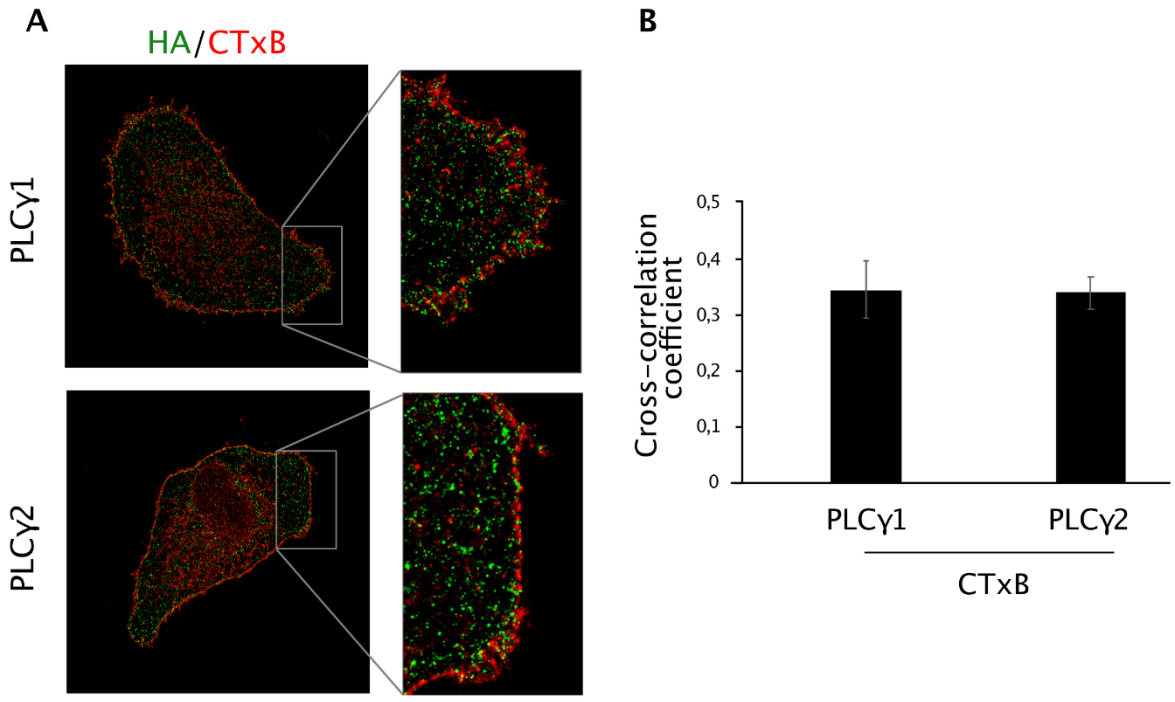

Appendix Figure S2. No differences in the co-clustering of PLCγ1 vs. PLCγ2 with CTxB upon EGF stimulation.

A. *HeLa* cells expressing HA-tagged forms of either PLCγ1 or PLCγ2 were stimulated for 1 min with EGF 100 ng/ml at 37°C, then fixed, permeabilized and stained with anti-HA and CTxB-Alexa-647 (red). HA was revealed with an Cy3 secondary *antibody (green). Cells were analyzed by STORM.* ***B.*** *Cross-correlation coefficient proportional to the fraction of co-clustered HA and CTxB signals within 40 nm of the PM is shown. Experiments were performed with the help of Stefano Freddi from our lab, and Simone Pelicci and Mario Faretta (Imaging Development Unit, IEO).*

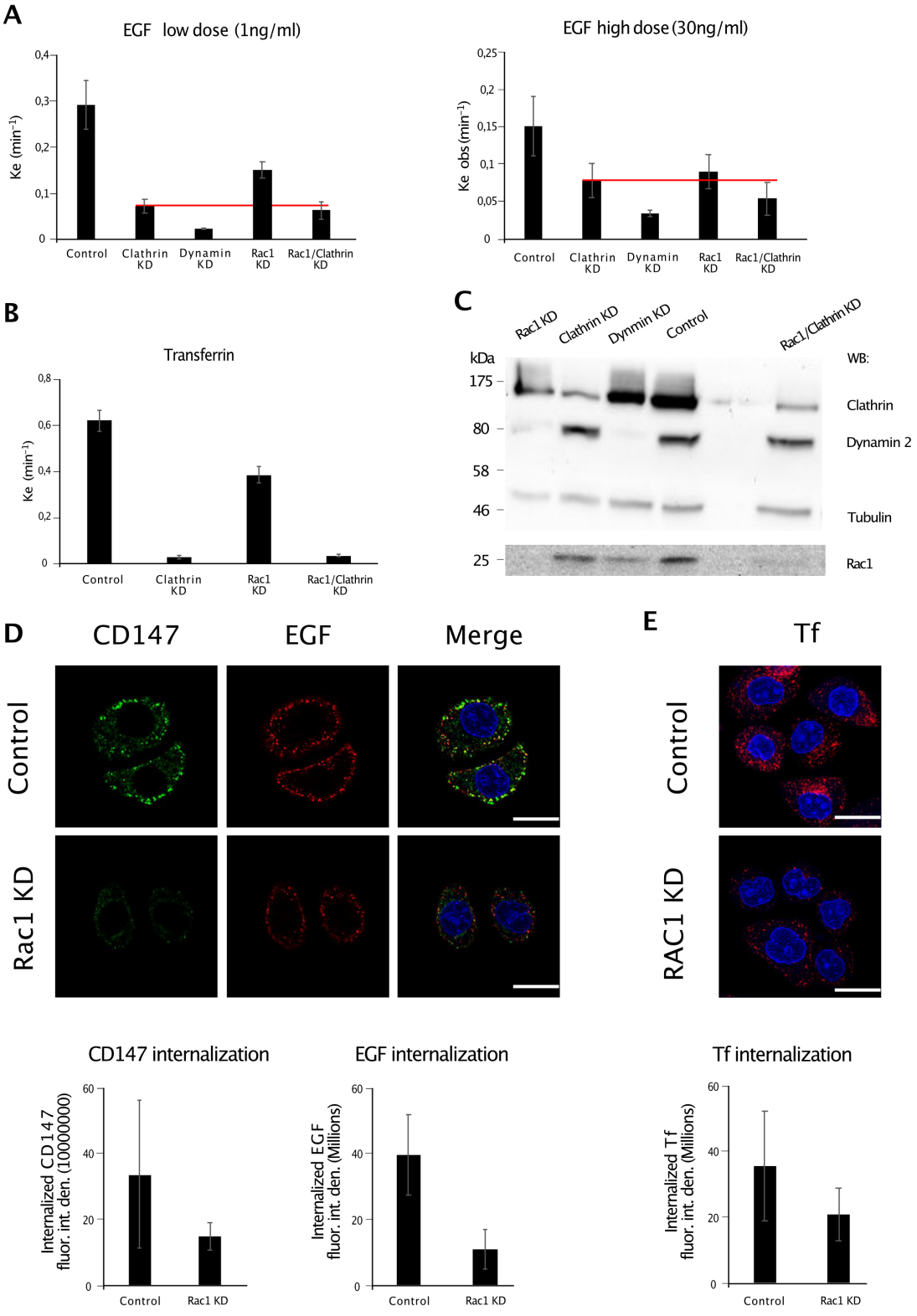

Appendix Figure S3. Rac1 KD decreased internalization of EGF and CD147.

A. *HeLa cells subjected to the indicated KDs were stimulated with low and high dose ^{125}I-EGF. The kinetics of ^{125}I- EGF internalization were followed at early time points (0-8 min).*

Internalization constants (Ke) were extrapolated from the internalization curves and correspond to the slopes of the best-fit curves. Red lines indicate the level of ^{125}I-EGF internalization in clathrin KD cells to be compared to the level observed upon Rac1+clathrin KD. ***B.*** *K_e of ^{125}I-labeled Tf (1 μg/ml) internalization in the indicated conditions.* ***A, B.*** *Results are mean+/-SD of three independent experiments* ***C.*** *Efficiency of the indicated KD was assessed by WB. Tubulin, loading control. MW: Molecular weight markers are shown on the left.* ***D.*** *Top, CD147 internalization in the presence of high dose Alexa-555-EGF (~30 ng/ml, red) was followed in vivo with an anti-CD147 antibody, as described [63]. Cells were subjected to an acid wash treatment prior to fixation to remove the PM-bound antibody. Internalized CD147 was revealed with an Alexa-488 secondary antibody (green) on permeabilized cells. Bottom left, internalized CD147 was quantified with an ad hoc designed ImageJ macro. Mean integrated fluorescence intensity ± SD is reported as % of control cells. Bottom right, EGF signal was highlighted applying an intensity-based threshold (Default method), and then fluorescence intensity per field was calculated using the "Measure" command, limiting measurement to the threshold. This value was then divided by the number of nuclei in the field, counted using the DAPI signal, to calculate the EGF fluorescence intensity per cell. Mean integrated fluorescence intensity ± SD.* ***E.*** *Top, HeLa cells were stimulated with Alexa-488-Tf for 15 min and subjected to acid wash before fixation. Bottom, Tf signal was highlighted applying an intensity-based threshold (Default method), and then fluorescence intensity per field was calculated using the "Measure" command, limiting measurement to the threshold. This value was then divided by the number of nuclei in the field, counted using the DAPI signal, to calculate the Tf fluorescence intensity per cell. Mean integrated fluorescence intensity ± SD. Blue, DAPI. Bar, 20 μm. Experiment was performed twice. The experiments from "A", "B" and "C" were performed with the help of Elisa Barbieri and Giusi Caldieri from our lab.*

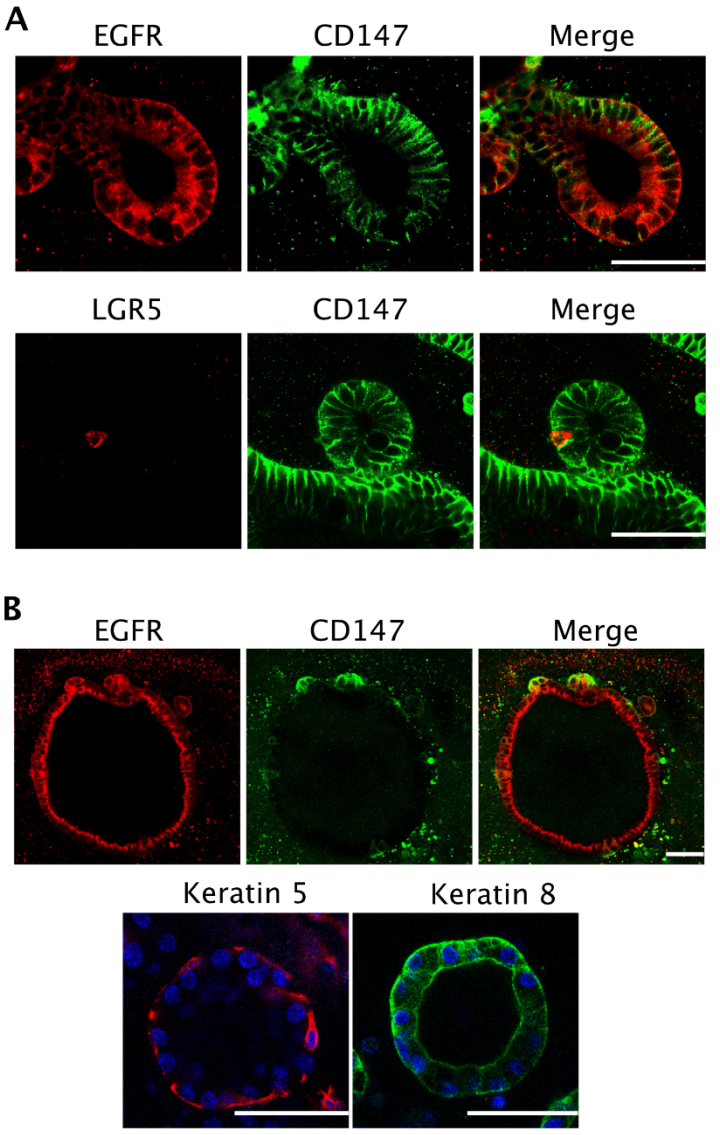

Appendix Figure S4. IF staining of intestinal and mammary organoids.

A. *IF staining of crypts from intestinal organoids with the indicated antibodies (EGFR, CD147, LGR5). LGR5 is a marker of stem cell of the crypt.* ***B.*** *IF staining of mammary organoids with the indicated antibodies (EGFR, CD147, CK5, CK8). CK5 is a basal layer marker, CK8 is a luminal layer marker. Blue, DAPI. Bar, 50 μm.*

7. REFERENCES

1. Di Fiore, P.P. and P. De Camilli, *Endocytosis and signaling. an inseparable partnership.* Cell, 2001. **106**(1): p. 1-4.
2. Sigismund, S., et al., *Endocytosis in the context-dependent regulation of individual and collective cell properties.* Nat Rev Mol Cell Biol, 2021. **22**(9): p. 625-643.
3. Doherty, G.J. and H.T. McMahon, *Mechanisms of endocytosis.* Annu Rev Biochem, 2009. **78**: p. 857-902.
4. Thottacherry, J.J., et al., *Spoiled for Choice: Diverse Endocytic Pathways Function at the Cell Surface.* Annu Rev Cell Dev Biol, 2019. **35**: p. 55-84.
5. Schiano Lomoriello, I., S. Sigismund, and K.J. Day, *Biophysics of endocytic vesicle formation: A focus on liquid-liquid phase separation.* Curr Opin Cell Biol, 2022. **75**: p. 102068.
6. Freeman, S.A. and S. Grinstein, *Phagocytosis: receptors, signal integration, and the cytoskeleton.* Immunol Rev, 2014. **262**(1): p. 193-215.
7. Lim, J.P. and P.A. Gleeson, *Macropinocytosis: an endocytic pathway for internalising large gulps.* Immunol Cell Biol, 2011. **89**(8): p. 836-43.
8. Mayor, S. and R.E. Pagano, *Pathways of clathrin-independent endocytosis.* Nat Rev Mol Cell Biol, 2007. **8**(8): p. 603-12.
9. McMahon, H.T. and E. Boucrot, *Molecular mechanism and physiological functions of clathrin-mediated endocytosis.* Nat Rev Mol Cell Biol, 2011. **12**(8): p. 517-33.
10. Kaksonen, M. and A. Roux, *Mechanisms of clathrin-mediated endocytosis.* Nat Rev Mol Cell Biol, 2018. **19**(5): p. 313-326.
11. Dambournet, D., et al., *Genome-edited human stem cells expressing fluorescently labeled endocytic markers allow quantitative analysis of clathrin-mediated endocytosis during differentiation.* J Cell Biol, 2018. **217**(9): p. 3301-3311.
12. Kirchhausen, T., *Clathrin.* Annu Rev Biochem, 2000. **69**: p. 699-727.
13. Hinshaw, J.E. and S.L. Schmid, *Dynamin self-assembles into rings suggesting a mechanism for coated vesicle budding.* Nature, 1995. **374**(6518): p. 190-2.
14. Puertollano, R., *Clathrin-mediated transport: assembly required. Workshop on Molecular Mechanisms of Vesicle Selectivity.* EMBO Rep, 2004. **5**(10): p. 942-6.

15. Fuchs, M., J.H. Brandstatter, and H. Regus-Leidig, *Evidence for a Clathrin-independent mode of endocytosis at a continuously active sensory synapse.* Front Cell Neurosci, 2014. **8**: p. 60.
16. Takei, K., et al., *Generation of coated intermediates of clathrin-mediated endocytosis on protein-free liposomes.* Cell, 1998. **94**(1): p. 131-41.
17. Maxfield, F.R. and T.E. McGraw, *Endocytic recycling.* Nat Rev Mol Cell Biol, 2004. **5**(2): p. 121-32.
18. Kaur, G. and A. Lakkaraju, *Early Endosome Morphology in Health and Disease.* Adv Exp Med Biol, 2018. **1074**: p. 335-343.
19. Scott, C.C., F. Vacca, and J. Gruenberg, *Endosome maturation, transport and functions.* Semin Cell Dev Biol, 2014. **31**: p. 2-10.
20. Takei, K. and V. Haucke, *Clathrin-mediated endocytosis: membrane factors pull the trigger.* Trends Cell Biol, 2001. **11**(9): p. 385-91.
21. Anderson, R.G., M.S. Brown, and J.L. Goldstein, *Role of the coated endocytic vesicle in the uptake of receptor-bound low density lipoprotein in human fibroblasts.* Cell, 1977. **10**(3): p. 351-64.
22. Gorden, P., et al., *Epidermal growth factor: morphological demonstration of binding, internalization, and lysosomal association in human fibroblasts.* Proc Natl Acad Sci U S A, 1978. **75**(10): p. 5025-9.
23. Mayle, K.M., A.M. Le, and D.T. Kamei, *The intracellular trafficking pathway of transferrin.* Biochim Biophys Acta, 2012. **1820**(3): p. 264-81.
24. Tao, W., et al., *Endocytic adaptors Arh and Dab2 control homeostasis of circulatory cholesterol.* J Lipid Res, 2016. **57**(5): p. 809-17.
25. Hanyaloglu, A.C. and M. von Zastrow, *Regulation of GPCRs by endocytic membrane trafficking and its potential implications.* Annu Rev Pharmacol Toxicol, 2008. **48**: p. 537-68.
26. Jean-Charles, P.Y., S. Kaur, and S.K. Shenoy, *G Protein-Coupled Receptor Signaling Through beta-Arrestin-Dependent Mechanisms.* J Cardiovasc Pharmacol, 2017. **70**(3): p. 142-158.
27. Stoddart, A., et al., *Lipid rafts unite signaling cascades with clathrin to regulate BCR internalization.* Immunity, 2002. **17**(4): p. 451-62.

28. Rollason, R., et al., *Clathrin-mediated endocytosis of a lipid-raft-associated protein is mediated through a dual tyrosine motif.* J Cell Sci, 2007. **120**(Pt 21): p. 3850-8.
29. Parton, R.G., K.A. McMahon, and Y. Wu, *Caveolae: Formation, dynamics, and function.* Curr Opin Cell Biol, 2020. **65**: p. 8-16.
30. Busija, A.R., H.H. Patel, and P.A. Insel, *Caveolins and cavins in the trafficking, maturation, and degradation of caveolae: implications for cell physiology.* Am J Physiol Cell Physiol, 2017. **312**(4): p. C459-C477.
31. Cheng, J.P.X. and B.J. Nichols, *Caveolae: One Function or Many?* Trends Cell Biol, 2016. **26**(3): p. 177-189.
32. Williams, T.M. and M.P. Lisanti, *The caveolin proteins.* Genome Biol, 2004. **5**(3): p. 214.
33. Shen, L. and J.R. Turner, *Actin depolymerization disrupts tight junctions via caveolae-mediated endocytosis.* Mol Biol Cell, 2005. **16**(9): p. 3919-36.
34. Henley, J.R., et al., *Dynamin-mediated internalization of caveolae.* J Cell Biol, 1998. **141**(1): p. 85-99.
35. Parton, R.G., *Ultrastructural localization of gangliosides; GM1 is concentrated in caveolae.* J Histochem Cytochem, 1994. **42**(2): p. 155-66.
36. Anderson, H.A., Y. Chen, and L.C. Norkin, *Bound simian virus 40 translocates to caveolin-enriched membrane domains, and its entry is inhibited by drugs that selectively disrupt caveolae.* Mol Biol Cell, 1996. **7**(11): p. 1825-34.
37. Torgersen, M.L., et al., *Internalization of cholera toxin by different endocytic mechanisms.* J Cell Sci, 2001. **114**(Pt 20): p. 3737-47.
38. Matthaeus, C. and J.W. Taraska, *Energy and Dynamics of Caveolae Trafficking.* Front Cell Dev Biol, 2020. **8**: p. 614472.
39. Ringerike, T., et al., *Cholesterol is important in control of EGF receptor kinase activity but EGF receptors are not concentrated in caveolae.* J Cell Sci, 2002. **115**(Pt 6): p. 1331-40.
40. Roepstorff, K., et al., *Sequestration of epidermal growth factor receptors in non-caveolar lipid rafts inhibits ligand binding.* J Biol Chem, 2002. **277**(21): p. 18954-60.
41. Lo, H.P., et al., *The caveolin-cavin system plays a conserved and critical role in mechanoprotection of skeletal muscle.* J Cell Biol, 2015. **210**(5): p. 833-49.
42. Parton, R.G., et al., *Caveolae: The FAQs.* Traffic, 2020. **21**(1): p. 181-185.

43. Hetmanski, J.H.R., et al., *Membrane Tension Orchestrates Rear Retraction in Matrix-Directed Cell Migration.* Dev Cell, 2019. **51**(4): p. 460-475 e10.
44. Meister, M. and R. Tikkanen, *Endocytic trafficking of membrane-bound cargo: a flotillin point of view.* Membranes (Basel), 2014. **4**(3): p. 356-71.
45. Riento, K., et al., *Endocytosis of flotillin-1 and flotillin-2 is regulated by Fyn kinase.* J Cell Sci, 2009. **122**(Pt 7): p. 912-8.
46. Frick, M., et al., *Coassembly of flotillins induces formation of membrane microdomains, membrane curvature, and vesicle budding.* Curr Biol, 2007. **17**(13): p. 1151-6.
47. Meister, M., A. Zuk, and R. Tikkanen, *Role of dynamin and clathrin in the cellular trafficking of flotillins.* FEBS J, 2014. **281**(13): p. 2956-76.
48. Solis, G.P., et al., *Reggies/flotillins interact with Rab11a and SNX4 at the tubulovesicular recycling compartment and function in transferrin receptor and E-cadherin trafficking.* Mol Biol Cell, 2013. **24**(17): p. 2689-702.
49. Johannes, L. and A. Billet, *Glycosylation and raft endocytosis in cancer.* Cancer Metastasis Rev, 2020. **39**(2): p. 375-396.
50. Lakshminarayan, R., et al., *Galectin-3 drives glycosphingolipid-dependent biogenesis of clathrin-independent carriers.* Nat Cell Biol, 2014. **16**(6): p. 595-606.
51. Renard, H.F., et al., *Endophilin-A2 functions in membrane scission in clathrin-independent endocytosis.* Nature, 2015. **517**(7535): p. 493-6.
52. Howes, M.T., et al., *Clathrin-independent carriers form a high capacity endocytic sorting system at the leading edge of migrating cells.* J Cell Biol, 2010. **190**(4): p. 675-91.
53. Thottacherry, J.J., et al., *Mechanochemical feedback control of dynamin independent endocytosis modulates membrane tension in adherent cells.* Nat Commun, 2018. **9**(1): p. 4217.
54. Naslavsky, N., R. Weigert, and J.G. Donaldson, *Characterization of a nonclathrin endocytic pathway: membrane cargo and lipid requirements.* Mol Biol Cell, 2004. **15**(8): p. 3542-52.
55. Wong, K.W. and R.R. Isberg, *Arf6 and phosphoinositol-4-phosphate-5-kinase activities permit bypass of the Rac1 requirement for beta1 integrin-mediated bacterial uptake.* J Exp Med, 2003. **198**(4): p. 603-14.

56. Donaldson, J.G., *Phospholipase D in endocytosis and endosomal recycling pathways.* Biochim Biophys Acta, 2009. **1791**(9): p. 845-9.

57. Van Acker, T., J. Tavernier, and F. Peelman, *The Small GTPase Arf6: An Overview of Its Mechanisms of Action and of Its Role in Host(-)Pathogen Interactions and Innate Immunity.* Int J Mol Sci, 2019. **20**(9).

58. Krauss, M., et al., *ARF6 stimulates clathrin/AP-2 recruitment to synaptic membranes by activating phosphatidylinositol phosphate kinase type Igamma.* J Cell Biol, 2003. **162**(1): p. 113-24.

59. Eyster, C.A., et al., *Discovery of new cargo proteins that enter cells through clathrin-independent endocytosis.* Traffic, 2009. **10**(5): p. 590-9.

60. Boucrot, E., et al., *Endophilin marks and controls a clathrin-independent endocytic pathway.* Nature, 2015. **517**(7535): p. 460-5.

61. Chan Wah Hak, L., et al., *FBP17 and CIP4 recruit SHIP2 and lamellipodin to prime the plasma membrane for fast endophilin-mediated endocytosis.* Nat Cell Biol, 2018. **20**(9): p. 1023-1031.

62. Sigismund, S., et al., *Threshold-controlled ubiquitination of the EGFR directs receptor fate.* EMBO J, 2013. **32**(15): p. 2140-57.

63. Caldieri, G., et al., *Reticulon 3-dependent ER-PM contact sites control EGFR nonclathrin endocytosis.* Science, 2017. **356**(6338): p. 617-624.

64. London, E., *How principles of domain formation in model membranes may explain ambiguities concerning lipid raft formation in cells.* Biochim Biophys Acta, 2005. **1746**(3): p. 203-20.

65. Simons, K. and E. Ikonen, *Functional rafts in cell membranes.* Nature, 1997. **387**(6633): p. 569-72.

66. Wisniewska, A., J. Draus, and W.K. Subczynski, *Is a fluid-mosaic model of biological membranes fully relevant? Studies on lipid organization in model and biological membranes.* Cell Mol Biol Lett, 2003. **8**(1): p. 147-59.

67. Sedwick, C.E. and A. Altman, *Ordered just so: lipid rafts and lymphocyte function.* Sci STKE, 2002. **2002**(122): p. re2.

68. Zaman, S.N., M.E. Resek, and S.M. Robbins, *Dual acylation and lipid raft association of Src-family protein tyrosine kinases are required for SDF-1/CXCL12-mediated*

chemotaxis in the Jurkat human T cell lymphoma cell line. J Leukoc Biol, 2008. **84**(4): p. 1082-91.

69. Simons, K. and D. Toomre, *Lipid rafts and signal transduction.* Nat Rev Mol Cell Biol, 2000. **1**(1): p. 31-9.
70. Brown, D.A. and J.K. Rose, *Sorting of GPI-anchored proteins to glycolipid-enriched membrane subdomains during transport to the apical cell surface.* Cell, 1992. **68**(3): p. 533-44.
71. Klymchenko, A.S. and R. Kreder, *Fluorescent probes for lipid rafts: from model membranes to living cells.* Chem Biol, 2014. **21**(1): p. 97-113.
72. Chadda, R., et al., *Cholesterol-sensitive Cdc42 activation regulates actin polymerization for endocytosis via the GEEC pathway.* Traffic, 2007. **8**(6): p. 702-17.
73. Parton, R.G., M.M. Kozlov, and N. Ariotti, *Caveolae and lipid sorting: Shaping the cellular response to stress.* J Cell Biol, 2020. **219**(4).
74. Sigismund, S., et al., *Clathrin-mediated internalization is essential for sustained EGFR signaling but dispensable for degradation.* Dev Cell, 2008. **15**(2): p. 209-19.
75. Niekamp, P., et al., *Sphingomyelin Biosynthesis Is Essential for Phagocytic Signaling during Mycobacterium tuberculosis Host Cell Entry.* mBio, 2021. **12**(1).
76. Mollinedo, F. and C. Gajate, *Lipid rafts as signaling hubs in cancer cell survival/death and invasion: implications in tumor progression and therapy: Thematic Review Series: Biology of Lipid Rafts.* J Lipid Res, 2020. **61**(5): p. 611-635.
77. Alonso, M.A. and J. Millan, *The role of lipid rafts in signalling and membrane trafficking in T lymphocytes.* J Cell Sci, 2001. **114**(Pt 22): p. 3957-65.
78. Varshney, P., V. Yadav, and N. Saini, *Lipid rafts in immune signalling: current progress and future perspective.* Immunology, 2016. **149**(1): p. 13-24.
79. Polo, S. and P.P. Di Fiore, *Endocytosis conducts the cell signaling orchestra.* Cell, 2006. **124**(5): p. 897-900.
80. von Zastrow, M. and A. Sorkin, *Signaling on the endocytic pathway.* Curr Opin Cell Biol, 2007. **19**(4): p. 436-45.
81. Disanza, A., et al., *Endocytosis and spatial restriction of cell signaling.* Mol Oncol, 2009. **3**(4): p. 280-96.

82. Dobrowolski, R. and E.M. De Robertis, *Endocytic control of growth factor signalling: multivesicular bodies as signalling organelles.* Nat Rev Mol Cell Biol, 2011. **13**(1): p. 53-60.

83. Raiborg, C. and H. Stenmark, *The ESCRT machinery in endosomal sorting of ubiquitylated membrane proteins.* Nature, 2009. **458**(7237): p. 445-52.

84. Garay, C., et al., *Epidermal growth factor-stimulated Akt phosphorylation requires clathrin or ErbB2 but not receptor endocytosis.* Mol Biol Cell, 2015. **26**(19): p. 3504-19.

85. Lucarelli, S., et al., *Similar requirement for clathrin in EGF- and HGF- stimulated Akt phosphorylation.* Commun Integr Biol, 2016. **9**(3): p. e1175696.

86. Kermorgant, S. and P.J. Parker, *Receptor trafficking controls weak signal delivery: a strategy used by c-Met for STAT3 nuclear accumulation.* J Cell Biol, 2008. **182**(5): p. 855-63.

87. Miaczynska, M., L. Pelkmans, and M. Zerial, *Not just a sink: endosomes in control of signal transduction.* Curr Opin Cell Biol, 2004. **16**(4): p. 400-6.

88. Joffre, C., et al., *A direct role for Met endocytosis in tumorigenesis.* Nat Cell Biol, 2011. **13**(7): p. 827-37.

89. Sorkin, A. and M. von Zastrow, *Endocytosis and signalling: intertwining molecular networks.* Nat Rev Mol Cell Biol, 2009. **10**(9): p. 609-22.

90. Moreno-Layseca, P., et al., *Integrin trafficking in cells and tissues.* Nat Cell Biol, 2019. **21**(2): p. 122-132.

91. Alanko, J., et al., *Integrin endosomal signalling suppresses anoikis.* Nat Cell Biol, 2015. **17**(11): p. 1412-21.

92. Paul, N.R., G. Jacquemet, and P.T. Caswell, *Endocytic Trafficking of Integrins in Cell Migration.* Curr Biol, 2015. **25**(22): p. R1092-105.

93. Sigismund, S., et al., *Endocytosis and signaling: cell logistics shape the eukaryotic cell plan.* Physiol Rev, 2012. **92**(1): p. 273-366.

94. Pietila, M., et al., *SORLA regulates endosomal trafficking and oncogenic fitness of HER2.* Nat Commun, 2019. **10**(1): p. 2340.

95. Al-Akhrass, H., et al., *A feed-forward loop between SorLA and HER3 determines heregulin response and neratinib resistance.* Oncogene, 2021. **40**(7): p. 1300-1317.

96. Jeffers, M., et al., *Degradation of the Met tyrosine kinase receptor by the ubiquitin-proteasome pathway.* Mol Cell Biol, 1997. **17**(2): p. 799-808.

97. Barrow-McGee, R. and S. Kermorgant, *Met endosomal signalling: in the right place, at the right time.* Int J Biochem Cell Biol, 2014. **49**: p. 69-74.

98. Lanzetti, L. and P.P. Di Fiore, *Endocytosis and cancer: an 'insider' network with dangerous liaisons.* Traffic, 2008. **9**(12): p. 2011-21.

99. Khan, I. and P.S. Steeg, *Endocytosis: a pivotal pathway for regulating metastasis.* Br J Cancer, 2021. **124**(1): p. 66-75.

100. Chen, P.H., et al., *Crosstalk between CLCb/Dyn1-Mediated Adaptive Clathrin-Mediated Endocytosis and Epidermal Growth Factor Receptor Signaling Increases Metastasis.* Dev Cell, 2017. **40**(3): p. 278-288 e5.

101. Thien, C.B. and W.Y. Langdon, *Cbl: many adaptations to regulate protein tyrosine kinases.* Nat Rev Mol Cell Biol, 2001. **2**(4): p. 294-307.

102. Peschard, P. and M. Park, *Escape from Cbl-mediated downregulation: a recurrent theme for oncogenic deregulation of receptor tyrosine kinases.* Cancer Cell, 2003. **3**(6): p. 519-23.

103. Yarden, Y., *The EGFR family and its ligands in human cancer. signalling mechanisms and therapeutic opportunities.* Eur J Cancer, 2001. **37 Suppl 4**: p. S3-8.

104. Roskoski, R., Jr., *The ErbB/HER family of protein-tyrosine kinases and cancer.* Pharmacol Res, 2014. **79**: p. 34-74.

105. Lemmon, M.A., *Ligand-induced ErbB receptor dimerization.* Exp Cell Res, 2009. **315**(4): p. 638-48.

106. Huang, F., et al., *Differential regulation of EGF receptor internalization and degradation by multiubiquitination within the kinase domain.* Mol Cell, 2006. **21**(6): p. 737-48.

107. Bae, J.H. and J. Schlessinger, *Asymmetric tyrosine kinase arrangements in activation or autophosphorylation of receptor tyrosine kinases.* Mol Cells, 2010. **29**(5): p. 443-8.

108. Sigismund, S., D. Avanzato, and L. Lanzetti, *Emerging functions of the EGFR in cancer.* Mol Oncol, 2018. **12**(1): p. 3-20.

109. Wilson, K.J., et al., *Functional selectivity of EGF family peptide growth factors: implications for cancer.* Pharmacol Ther, 2009. **122**(1): p. 1-8.

110. Li, Y., et al., *Quantitation of the effect of ErbB2 on epidermal growth factor receptor binding and dimerization.* J Biol Chem, 2012. **287**(37): p. 31116-25.

111. Freed, D.M., et al., *EGFR Ligands Differentially Stabilize Receptor Dimers to Specify Signaling Kinetics.* Cell, 2017. **171**(3): p. 683-695 e18.

112. Roepstorff, K., et al., *Differential effects of EGFR ligands on endocytic sorting of the receptor.* Traffic, 2009. **10**(8): p. 1115-27.

113. Yarden, Y. and M.X. Sliwkowski, *Untangling the ErbB signalling network.* Nat Rev Mol Cell Biol, 2001. **2**(2): p. 127-37.

114. Decker, S.J., *Epidermal growth factor and transforming growth factor-alpha induce differential processing of the epidermal growth factor receptor.* Biochem Biophys Res Commun, 1990. **166**(2): p. 615-21.

115. Revillion, F., et al., *ErbB/HER ligands in human breast cancer, and relationships with their receptors, the bio-pathological features and prognosis.* Ann Oncol, 2008. **19**(1): p. 73-80.

116. Lemos-Gonzalez, Y., et al., *Alteration of the serum levels of the epidermal growth factor receptor and its ligands in patients with non-small cell lung cancer and head and neck carcinoma.* Br J Cancer, 2007. **96**(10): p. 1569-78.

117. Ciarloni, L., S. Mallepell, and C. Brisken, *Amphiregulin is an essential mediator of estrogen receptor alpha function in mammary gland development.* Proc Natl Acad Sci U S A, 2007. **104**(13): p. 5455-60.

118. Plowman, G.D., et al., *The amphiregulin gene encodes a novel epidermal growth factor-related protein with tumor-inhibitory activity.* Mol Cell Biol, 1990. **10**(5): p. 1969-81.

119. Baillo, A., C. Giroux, and S.P. Ethier, *Knock-down of amphiregulin inhibits cellular invasion in inflammatory breast cancer.* J Cell Physiol, 2011. **226**(10): p. 2691-701.

120. Lee, S., et al., *Alterations of gene expression in the development of early hyperplastic precursors of breast cancer.* Am J Pathol, 2007. **171**(1): p. 252-62.

121. Chung, E., et al., *Differential effects of amphiregulin and TGF-alpha on the morphology of MDCK cells.* Exp Cell Res, 2005. **309**(1): p. 149-60.

122. Willmarth, N.E. and S.P. Ethier, *Autocrine and juxtacrine effects of amphiregulin on the proliferative, invasive, and migratory properties of normal and neoplastic human mammary epithelial cells.* J Biol Chem, 2006. **281**(49): p. 37728-37.

123. Sigismund, S., et al., *Clathrin-independent endocytosis of ubiquitinated cargos.* Proc Natl Acad Sci U S A, 2005. **102**(8): p. 2760-5.

124. Caldieri, G., et al., *EGFR Trafficking in Physiology and Cancer.* Prog Mol Subcell Biol, 2018. **57**: p. 235-272.

125. Barbieri, E., P.P. Di Fiore, and S. Sigismund, *Endocytic control of signaling at the plasma membrane.* Curr Opin Cell Biol, 2016. **39**: p. 21-7.

126. Pascolutti, R., et al., *Molecularly Distinct Clathrin-Coated Pits Differentially Impact EGFR Fate and Signaling.* Cell Rep, 2019. **27**(10): p. 3049-3061 e6.

127. Savio, M.G., et al., *USP9X Controls EGFR Fate by Deubiquitinating the Endocytic Adaptor Eps15.* Curr Biol, 2016. **26**(2): p. 173-183.

128. Di Fiore, P.P., *Endocytosis, signaling and cancer, much more than meets the eye. Preface.* Mol Oncol, 2009. **3**(4): p. 273-9.

129. Levkowitz, G., et al., *c-Cbl/Sli-1 regulates endocytic sorting and ubiquitination of the epidermal growth factor receptor.* Genes Dev, 1998. **12**(23): p. 3663-74.

130. Jiang, X., et al., *Grb2 regulates internalization of EGF receptors through clathrin-coated pits.* Mol Biol Cell, 2003. **14**(3): p. 858-70.

131. Iacono, K.T., et al., *CD147 immunoglobulin superfamily receptor function and role in pathology.* Exp Mol Pathol, 2007. **83**(3): p. 283-95.

132. Yan, L., S. Zucker, and B.P. Toole, *Roles of the multifunctional glycoprotein, emmprin (basigin; CD147), in tumour progression.* Thromb Haemost, 2005. **93**(2): p. 199-204.

133. Eyster, C.A., et al., *MARCH ubiquitin ligases alter the itinerary of clathrin-independent cargo from recycling to degradation.* Mol Biol Cell, 2011. **22**(17): p. 3218-30.

134. Muramatsu, T., *Basigin (CD147), a multifunctional transmembrane glycoprotein with various binding partners.* J Biochem, 2016. **159**(5): p. 481-90.

135. Weidle, U.H., et al., *Cancer-related issues of CD147.* Cancer Genomics Proteomics, 2010. **7**(3): p. 157-69.

136. Schikorski, T., S.M. Young, Jr., and Y. Hu, *Horseradish peroxidase cDNA as a marker for electron microscopy in neurons.* J Neurosci Methods, 2007. **165**(2): p. 210-5.

137. Regad, T., *Targeting RTK Signaling Pathways in Cancer.* Cancers (Basel), 2015. **7**(3): p. 1758-84.

138. Kwon, Y., et al., *Targeting Autophagy for Overcoming Resistance to Anti-EGFR Treatments.* Cancers (Basel), 2019. **11**(9).

139. Wee, P. and Z. Wang, *Epidermal Growth Factor Receptor Cell Proliferation Signaling Pathways.* Cancers (Basel), 2017. **9**(5).

140. Katan, M. and S. Cockcroft, *Phosphatidylinositol(4,5)bisphosphate: diverse functions at the plasma membrane.* Essays Biochem, 2020. **64**(3): p. 513-531.

141. Andl, C.D., et al., *EGFR-induced cell migration is mediated predominantly by the JAK-STAT pathway in primary esophageal keratinocytes.* Am J Physiol Gastrointest Liver Physiol, 2004. **287**(6): p. G1227-37.

142. David, M., et al., *STAT activation by epidermal growth factor (EGF) and amphiregulin. Requirement for the EGF receptor kinase but not for tyrosine phosphorylation sites or JAK1.* J Biol Chem, 1996. **271**(16): p. 9185-8.

143. Quesnelle, K.M., A.L. Boehm, and J.R. Grandis, *STAT-mediated EGFR signaling in cancer.* J Cell Biochem, 2007. **102**(2): p. 311-9.

144. Gresset, A., J. Sondek, and T.K. Harden, *The phospholipase C isozymes and their regulation.* Subcell Biochem, 2012. **58**: p. 61-94.

145. Carpenter, G. and Q. Ji, *Phospholipase C-gamma as a signal-transducing element.* Exp Cell Res, 1999. **253**(1): p. 15-24.

146. Kania, E., et al., *IP3 Receptor-Mediated Calcium Signaling and Its Role in Autophagy in Cancer.* Front Oncol, 2017. **7**: p. 140.

147. Kang, J.H., et al., *Protein kinase C (PKC) isozyme-specific substrates and their design.* Biotechnol Adv, 2012. **30**(6): p. 1662-72.

148. Hajicek, N., et al., *Structural basis for the activation of PLC-gamma isozymes by phosphorylation and cancer-associated mutations.* Elife, 2019. **8**.

149. Gresset, A., et al., *Mechanism of phosphorylation-induced activation of phospholipase C-gamma isozymes.* J Biol Chem, 2010. **285**(46): p. 35836-47.

150. Kim, H.K., et al., *PDGF stimulation of inositol phospholipid hydrolysis requires PLC-gamma 1 phosphorylation on tyrosine residues 783 and 1254.* Cell, 1991. **65**(3): p. 435-41.

151. Koss, H., et al., *Dysfunction of phospholipase Cgamma in immune disorders and cancer.* Trends Biochem Sci, 2014. **39**(12): p. 603-11.

152. Choi, J.H., et al., *Grb2 negatively regulates epidermal growth factor-induced phospholipase C-gamma1 activity through the direct interaction with tyrosine-phosphorylated phospholipase C-gamma1.* Cell Signal, 2005. **17**(10): p. 1289-99.

153. Timsah, Z., et al., *Competition between Grb2 and Plcgamma1 for FGFR2 regulates basal phospholipase activity and invasion.* Nat Struct Mol Biol, 2014. **21**(2): p. 180-8.

154. Choi, J.H., et al., *Phospholipase C-gamma1 is a guanine nucleotide exchange factor for dynamin-1 and enhances dynamin-1-dependent epidermal growth factor receptor endocytosis.* J Cell Sci, 2004. **117**(Pt 17): p. 3785-95.

155. Walliser, C., et al., *Rac-mediated Stimulation of Phospholipase Cgamma2 Amplifies B Cell Receptor-induced Calcium Signaling.* J Biol Chem, 2015. **290**(28): p. 17056-72.

156. Zhou, X., et al., *Rac1/osmosensing scaffold for MEKK3 contributes via phospholipase C-gamma1 to activation of the osmoprotective transcription factor NFAT5.* Proc Natl Acad Sci U S A, 2011. **108**(29): p. 12155-60.

157. Jang, H.-J., et al., *Phosphoinositide-Specific Phospholipase C (PI-PLC)*, in *Encyclopedia of Signaling Molecules*, S. Choi, Editor. 2018, Springer International Publishing: Cham. p. 3973-3988.

158. Wilde, J.I. and S.P. Watson, *Regulation of phospholipase C gamma isoforms in haematopoietic cells: why one, not the other?* Cell Signal, 2001. **13**(10): p. 691-701.

159. Kataoka, K., et al., *Integrated molecular analysis of adult T cell leukemia/lymphoma.* Nat Genet, 2015. **47**(11): p. 1304-15.

160. Vaque, J.P., et al., *PLCG1 mutations in cutaneous T-cell lymphomas.* Blood, 2014. **123**(13): p. 2034-43.

161. Zhou, Q., et al., *A hypermorphic missense mutation in PLCG2, encoding phospholipase Cgamma2, causes a dominantly inherited autoinflammatory disease with immunodeficiency.* Am J Hum Genet, 2012. **91**(4): p. 713-20.

162. Ombrello, M.J., et al., *Cold urticaria, immunodeficiency, and autoimmunity related to PLCG2 deletions.* N Engl J Med, 2012. **366**(4): p. 330-8.

163. Takalo, M., et al., *The Alzheimer's disease-associated protective Plcgamma2-P522R variant promotes immune functions.* Mol Neurodegener, 2020. **15**(1): p. 52.

164. Jang, H.J., et al., *PLCgamma1: Potential arbitrator of cancer progression.* Adv Biol Regul, 2018. **67**: p. 179-189.

165. Threadgill, D.W., et al., *Targeted disruption of mouse EGF receptor: effect of genetic background on mutant phenotype.* Science, 1995. **269**(5221): p. 230-4.

166. Sato, T., et al., *Single Lgr5 stem cells build crypt-villus structures in vitro without a mesenchymal niche.* Nature, 2009. **459**(7244): p. 262-5.

167. Abud, H.E., W.H. Chan, and T. Jarde, *Source and Impact of the EGF Family of Ligands on Intestinal Stem Cells.* Front Cell Dev Biol, 2021. **9**: p. 685665.
168. Takahashi, T. and A. Shiraishi, *Stem Cell Signaling Pathways in the Small Intestine.* Int J Mol Sci, 2020. **21**(6).
169. Yarden, Y. and G. Pines, *The ERBB network: at last, cancer therapy meets systems biology.* Nat Rev Cancer, 2012. **12**(8): p. 553-63.
170. Tanner, M., P. Jarvinen, and J. Isola, *Amplification of HER-2/neu and topoisomerase IIalpha in primary and metastatic breast cancer.* Cancer Res, 2001. **61**(14): p. 5345-8.
171. Rosell, R., et al., *Erlotinib versus standard chemotherapy as first-line treatment for European patients with advanced EGFR mutation-positive non-small-cell lung cancer (EURTAC): a multicentre, open-label, randomised phase 3 trial.* Lancet Oncol, 2012. **13**(3): p. 239-46.
172. Hirsch, F.R., et al., *Epidermal growth factor receptor inhibition in lung cancer: status 2012.* J Thorac Oncol, 2013. **8**(3): p. 373-84.
173. Frampton, J.E., *Cetuximab: a review of its use in squamous cell carcinoma of the head and neck.* Drugs, 2010. **70**(15): p. 1987-2010.
174. Krawczyk, P.A. and D.M. Kowalski, *Genetic and immune factors underlying the efficacy of cetuximab and panitumumab in the treatment of patients with metastatic colorectal cancer.* Contemp Oncol (Pozn), 2014. **18**(1): p. 7-16.
175. Jaramillo, M.L., et al., *Effect of the anti-receptor ligand-blocking 225 monoclonal antibody on EGF receptor endocytosis and sorting.* Exp Cell Res, 2006. **312**(15): p. 2778-90.
176. Ferraro, D.A., et al., *Inhibition of triple-negative breast cancer models by combinations of antibodies to EGFR.* Proc Natl Acad Sci U S A, 2013. **110**(5): p. 1815-20.
177. Sigismund, S., et al., *Threshold-controlled ubiquitination of the EGFR directs receptor fate.* The EMBO journal, 2013. **32**(15): p. 2140-57.
178. Marsault, R., et al., *Domains of high Ca2+ beneath the plasma membrane of living A7r5 cells.* EMBO J, 1997. **16**(7): p. 1575-81.
179. Bonora, M., et al., *Subcellular calcium measurements in mammalian cells using jellyfish photoprotein aequorin-based probes.* Nature protocols, 2013. **8**(11): p. 2105-18.
180. Heilemann, M., et al., *Subdiffraction-resolution fluorescence imaging with conventional fluorescent probes.* Angewandte Chemie, 2008. **47**(33): p. 6172-6.

181. Thompson, R.E., D.R. Larson, and W.W. Webb, *Precise nanometer localization analysis for individual fluorescent probes.* Biophysical journal, 2002. **82**(5): p. 2775-83.
182. Pelicci, S., et al., *Novel Tools to Measure Single Molecules Colocalization in Fluorescence Nanoscopy by Image Cross Correlation Spectroscopy.* Nanomaterials (Basel), 2022. **12**(4).
183. Wilson, B.S., J.R. Pfeiffer, and J.M. Oliver, *Observing FcepsilonRI signaling from the inside of the mast cell membrane.* J Cell Biol, 2000. **149**(5): p. 1131-42.
184. Lagache, T., et al., *Analysis of the spatial organization of molecules with robust statistics.* PLoS One, 2013. **8**(12): p. e80914.
185. Nikolaev, M., et al., *Homeostatic mini-intestines through scaffold-guided organoid morphogenesis.* Nature, 2020. **585**(7826): p. 574-578.
186. Nguyen-Ngoc, K.V., et al., *3D culture assays of murine mammary branching morphogenesis and epithelial invasion.* Methods Mol Biol, 2015. **1189**: p. 135-62.
187. Wilson, B.S., et al., *High resolution mapping of mast cell membranes reveals primary and secondary domains of Fc(epsilon)RI and LAT.* J Cell Biol, 2001. **154**(3): p. 645-58.
188. Zhukovsky, M.A., et al., *Phosphatidic acid in membrane rearrangements.* FEBS Lett, 2019. **593**(17): p. 2428-2451.
189. Takahashi, D., et al., *Crystal structure and calcium-induced conformational changes of diacylglycerol kinase alpha EF-hand domains.* Protein Sci, 2019. **28**(4): p. 694-706.
190. Medina, D.L., et al., *Lysosomal calcium signalling regulates autophagy through calcineurin and TFEB.* Nat Cell Biol, 2015. **17**(3): p. 288-99.
191. Rao, A., C. Luo, and P.G. Hogan, *Transcription factors of the NFAT family: regulation and function.* Annu Rev Immunol, 1997. **15**: p. 707-47.
192. Singh, B., G. Carpenter, and R.J. Coffey, *EGF receptor ligands: recent advances.* F1000Res, 2016. **5**.
193. Waterman, H., et al., *Alternative intracellular routing of ErbB receptors may determine signaling potency.* J Biol Chem, 1998. **273**(22): p. 13819-27.
194. Sanders, J.M., et al., *Molecular determinants of epidermal growth factor binding: a molecular dynamics study.* PLoS One, 2013. **8**(1): p. e54136.
195. Li, P., et al., *Measuring Sharp Waves and Oscillatory Population Activity With the Genetically Encoded Calcium Indicator GCaMP6f.* Front Cell Neurosci, 2019. **13**: p. 274.

196. Abulrob, A., et al., *Nanoscale imaging of epidermal growth factor receptor clustering: effects of inhibitors.* J Biol Chem, 2010. **285**(5): p. 3145-56.

197. Wang, Y., et al., *Regulation of EGFR nanocluster formation by ionic protein-lipid interaction.* Cell Res, 2014. **24**(8): p. 959-76.

198. Bugaj, L.J., et al., *Regulation of endogenous transmembrane receptors through optogenetic Cry2 clustering.* Nat Commun, 2015. **6**: p. 6898.

199. Petrelli, A., et al., *The endophilin-CIN85-Cbl complex mediates ligand-dependent downregulation of c-Met.* Nature, 2002. **416**(6877): p. 187-90.

200. Kirk, P., et al., *CD147 is tightly associated with lactate transporters MCT1 and MCT4 and facilitates their cell surface expression.* EMBO J, 2000. **19**(15): p. 3896-904.

201. Su, J., et al., *CD147 silencing inhibits tumor growth by suppressing glucose transport in melanoma.* Oncotarget, 2016. **7**(40): p. 64778-64784.

202. Debnath, J., S.K. Muthuswamy, and J.S. Brugge, *Morphogenesis and oncogenesis of MCF-10A mammary epithelial acini grown in three-dimensional basement membrane cultures.* Methods, 2003. **30**(3): p. 256-68.

203. Sato, T. and H. Clevers, *Growing self-organizing mini-guts from a single intestinal stem cell: mechanism and applications.* Science, 2013. **340**(6137): p. 1190-4.

204. Chiang, C.Y., et al., *Phospholipase Cgamma-2 and intracellular calcium are required for lipopolysaccharide-induced Toll-like receptor 4 (TLR4) endocytosis and interferon regulatory factor 3 (IRF3) activation.* J Biol Chem, 2012. **287**(6): p. 3704-9.

205. Maguire, E., et al., *PIP2 depletion and altered endocytosis caused by expression of Alzheimer's disease-protective variant PLCgamma2 R522.* EMBO J, 2021. **40**(17): p. e105603.

206. Delos Santos, R.C., et al., *Selective regulation of clathrin-mediated epidermal growth factor receptor signaling and endocytosis by phospholipase C and calcium.* Mol Biol Cell, 2017. **28**(21): p. 2802-2818.

207. Alava, M.A., et al., *Increased intracellular cyclic AMP inhibits inositol phospholipid hydrolysis induced by perturbation of the T cell receptor/CD3 complex but not by G-protein stimulation. Association with protein kinase A-mediated phosphorylation of phospholipase C-gamma 1.* Biochem J, 1992. **284 (Pt 1)**: p. 189-99.

208. Bae, S.S., et al., *Regulation of phospholipase C-gamma1 by protein kinase A-dependent phosphorylation.* Adv Enzyme Regul, 2002. **42**: p. 195-211.

209. Guittard, G., et al., *The Cish SH2 domain is essential for PLC-gamma1 regulation in TCR stimulated CD8(+) T cells.* Sci Rep, 2018. **8**(1): p. 5336.

210. Jeon, M.S., et al., *Essential role of the E3 ubiquitin ligase Cbl-b in T cell anergy induction.* Immunity, 2004. **21**(2): p. 167-77.

211. Sohn, H.W., H. Gu, and S.K. Pierce, *Cbl-b negatively regulates B cell antigen receptor signaling in mature B cells through ubiquitination of the tyrosine kinase Syk.* J Exp Med, 2003. **197**(11): p. 1511-24.

212. Tvorogov, D. and G. Carpenter, *EGF-dependent association of phospholipase C-gamma1 with c-Cbl.* Exp Cell Res, 2002. **277**(1): p. 86-94.

213. Matsuda, M., et al., *Real time fluorescence imaging of PLC gamma translocation and its interaction with the epidermal growth factor receptor.* J Cell Biol, 2001. **153**(3): p. 599-612.

214. Rodriguez, R., et al., *Requirements for distinct steps of phospholipase Cgamma2 regulation, membrane-raft-dependent targeting and subsequent enzyme activation in B-cell signalling.* Biochem J, 2003. **374**(Pt 1): p. 269-80.

215. Ioannou, G.N., et al., *Cholesterol crystallization within hepatocyte lipid droplets and its role in murine NASH.* J Lipid Res, 2017. **58**(6): p. 1067-1079.

216. Munro, S., *Lipid rafts: elusive or illusive?* Cell, 2003. **115**(4): p. 377-88.

217. Nichols, B.J., *GM1-containing lipid rafts are depleted within clathrin-coated pits.* Curr Biol, 2003. **13**(8): p. 686-90.

218. Hansen, G.H., et al., *Cholera toxin entry into pig enterocytes occurs via a lipid raft- and clathrin-dependent mechanism.* Biochemistry, 2005. **44**(3): p. 873-82.

219. Siraliev-Perez, E., et al., *Dynamics of allosteric regulation of the phospholipase C-gamma isozymes upon recruitment to membranes.* Elife, 2022. **11**.

220. Park, M.J., et al., *SH2 Domains Serve as Lipid-Binding Modules for pTyr-Signaling Proteins.* Mol Cell, 2016. **62**(1): p. 7-20.

221. Haugh, J.M., et al., *Effect of epidermal growth factor receptor internalization on regulation of the phospholipase C-gamma1 signaling pathway.* J Biol Chem, 1999. **274**(13): p. 8958-65.

222. Tan, X., et al., *Emerging roles of PtdIns(4,5)P2--beyond the plasma membrane.* J Cell Sci, 2015. **128**(22): p. 4047-56.

223. Manna, A., et al., *Cooperative assembly of a four-molecule signaling complex formed upon T cell antigen receptor activation.* Proc Natl Acad Sci U S A, 2018. **115**(51): p. E11914-E11923.

224. Piechulek, T., et al., *Isozyme-specific stimulation of phospholipase C-gamma2 by Rac GTPases.* J Biol Chem, 2005. **280**(47): p. 38923-31.

225. Walliser, C., et al., *rac regulates its effector phospholipase Cgamma2 through interaction with a split pleckstrin homology domain.* J Biol Chem, 2008. **283**(44): p. 30351-62.

226. Bunney, T.D., et al., *Structural insights into formation of an active signaling complex between Rac and phospholipase C gamma 2.* Mol Cell, 2009. **34**(2): p. 223-33.

227. Choi, J.H., S.H. Ryu, and P.G. Suh, *On/off-regulation of phospholipase C-gamma 1-mediated signal transduction.* Adv Enzyme Regul, 2007. **47**: p. 104-16.

228. Walliser, C., et al., *The Phospholipase Cgamma2 Mutants R665W and L845F Identified in Ibrutinib-resistant Chronic Lymphocytic Leukemia Patients Are Hypersensitive to the Rho GTPase Rac2 Protein.* J Biol Chem, 2016. **291**(42): p. 22136-22148.

229. Cizmecioglu, O., et al., *Rac1-mediated membrane raft localization of PI3K/p110beta is required for its activation by GPCRs or PTEN loss.* Elife, 2016. **5**.

230. Itoh, R.E., et al., *Activation of rac and cdc42 video imaged by fluorescent resonance energy transfer-based single-molecule probes in the membrane of living cells.* Mol Cell Biol, 2002. **22**(18): p. 6582-91.

231. Woyach, J.A., et al., *Resistance mechanisms for the Bruton's tyrosine kinase inhibitor ibrutinib.* N Engl J Med, 2014. **370**(24): p. 2286-94.

232. Magno, L., et al., *Alzheimer's disease phospholipase C-gamma-2 (PLCG2) protective variant is a functional hypermorph.* Alzheimers Res Ther, 2019. **11**(1): p. 16.

233. Francia, V., et al., *Limits and challenges in using transport inhibitors to characterize how nano-sized drug carriers enter cells.* Nanomedicine (Lond), 2019. **14**(12): p. 1533-1549.

234. Sandvig, K., S. Kavaliauskiene, and T. Skotland, *Clathrin-independent endocytosis: an increasing degree of complexity.* Histochem Cell Biol, 2018. **150**(2): p. 107-118.

235. Wang, K., et al., *CD147-spike protein is a novel route for SARS-CoV-2 infection to host cells.* Signal Transduct Target Ther, 2020. **5**(1): p. 283.

236. Radzikowska, U., et al., *Distribution of ACE2, CD147, CD26, and other SARS-CoV-2 associated molecules in tissues and immune cells in health and in asthma, COPD, obesity, hypertension, and COVID-19 risk factors.* Allergy, 2020. **75**(11): p. 2829-2845.

237. Jorissen, R.N., et al., *Epidermal growth factor receptor: mechanisms of activation and signalling.* Exp Cell Res, 2003. **284**(1): p. 31-53.

238. Chen, P., K. Gupta, and A. Wells, *Cell movement elicited by epidermal growth factor receptor requires kinase and autophosphorylation but is separable from mitogenesis.* J Cell Biol, 1994. **124**(4): p. 547-55.

239. Chen, P., et al., *Epidermal growth factor receptor-mediated cell motility: phospholipase C activity is required, but mitogen-activated protein kinase activity is not sufficient for induced cell movement.* J Cell Biol, 1994. **127**(3): p. 847-57.

240. van Leeuwen, F.N., et al., *Rac regulates phosphorylation of the myosin-II heavy chain, actinomyosin disassembly and cell spreading.* Nat Cell Biol, 1999. **1**(4): p. 242-8.

241. Chen, P., J.E. Murphy-Ullrich, and A. Wells, *A role for gelsolin in actuating epidermal growth factor receptor-mediated cell motility.* J Cell Biol, 1996. **134**(3): p. 689-98.

242. Wells, A., et al., *Epidermal growth factor receptor-mediated motility in fibroblasts.* Microsc Res Tech, 1998. **43**(5): p. 395-411.

243. Dearden-Badet, M.T. and G. Mouchiroud, *Re-distribution of phospholipase C gamma 2 in macrophage precursors is mediated by the actin cytoskeleton under the control of the Src kinases.* Cell Signal, 2005. **17**(12): p. 1560-71.

244. Cremasco, V., et al., *Phospholipase C gamma 2 is critical for development of a murine model of inflammatory arthritis by affecting actin dynamics in dendritic cells.* PLoS One, 2010. **5**(1): p. e8909.

245. Faix, J. and I. Weber, *A dual role model for active Rac1 in cell migration.* Small GTPases, 2013. **4**(2): p. 110-5.

246. Janmey, P.A., *Phosphoinositides and calcium as regulators of cellular actin assembly and disassembly.* Annu Rev Physiol, 1994. **56**: p. 169-91.

247. Antonescu, C.N., G. Danuser, and S.L. Schmid, *Phosphatidic acid plays a regulatory role in clathrin-mediated endocytosis.* Mol Biol Cell, 2010. **21**(16): p. 2944-52.

248. Lai, M.M., et al., *The calcineurin-dynamin 1 complex as a calcium sensor for synaptic vesicle endocytosis.* J Biol Chem, 1999. **274**(37): p. 25963-6.

249. Saheki, Y. and P. De Camilli, *Synaptic vesicle endocytosis.* Cold Spring Harb Perspect Biol, 2012. **4**(9): p. a005645.

250. Nishida, M., et al., *Amplification of receptor signalling by Ca2+ entry-mediated translocation and activation of PLCgamma2 in B lymphocytes.* EMBO J, 2003. **22**(18): p. 4677-88.

251. Liu, Y., et al., *Structural insights and activating mutations in diverse pathologies define mechanisms of deregulation for phospholipase C gamma enzymes.* EBioMedicine, 2020. **51**: p. 102607.

252. Francavilla, C., et al., *Multilayered proteomics reveals molecular switches dictating ligand-dependent EGFR trafficking.* Nat Struct Mol Biol, 2016. **23**(6): p. 608-18.

253. Doerner, A., R. Scheck, and A. Schepartz, *Growth Factor Identity Is Encoded by Discrete Coiled-Coil Rotamers in the EGFR Juxtamembrane Region.* Chem Biol, 2015. **22**(6): p. 776-84.

254. Sinclair, J.K.L., et al., *Mechanism of Allosteric Coupling into and through the Plasma Membrane by EGFR.* Cell Chem Biol, 2018. **25**(7): p. 857-870 e7.

255. Gao, J., et al., *Mechanistic insights into EGFR membrane clustering revealed by super-resolution imaging.* Nanoscale, 2015. **7**(6): p. 2511-9.

256. Ichinose, J., et al., *EGF signalling amplification induced by dynamic clustering of EGFR.* Biochem Biophys Res Commun, 2004. **324**(3): p. 1143-9.

257. Michailidis, I.E., et al., *Phosphatidylinositol-4,5-bisphosphate regulates epidermal growth factor receptor activation.* Pflugers Arch, 2011. **461**(3): p. 387-97.

258. Gratacap, M.P., et al., *Phosphatidylinositol 3,4,5-trisphosphate-dependent stimulation of phospholipase C-gamma2 is an early key event in FcgammaRIIA-mediated activation of human platelets.* J Biol Chem, 1998. **273**(38): p. 24314-21.

259. Xin, X., et al., *CD147/EMMPRIN overexpression and prognosis in cancer: A systematic review and meta-analysis.* Sci Rep, 2016. **6**: p. 32804.

260. Xiong, L., C.K. Edwards, 3rd, and L. Zhou, *The biological function and clinical utilization of CD147 in human diseases: a review of the current scientific literature.* Int J Mol Sci, 2014. **15**(10): p. 17411-41.

261. Landras, A., et al., *CD147 Is a Promising Target of Tumor Progression and a Prognostic Biomarker.* Cancers (Basel), 2019. **11**(11).

262. Li, X., et al., *The altered glucose metabolism in tumor and a tumor acidic microenvironment associated with extracellular matrix metalloproteinase inducer and monocarboxylate transporters.* Oncotarget, 2016. **7**(17): p. 23141-55.

263. Huang, L., et al., *EGFR promotes the apoptosis of CD4(+) T lymphocytes through TBK1/Glut1 induced Warburg effect in sepsis.* J Adv Res, 2022.

264. LaMarca, H.L. and J.M. Rosen, *Estrogen regulation of mammary gland development and breast cancer: amphiregulin takes center stage.* Breast Cancer Res, 2007. **9**(4): p. 304.

265. Palamidessi, A., et al., *Unjamming overcomes kinetic and proliferation arrest in terminally differentiated cells and promotes collective motility of carcinoma.* Nat Mater, 2019. **18**(11): p. 1252-1263.

ACKNOWLEDGMENTS

The conclusion of this PhD has been possible thanks to the help of many people.

First of all, I would like to thank my PhD Supervisor, Professor Pier Paolo Di Fiore for giving me the opportunity to work on this exciting project and for his constant guidance and scientific advices.

I would like to thank also my added Supervisor, Professor Sara Sigismund for her everyday supervision, support and scientific discussions during the years. She stimulated me to become more creative, confident and to overcome bad results and never give up.

Special acknowledgments to Giusi Caldieri and Elisa Barbieri, former lab members, who started this project. Thanks to Giusi for introducing me with the project, and for hers and Elisa's advices and help in many ways.

I want to thank Deborah Salvi Mesa, who shared this project with me along these years trying to give our best and always being there for me.

I am very grateful for the suggestions and feedback of my external advisor Professor Yosef Yarden, from the Weizmann Institute of Science, and my internal advisor Professor Giorgio Scita, from IFOM.

I also acknowledge the help of Rosalind Gunby for critically reading my thesis.

I would like to thank all our collaborators, whose work and suggestions have been fundamental for this project: Andrea Raimondi and Professor Carlo Tacchetti from San Raffaele Institute, Milan; Massimo Bonora and Professor Paolo Pinton from University of Ferrara, Ferrara. Thanks to all IEO facilities, especially Imaging Development Unit: Mario Faretta and Simone Pelicci, and Imaging Unit: Simona Rodighiero and Chiara Soriani.

I want also to thank all Sigismund group: our office crew (Chia, Ire, Matte, Andre + externals Cecia and Debi) + extended members (Ste, Giorgia, Ale, Marghe, MG, Stefano, Bronia) + former members (Cami and Ele) for all help, support and advices through these years.

I need to acknowledge also all the people that side-by-side shared with me all good and bad scientific and non-scientific moments: Angeli, Amir, Catiana, Eirini, Sara, Johannes and Marija.

Hvala mojoj porodici i prijateljima, što su uvek bili tu za mene i verovali u mene!

Hvala mojoj mami, sestri i Aci na bezuslovnoj ljubavi i podršci!

I hvala mom Mićoniju, mom večitom osloncu i najvećoj ljubavi!